A comprehensive characterization of brain and retina synaptic vesicle proteome by quantitative mass spectrometry.

Dissertation

for the award of the degree

“Doctor of Philosophy” (Ph.D.)

Division of Mathematics and Natural Sciences

of the Georg-August-Universität Göttingen

Submitted by

Sunit Mandad

from Pilani, India

Göttingen, May 2015

Members of the Thesis Committee

Prof. Dr. Henning Urlaub (Supervisor and First Referee)	Department of Bioanalytical Mass Spectrometry Max Planck Institute for Biophysical Chemistry, And Bioanalytics, Department of clinical chemistry University Medical Center Göttingen, Germany.
Prof. Dr. Reinhard Jahn (Second Referee)	Department of Neurobiology Max Planck Institute for Biophysical Chemistry Göttingen, Germany.
Prof. Dr. Tobias Moser	Department of Otorhinolaryngology Center for Molecular Physiology of the Brain Bernstein Center for Computational Neuroscience University of Göttingen Medical Center Göttingen, Germany

Additional Members of the Examination Board

Prof. Dr. Silvio O. Rizzoli	Department of Neuro- and Sensory Physiology University Medical Center Göttingen Georg-August-University Göttingen, Germany.
Prof. Dr. Detlef Doenecke	Institute for Molecular Biochemistry University Medical Center Göttingen Georg-August-University Göttingen, Germany.
Prof. Dr. Mikael Simons	Department of Cellular Neuroscience Max Planck Institute for Experimental Medicine Göttingen, Germany

Date of oral examination: 09.06. 2015

Dedicated to my family and friends

Summary

Synaptic vesicles (SVs) are essential organelles for the transfer of information between a pre-synaptic nerve terminal and a post-synaptic target. SVs release their neurotransmitter content into the synaptic cleft in a tightly regulated process, requiring the orchestrated interaction of a number of proteins involved in exocytosis, endocytosis and vesicular recycling. While the molecular anatomy of brain SV is known, the molecular profile of SVs of sensory systems, such as the retina, is not well understood. The major reason is the unavailability of reliable and efficient isolation protocol for SVs with low amounts of starting material.

In this study, establishment of a modified isolation protocol resulted in successfully purifying highly pure SVs from retina that formed the basis for a reliable determination of its absolute proteome quantification and molecular composition. Remarkably, this protocol allowed recovery of microgram quantities of highly pure and functional SVs from as low as eight bovine retinas. Maximal vesicle recovery was achieved by the introduction of a harsh homogenization step (powdering the tissue in liquid nitrogen using mortar and pestle and subsequent homogenization using Ultra-turrax) followed by subcellular fractionation. Notably, after fractionation by differential and rate-zonal centrifugation, performing an immunoprecipitation with a monoclonal antibody against synatophysin greatly improved the purity and yield of SVs from retina. The purity of the preparation was ensured by western blotting, electron microscopy and mass spectrometry.

The data derived from the iBAQ-MS based absolute quantification of proteins in purified bovine brain and retina SVs from frozen starting materials showed that the copies of SV-integral proteins such as synaptotagmin, SCAMP5, VGlut1 and synaptophysin were similar, if not identical, in bovine brain and retina SVs. Interestingly, however, the copies of v-SNARE protein VAMP2 and tetraspanin protein synaptogyrin-1 were drastically reduced; ~ 6 and 2 fold, respectively, in retina as compared to brain. On the other hand, surprisingly, a three to four fold increase in the copy number of the membrane glycoprotein SV2 were quantified in retina as compared to brain. In addition to differences observed in SV integral proteins, intriguing observations also surfaced when SV associated proteins were quantified. Three copies of the ribbon synapse specific protein syntaxin-3 were found associated to the purified retina SVs, however its brain-specific isoform syntaxin1A/B was totally absent. In addition, the brain-specific Rab3a and synapsin were not quantifiable in our pure retina SVs, suggesting the preparation of SVs to be of majorly ribbon in origin.

These striking differences in the retina SV proteome to that of brain highlights the specialized functionality of retina synapses. Although the molecular profile of synaptic proteins in transverse sections of retina is reported in literature, this is the first study where retina and brain SV proteome have been compared in terms of

absolute copies. The findings put forward in this study provides a basis for detailed functional analysis in the future.

In parallel, highly pure rat brain synaptosomes were quantified by iBAQ mass spectrometry in an aim to characterize the average number of presynaptic proteins. As a further validation of the obtained results, a battery of quantitative western blots was run for a selected group of proteins. These results, in combination with additional biophysical and biochemical data, were used to build a three-dimensional model of an average synaptic nerve terminal.

As an independent project, the temporal turnover of synaptic proteins in nerve terminals of the brain and retina were analyzed using a modified version of the SILAC mice approach. To our knowledge this is the first study where a lysine$_6$ diet has been used for labelling proteins over various timeframes to determine protein turnover *in vivo*. The mice were fed with lysine$_6$ diet for 5, 14 and 21 days and its incorporation in the proteins of brain and retina were analysed by quantitative mass spectrometry. The data shows that the turnover of synaptic proteins in retina is faster than in brain. Strikingly, the turnover of proteins that are involved in similar SV-recycling pathways, correlated well with their respective copy numbers. Future work should be focussed on elucidating the physiological meaning of these interesting observations.

Table of contents

List of Figures

List of Tables

List of Abbreviations

° C	Degree Celcius
µg	microgram
µM	micromolar
µl	microliter
µm	micrometer
ADP	Adenosine diphosphate
AGC	Automatic gain control
APEX	Absolute protein expression
ATP	Adenosine-1, 4, 5-triphosphate
AZ	Active zone
Ca^{2+}	Calcium
cAMP	cyclic AMP
CASK	Calcium/calmodulin-dependent serine protein kinase
Cl.	Clone
cpm	counts per minute
CtBP2	C-terminal binding protein 2
DAVID	Database for Annotation, Visualization and Integrated Discovery
DDA	Data-dependent acquisition
ER	Endoplasmic reticulum
ECD	Electron captured dissociation
ECL	Enhanced chemiluminescence (ECL)
EM	Electron microscope (EM)
ELKS/Rab6	Interacting/CAST family proteins (ERCs)
emPAI	Exponentially modified protein abundance index
ESI	Electrospray ionization
ETD	Electron- dissociation energy
FCS	Fluorescence correlation spectroscopy

FDR	Fast discovery rate
FT-ICR	Fourier-transform ion-cyclotron resonance
FTMS	Fourier Transform Mass Spectrometry
GDP	Guanosine diphosphate
GTP	Guanosine triphosphate
GO	Gene ontology
HCD	High energy collision dissociation
HEPES	*4-(2-hydroxyethyl)-1-piperazineethanesulfonic acid*
HRP	Horseradish peroxidase
iBAQ	Intensity-based-absolute quantitation
ICAT	Isotope-coded affinity tag
IPL fraction	Inner plexiform layer fraction
ITP	Inositol-1,4,5-triphosphate
iTRAQ	Isobaric tags for relative and absolute quantification
kDa	Kilo dalton
LC-MS	Liquid chromatography-mass spectrometry
LTQ	Linear Trap Quadrupole
mA	Milliampere
MALDI	Matrix assisted laser desorption ionization
MALDI-TOF	Matrix Assisted Laser Desorption/Ionization-time-of-flight
MALS	Mammalian LIN-7
mg	milligram
mM	Millimolar
MS	Mass spectrometry
m/z	Mass to charge ratio
CID	Collision induced dissociation
NaCl	Sodium chloride
NMDA	N-methyl-D-aspartate receptor subunit NR1
NSF	N-ethylmaleimide-sensitive fusion protein

LDS	Lithium dodecyl sulfate
MOPS	3-Morpholinepropanesulfonic acid
$MgSO_4$	Magnesium sulfate
OPL fraction	Outer plexiform layer fraction
PAGE	Polyacrylamide gel electrophoresis
P1	Pellet after first centrifugation
P2	Pellet after second centrifugation
P3	Pellet after third centrifugation
P4	Pellet after third centrifugation
S1	Supernatant after first centrifugation
S2	Supernatant after second centrifugation
S3	Supernatant after third centrifugation
PAI	Protein abundance index
PBS	Phosphate Buffer Saline
PIP_2	Phosphatidylinositol 4,5-bisphosphate
PIPK 1ϒ	Phosphatidylinositol 4-phosphate 5-kinase type 1 gamma
PMF	Peptide mass fingerprinting
PSD95	Postsynaptic density protein 95
pSILAC	pulsed Stable Isotope Labeling with Amino acids in cell culture
pSILAM	pulse Stable Isotope Labeling in Mammals
PVDF	Polyvinylidene fluoride
R^2	Coefficient of correlation
RBP	RIM binding protein
RIM	Rab3 interacting molecule
rpm	Rotation per minute
SCAMP	Secretory carrier-associated membrane protein 1
SDHA	Succinate dehydrogenase
SDS-PAGE	Sodium dodecyl sulphate-polyacrylamide gel electrophoresis
SILAC	Stable isotope labeling with amino acids in cell culture

SILAM	Stable isotope labeling by/with amino acids in mammals
SIMS	Secondary Ion mass spectrometry
SNARE	Soluble NSF attachment protein receptor
SV	Synaptic vesicles
Syp	Synaptophysin
TBST	Tris-Buffered Saline and Tween 20
TEMED	N, N, N',N'- Tetramethylethane-1,2-diamine
TOF	Time-of-flight
Tris-HCl	Tris(hydroxymethyl) aminomethane
UPS2	Universal Proteomics Standard-2
V	Volts
VAMP2	Vesicle-associated membrane protein 2
vATPase	Vacuolar-type H+-ATPase
VGAT/VIAAT	Vesicular inhibitory amino acid transporter
VGlut	Vesicular glutamate transporter
α-SNAP	α-soluble NSF attachment protein

1 Introduction

As the old adage goes "*we are what we think".* The thought process, a unique feature of humans, influences our actions, behavior and how we respond to internal and external cues. In turn, the thought process is shaped by sensory perception. Sensory perception is a series of events of receiving a sensory stimulus, converting it to a molecular signal, and finally recognizing and characterizing the signal. Our brain serves as the centre where our sensory perception is processed and expressed as a response to a received sensory stimulus, thus coordinating physiological processes. For example, vision is one of the remarkable physiological phenomena that represents a highly co-ordinated action between the brain and the eyes. Static picture, its colors and movement are the three kinds of light-evoked information captured by our eye. It is faithfully converted into electrochemical signal and sent to the brain. In response, brain decodes the information and commands the body to react accordingly. Emil du Bois-Reymond, known as the father of experimental electrophysiology, initiated modern neuroscience with the discovery of action potential and chemical transmission at neuromuscular junctions (Wassle, 2004). The whole process of coordination by the brain is highly complex than it seems, and still far from being understood.

1.1 Synapse

The functional unit of brain is a neuron. The neuron is an electrically excitable cell that can transmit electrical as well as chemical signals from one neuron to another (Cajal, 2006). S. Ramon Cajal and C Sherrington, fathers of modern neuroscience, proposed that the neurons communicate with each other via a special structure called synapse. This process is mediated by neurotransmitters (Cajal, 2006). After this discovery, there were debates whether the information transferred is in the form of electrical or chemical signal. These debates are referred in the history as 'The War of Soup and the Sparks' (Valenstein ES., 2006). Initial findings led to discovery of chemical synapses. S. R. Cajal found that the information transfer does occur in the neuron by neurotransmitters (Cajal, 2006), and these neurotransmitters are present only at specific locations of neuron and not all over the neuron body (Valenstein ES., 2006) (Pereda, 2014). Later, T.R. Elliot (1905) and O. Loewi (1924) established the existence of neurotransmitters at the postsynaptic site occurring in millisecond of time (Elliot, 1905). Katz B *et al* worked on frog neuromuscular junction and found that signal relay was electrically

mediated, calcium-dependent and occurred within millisecond (Katz and Miledi, 1969). In contrast to the chemical nature of synapses, some years later an interesting study by D. Potter led to discovery of electrical synapses. He demonstrated in Cray fish that the transmission was bidirectional and voltage dependent (Furshpan and Potter, 1959).

A synapse is the contact region of two neurons where exchange of information takes place with the help of various chemicals such as acetylcholine, dopamine, and glutamate collectively called as neurotransmitters (Elliot, 1905). The synaptic area of a neuron that transfers the neurotransmitters is called the pre-synaptic, while the neuron that receives the neurotransmitters is called the post synapse. The space between the pre- and post-synapse where the neurotransmitters are released is called the synaptic cleft (fig 1-3).

1.1.1 Types of synapses

Synapses are divided into two types based on their morphology and function: chemical synapses and electrical synapses. Electrical synapses are the synapses that are electrically excitable and transfer information via gap-junction (Bennett and Zukin, 2004).

The gap-junctions are approximately 1.2 nm (in diameter) hydrophilic pores on membrane that allow flow of ions and small molecules for example cyclic AMP, calcium and inositol-1, 4, 5-triphosphate. The information transfer is very fast and bidirectional in electrical synapses ((Bennett and Zukin, 2004; Goodenough and Paul, 2009).

The other class of synapses are called chemical synapses. Here, the information is transferred by chemicals called neurotransmitters mediated by synaptic vesicles. Based on their location and function, chemical synapses are sub-divided into two kinds: Conventional and Ribbon synapses. Conventional synapses (fig. 1-1(a)) are present in brain (fig. 1-1(a)) and spinal cord. Ribbon synapses are present at the sensory systems like retina (fig. 1-1(b)) and hair cell in cochlea (Lenzi and von Gersdorff, 2001; Sterling and Matthews, 2005). The differences between conventional synapses and retina ribbon synapses are summarized in Table 1-1 (section 1.1.1.2.1). In brain as well as retina, the electrical and the chemical synapses co-exist and interact to perform function (Bargmann, 2012; Connors and Long, 2004; Pereda, 2014).

(a) (b)

BRAIN RETINA

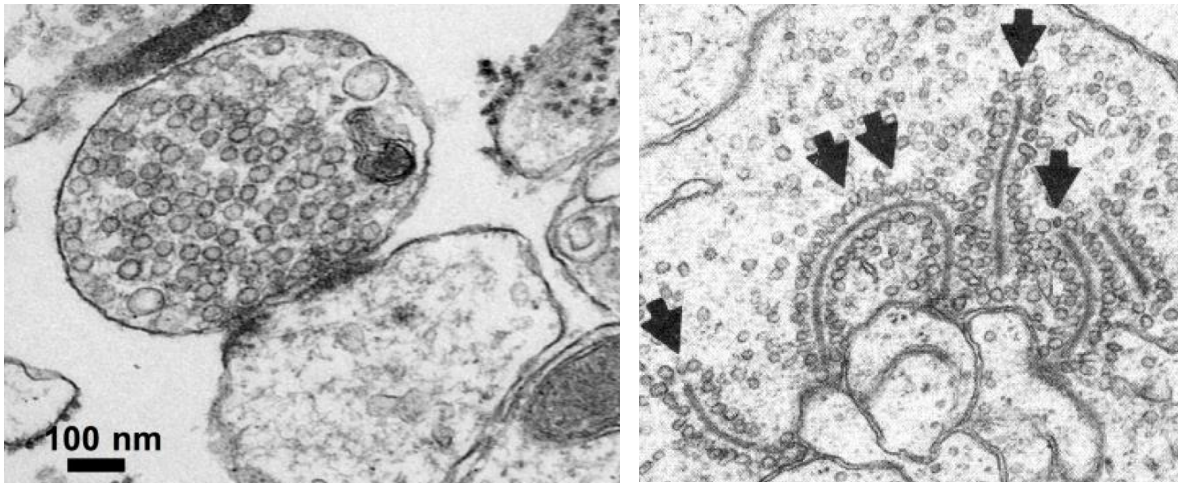

Z. Taoufiq (2013) Dowling J E and Werblin FS., (1969)

Figure 1-1: ***Brain and retina synapse.*** EM picture depicting (a) Conventional synapse from a rat brain synaptosome and (b) Ribbon synapses in guinea pig retina. Figure adapted from Taoufiq Z (2013) *(left)*, Dowling JE and Werblin FS (1969) *(right)* with permission.

Apart from the above-mentioned synapses, there are other two important types of synapses named peripheral neuromuscular junctions and Calyx of Held. Neuromuscular junctions connect the nervous system with muscle fibers while Calyx of Held is located at auditory nervous system (Borst and van Hoeve, 2012).

1.1.1.1 Brain synapse

The human brain contains approximately 10^{12} neurons that form approximately 10^{15} chemical synapses to communicate and coordinate our body (Pocklington et al., 2006). The pre-synaptic region is predominated by a dense proteinaceous region containing synaptic vesicles (SVs) called Active Zone (AZ) (Sudhof, 2004). Upon arrival of a signal, various proteins interact and lead to exocytosis of neurotransmitters into the synaptic cleft (for more information, section 1.1.1.1.2). These neurotransmitters bind to their receptors present at the post-synaptic region and activate the down-stream signaling cascade. In this way, signal is transferred chemically from one neuron to other.

Apart from this, brain cells also transfer electrical signals via gap-junctions (section 1.2). However, a major population of brain synapses is chemical in nature (Wassle, 2004).

1.1.1.1.1 Brain Synaptic Vesicle

In 1950, Bernhard Katz first observed a calcium-dependent quantal release at synapses in neuromuscular junctions of frog (Katz, B., Nobel lecture, 1970). The general hypothesis of the general release of a certain quantal unit (later termed as SV) from pre-synaptic region upon induction by calcium was given by Katz. The identity of the released quantal unit from the synapses was not exactly known until the seminal work by George Palade. In 1956, George Palade and Eduardo De Robertis first observed synapses under electron microscope (EM) and named the quantal unit as 'synaptic vesicle' (Derobertis and Bennett, 1955; Palade, 1954). Synaptic Vesicles (SVs) are the smallest known organelles. They are the information units of neurons. SVs are spherical in structure with varying sizes between 30 to 60 nm in diameter. They are made of proteins and lipid, with neurotransmitters filled in their lumen. SVs are known to function in uptake and release of neurotransmitters like glutamate (Jahn, 2006; Jahn and Sudhof, 1994). In 1970, John Heuser and Bruno Ceccarelli worked on SV recycling and later Heuser captured stimulus dependent SV exocytosis by rapid-freezing technique (Heuser et al., 1979; Hurlbut and Ceccarelli, 1974). Years after 1980 are referred as the "golden age" of molecular discoveries because it has led to the discovery and investigation of various SV associated proteins that assist in the proper functioning of synapses for information transfer (Jahn and Sudhof, 1994; Sudhof, 2004) (Jahn, R and Boyken J., 2013).

A synaptic vesicle is continuously endocytosed and exocytosed in a process termed SV cycle (explained in section 1.5). A SV contains two major classes of proteins: (a) transporters that are meant to uptake various neurotransmitters into the SV lumen, and (b) trafficking proteins that aid the SV through various steps of the SV cycle. Transporter proteins consist of a vacuolar-type proton pump that generates an electrochemical gradient by transferring protons into the lumen of the SV. This fuels neurotransmitter uptake by respective transporters. On the other hand, trafficking proteins constitute an array of proteins that function in a complex manner to orchestrate multistep pathways like exocytosis and endocytosis, by mediating protein-protein interaction, protein-lipid modification and undergoing post-translational modification to fulfil a specific function (Sudhof, 2004). The SV proteins with their copy numbers per vesicle and possible role in SV-recycling are given in Fig. 1.2.

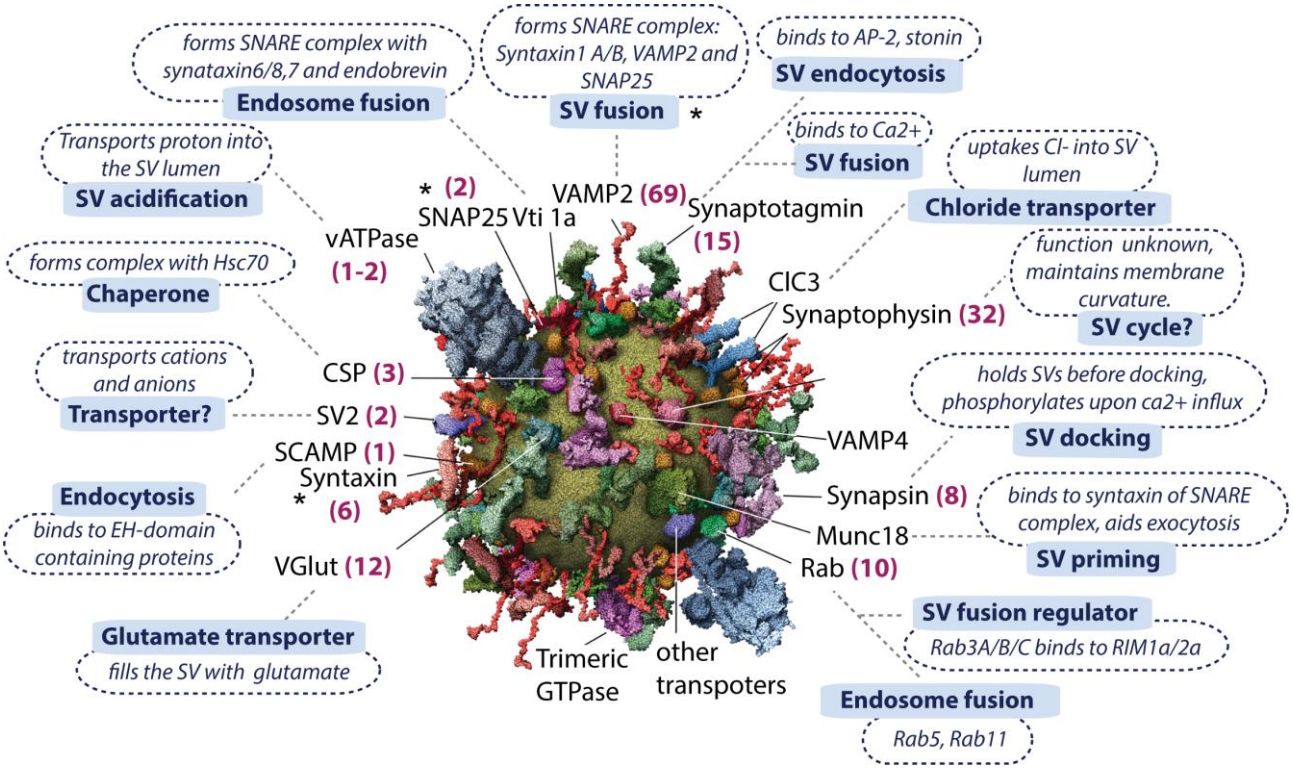

Figure 1-2: ***Molecular model of SV.*** Various SV integral and associated proteins are labelled with their possible 3-dimensional structure. The function of SV proteins are shown in bold letters (filled blue boxes) along with details (blue dotted boxes, in italics). Copy number (in brackets) for protein are shown in bold red color. Figure adapted from (Sudhof, 2004; Takamori et al., 2006) with permission.

Unlike other organelles, SVs exhibit very definite proteome and lipids composition in a ratio of Protein(1):Lipid(3). The lipid composition (wt/wt) contains 40% phosphatidylcholine, 10% cholesterol, 12% phosphatidylserine and 5% phosphatidylinositol (Benfenati et al., 1989). In a landmark study, Takamori *et al.,* (2006) accomplished the biophysical, biochemical and molecular characterization of the major protein constituents of synaptic vesicles, which led to the construction of a 3-dimensional model of a SV (Takamori et al., 2006) (fig 1.2).

1.1.1.1.2 Brain Synaptic Vesicle Cycle

In order to maintain the continuous synaptic transmission, the neuron must undergo continuous exocytosis and endocytosis of SVs at synapse. The SV cycle is divided into 8 major steps (Chua et al., 2010) as described below (fig. 1-3):

Step 1: Loading of Neurotransmitter in empty SVs

Loading of neurotransmitters requires generation of an electrochemical proton gradient across the SV membrane. The proton gradient is maintained by vacuolar H^+ ATPase. Glutamate is the major component filled inside the SVs transported by vesicular glutamate transporter (VGlut).

Step 2: Docking of SV

Upon arrival of an action potential, the voltage-gated calcium channels (N-type ($Ca_v2.2$) or P/Q type ($Ca_v2.1$)) allow influx of calcium ions into the synapse. This creates a microenvironment with by high calcium concentration. For docking, a few protein-protein interactions and protein modifications are characterized, however most of the steps are not well understood.

One of the well-known pathways is calmodulin-dependent phosphorylation cascade leading to phosphorylation of synapsin (Deremer et al., 1992a; Deremer et al., 1992b; Jia et al., 1992; Sihra et al., 1992). Synapsin contains a short N-terminal domain (20 residues, conserved for phosphorylation at seven sites by multiple protein kinases, a linker sequence and a large central C domain (300 residues) conserved in the synapsin family. Phosphorylation of synapsin is a critical signal, which leads to its dissociation from the SV. The free SVs move towards the nerve terminal and meet their potential interacting partners present in the active zone (Rodnight and Wofchuk, 1992). Potential interaction might occur with large multidomain proteins such as Bassoon, Piccolo, ELKS/Rab6-interacting/CAST family proteins (ERCs), liprin-α, MINT1 (Rogelj et al., 2006), MALS (Olsen et al., 2006) and CASK (Hsueh, 2006) which form the protein matrix of the active zone. The close positioning of the SVs to the pre-synaptic membrane is referred as docking (Verhage and Sorensen, 2008).

Step 3: Priming

Priming is an ATP dependent process that triggers docked SVs to fuse with the plasma membrane. The docked SV undergo exocytosis upon influx of calcium ion (Verhage and Sorensen, 2008) (fig. 1.3; step 3). Priming is also regulated independently of by Munc13 (Ma et al., 2011) and RIM (Rizo and Rosenmund, 2008).

In addition, the Ras-related small monomeric GTPase Rab3 also plays an important role in priming (fig. 1.3; step 3). Rab3A has been very well studied (Schluter O.M. *et al*., 1999). It binds to GTP, which poses the “ON” signal for exocytosis. This allows RIM (Rab3 interacting protein) to bind to Rab3a. The catalysis of GTP to GDP conversion is “OFF” signal. Binding of GTP to Rab3 activates SV for fusion (Jahn R and Boyken J., 2013).

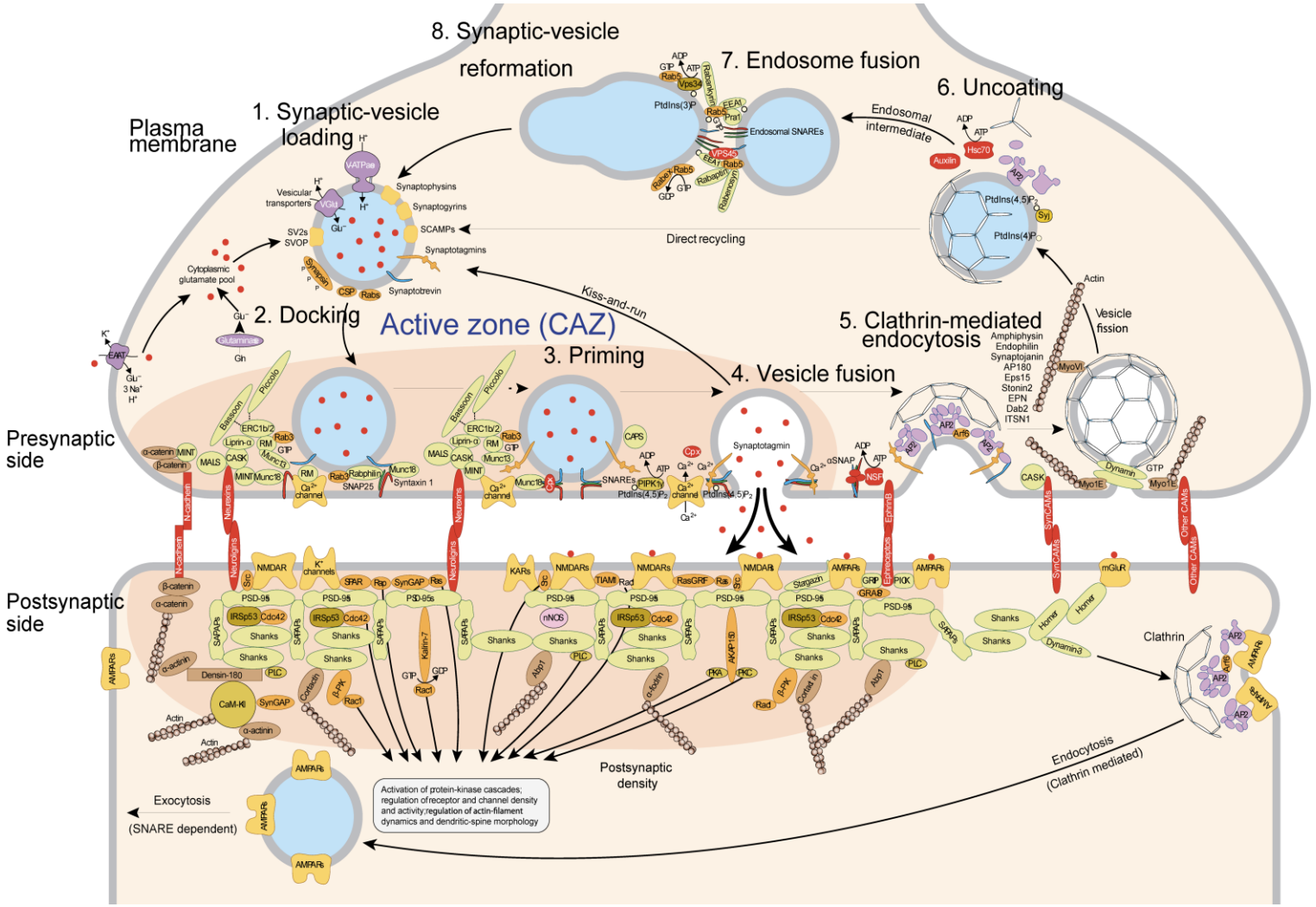

Figure 1-3: ***Synaptic Vesicle cycle model.*** Schematic representation of various known proteins involved at 8 steps of SV cycle viz., 1. SV loading, 2. Docking, 3. Priming, 4. Vesicle fusion, 5. Clathrin-mediated endocytosis, 6. Uncoating, 7. Endosome fusion and 8. Synaptic vesicle reformation. Picture adapted from Chua J J *et al*., (2010) with permission.

Priming includes synthesis of phosphatidylinositol (4,5)-bisphosphate and disassembly of assembled soluble NSF attachment protein receptor (SNARE) complexes by AAA+-ATPase N-ethylmaleimide-sensitive fusion protein (NSF) and its cofactor α-soluble NSF attachment protein (α-SNAP) (fig. 1-3) (Chua et al., 2010).

Step 4: Vesicle fusion

The elevated micro-calcium environment is detected by calcium sensor synaptotagmin. Binding of calcium to two C2 domains of synaptotagmin increases its affinity towards phospholipids and thus binds to the plasma membrane (Matthew et al., 1981 (Sudhof and Rizo, 2011). High calcium also dissociates the fusion clamp complexin proteins from SNARE complexes thus triggering exocytosis (Kummel et al., 2011; Li et al., 2011; Malsam et al., 2012; Martin et al., 2011).

SNAP25, syntaxin1 and VAMP2 form synaptic SNARE complex in a zipper-like fashion initiated from N-terminus region and proceeding towards the C-terminus of proteins resulting in a driving force for vesicle fusion (Jahn and Scheller, 2006). This zippering bridges the gap of opposing membrane forces. The mechanical energy released during this process is used to overcome the energy barrier for merging the two membranes; SV membrane to plasma membrane (Honing et al., 2005; Jahn and Scheller, 2006; Jahn and Sudhof, 1994; Sudhof, 2004). The fusion of vesicle releases the neurotransmitters into the synaptic cleft.

Interestingly, VAMP2 is also the site of action for tetanus and Botulinum toxins. Each toxin contains a light chain and a heavy chain. The light chain is a Zn^{2+} dependent protease that selectively cleaves VAMP2 (and not other VAMPs). The heavy chain binds to the SV2 and synaptotagmin proteins, thus channels on SV while endocytosis. The toxin binds to the cytoplasmic part of VAMP2 and cleaves it, hence leading to no recognition of VAMP2 by the Syntaxin1 and SNAP25, further stopping the exocytosis and thus inhibition of neurotransmission.Step 5: Clathrin-mediated endocytosis

After fusion of SV into the plasma membrane to empty its contents, the process of endocytosis retrieves empty SV. There are four pathways described for endocytosis of SV as described below:

Clathrin-mediated endocytosis: Among all four pathways for endocytosis of a synaptic vesicle, clathrin-mediated endocytosis is the most well studied process. The first step for endocytosis is invagination of the plasma membrane to form a structure called pit. The crucial component for the formation of pit is membrane

lipid phosphatidylinositol 4,5-bisphosphate (PIP_2) generated by phosphorylation of PIP by phosphatidylinositol 4-phosphate 5-kinase type 1 gamma (PIPK 1ϒ) (Wenk and De Camilli, 2004). Adaptor proteins are present either in monomeric form like stonin or tetrameric form like the AP-2 complex. Cargo AP-2 stimulates the PIPK 1ϒ to initiate assembling of clathrin coat around invaginated plasma membrane pit. Proteins like Epsin, EPS-15 and intersectin assist AP-2 adaptor protein to form curvature surrounding the pit (Ford et al., 2002; Henne et al., 2010; Saheki and De Camilli, 2012). Finally, dynamin cleaves the two membranes apart releasing the clathrin-coated vesicle inside the pre-synaptic region.

Kiss and Run: According to this hypothesis, the SV does not fuse but adheres transiently to the plasma membrane. As soon as the neurotransmitters are released through a short-lived pore, the empty SV is endocytosed (Rizzoli and Jahn, 2007; Smith et al., 2008).

Bulk endocytosis: This is the most widely accepted hypothesis for SV endocytosis. According to this theory, the large number of SV exocytosis adds extra length to the plasma membrane and make it wavier, thus, invaginates and pinches individual SV via clathrin-mediated endocytosis (Ferguson et al., 2007).

Endosomal sorting: The endocytosed SV might undergo an extra sorting step in order to maintain the integration of SV proteome. Thus, rather than recycling vesicle material, endosomal resorting seems to be a better way. This sorting is expected to take place in early endosomes where the definite protein composition is maintained.

Step 6-8: Uncoating

Several independent processes mediate disassembly of clathrin. The Phosphatildyinositol-(4,5)P2 is dephosphorylated into phosphatidylinositol-4-phosphate either by phosphatase synaptojanin or by ADP ribosylation factor 1. Auxillin binds to the phosphatidylinositol-4-phosphate and along with chaperones like Hsc70 to remove the Clathrin coat (McMahon and Boucrot, 2011; Schlossman et al., 1984; Schmid et al., 1984; Taylor et al., 2012; Ungewickell et al., 1995; Xing et al., 2010) (fig. 1.3; step 6).

Step 7: Endosomal fusion

After the uncoating of newly formed vesicle, it fuses with endosomes. This process is mediated by endosomal proteins like Rabenosyn, Rab5.

Step 8: Synaptic vesicle reformation

After the fusion of vesicle into the endosome, endosomal-sorting buds a new synaptic vesicle where the protein and lipid content is kept to maintain the structural integration of SV. Syndapin in conjugation with actin cytoskeleton is believed to mediate this reformation (Kessels and Qualmann, 2004) (fig. 1.3; step 8).

1.1.1.2 Retina synapses

The retina is a neuronal tissue ~200 µm in thickness that is found in the eyes (Sjostrand, 1953d). It is a complex tissue containing six major layers of cells (fig. 1.4).

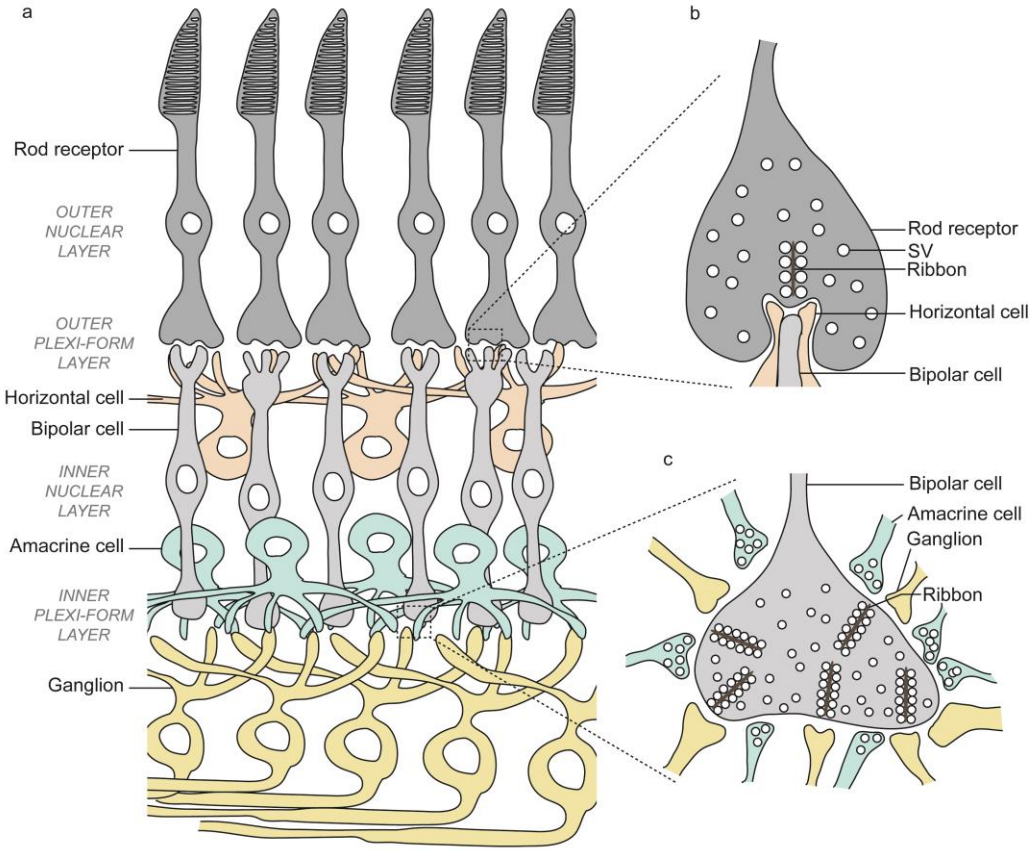

Figure 1-4: ***Layers of retina.*** (a) Various cell layers found in retina viz., rod and cone cells, outer nuclear layer, outer-plexiform layer, inner nuclear layer, inner-plexiform layer and ganglion layer. Rod and cone layer faces the vitreous humor of the eye. (b) The outer plexiform layer contains ribbon synapses of rod/cone cells and conventional synapses of horizontal and amacrine cells. (c) The inner-plexiform layer contains ribbon synapses of bipolar cells and conventional synapses of amacrine cells. Figure redrawn from Wassle, 2004.

The outermost layer of the retina that is directly in contact with the vitreous humor of the eye contains (1) photoreceptors: rod and cone cells. These specialized cells transfer the light-evoked signals to bipolar and horizontal cells lying at the inner layer of the retina. Cone cells are responsible for colour vision. Various forms of retinal proteins like rhodopsin in rod cells absorb the light in the visible range of wavelength. Upon excitation, they encode the visual information into chemical signals and the ribbon synapse that is present at the basal end performs exocytosis. This information is transferred to bipolar cells that receive the information encoded and faithfully transfer it to the optic nerve via ganglions (Wassle, 2004). Other layers of retina are (2) the outer-nuclear layer containing

nuclear portion of cone and rod cells, (3) the outer-plexiform layer containing the synapses formed by rod/cone with the bipolar/amacrine cells followed by (4) the inner nuclear layer containing nuclei from bipolar cells, amacrine cells, horizontal cells. The next layer is (5) the inner-plexiform layer, which contains mostly the synapse formed by bipolar cells and amacrine cells and ganglion, while the inner most layer consist of nucleus (6) ganglions that further lead to optic nerve which connects the retina to brain.

It is very interesting that only three kinds of cells of retina i.e. rod, cone and bipolar cells form the ribbon synapses. The rest of the retina cells for instance amacrine cells and ganglions form conventional synapses. In addition, there are substantial differences between the three kinds of ribbon synapse forming cells of retina (table 1.1). Electrical synapses, that are formed by gap junction, also exist in addition to chemical synapses (Wassle, 2004).

1.1.1.2.1 Retina Ribbon Synapse

By EM, Sjostrand F.S. (1953) first attempted to study various layers of guinea brain and retina. Later, he discovered the synaptic ribbon in retina and reported its plate-like structure by serial sectioning and examining under electron microscope (Sjostrand, 1958). Since then, the word “ribbon synapse” became a generic word to describe ribbon synapses. Later, Dowling J.E. and Boycott B.B. (1966) compared the retina with conventional synapses and reported the ribbon synapses as distinct structures specific for retina. Morphologically, ribbon synapses are distinguished from conventional synapses by the presence of a special bar like structure called ‘Ribbon’ (Dowling and Boycott, 1966). The ribbons are the characteristic feature for chemical synapses with loads of work like hair cell and retina (Lenzi and von Gersdorff, 2001; Sterling and Matthews, 2005). At the molecular level, there are few proteins reported to be uniquely present in ribbons (Schmitz et al., 2000) (section 1.8).

A typical mammalian rod cell contains a single active zone clustering approximately 770 SVs (Sterling and Matthews, 2005). 130 of these are anchored to the basal row of the ribbon and are known as docked SVs while the remaining 640 associated to the ribbons are called tethered SVs. Mammalian ribbons in cone cells are slightly shorter (approximately 2 µm long, 0.2 µm high) than the rod (approximately 2 µm long, 0.4 µm high). The total ribbon surface and number of ribbon tethered SVs in cone is much larger than in the rod cell (Heidelberger et al., 2005; Jackman et al., 2009; Sterling and Matthews, 2005; Thoreson, 2007). A cat

cone cells can bind to approximately 3600 vesicles out of which 600 are docked while the remaining 3000 are tethered SVs (Sterling and Matthews, 2005).

Table 1.1: Comparison of various attributes of brain synapses with all three kinds of ribbon synapses found in retina.

Attributes	Retina ribbon synapse			Brain synapse
	Rod	Cone	Bipolar	
SVs per synapse	10^6	10^6	$4x10^5$-10^6	200, 380
Ribbons per synapses	1	10-12-<50	30 -<100	0
Size of ribbons per synapses				
Length (µm)	1	1	0.150	-
Height	0.4	0.2	0.400	-
thickness	35	>35	0.25 µm	-
Total SVs tethered per ribbon	770	3600	6000	-
docked SVs per ribbon/synapse	130	600	1200	8-10

Information given in this table is extracted from the following sources- (Heidelberger et al., 2005; Rizzoli and Betz, 2005; vonGersdorff et al., 1996; Wilhelm et al., 2014a) (vonGersdorff et al., 1996) (Schokoriski and Stevens, 1997)

In goldfish, each bipolar cell contains 45-65 small ribbons. Each ribbon is associated with approximately 110 SVs out of which 22 are docked while 110 are tethered. Thus for a single bipolar cell, there are total of approximately 6000 SV associated with all ribbons out of which 1200 SV are docked (Lenzi and von Gersdorff, 2001).

Although the basic structural and functional units of ribbon synapses are similar to the conventional synapses, there are many differences that make ribbon synapses unique. Functionally, these special chemical synapses are capable of faithfully transmitting graded signal, and have the ability for tonic release of SVs mostly containing glutamate, for long periods of time (Heidelberger et al., 2005; Sterling and Matthews, 2005). In contrast, the conventional synapses (a) do not reliably convert all the action potential into exocytic function (b) respond to the action potential and (c) show phasic release of SVs. In order to transduce fast and transient as well as slow and sustained signals, the ribbon synapses have large reservoir of readily releasable pool of SVs. Electro-physiologically, it has been

shown that the ribbon synapses (frog retina) have the capability to exocytose around 400 SVs per second (Heidelberger et al., 2005; Sterling and Matthews, 2005; Wassle, 2004).

1.1.1.2.1.1 Retina Ribbon

Ribbons vary in their size depending upon the kind of cell/synapse (Table 1.1). A ribbon is a slender bar-like structure typically ~30 nm thick, ~1µm high and ~1-2 µm wide (Heidelberger et al., 2005; Sterling and Matthews, 2005). Typically, it is a curved structure but always maintains a vertical orientation over a trough-like form structure known as arciform density (Dowling and Werblin, 1969; Heidelberger et al., 2005; Lasansky, 1973; Lenzi and von Gersdorff, 2001; Raviola and Gilula, 1975; Sterling and Matthews, 2005). Ribbon is planar, plate-shaped structures providing huge surface area, approximately 0.77 μm^2 in mammalian rods (Sterling and Matthews, 2005).

Rod cells contain one ribbon per synapses however; the cone and bipolar cells contain more than one ribbon per synapse (Sterling and Matthews, 2005; Wassle, 2004).

Multiple roles of ribbons have been proposed but the precise function is still unclear (LoGiudice et al., 2009; Parsons and Sterling, 2003; Sterling and Matthews, 2005). The function of the ribbon depends on its protein composition of ribbon and various attempts are going on to identify the molecular composition of ribbon (Alpadi et al., 2008; Kantardzhieva et al., 2012; Schmitz et al., 2000; Wahl et al., 2013).

Through immuno-labeling, Schmitz discovered that a nuclear protein C-terminal binding protein 2 (CtBP2) specific antibody could cross-react with the ribbon as well and named it as RIBEYE protein. It is known to form the major component of ribbons. Based on CtBP2 antibody and electron microscopy, he also established protocol to purify ribbons (Schmitz et al., 1996; Schmitz et al., 2000). RIBEYE is a 120 kDa protein and an integral/built-in component to ribbon synapses (Schmitz et al., 2000). RIBEYE can form homo-dimer as well as hetero-dimer with its variants (Schmitz, 2009; Schmitz et al., 2000). Through comparative western blot analysis of bovine retinal homogenate, crude OPL fraction and purified ribbon fraction, it was confirmed that rabphilin, synapsin, synaptotagmin, SNAP23, syntaxin1/3 were ribbons associated (Von Kriegstein et al., 1999).

Knock-out mice for CtBP2 was lethal at embryonic stage (Hildebrand and Soriano, 2002). However the CtBP2 knock-down of RIBEYE using morpholino in zebra-fish

larvae was found to be deficient for ribbons suggesting its role in structural formation of ribbons (Wan et al., 2005).

Apart from RIBEYE, KIF3A, piccolo and bassoon are important proteins for ribbon synapses. The kinesin like protein KIF3A is reported to be present on the ribbon matrix and on docked SVs (Muresan et al., 1999). Bassoon is found at the base of the ribbon. Knock-out mice of bassoon showed floating ribbons, thus, it was predicted that bassoon is responsible for binding the ribbons to the arciform density. Piccolo is present at distal part of the ribbons (Dieck et al., 2005).

1.1.1.2.1.2 Retina Ribbon Synaptic Vesicles

Ribbon SVs vary in range from 20 to 65 nm (Derobertis and Franchi, 1956). Studies in rodents, monkey and salamander retina suggest that synapsin is absent in ribbon synapses (Geppert et al., 1994; Mandell et al., 1992; Mandell et al., 1990; Ullrich and Sudhof, 1994; Von Kriegstein et al., 1999). However, it was also reported that the absence of synapsin is species-specific, when synapsin was found in the OPL fraction of bovine retina (Von Kriegstein et al., 1999). In addition, rabphilin was also found to be absent in bovine the OPL but present in murine the OPL showing species-specific pattern similar to synapsin. SV2B was found to be present more prominently in the OPL than the IPL while its variant SV2A showed high abundance in IPL region. Thus, it was suggested that the ribbon SVs contains SV2B isoform. Similar to conventional synapses, the SVs of ribbons contain synaptophysin, synaptobrevin, synaptotagmin1/2, SCAMP and synaptogyrin (Von Kriegstein et al., 1999). Rab3 was absent in ribbon synapses (Grabs et al., 1996), however it was later reported that Rab3 proteins were found in the OPL as well as the IPL fraction of bovine, mouse and rat retina (Von Kriegstein et al., 1999).

In addition to SV proteins, endocytic proteins like amphiphysin and clathrin light chain were detected in the OPL, thus also suggesting that endocytosis of SV is a clathrin-mediated process (Wahl et al., 2013). In addition, PSD95 and NMDA receptors were also observed in the OPL fraction suggesting the glutamate based signaling similar to the conventional synapses (Von Kriegstein et al., 1999).

Anatomical studies by electron microscopy suggest that conventional and ribbon synapses lie in close proximity in the retina. (Dowling and Boycott, 1966); Fig 1.4). Thus, it is very difficult to separate these two kinds of synapses from each other. Further, although the ribbon synapses occur majorly in the OPL than the IPL (Heidelberger et al., 2005; Sterling and Matthews, 2005), it is difficult to decide whether a protein is truly ribbon or not, based on their presence in OPL.

1.1.1.2.2 Synaptic vesicle cycle in retina Ribbon Synapses

Synaptic vesicle cycle of ribbon synapses is quite similar to that of conventional synapses. However, along with some proteome differences, ribbon is the major structural component that makes ribbon synapse distinct. It tethers thousands of SVs around its surface suggesting a unique way of docking and priming in ribbon synapses. Nevertheless, most of the steps of SV exocytosis, SV fusion and SV endocytosis in ribbon synapses are ill defined (Heidelberger et al., 2005; Paillart et al., 2003; Sterling and Matthews, 2005; Wahl et al., 2013).

Table 1.2: Proteome comparison of retina ribbon synapses versus conventional brain synapses. Various proteins present in retina ribbon synapses along with the information about their identity and possible function in conventional synapse. The table was partially adapted from (Zanazzi and Matthews, 2009)

Protein	Photoreceptor synapses	Bipolar synapses	Brain Synapse
Amphiphysin	+	+	+
AP180	+		+
Bassoon	+	+	+
Calcium channels	L type	L type	P/Q, N type
Clathrin	+	+	+
Complexin	3/4	3/4	1/2
CSP	+		+
Dynamin	+	+	+
GLT1/EAAT2	+	+	+
Munc13	+	?	+
Munc18	+	?	+
Munc119/RG4	+	?	?
NSF	+	?	+
Rab3a	+	-	+
	-		

Rabphilin	+	?	+
RIBEYE	+	+	-
SNAP23	+	?	+
SNAP25	+ -	+	+
SV2	+ - SV2B	+ -	+
Synapsin1	+ -	-	+
Synapsin2	-	-	+
Synaptobrevin	+	+	+
Synaptophysin1/2	+	+	+
Synaptotagmin1/2	+ -	+ -	+
Syntaxin	3	3	1A/B
VGAT/VIAAT	-	+	+
VGLUT1	+	+	+

The information for the proteins was extracted from following publications: Amphiphysin (Sherry and Heidelberger, 2005), AP180 (Yao et al., 2002),Bassoon (Dieck et al., 2005) Calcium channel (Morgans, 2001)Clathrin (Sherry and Heidelberger, 2005), Complexins (Hirano et al., 2005; Reim et al., 2009), CSP (Schmitz et al., 2006), Dynamin (Sherry and Heidelberger, 2005; Ullrich and Sudhof, 1994), Munc13 (Schmitz et al., 2001; tom Dieck et al., 2005), Munc18 (Ullrich and Sudhof, 1994), Munc119/RG4 (Higashide et al., 1998), Rab3a (Grabs et al., 1996; Ullrich and Sudhof, 1994; Von Kriegstein et al., 1999), RIBEYE (Schmitz et al., 2000)SNAP-25 (Brandstatter et al., 1996b; Catsicas et al., 1992; Grabs et al., 1996; Ullrich and Sudhof, 1994; Von Kriegstein et al., 1999), Raphilin (Von Kriegstein et al., 1999),SNAP 23 (Von Kriegstein et al., 1999), SV2(Johnson et al., 2003; Mandell et al., 1993; Mandell et al., 1990; Schmied and Holtzman, 1987; Von Kriegstein et al., 1999; Wang et al., 2003; Yang et al., 2002), Synapsin1/2 (Ullrich and Sudhof, 1994; Von Kriegstein et al., 1999; Yang et al., 2002) VAMP (Greenlee et al., 2001; Von Kriegstein et al., 1999) synaptophysin (Grabs et al., 1996; Greenlee et al., 2001; Ullrich and Sudhof, 1994; Von Kriegstein et al., 1999), Synaptotagmin 1/2 (Grabs et al., 1996; Ullrich and Sudhof, 1994; Von Kriegstein et al., 1999), Syntaxin 1/3(Brandstatter et al., 1996a; Grabs et al., 1996; Morgans, 2000a, b; Morgans et al., 1996; Ullrich and Sudhof, 1994; Von Kriegstein et al., 1999), VGAT/VIAAT (Cueva et al., 2002; Jellali et al., 2002), VGlut1 (Johnson et al., 2003; Sherry et al., 2003).

Step 1-2: Loading of neurotransmitters and Docking of SV

No detail is available on if the ribbon synapses have any special proteins for filling neurotransmitters. However, the fast rates of SV exocytosis suggest that there is continuous refilling of neurotransmitters going on to maintain its optimum function of ribbon synapses.

The docking process in ribbon synapses is different from that of conventional synapses. Unlike in the conventional synapses, the calcium channel is present right at the base called the arciform of ribbons. The close location might help in faithful signaling for exocytosis. Upon arrival of an action potential, the voltage-gated calcium channels (L type) allow endocytosis of calcium ions right near the ribbon arciform (Bech-Hansen et al., 1998; Firth et al., 2001; Morgans, 2001; Morgans et al., 2001; Read et al., 2001; Strom et al., 1998). This creates a microenvironment that has very high calcium concentration.

Unlike conventional synapses, the lack of synapsin in ribbon synapses makes SVs much more mobile. The free SVs move by Brownian motion and thus there is just a probability that few SVs will migrate near the active zone. Apparently, this is the possible reason ribbon synapses have a special ribbon structure, which tethers SVs, although it is not yet known which proteins of the ribbon tethers the SVs (Heidelberger et al., 2005; Lenzi and von Gersdorff, 2001; Matthews and Fuchs, 2010; Morgans, 2000a; Schmitz, 2009; Sterling and Matthews, 2005). It is proposed that this may be assisted by Piccolo, RIM or Bassoon.

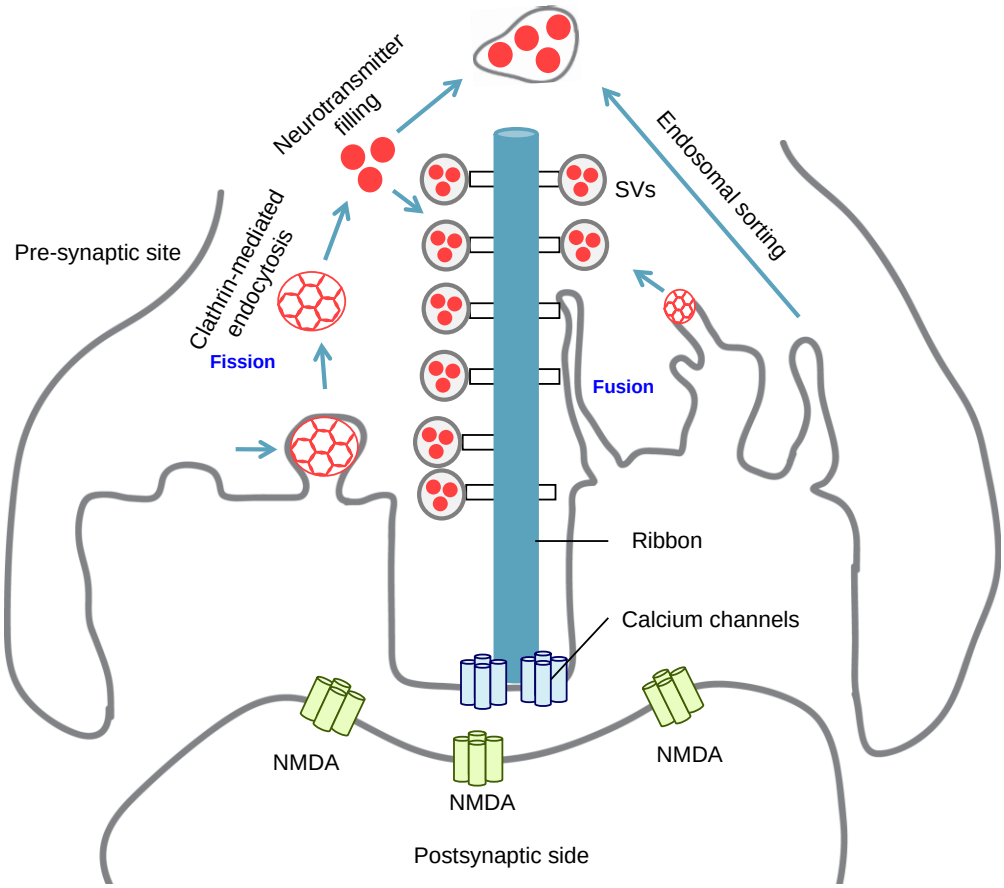

Figure 1-5: ***Synaptic Vesicle cycle in retina ribbon synapse.*** Possible SV exo-endocytosis cycle based on the electron microscopy scan. Picture redrawn from Gray and Pease, 1971.

Step 3-4: Priming and Vesicle Fusion

Upon arrival of membrane potential, the docked SVs (step 2) undergo priming and exocytosis. How exactly does the docked ribbon SVs migrate from ribbon and fuse, is still an open question.

In rod photoreceptors, the distances between the docked SVs at the base of ribbon to the pre-synaptic plasma membrane is about 1 μm. So far, it is still a question how SVs travels and fuses to the adjacent plasma membrane. One possibility is by using some kind of active transport or protein-protein interaction. Ribbon-associated proteins found at the distal position like Piccolo could aid this exocytosis (Dieck et al., 2005). Based on the analysis by fluorescence microscopy, it was reported that the SVs do not follow a highly directed motion before fusion in this 1 μm distance (Holt et al., 2004; Zenisek et al., 2003). In support of this, microtubules and actin filaments, requisite for typical directed movement are absent in this area (Usukura and Yamada, 1987; Gray, 1976). Second possibility could be detachment of docked SV upon high concentration of calcium, and allowing diffusion of SV with the plasma membrane. A third possibility could be by a kind of fusion at play, which

allows only the bottom row of SVs to fuse directly with the plasma membrane (Edmonds et al., 2004; Parsons and Sterling, 2003). Subsequently, the next row of SVs fuse with the first and so on, depending on the sustained time required to relay the signal information faithfully. Because of a lack of evidence, it is unclear which of the above-mentioned hypotheses might be true and appropriate (Heidelberger et al., 2005).

In cone photoreceptors and bipolar cells, neither of the above-mentioned hypothesis for fusion of SV could be applied. This is because of the mere fact that their cytoplasms are filled up with hindrances like endosomes and vesicle. Brownian induced fusion does not correlate well with their fusion rates (Heidelberger et al., 2005; Luby-Phelps, 2000).

After the migration of primed SV to the plasma membrane, SNARE complex is the universal machinery required for fusion of ribbon synapse SV. However, in retina ribbon synapses, syntaxin1 is replaced by its isoform syntaxin3 (Morgans et al., 1996). It was also shown by competitive co-immunoprecipitation that syntaxin3 has higher affinity for its SNARE partners than syntaxin1, thus suggesting its function in increased rate of exocytosis in ribbon synapse (Morgans, 2000a, b; Morgans et al., 1996). Syntaxin3 and SNAP25 waits at the plasma membrane to form complex with VAMP to initiate fusion. VAMP2 is found in both conventional as well as ribbon synapses of mouse retina, while VAMP1 is only limited to photoreceptor ribbon synapses and some ganglions and not present in the bipolar synapses (Sherry et al., 2003).

Apart from the SNARE complex, complexins are also reported in the retina ribbon synapses. Unlike the brain synapses, which have complexin1 and 2, the retina ribbon synapses contain complexin3 and 4 (Reim et al., 2009). In addition, the retina ribbon synapses do not contain Rab3 protein that negatively regulates fusion of vesicle. Perhaps, the activity is displaced by RIM (Rab3 interacting molecule), which clusters around the ribbon.

The calcium sensor synaptotagmin1/2 are found in conventional synapses as well as the photoreceptor synapses of mouse retina (Berntson and Morgans, 2003; Heidelberger et al., 2003). However, synaptotagmin 1 was observed only in outerplexiform layer (Von Kriegstein et al., 1999). Synaptotagmin 3 reported as plasma membrane protein (Shin et al., 2002; Sudhof, 2002) was also reported in outer plexiform layer of goldfish and mouse (Von Kriegstein et al., 1999). *In vitro* studies suggest that C2A domain of synaptotagmin3 responds more to the high calcium pool than that of synaptotagmin1 (Sugita et al., 2002; Thoreson et al., 2004).

Similar to conventional synapses, photoreceptor and bipolar synapses have SCAMP1, synaptogyrin, Munc18 and synaptophysin1 (Brandstatter et al., 1996a; Brandstatter et al., 1996b; Morgans, 2000a, b; Morgans et al., 1996; Sherry et al., 2003; Sherry et al., 2001; Ullrich and Sudhof, 1994). SV2B is present at all ribbon synapses in retina while SV2A is present exclusively on cone terminals and not on rods (Wang et al., 2003). RIM binding protein (RBP) co-localizes with SV2 and Ca^{2+} channels on photoreceptor terminals. At present, how these proteins interact specifically to make ribbon synapses special is still unclear (Heidelberger et al., 2005).

High calcium concentrations are known to facilitate vesicle fusion in many systems and could also be possible for SVs fusion in ribbon synapse (Gratzl et al., 1977). In addition, elevated calcium is also reported to accelerate refilling of readily releasable pool (Matthews 1994; (Gomis et al., 1999; Vongersdorff and Matthews, 1994) and might work similarly for ribbon synapses.

Step 5-8: Endocytosis and vesicle recycling at ribbon synapses

The pre-synaptic plasma membrane of ribbon synapses gain enormous length because of exocytosis of large number of SVs for long periods. Thus, it has been shown that the ribbons synapses functionally exhibit compensatory endocytic activity to maintain its regular surface area (Heidelberger, 2001; Vongersdorff and Matthews, 1994). However, the whole process of endocytosis seems to be very different from conventional synapses because of 3 known facts. Unlike conventional synapses, (a) endocytic activity of the ribbon synapses is inhibited by increased calcium concentration, (b) endocytic activity of the ribbon synapses remains unaltered by GTPase inhibitors and (c) have a huge reserve of SV pool approximately $5x10^5$ SVs (vonGersdorff et al., 1996), that creates hindrance in the ribbon synapses (Heidelberger et al., 2002). It was observed on a dissected bipolar cell that upon constant stimulation, causing heavy exocytosis of SVs, there were accumulation of large membrane cisterns. However, the pathway for endocytosis remained unclear (Paillart et al., 2003).

The electron micrographs of retina of photoreceptors reveal presence of coated buds and coated vesicles at the pre-synaptic plasma membrane lateral to synaptic ribbon (Gray and Pease, 1971). Thus, it is clear that ribbon synapse undergo clathrin-mediated endocytosis for regeneration of SVs. Using distinct antibodies Schmitz F (2013) reported that CHC-V1 and not CHC-V2 is localized near the synaptic ribbon. In addition, endocytic proteins like dynamin, syndapin,

amphiphysin and calcineurin proteins were highly abundant in active zone of rod synapse (Wahl et al., 2013).

Besides all the protein identifications, it is still unclear if the distinct feature of ribbon is ribbon-driven or SV driven. The literature so far suggests that there are special proteins present on the plasma membrane, the ribbon as well as the SV that may contribute to the uniqueness of ribbon synapses.

1.1.2 Isolation procedures for synaptic structures

1.1.2.1 Brain preparations

The invention of electron microscopy not only led to the discovery of ribbons but also contributed to the field of purification of subcellular like SVs and ribbon preparation. The observation of phenomenon of formation of artificial nerve-bouton so-called synaptosomes was solely by EM technique. Whittaker first attempted to homogenize brain tissue to purify synaptic vesicles. While doing so, he observed that the nerve terminal pinches off and re-sealed back. The re-sealed bouton were named as “synaptosomes” (Gray and Whittaker, 1962; Whittaker et al., 1964). Initially the synaptosomes were isolated by differential centrifugation or sucrose (Gray and Whittaker, 1962; Whittaker et al., 1964) and later by Ficoll/sucrose (Booth et al., 1978) or Percoll (Nagy et al., 1976) density gradient centrifugation. Since then, studies showed that the structural and functional of synaptosome maintain integrity with the endogenous nerve-terminus. This protocol has been little bit modified by various groups in order to get pure population of similar boutons.

The classical SV isolation protocol was established to acquire highly pure SVs. However, this protocol gave low yield of SVs (Huttner et al., 1983; Nagy et al., 1976). This is where the purification of synaptosome is superior. Briefly, the synaptosomes were osmotically lysed. The released SVs can be pelleted (known as LP2 fraction) down at a particular speed on the basis of its density.

Various attempts to purify synaptic vesicle have been tried to achieve high yield. When the brain tissue was homogenized, it releases certain amount of SVs into the cytosol. In order to get high yield, wide variety of protocols was established in which the brain cells were ruptured by freeze-thaw steps. These types of protocols are known to have high yield but less purity.

1.1.2.2 Retina preparation

The limitation for working with retina sample is the amount of protein. Frank Schmitz attempted first, to purify the ribbons from 200 bovine retinae successfully (Schmitz et al., 1996).

After the establishment of brain synaptosome preparation, Neal (1974) attempted to purified ribbon synaptosomes. Unlike brain synaptosomes, retina ribbon synapses first of all do not efficiently disrupt with glass-douncers, secondly they do not re-seal back to form synaptosomes. In addition, it was observed that the conventional synapses of retina form synaptosomes upon homogenization (Neal and Atterwil.Ck, 1974).

For isolation of SVs, there is no better working protocol available. In 2010, Hudspeth and Uthaiah attempted to isolate various ribbon associated complexes from cochlea and retina (Uthaiah and Hudspeth, 2010). However, due to the above mentioned fact that retina ribbon synapses do not rupture and reseal to form synaptosomes, their protocol is still unreliable to follow.

1.2 Mass spectrometry

1.2.1 Key events: invention, advancement in mass spectrometry

The word 'mass spectrometry' is a misnomer of this technique. The mass measured is not the actual mass of the molecule (or precursor) instead in mass spectrometry calculates mass-to-charge ratio (*m/z*) of a molecule is measured. A mass spectrum is a plot of the *m/z* of various ions versus their intensity at a given time. The mass spectrum is recorded in a gas phase and only for charged precursors. The whole idea of a mass spectrometer was initiated when JJ Thompson (1911) discovered cathode rays. Thompson measured the mass-to-charge ratio of cathode rays by constructing the first mass spectrometer called parabola spectrograph (Griffiths, 2008). Later, his student, Francis William Aston (1919) invented a fully functional mass spectrometer and identified various isotopes of Bromine (Br^{35}, Br^{37}), Chlorine (Cl^{35}, Cl^{37}) and Krypton (K^{78}, K^{80}, K^{82}, K^{83}, K^{86}) (Squires G., 1998) for which later in 1922, he was awarded the Nobel prize in Chemistry. However, the first modern mass spectrometer was developed by Arthur Jeffrey Dempster (1920) that was 100 times more accurate than the previous versions (Squires version). Using this modern mass spectrometer, Dempster discovered the uranium isotope U^{235}. After the age of discoveries of isotopes, mass spectrometer was widely used to identify large molecules like polymers, proteins. Prior to the modern application of mass spectrometry to large scale identification of proteins, Edman degradation was the only known technique during that time for sequencing proteins (Edman, 1949). This was due to the absence of 'soft-ionization' methods, meaning that molecules could not be charged (for *m/z* measurement) without extensive analyte fragmentation. Soon advancements were made in studying ways to ionize biomolecules like proteins in mass spectrometer. The first attempt for soft ionization was originated by Malcolm Dole, where he tried to measure the molecular weight of oligomers of synthetic polymers based on electrospray ionization (ESI) (Dole et al., 1968). In this attempt, Dole introduced the concept of how to form solute ions (Dole et al., 1968). However, Dole's set-up could not ionize proteins (Fenn, 2002).

Using a different approach, Franz Hillenkamp and Micheal Karas (1985) introduced the first working soft ionization technique for proteins and named it "matrix assisted laser desorption ionization" (MALDI). In MALDI, the sample is mixed with matrix (generally aromatic acid), irradiated in pulses on the target plate, dried and the intact precursors were observed when the laser power was introduced (Karas et al., 1985; Karas and Hillenkamp, 1988) (Tanaka K., Nobel prize lecture, 2002). Soon, John Fenn modified Dole's mass spectrometer and introduced the N_2 spray

at right angle to the precursor inlet (Whitehouse et al., 1985). In Dole's model, the precursor and the N_2 inlet were kept parallel. It was for the first time that Fenn could see mass spectrum for proteins of wide range masses like insulin (5.7 kDa), cytochrome c (12.4 kDa), lysozyme (14.3 kDa), myoglobin (17 kDa), chymotrypsinogen A (25.7 kDa), alcohol dehydrogenase (39.8 kDa), amylase (54.7 kDa) and Conalbumin (76 kDa). Initially, the obtained spectrum was difficult to deconvolute the molecular mass of precursor because of appearance of many peaks showing Gaussian distribution. Soon, Fenn deconvoluted the spectrum and discovered that fact that ESI can detect multiply charged precursors (Fenn et al., 1989). In his Nobel lecture, he introduced ESI as 'Electrospray wings to molecular elephants' (Fenn, 2002).

1.2.2 Mass analysers for mass spectrometer

Mass analysers, as the name suggests, are the devices that measure the mass-to-charge ratio of precursor. For mass spectrometry, it is important that the mass analysers measure the precursor *m/z* accurately (very close to the real value) and precisely (with small variability). In mass spectrometric terms, precise means resolution i.e. ability to resolve two adjacent precursors. The 6 major types of mass analysers used are time-of-flight (TOF), quadrupole, ion-trap, Fourier-transform ion-cyclotron resonance (FT-ICR), sectors and orbitraps. Two most commonly used mass analyzers are:

Time of flight: This method relies on the differences in the velocity of the charged molecules pulsed together in the mass spectrometer. The mass spectrometer records time, which the precursors needs the end of TOF tube. Higher the mass-to-charge ratio value, longer will be the time taken by the precursor to travel the given distance.

Orbitrap: This is the latest developed mass spectrometer (Makarov 2000). A static voltage is applied that results in generation of radial logarithmic potential between the two electrodes. This results into various precursors (charged molecules) moving inside the orbitrap following a particular trajectory. The precise m/z of the precursors can be extracted based on the Fourier transformation of the signals recorded from the harmonic movement (Makarov, 2000).

1.2.3 Tandem mass spectrometry for protein identification

Initially mass spectrometry allowed the identification of proteins based on measurement of peptide masses of digested proteins known as the Peptide mass fingerprinting (PMF). However, when the genome was sequenced, it was realized

that the two or more proteins might result into peptides that have similar *m/z*. Thus, there was a pre-requisite to define the exact sequence of amino acids present in a peptide. Unlike harsh ionization, soft ionization technique kept the molecule intact during the ionization process and the charged molecule could be subjected to more controlled mode of fragmentation. There are two most commonly used techniques for fragmentation of molecules. First is collision-induced dissociation (CID), also called collision-activated dissociation. For this, the isolated protonated peptide collides with neutral gas like N_2 and He. Generally, the peptide bond is the most stable bond, but small amount of vibrational energy on protonated -CO-NH- peptide bond induces a nucleophilic attack on nitrogen of –NH-, thus breaking the -CO-NH- bond of peptide resulting in formation of b and y ions (Wells and McLuckey, 2005). The second type of fragmentation is by electron- transfer dissociation (ETD) (Syka et al., 2004) and electron captured dissociation (ECD) (Zubarev, 2004, 2009; Zubarev et al., 1998). In this type of fragmentation, the protonated peptide is allowed to react with enough amounts of electrons (from fluoranthene radical anions in case of ETD). This extra electron destabilizes the peptide bond and induces re-arrangement that results in the breaking of –NH-C^{α}- bond, finally ending up as *c* and *z'* ions (Syka et al., 2004).

For protein identification, the mass spectrometer first scans for all the precursors (or protonated peptides) called MS or MS1. It provides accurate mass of the precursors. In the next step, the mass spectrometer precisely selects individual MS1 precursors according to the method file criteria (like top N peaks; top most N intense peaks, N is a natural number) with higher energy, the precursors are isolated individually and fragmented to yield a spectrum called MS/MS or MS2. The fragmentation pattern gives the identity of the peptide sequence. This fragmentation pattern can be used for *de-novo* sequencing of unknown peptides.

For routine protein identification, most mass spectrometers operate in data-dependent acquisition (DDA) mode. This means that top N most intense ions are isolated individually and fragmented to prove their identity. Number of MS/MS scan in MS cycle is solely dependent on the speed of mass analyser and is requires optimization for complex protein sample (Michalski et al., 2011; Michalski et al., 2012)

Coupling of reversed-phase liquid chromatography (LC) with ESI allowed high number of protein identifications and opened the gates to the era of proteomics. The first shot-gun proteomic analysis allowed many proteins to be identified in yeast-cell lysate from a single experiment (Washburn et al., 2001). Soon with the genomic sequence information, large-scale protein identification was reported

using database for yeast (Peng et al., 2003) (fig. 1.6). Introduction of quadrupole to isolate specific ion for fragmentation and orbitrap to analyse the mass/charge ratio were performed highly accurately. This combination of quadrupole and orbitrap lead to automatization of protein identification (fig. 1.6).

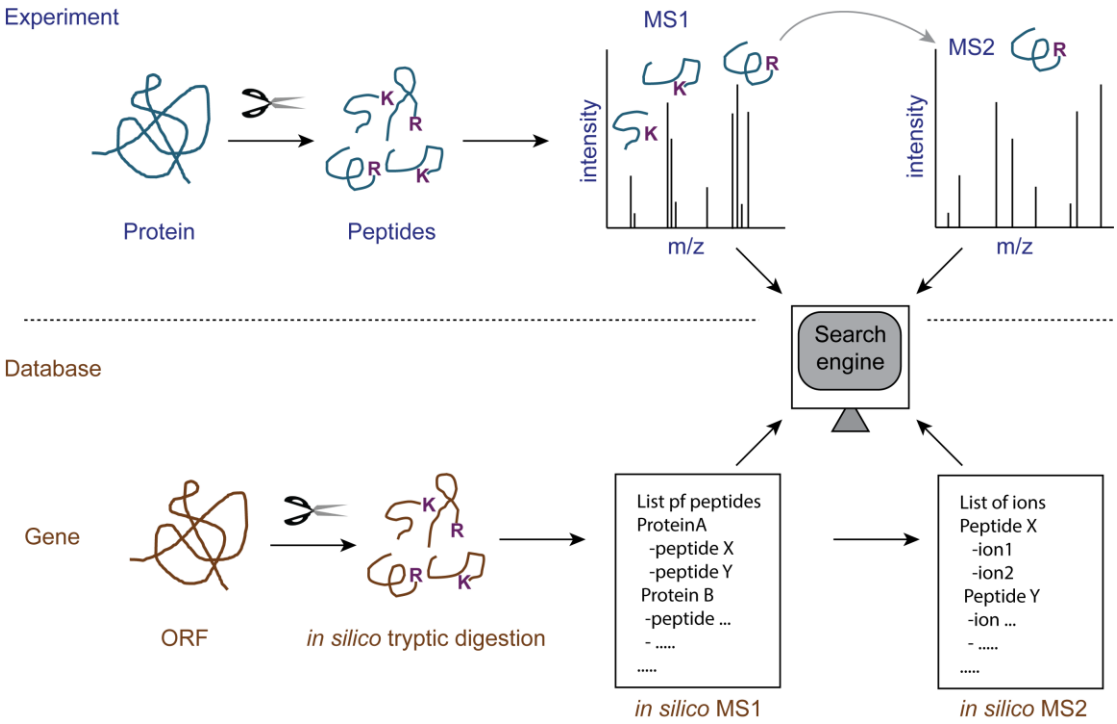

Figure 1-6: ***Workflow of protein identification by mass spectrometry.*** The crude protein sample is digested with endo-protease to get peptides. The generated peptides are injected into mass spectrometer where-in MS1 and MS2 takes place for peptides (upper half of diagram). MS1 refers to the scanning of peptide mass while MS2 refers to the ions obtained after fragmenting specific peptide/MS1. After the data acquisition, the search (MS2) engine digests the protein into theoretical peptides (MS1) and their respective fragmentation ions from the database (lower half of diagram). Finally the search engine tries to match every experimental MS1 and MS2 spectrum to every theoretical MS1 and MS2 and identifies the peptide and finally the protein with an acceptable score.

Presently, fractionation of protein via SDS-PAGE (Shevchenko et al., 2006), strong cation exchange followed by automatizated identification has led to identification of strikingly increased proteins ~90% of the total sequenced genome (Nagaraj et al., 2011) (Fig. 1.6).

1.2.4 Quantitative Proteomics

Classical methods of protein quantitation including use of dyes, fluorophore, radioactivity and quantitative western blotting have provided good sensititvity, linearity and dynamic range, but they suffer shortcomings. First, they can be applied only to isolated proteins of high abundance and purity, thus require high-

resolution chromatography/isolation step for purification of the protein of interest. Secondly especially, in case of western blotting, recombinant purified protein is required along with its antibody for detection. However, mass spectrometry outperforms these difficulties because of its ability of unbiased approach of identification of the protein, far more than any known technique (Bantscheff et al., 2007) (fig. 1.6). Basically the quantitative proteomics has been divided into 2 kinds: (a) relative quantification for comparison of proteome of two or more samples and (b) absolute quantification for calculation of exact amounts of proteins. Traditionally, accurate amount of proteins was quantified by conjugation of specific tags and immunoblotting. Only from the last decade, with the advancement in quadrupole to isolate specific mass, TOFs and orbitrap to analyse mass accurately and synthesis of isotopic standards peptides called AQUA, mass spectrometry has been projected as a potential technique to accurately quantify proteins. The well known technique AQUA is based on the titration of peptides, derived from endogenous proteins, with known amount of isotopic peptide of same amino-acid sequence. This technique is highly accurate when the protein is quantified in the linear range (Gerber et al., 2007; Gerber et al., 2003).

Based on various tags required for labelling different samples, quantitative proteomics is divided into two subgroups:

1.2.4.1 Label-free Protein Quantitation

Recently in the last decade, label-free quantification has been widely used to quantify proteins without introduction of any tag (section 1.12.1). Labelling strategies are considered highly accurate in quantitating protein abundance; however, these techniques require expensive isotope labels. However not every protein can be labelled completely because of uncertain efficiency of labelling reaction. Label-free quantification has only been possible due to the introduction of sensitive mass spectrometer, stable spray and liquid chromatography. Label-free approach can be used for both kinds of quantitation i.e. relative as well as absolute abundances (Bantscheff et al., 2007).

Label-free protein quantification strategy is based on either measuring and comparing the intensity of peptides of proteins or counting and comparing the number of fragment spectra identifying peptides of proteins. Label-free quantitation approaches known so far like protein abundance index (PAI) (Rappsilber et al., 2002), exponentially modified protein abundance index (emPAI) (Ishihama et al., 2005), APEX (Lu et al., 2007), intensity-based-absolute quantitation (iBAQ) (Schwanhausser et al., 2011) used for quantitation of proteins from various crude samples. In addition to the types of label-free quantitation, advancements have

been made using computational models that predict which peptides of a given protein is likely to be detected by mass spectrometer to provide better, reproducible and highly accurate abundance (Craig R et al., 2005; Tang H et al., 2006; (Lu et al., 2007; Mallick et al., 2007). Among the various computational model based software engines, the Andromeda (Cox et al., 2011) software that uses MaxQuant (Cox and Mann, 2008) as interface is highly popular because of its quantitation accuracy and ease of handling.

Among all label-free protein quantification techniques, iBAQ outperforms other techniques for most reliable and accurate quantification (Schwanhausser et al., 2011).

1.2.4.1.1 iBAQ: intensity-based-absolute-quantitation

Schwanhausser 2011 first introduced intensity based absolute quantitation or iBAQ of proteins. iBAQ is based on normalization of protein intensity based on the number of theoretical peptides, and well explained in detail in Fig. 1.7.

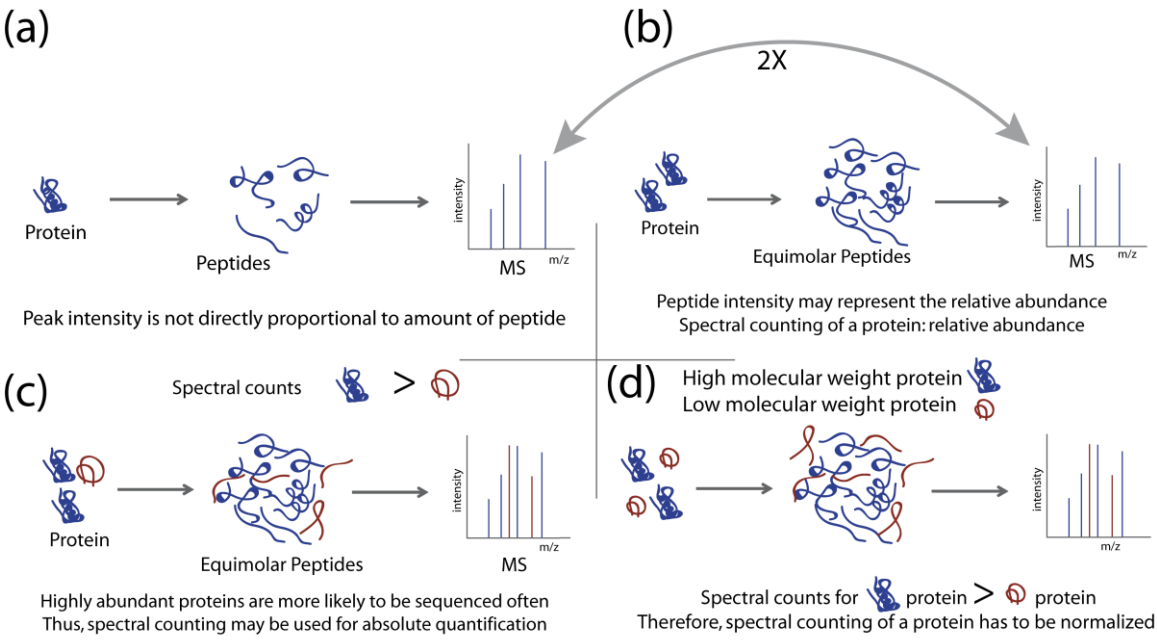

Figure 1-7: *iBAQ normalized total protein intensity by the number of peptides to give accurate abundance.* (a) The total protein intensity of protein represents its ionizability in mass spectrometer. (b) Total protein intensity for same protein can be compared in two or more samples. However it is difficult to account abundance based on the total intensity. (c) The reason for high value for total peptide intensity can be the higher molecular weight, thus represent large number of peptides for total intensity. (d) Hence, the iBAQ normalizes the total protein by the theoretical observable peptides to report accurate abundance.

iBAQ sums the intensity of all peptides of protein and divides it by the theoretical number of peptides (Schwanhausser et al., 2011). Recently, iBAQ has been used to calculate stoichiometry of various protein complexes (Fabre et al., 2014) and protein abundances in complex lysate (Ahrne et al., 2013; Arike et al., 2012; Geiger et al., 2012; Kuster, 2014; Mann and Edsinger, 2014; Mann and Mann, 2013; Shalit et al., 2015; Soufi et al., 2015; Wilhelm et al., 2014b).

1.2.4.2 Isotopic labelling based quantitation

In this technique, multiple digested samples can be conjugated with differential tags. The differential tags available introduce a certain mass to the peptides, without influencing the hydrophobicity. Hence, peptides of same amino-acid sequence containing differential tags co-elute in a reversed-phase LC. Comparison of the intensities of the two or more peptides containing tags cab be used to derive the differences in their relative abundance. Examples of these tags are iTRAQ, ICAT, dimethyl-labelling reagents. Relative proteome quantification can be measured using this approach.

1.2.4.2.1 Metabolic labelling

One of the most widely used technique to quantify relative abundances of proteome is Stable Isotope Labelling with Amino-acids in Cell culture also referred as SILAC (Ong et al., 2002). In this technique, amino-acids containing stable isotopes like C13, N15 are introduced the cellular culture and incorporated into the proteins through the cellular metabolism. The relative intensities of peptides from different experiments represent their relative amounts in the two cell lines. This technique was first applied to quantify proteome changes during the process of muscle differentiation (Ong et al., 2002).

A modification of the SILAC approach is SILAM, Stable Isotope Labelling in Mammals (McClatchy and Yates, 2014). For this, spirulina algae were first completely labelled with N^{15} by growing them on N^{15} containing media for several generations. Later, rats were fed on dried pellet prepared from 100% N^{15} spirulina for certain period of time (McClatchy and Yates, 2008, 2014; Rauniyar et al., 2013). During the same time, SILAC mouse containing $lysine_6$ was also reported. SILAC mouse was used to study the effects of Kindlin-3 protein expression in various tissues of mice (Kruger et al., 2008).

1.2.4.2.1.1 pulse experiment using stable isotopes

Protein turnover describes the overall balance between protein synthesis and protein degradation (Pratt et al., 2002) (fig. 1.8). Protein turnover is the measure of rate of loss of already synthesized protein or gain of newly synthesized protein (Schoenheimer and Rittenberg, 1938; Schoenheimer et al., 1938). To understand this proteome dynamics, traditionally, rats were either subjected to simultaneous tracer infusion or by injecting large amount of radioactive amino-acids like L-(U-^{14}C) threonine, L-(U-^{14}C) lysine, L-(U-^{14}C) tyrosine, L-(U-^{14}C) phenylalanine and L-(U-^{14}C) leucine. (Obled, CF et al., 1989; 1991). Using this approach, Obled et al., studied amino-acid turnover in whole body. However, the turnover of specific proteins cannot be estimated using this approach.

Introduction of stable isotopic amino acid coupled to mass spectrometry overthrows the traditional radioactivity based technique. In heavy SILAC, the cells are fed on media containing heavy lysine and arginine. However, heavy arginine cannot be used for mammals because it is known to be metabolized into other amino acids.

For the first time, the SILAC approach was applied as a function of time on cell cultures to calculate the protein turnover of HeLa cells and was termed as pulse-SILAC (Schwanhausser et al., 2011). pSILAC allows incorporation of heavy stable isotope over a certain period of time. Recently, it has also been applied to calculate the protein turnovers of primary neurons in culture system (Cohen et al., 2013).

Using this approach, Price et al., compared the newly synthesized proteome population of proteins in various tissue i.e. brain and liver (Price et al., 2010). The same group also observed very long-lived proteome by pulsing the mice for almost 6 to 12 month for N15 labelled diet. They reported that certain cellular proteins like myelin basic protein, Nup are very stable proteins because these proteins were not even 50% N15 labelled even after feeding the rats for nine months (Toyama et al., 2013). The basic idea behind pSILAM experiment is described in Fig. 1.8.

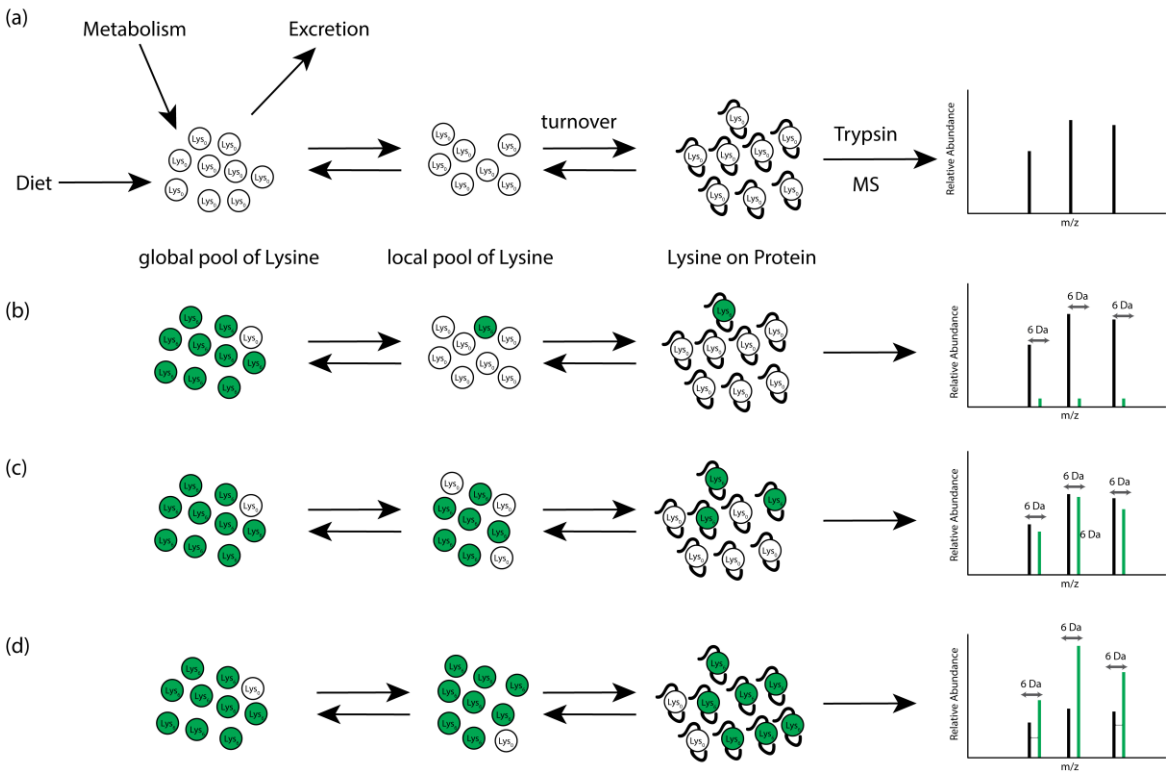

Figure 1-8: MS-based quantitation of newly incorporated Lysine$_6$ (green coloured dots) in background of Lysine$_0$ (white coloured dots) in body. (a) The whole proteome of mice contains lysine$_0$ before the experiment. This may be regarded as a very long pulse of lysine$_0$ food. This lysine$_0$ enters the local pool of body viz., blood stream, tissue, cells and finally in the newly synthesized protein. (b) After a long pulse of 2 months, they can be chased for certain time with lysine$_6$. With longer chase (c,d), the amount of lysine$_6$ increases. The lysine$_6$ differ from lysine$_0$ by replacing all C^{12} with its isotope C^{13}. Same peptides containing lysine$_6$ and lysine$_0$ co-elute on a reversed-phase LC but can be resolved based on their mass in MS1. The (lysine$_6$/ lysine$_0$) of intensities can be compared over time to calculate the rate of synthesis of individual protein. Figure is re-drawn from Price et al., (2012).

Briefly, the body metabolism is influenced by various factors like diet, excretion and protein stability (Obled et al., 1989; Olsen et al., 2006; Schoenheimer and Rittenberg, 1938; Schoenheimer et al., 1938). There is certain amount of protein that the animal will feed on. Out of the consumed protein, only a portion will be available for specific tissue. This will also depend on the absorbability of the tissue. Finally, out of all the absorbed amino-acid pool, certain amount will be used to synthesize a particular protein. And this will totally depend on the stability of protein. The rate of degradation and rate of synthesis of protein in a particular cell is always in equilibrium to maintain the homeostasis of body (Doherty and Beynon, 2006). And finally this rate can be determined by calculating the rate of incorporation of lysine6 in a particular tissue. pSILAM for more than two time-points may help in accurate calculation of rate kinetics (Doherty and Beynon, 2006; Price et al., 2010; Reckow and Webhofer, 2014).

1.3 Mass spectrometry in Neuroscience

With the advancement of large-scale protein identification, quantification techniques and automatization of data analysis has made ease to use mass spectrometry for every field of science. Recently, it is also been used to understand the synapse proteome.

1.3.1 Brain Proteomics

More than a decade ago, the first large-scale proteomic analysis was done on co-immunoprecipitated NMDA receptor resulting in the identification of 186 proteins from rat brain interacting NMDA receptor for down-stream signalling in post-synaptic region (Husi et al., 2000). Around the same time, proteins from purified PSD fractions were analysed by mass spectrometry (Walikonis et al., 2000). Since then, mass spectrometry has been used for large-scale in-depth proteome identification for synaptic structures (Jordan et al., 2004; Jordan et al., 2006; Peng et al., 2004; Yoshimura et al., 2004).

Relative protein quantitation approach by using cysteine reacting tags like ICAT was applied for characterization of synaptosomes proteome isolated from mouse brain (Schrimpf et al., 2005). Using similar approach, the effect of chronic morphine exposure was quantitatively studied on synaptic plasma membrane (Prokai-Tatrai et al., 2005).

Shot-gun proteomic analysis with ESI-LC after in-solution digestion of isolated synaptosomes identified a total of 209 unique proteins. Another approach based on separation of protein on 2-D gel electrophoresis separation followed by MALDI-TOF and LC-MS identified, in total, 85 proteins (Kai F et al., 2007).

Two independent studies analyzed the SV proteome comprehensively and identified 185 (Morciano et al., 2005) and 422 (Takamori et al., 2006) proteins respectively. The later study represents the major step towards the whole proteome of synaptic vesicles. Recently, Boyken extensively studied the free and docked SV proteome after separation on density-gradient centrifugation (continuous gradient) and using iTRAQ reagent (Boyken et al., 2013).

SILAC approach was applied to see the relative changes in proteome while stimulating cultured primary neurons by brain-derived neurotrophic factor, BDNF (Spellman et al., 2008).

1.3.2 Retina Proteomics

Using SIMS (secondary Ion mass spectrometry) approach (section 1.11), the distribution of various ions like Ca^{2+}, Ba^{2+} through various layers of retina was reported (Bellhorn and Lewis, 1976).

In 2010, the first report of mouse retina was published with identification of 42 unique proteins responsible for rod photoreceptor genesis by combination of 2DE followed by MALDI-TOF MS/MS (Barnhill et al., 2010). While the same year, Uthaiah and Hudspeth, homogenized and isolated various protein complexes on density-gradient centrifugation followed by LC-MS and reported lists of ear and retina proteins (Uthaiah and Hudspeth, 2010). 896 proteins were reported by cryo-sectioning of retina transversely followed by proteomic analysis (Reidel et al., 2011).

Recently, whole synaptic ribbon proteome was comprehensively studied by immunoprecipitation followed by LC-MS analysis (Kantardzhieva et al., 2012).

In addition to pSILAM studies, there were some retina proteins reported to be very long lived (Toyama et al., 2013).

1.4 Aim of the study

In recent years, an explosion in studies on synaptic vesicle (SV) proteins (both integral and associated) has vastly improved our understanding on the molecular basis of SV biogenesis, recycling and synaptic transmission in general. These studies provided an understanding of the composition and function of brain and sensory synapses and underlying differences in their mode of synaptic transmission. A large body of evidence on the function and composition of SV proteome has been gained by genetic and biochemical analysis. However, the picture is far from complete. Deciphering the quantitative composition of synaptic molecular machineries present in these two systems would aid in defining the molecular identity in terms of form and function. The major focus of this thesis work is to investigate the similarities and differences in the proteome of SVs derived from retina and brain by quantitative mass spectrometry.

One of the aims is to establish a method for isolation of SVs from bovine retina with high purity and yield suitable for large-scale proteome quantification. The proteome of the isolated SVs from bovine retina and brain will be quantified using label-free protein quantitation technique called intensity-based-absolute-quantitation (iBAQ) to decipher the absolute amounts of the proteins present on retina and brain SV. Further, this study aims to quantify the proteome of highly pure rat brain SVs and synaptosomes.

Synaptic vesicle biogenesis and recycling events are highly dynamic and related processes that require a tightly regulated balance in the availability of SV proteins. It is quite intriguing that although the brain SV proteome is quite similar to sensory synapses like retina, significant differences like a rapid exocytosis in retina, particularly in ribbon synapses, exist. However, the molecular basis for this difference in dynamics is not well understood. Analysis of the brain and retina SV proteome dynamics would provide significant insights into the regulation of these biological processes at the molecular level, which constitutes another focus of this study. For this purpose, a modified approach of SILAC mice generation will be employed to quantify the turnover of proteins in retina and brain by quantitative mass spectrometry.

2 Materials and Methods

2.1 Materials

Standard Chemicals used in this study were bought from either of the following suppliers: Sigma-Aldrich (Steinheim, Germany), Roth (Karlsruhe, Germany), Merck (Darmstadt, Germany), Boehringer (Ingelheim, Germany), Fluka (Buchs, Germany), Serva (Heidelberg, Germany), Roche (Basel, Switzerland) or Waters (Eschborn, Germany). All chemicals used for this study had at least analytical purity.

2.1.1 Chemicals

CHEMICAL	**SOURCE**
Phenylmethylsulfonylfluoride (PMSF)	Roth
Eupergit C1Z beads	Roehm Pharma
C18 matrix	Empore
RapiGest	Waters
Formic acid	Fluka
Dithiothretol	Calbiochem
Iodoacetaminde	Sigma Aldrich
UPS2-Universal Human Protein Standard	Sigma Aldrich
$Lysine_6$ diet	Silantes
Lichrosolv Water	Merck
Lichrosolv Methanol	Merck
Lichrosolv Acetonitrile	Merck

2.1.2 Enzymes

ENZYME	**SOURCE**	**USAGE**
Trypsin	Serva	In-gel digestion
Trypsin (sequence grade modified)	ProMega	In-solution and on bead digestion

Benzonase	Calbiochem	DNA digestion

2.1.3 Commercial Kits

KITS	**SOURCE**
Western Lightening™ Plus ECL	Perkin Elmer
Pierce BCA Protein Assay	ThermoFisher
NuPAGE Antioxidant	Invitrogen
NuPAGE LDS sample buffer (4x)	Invitrogen
NuPAGE MOPS running buffer (20x)	Invitrogen
NuPAGE Novex 4-12% Bis-Tris gels, 1mm	Invitrogen
NuPAGE sample reducing buffer	Invitrogen

2.1.4 Antibodies

ANTIBODY	SPECIES	APPLICATION	SOURCE
Synaptophysin 7.2	mouse monoclonal	WB (1:1000), IP	SySy
Synaptophysin G96	rabbit polyclonal	WB (1:1000)	Jahn *et al.,* 1985
Synaptobrevin 69.1	mouse monoclonal	WB (1:2000)	SySy
Synaptotagmin	mouse monoclonal	WB (1:1000)	SySy
VGlut1	Rabbit polyclonal	WB (1:2000)	Takamori *et al* 2000
Syntaxin1	Mouse monoclonal	WB (1:1000)	SySy
Syntaxin3	Rabbit polyclonal	WB (1:500)	SySy
Syntaxin3	Mouse monoclonal	WB (1:1000)	SySy
Rab3a	Monoclonal	WB (1:1000)	SySy
RabGDI	Monoclonal	WB (1:1000)	SySy
NR1	Mouse monoclonal	WB (1:1000)	SySy
CtBP2	Mouse monoclonal	WB (1:1000)	Abcam

Spliceosome complex (115 kDa)	Rabbit polyclonal	WB (1:1000)	Prof. Reinhard Lührmann lab
VAMP7	Rabbit polyclonal	WB (1:500)	Jahn et al., 1999
Calnexin	Rabbit polyclonal	WB (1:1000)	Abcam
Spliceosome complex (44 kDa)	Rabbit polyclonal	WB (1:1000)	Prof. Reinhard Lührmann lab
SDHA	Mouse monoclonal	WB (1:2000)	Abcam
PSD95	Mouse monoclonal	WB (1:1000)	Neuramab
Rabbit IgG (Cy3 labelled)	Goat polyclonal	WB (1:1000)	Jackson Immunoresearch
Mouse IgG (HRP labelled)	Goat ploYclonal	WB (1:2000)	BioRad
Rabbit IgG (HRP labelled)	Goat polyclonal	WB (1:2000)	BioRad
Sheep IgG (HRP labelled)	Goat polyclonal	WB (1:1000)	BioRad

2.1.5 Buffers and solutions

BUFFER	**COMPOSITION**
PBS	2.7 mM KCl, 1.5 mM K_2HPO_4, 137 mM NaCl, 8 mM Na_2HPO_4, pH 7.3
TBST	15 mM Tris-HCl, pH 7.4, 150 mM NaCl, 0.5% (v/v) Tween 20
SDS running buffer	25 mM Tris-HCl, 192 mM Glycine, 0.1% SDS
SDS-PAGE running buffer	1 M Tris-HCl, pH 8, 10% SDS (w/v), 10% Ammonium per sulphate, 5 μl TEMED
SDS-PAGE stacking buffer	1 M Tris-HCl, pH 6.8, 10% SDS (w/v), 10% Ammonium per sulphate, 2 μl TEMED
Transfer buffer	200 mM Glycine, 25 mM Tris, 0.04% SDS, 20% Methanol
Homogenization buffer	320 mM sucrose, 5 mM HEPES-NaOH, pH 7.4
Sucrose 0.7 M	700 mM sucrose, 5 mM HEPES-KOH, pH 7.4
Sucrose 1 M	1 M sucrose, 5 mM HEPES-KOH, pH 7.4
2X IP buffer	2X PBS, 5 mM HEPES pH 8, 6 mg/ml BSA

1X IP buffer	1X PBS, 5 mM HEPES pH 8, 3 mg/ml BSA
Blocking buffer	5% (w/v) low fat milk powder, 0.1% (v/v) Tween 20 in PBS
Coomassie staining solution	0.08% (w/v) Coomassie Brilliant Blue, 1.6% (v/v) ortho-phosphoric acid, 8% (w/v) ammonium sulphate, 20% (v/v) Methanol
Ringer's solution	153 mM NaCl, 2.6 mM KCl, 1 mM $MgCl_2$, 0.5 mM $CaCl_2$, 10 mM HEPES, pH 7.6, osmolarity 310-315 mOsm. Add 100 mg to 50 ml of solution freshly.
SDS sample buffer	50 mM Tris-HCl, pH 6.8, 12% (v/v) Glycerol, 4% (w/v) SDS, 2% (v/v) beta-mercaptoethanol, 0.01% Bromophenol Blue
Buffer ABC	25 mM ammonium bicarbonate, pH 8
Buffer H	5% acetonitrile, 0.1% formic acid in Lichrosolv water
LC buffer A	95% Acetonitrile, 0.1% formic acid in Lichrosolv water.
LC buffer B	0.1% formic acid in Lichrosolv water.
ABC buffer	25 mM Ammonium bicarbonate in Lichrosolv Water
Buffer A	0.1% formic acid in Lichrosolv water
Buffer B	0.1% formic acid, 95% acetonitrile in Lichrosolv water
Buffer C	0.1% formic acid, 80% acetonitrile in Lichrosolv water
Buffer H	0.1% formic acid, 5% acetonitrile in Lichrosolv water

2.1.6 Centrifuges

CENTRIFUGE	**SPECIFICATION**
Optima TL-100 Ultracentrifuge	Beckman Coulter (Krefeld, Germany)
Optima L-90K Ultracentrifuge	Beckman Coulter (Krefeld, Germany)
Optima L-70 Ultracentrifuge	Beckman Coulter (Krefeld, Germany)
RC 5C Plus centrifuge	Sorvall (Bad Homburg, Germany)
RC 5B centrifuge	Sorvall (Bad Homburg, Germany)
Fresco 21 Heraeus Tabletop	Thermo Fisher Scientific (Langenselbold, Germany)

2.1.7 Rotors

CENTRIFUGE	**SPECIFICATION**
SS34	Sorvall (Bad Homburg, Germany)
SW28	Beckman Coulter (Krefeld, Germany)
SW41	Beckman Coulter (Krefeld, Germany)
Ti 70.1	Beckman Coulter (Krefeld, Germany)

2.1.8 Other instruments

INSTRUMENT	**SPECIFICATION**
Electrophoresis power supplies	BioRad, Munich, Germany
NanoDrop ND/1000	Peqlab, Erlangen, Germany
pH meter	Metler/Toledo, Giesen
Sonication bath SONOREX Super	BANDELIN Electronic, Berlin, Germany
SpeedVac Savant SPD121P	Thermo Scientific, Braunschweig, Germany
Thermomixer Comfort	BioRad, Munich, Germany

2.1.9 Mass spectrometers

MASS SPECTROMETERS		**APPLICATION IN THIS STUDY**
Velos	Thermo Fisher Scientific, Bremen, Germany.	-Ribbon protein identification -Docked and free SV protein identification -Synaptosome protein quantification -SV protein quantification
Q-Exactive HF	Thermo Fisher Scientific, Germany.	-Brain and retina proteome -Bovine retina and brain SV proteome quantification -Protein Turnover analysis

2.1.10 Softwares

SOFTWARES	**SPECIFICATION**
MaxQuant versions 1.0.3.5, 1.5.2.8, 1.5.3.0	Max Planck institute for Biochemistry, Germany
R language	R foundation for statistical computing
Adobe Creative Suite 6	Adobe Systems, USA
Venny version 2.2	Computational Genomics, CNB-CSIC
Biovenn	Hulsen et al., 2008
DAVID Bioinformatic Resources	2013-2015 (version 6.7)
ImageJ version 1.48U	Wayne Rasband, NIH, USA

2.2 Methods

2.2.1 Synaptic sample preparation

2.2.1.1 Dissection of Retina

The bovine eyes were kind gift from Seberts' slaughter house and were transferred quickly to the lab on ice.

Eyes and isolated retina were kept submerged in Ringer's solution during the dissection as described previously (Wan et al., 2008). Briefly, the extra tissue around eye was removed with sharp scissors. Eye was cut around iris by holding the optic nerve. Iris and lens was pulled out. Transverse cut were made in order to pull out the vitrous humor. Eye-cups were transferred in fresh Ringer's solution and by grasping the eye-cup with forceps, with little shaking, the retina was gently dissected out. The dissected retina were labelled and snap-frozen.

2.2.1.2 Preparation of Ribbons from Bovine retina

Retina tissue from eight bovine eyes was used for purification of ribbons by the protocol reported previously (section 3.2.1) (Schmitz et al., 1996). Briefly, freshly dissected retinas were homogenized by using UltraTurrax, in 20 ml of Tris-HCl buffer pH 7.6. The homogenate was overlayed on 0.5 M sucrose cushion and centrifuged in SS34 rotor at 15,000 rpm at 4°C. Ribbons migrated in the middle of the sucrose cushion. This crude ribbon fraction was isolated carefully by pipetting and overlayed on a 50-35% continuous sucrose gradient. It was again centrifuged using SW28 rotor at 13,000 rpm for 75 min. Ribbons migrated to 40% sucrose

forming a clear band. This band was carefully isolated and treated with 1% triton detergent for 30 min at 4°C. Detergent solubilized all the SVs and associated proteins. Ribbons are known for high salt and triton resistance (Schmitz et al., 1996). The triton treated ribbons were resuspended in 20% sucrose and overlayed on a 4-step discontinuous sucrose gradient (70%, 50%, 40%, 30% sucrose) and centrifuged using SW41 at 11,000 rpm for 75 min at 4°C. The outer plexiform (OPL) ribbons were found at the interface of 50% and 70% sucrose while inner plexiform (IPL) ribbons were found at the interface of 30% and 40% sucrose gradient.

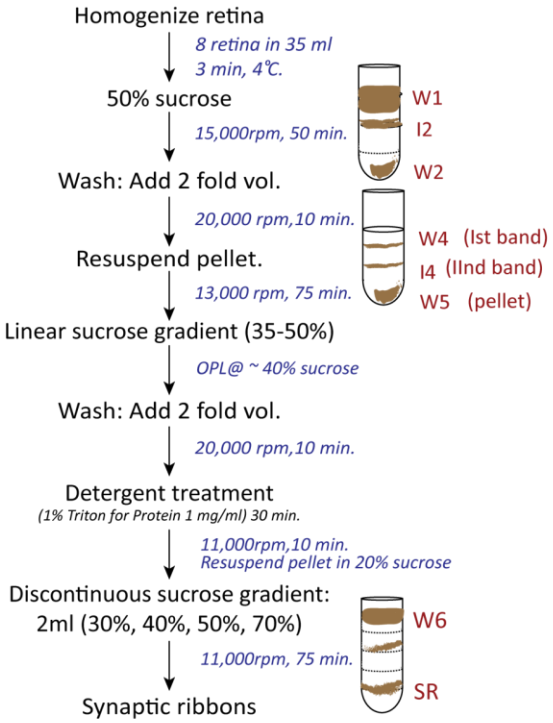

Figure 2-1: Schematic diagram for isolation of synaptic ribbons. Protocol drawn according to the protocol given by Schmitz F et al., 1996.

The protein concentration of OPL and IPL ribbons was determined by BCA analysis (section 2.2.2.1). The IPL ribbons were very dilute, thus only OPL fraction was processed for mass spectrometric analysis. Briefly, 20 μg of OPL ribbons were in-solution digested using trypsin (section 2.2.4.1) and the resulting peptides were analysed by LC-MS on LTQ-Orbitrap Velos (section 2.2.4.7, 2.2.4.14).

2.2.1.3 Preparation of Synaptic Vesicles from Bovine retina

The SV isolation protocol was modified based on the available SV isolation protocol to acquire high yield (Hell and Jahn 2006). We modified Jahn et al protocol (Hell and Jahn 2006) to obtain high purity and high yield for retina (fig. 3-3). The bovine

retina were enfolded in a muslin cloth and crushed by mortor and pestle using liquid nitrogen. Approximately, 3-4 g (by weight) of crushed retina sample was used for each preparation and suspended in 20 ml of homogenization buffer (Tris-HCl pH 7.6 buffer). This suspension was blended using an Ultra-turrax for 3 min at maximum speed. The homogenate was centrifuged using a SS34 rotor at 20,000 rpm for 10 min at 4°C. The supernatant (S1) was collected and stored in separate vial. The pellet (P1) was resuspended in 10 ml of homogenization buffer and re-blended using Ultraturax (3 min, max speed; as above) and-centrifuged at 20,000 rpm for 10 min. The pellet (P2) obtained at this step, was discarded while supernatant (S2) was pooled with S1. Pooled S1 and S2 was ultra-centrifuged using 70Ti rotor at 31,000 rpm for 40 min at 4°C. The supernatant (S3) was collected carefully in fresh falcon tube, while the pellet P3 was discarded. Finally, 4 ml of S3 supernatant was overlayed on a 2-step discontinuous gradient consist of 2 layers of sucrose: 3 ml of 1M sucrose and 4 ml of 0.7M sucrose and centrifuged at 41,000 rpm for 8 hours at 4°C. The SVs migrated at the interface of 0.7 M and 1 M sucrose and were carefully taken out and collected in fresh vial. This sucrose gradient fraction was further centrifuged using 70Ti rotor at 50,000 rpm for 2 hours at 4°C. The supernatant was discarded and the pellet (P4) was resuspended in 200 µl of 20 mM HEPES buffer using plastic spatula. The P4 fraction was passed through 20G needle and expelled out using 27G needle. This step is crucial to segregate the SVs. P4 was later used for EM and western blotting. For mass spectrometric analysis, the synaptophysin antibody *cl 7.2* was coupled to Eupergit beads (section 2.2.2.5). The synaptophysin antibody coupled to bead were used for immunoprecipitating the SVs from P4 fraction obtained from bovine brain and retina as described in section 2.2.2.6.

2.2.1.4 pulse-SILAM and sample preparation

2.2.1.4.1 Mice handling and dissection of brain and retina

3 months old mice strain C57BL/6 were fed with 99% lysine$_6$ containing diet medium (Silantes) for 5 days, 14 days and 21 days following regular animal ethic protocol in animal house facility (European Neuroscience Institute, Germany). For three time-points with three biological replicates, 36 mice were sacrificed for the whole study as described below:

Mice/experiment	Time point	Biological replicates	Total mice
4	~1 week (5 days)	3	12 mice
4	2 week (14 days)	3	12 mice
4	3 week (21 days)	3	12 mice

At the end of the mentioned feeding period, mice were decapitated, brain and eyes were dissected.

2.2.1.4.2 Preparation of brain and retina homogenate

For brain sample, cortexes from 4 mice was homogenized (9 strokes at 900 rpm) using glass douncer in 30 ml of ice cold homogenization buffer. Protein concentration was estimated (section 2.2.2.1)

The retinas were dissected under dissecting microscope within 1 hour of sacrifice (section 2.2.2.1). The eyes from mice fed on heavy lysine food were kind gift from Prof. Silvio Rizzoli (Uni-Goettingen).

10 µl of PBS buffer was added to each vial containing 1 mice retina or 50 µg of brain homogenate. Each of these samples was sonicated for 5 min (by alternating on and off 30 sec sonication) using Bioruptor. After sonication, 4 µl of Benzonase was added to each vial and incubated at 750 rpm for 30 min at RT on thermomixer. The samples were loaded on NuPAGE gel (section 2.2.2.2), in-gel digested (section 2.2.4.2). The extracted peptides (section 2.2.4.6) were run on Q-Exactive-HF (section 2.2.4.8) and analysed (section 2.2.4.11, 2.2.4.14).

2.2.1.5 Preparation of Rat brain synaptosomes

Synaptosomes were prepared from 2 months old rat brain. This preparation was performed by Benjamin Wilhelm (Prof Rizzoli lab, ENI, Goettingen) and the details were described in his PhD thesis.

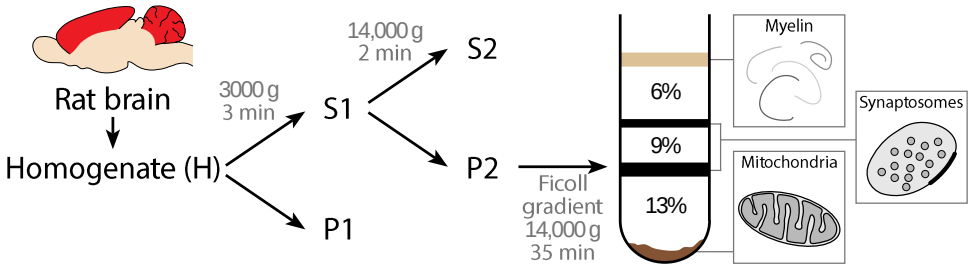

Figure 2-2: Schematic diagram of preparation of synaptosomes from rat brain. Figure adapted from Wilhelm *et al.*, 2014.

Briefly, 20 rats were decapitated and the cortex and cerebellum were dissected out. The cortex and cerebellum were suspended in 30 ml of homogenization buffer and homogenized using a glass douncer at 900 rpm (10 strokes). The homogenate was centrifuged using SS34 rotor at 5000 rpm for 2 min to pellet the nucleus and cell debris. The supernatant was re-centrifuged using SS34 rotor at 11,000 rpm for 12 min. The synaptosomes pelleted at this step. Thus, the pellet was resuspended in 5 ml of homogenization buffer. Dark brown pellet at the deep bottom was avoided because it majorly contains mitochondria. The resuspended pellet was overlayed on a 3 step discontinuous Ficoll gradient containing 3 ml of 13%, 2 ml of 9% and 3 ml of 6% and centrifuged using SW41 rotor at 22,500 rpm for 35 min. The lower band at interface of 13% and 9% Ficoll was carefully pipetted and washed once in 20 ml of homogenization. The synaptosomes were pelleted by centrifugation using SS34 rotor at 11,000 rpm for 12 min. The pellet was resuspended in 2 ml of homogenization buffer and used for immunofluorescence, western blotting, EM and mass spectrometry (Wilhelm, B., doctoral thesis, for mass spectrometry , section 3.4.2). The methods for immunofluorescence, EM and western blotting are very well described in PhD thesis of Benjamin Wilhelm (PhD in Prof Rizzoli lab, ENI, Goettingen) and (Wilhelm et al., 2014a).

For mass spectrometric analysis, the synaptosomes were in-solution digested (section 2.2.4.1), desalted (section 2.2.4.4), and loaded on LTQ-Velos (section 2.2.4.7, 2.2.4.10) and analysed (section 2.2.4.13, 2.2.4.14).

2.2.1.6 Preparation of Rat brain SVs

Highly pure synaptic vesicles were prepared from 20 rats following previously described protocol(Takamori et al., 2006). This preparation was performed in collaboration with Zohreh Farsi (Prof. Jahn, MPI for Biophysical Chemistry, Göttingen).

Briefly, 20 rats were decapitated and brains were homogenized in 30 ml of homogenization buffer at 900 rpm (9 strokes) using a glass douncer. The cell debris and nucleus was pelleted using SS34 rotor at 800*g* for 10 min. The supernatant was carefully collected and re-centrifuged at 10,000*g* for 15 min. The pellet was resuspended carefully and washed once with homogenization buffer. Next, the synaptosomes were osmotically lysed. The lysis was aided by homogenization step using glass douncer at maximum speed, 3 strokes. The lysed synaptosomes were centrifuged at 25,000*g* for 20 min. The supernatant was re-centrifuged at 200,000*g* for 2 hours. The resulting pellet was loaded on a sucrose gradient and centrifuged at 82500*g* for 4 hours. Syanptic vesicle band was collected from the gradient and then loaded on a long CGP bead column (1 meter long, 2 cm in diameter) and run overnight under gravity.

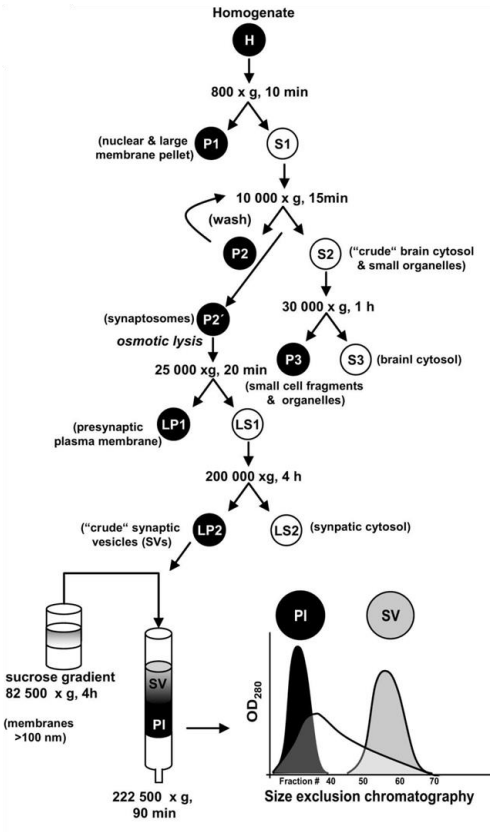

Figure 2-3: Schematic diagram of preparation of pure SVs from rat brain. Adapted from Takamori *et al*., 2006.

The acquired fractions were blotted against synaptophysin antibody by dot blot (section). Two peaks were observed in the chromatogram. The fractions of the second peak were pooled and centrifuged using 70Ti rotor at 200,000g for 2 hours. The pellet was resuspended in 200 μl of homogenization buffer and given for counting by FCS (full form). FCS studies were done by Sabrina (Walla Lab, MPI for Biophysical Chemistry) and well described in here PhD thesis. The SV fraction

was processed for in-solution digestion (section 2.2.4.1), desalted (section (2.2.4.4), loaded on LTQ-Velos (2.2.4.7, 2.2.4.10) and the data was analysed as described in section 2.2.4.13, 2.2.4.14.

2.2.2 Biochemical methods

2.2.2.1 Protein estimation

All the protein estimations were performed using reagents and the standard BCA protocol (Smith et al., 1985) as provided by Thermo Scientific online.

2.2.2.2 SDS-PAGE

Bio-Rad mini gel and in-house built gel chambers (dimension 15 cm x 20 cm) were prepared according to the recipe provided by Bio-Rad. 15% polyacrylamide running gels were casted with 4% of stacking. Samples were always boiled in Laemelli buffer and heated for 5 min at 95˚C. Gels were run at constant current of 30 mA for 3 hours (Bio-Rad) and for 3 hours (in-house built gel chamber). (Schagger, 2006; Schagger and von Jagow, 1987). All the parameters were followed as given by Bio-Rad mini gel manual available online.

NuPAGE pre-casted gels were run according to the details provided by Life-Science manual online. Gels were loaded with sample and run at constant voltage 200V for 53 min.

2.2.2.3 Western Blotting

Gels ran on SDS-PAGE or NuPAGE or in-house built was blotted in semi-dry condition using nitrocellulose (Portran) or PVDF membrane (Millipore). Proteins were transferred for 1 hour at constant voltage depending on its size (Towbin et al., 1989). For example, 1 BioRad gel or 1 NuPAGE was always run at constant 50 mA current for 1 hour. The membrane was blocked for 1 hour in milk buffer and incubated with primary antibody overnight in milk buffer. After three washing steps (10 min each), membrane was incubated with secondary antibody for 1 hour. After three washings (10 min each), the membrane was developed either by enhanced chemiluminescence (ECL) on a LumiImager or under fluorescence scanner (FLA-7000 Fujifilm). ImageJ software was used for quantification.

2.2.2.4 Dot Blot

A nitrocellulose membrane was cut 5x5 cm area. The area was divided into 25 equal squares (1cm^2 each). 2 μl of various fraction of SV sample (LP2 section 2.2.1.6) were pipetted on the nitrocellulose membrane squares. The membrane was air dried for 2 min. The membrane was blocked in milk (in TBST buffer) for 6 min. The membrane was incubated with primary antibody (Synaptophysin 1:500) for 6 min. The membrane was washed in milk (in TBST buffer) thrice, 3 min each. The membrane was incubated with secondary antibody (1:10,000) for 6 min. The membrane was washed in milk (in TBST) thrice, 3 min each. Finally, the membrane was washed in plain TBST buffer thrice, 3 min each. The membrane was developed using ECL kit.

2.2.2.5 Coupling of antibody to Eupergit beads

The basic principle of antibody/protein coupling to the beads is the reactivity of its amine group to the epoxy group of beads to form a stable covalent bond. This is a common strategy for binding antibodies like IgG to the beads in affinity purification.. We used Eupergit beads, which are known to have almost no unspecific binding.

First of all, the antibody Synaptophysin (*Cl* 7.2) was dialyzed against 150 mM NaCl for 3 days with 7 transfers. The dialyzed antibody was centrifuged at 10,000 g for 15 min. The protein concentration of dialyzed antibody was estimated using NanoDrop and further used for coupling. 40 mg of Eupergit beads were weighed, resuspended in 1 ml of double distilled water and sonicated by applying full power ultra-sonication at 50% pulsed for 3 min. The beads were vortexed rigorously and finally washed by spinning at 4,500 rpm for 6 min at RT. For coupling reaction, 40 mg of Eupergit beads was mixed with 375 μg (250 μl of 1.5 mg/ml) of dialyzed antibody and vortex vigorously. The protein to bead ratio is crucial for coupling (5 mg protein (minimum protein concentration of 1 mg/mg) is added to 0.5 g of beads). The coupling mixture was incubated at 21°C for 8 hours on rotating wheel. After the incubation, beads were centrifuged in SS34 at 4,500 rpm for 6 min. Coupling efficiency was checked by determination of unbound antibodies in the supernatant which can be reused. To block the non-specific binding 1,200 μl of 1 M glycine was added to the beads. After vortexed vigorously, incubated on rotating wheel at room temperature for overnight. Next morning, the beads were centrifuge in SS34 at 4,500 rpm for 6 min. Supernatant was discarded and beads were washed 6 times in total by alternating with Buffer A (0.1 M acetate, 0.5 M NaCl, pH 4.5) and buffer B (0.1 M Tris, 0.5 M NaCl, pH 8). Finally, the beads were washed with PBS buffer

and re-suspended by vortexing, spun as above, and stored frozen in total 4x dry volume assuming that 0.5 g beads = 0.5 ml (dh. 0.5 g beads in total 2 ml).

2.2.2.6 Immunoprecipitation of SVs using Eupergit beads coupled with antibody

Prior to use, 2 µl of Eupergit beads coupled with antibody/glycine were washed in PBS buffer by centrifugation at 4,500 rpm for 6 min. The pelleted beads were first resuspended in 600 µl of 2x IP buffer and 480 µl of double-distilled water by vortexing 120 µl of sample containing SV in 0.7 M sucrose was added to the beads by vortexing vigorously and incubated overnight on rotating wheel in cold room. Supernatant was discarded after centrifugation at 2,000 rpm for 3 min. and beads were resuspended in 1 ml PBS buffer and incubated for 15 min on ice. The above washing steps were repeated three times.

For embedding in electron microscopy, the sample was finally washed in 100 mM HEPES buffer to evade phosphate.

For mass spectrometric analysis, the beads were finally centrifuged at 10,000 rpm for 5 min and supernatant was removed and sample further processed for on-bead protein digestion.

2.2.3 Structural and functional studies of SVs

2.2.3.1 Negative staining by Electron Microscopy

All the SV containing fractions (P4; Fig 3.3)) were either washed or resuspended with/in 20 mM HEPES buffer to avoid phosphate contamination in electron microscopy. Negative staining was performed by Dr. Dietmar Reidel (MPI for Biophysical Chemistry, Goettingen). Briefly, samples were applied on a glow discharged carbon coated grid, washed once with 100 mM ammonium acetate and stained with 2% uranyl acetate (Maycox et al., 1988). Dark-field images were recorded at various magnifications using a CM 120 (FEI, Eindhoven, and The Netherlands) transmission electron microscope equipped with TemCam F416 CMOS camera (TVIPS, Gauting, Germany).

2.2.3.2 Embedding-Electron Microscopy

Dr. Dietmar Reidel (MPIbpc) performed all the EM steps. Briefly, immunoprecipitated SVs obtained from bovine retina and brain (section 2.2.2.6) were fixed by immersing in 2% glutarldehyde in 0.1% cacodylate buffer (pH 7.4)

overnight at 4°C. After fixation, the sample was immobilized in 2% agarose in fixation buffer. After fixation, the samples were applied with 1% osmium tetroxide. Next, the samples were pre-embeding stained with 1% uranyl acetate. The samples were dehydrated and embedded in agar 100. Finally, thin sections were sliced (approximately 80 nm) and examined under CM 120 transmission electron microscope (FEI, Eindhoven, and The Netherlands). Images were obtained using TemCam F416 CMOS camera (TVIPS, Gauting, Germany).

2.2.3.3 Glutamate Uptake assay

Vesicular glutamate transporter (VGlut) protein of synaptic vesicle have the ability to intake glutamate ions. The amount of glutamate uptake was detected by radiolabelled ^{3}H-glutamic acid (Maycox et al., 1988).

The uptake was measured in presence of 4 mM ATP, 50 μM K-glutamate, 4 mM chloride and 2 μCi 3H-glutamic acid (GE Healthcare, Hartmann Analytik GmbH) per data. The uptake buffer was 10 mM MOPS, pH 7.3, 2 mM $MgSO_4$ and 100 mL potassium Gluconate or 200 mM Glycine. 30 μg of SVs in 50-100 μl each from bovine brain, bovine retina and mouse brain were incubated by mixing with 10x uptake buffer. The mixture was incubated for 20 min at 32°C. The reaction mixture was pipetted in 3 ml of ice-cold uptake buffer. To stop the reaction, the reaction mixture was filtered through 0.45 μm nitrocellulose filters. The nitrocellulose filter was washed thrice with 3 ml of ice-cold uptake buffer. The SVs were trapped on the filters, thus the chloride uptake was detected in terms of radioactivity by liquid scintillation.

2.2.4 Mass spectrometric methods

2.2.4.1 In-solution digestion

10 μl of 1% RapiGest was added to 20 ug of protein sample (synaptosome or SV or *E. coli* lysate or UPS2 standard protein or OPL ribbon fraction or 7 fold amounts of marker proteins (appendix A10) and heated to 95°C for 5 min. All subsequent steps were performed at 750 rpm on a thermomixer at room temperature. 10 μl of ABC buffer was added to the sample and incubated for 5 min. To reduce the cysteines, 10 μl of 10 mM dithiothretol was added and incubated for 1 hour. Reduced cysteines were alkylated by adding 10 μl of 100 mM iodoacetamide and incubated for 20 min in dark. 180 μl of ABC was added to lower the detergent percentage to 0.1%. Finally, trypsin (1:50, ProMega) was added the sample for digestion and incubated for 16 hours.

For label-free quantification, the solubilized, reduced, alkylated synaptosomal proteins were incubated for 8, 12, 16, 24 and 48 hours.

Trypsinization process was stopped by adding 20 µl of 5% formic acid solution. The samples were incubated to deteriorate the RapiGest molecule. The samples were further desalted (section 2.2.4.4) and processed for LC-MS (section 2.2.4.8 and 2.2.4.9).

For spike-in iBAQ of SV, 1 µg of UPS2 standard protein mixture was spiked-in prior to digestion.

2.2.4.2 In-gel digestion

The proteins were processed for in-gel digestion following the protocol described previously (Shevchenko et al., 2006).

Briefly, 50 µg of mice brain and retina homogenates separately were added with NuPAGE sample loading buffer and heated for 10 min at 70°C. The pre-heated samples were vortexed, shortly spun and loaded on NuPAGE gel (4 -15%). The gel was run at constant Voltage (200 V) for 53 min. After the run, the gels were stained overnight with Coomassie and destained with water for 2-3 hours.

Each lane of gel was cut into 23 gel pieces using in-house built gel cutter. Each gel slice was further sliced into 8 pieces and placed on 96 well plate (Millipore) containing filter paper and pores at the bottom to wash away the solvents. All step henceforth were performed on a thermomixer at 350 rpm. All the gel slices were washed with water and 100% acetonitrile solvent alternatingly to wash away the impurities. The proteins will not wash away by this step. The solvent was always taken out using a motor pump (Millipore pump) by applying pressure less than -35 Pa. After washing, the gel slices were shrunken by incubating with acetonitrile. The acetonitrile was removed and the gel slices were incubated at 56°C for 1 hour in 100 µl of 10 mM dithiothretol reagent prepared in ABC buffer. The excess reagent was washed off and the gel slices were again washed and shrunk in acetonitrile. After removal of acetonitrile, the gel slices were incubated for 20 min in dark with 100 µl of 50 mM iodoacetamide reagent prepared in ABC buffer. The iodoacetamide was removed and the gel slices were further introduced with one step of incubation step in ABC buffer. Followed by two more steps of acetonitrile incubation to remove excess of Coomassie staining and to shrink the gel pieces. The acetonitrile was drained off and the gel slices and traces of acetonitrile were removed by a short speed-vac step for 2 min. Finally, each gel slice was added with 20 µl of buffer C solution containing trypsin. The gel slices were incubated at

4°C for 20 min to absorb the trypsin. Later, 10-15 ml of Buffer D was added and incubated overnight at RT.

Next morning, each well was incubated with 20 µl of 5% formic acid solution to stop the trypsin activity. Further, to dissolve and extract all the hydrophilic as well as hydrophobic peptides, the gel slices were incubated twice with 50% acetonitrile solution for 30 min. Finally, with the help of motor pump, the peptides were passed into a fresh 96 well plate (Millipore) present underneath by applying the pressure from the top. The extracted peptides were dried in a SpeedVac.

2.2.4.3 On-bead Digestion

On-bead digestion was performed as described previously (Boyken et al., 2013). Briefly, beads containing immunoprecipitated SV were efficiently solubilized by adding 30 µl of 1% Rapigest™ and heating to 95°C for 5 min. The sample was briefly centrifuged and vortexed to resuspend beads in following steps. 10 µl of ABC buffer was added to the solubilized sample. 20 µl of 100 mM dithiothretol was added to sample and incubated on a thermomixer at 750 rpm for 1 hour at room temperature for reducing the disulphide bonds. Reduced cysteines were blocked by alkylation with 20 µl of 50 mM iodoacetamide for 20 min in dark. The percentage of detergent was lowered to 0.1% by adding 180 µl of ABC buffer before adding trypsin. Finally, 5 µl of 0.1 mg/ml Trypsin (ProMega) was added and incubated overnight on thermomixer at 750 rpm at room temperature.

20 µl of 5% formic acid solution was added to the sample and incubated for 2 hours on thermomixer to quench the trypsin activity and breaks down the molecule of Rapigest™ into its non-detergent form. Further, the supernatant containing peptides were collected by centrifugation at 10,000 rpm and desalted (2.2.4.4).

2.2.4.4 Desalting

Four C18 plugs were filled up in a micropipette tip to make one column. Prior to use, the column was washed twice with 50 µl of methanol and equilibrated by passing 50 µl of 0.1% formic acid solution twice. The supernatant containing peptides was loaded on a pre-equilibriated column. While passing the supernatant through column, the peptides being hydrophobic will bind to the C18 matix. The column was washed four times with 50 µl of 0.1% formic acid solution. Finally, bound peptides were eluted by 50 µl of 80% acetonitrile, 0.1% formic acid solution twice. The eluted peptide solution was dried using SpeedVac.

2.2.4.5 Sample preparation for LC-MS: Immunoprecipitated bovine SV

The dried peptides from 5 immunoprecipitation were pooled together to run as one sample on mass spectrometer. The peptides were resuspended in 20 ml of buffer H and pooled together. For bovine retina and brain SV iBAQ quantitation, 1 μg of equivalent digested UPS2 standard protein mixture was spiked-in the digested immunoprecipitated bovine retina and brain SV peptides separately. The mixture of peptides was dried in SpeedVac. Finally, the peptides were resuspended in 20 μl of buffer H. 6 μl of the sample was injected in the Q-Exactive-HF for LC-MS analysis (section 2.2.4.9, 2.2.4.11).

2.2.4.6 Sample preparation for LC-MS: mice brain and retina

20 μl of buffer H (5% acetonitrile, 1% formic acid solution) was added to each well containing extracted dried peptides obtained from in-gel digestion (2.2.4.2). The peptides were sonicated for 3 min. Peptides from two consecutive wells were pooled together in a vial for preparation of 1 sample for LC-MS.

Briefly, from one sample, 23 wells in a 96 well microtitre plate contain extracted peptides from 23 gel slices. The peptides from two consecutive wells were pooled and LC-MS was performed as described below:

Sample for LC-MS	Peptides pooled from well	LC-MS gradient method
1	1+2	88 min
2	3+4	88 min
3	5+6	88 min
…	…	88 min
…	…	88 min
11	21+22	88 min
12	23 only	58 min

The acquired RAW data was analysed as described in section 2.2.4.12.

2.2.4.7 Sample preparation for LC-MS: rat brain SV and synaptosome

Dried peptides were resuspended in buffer H. Volume was adjusted according to the amount required for injection. The peptides were sonicated for 3 min. The

sample was centrifuged to 13,000 rpm for 2 min to pellet solid particles. The supernatant was pipetted into fresh LC glass vials and run for LC-MS.

2.2.4.8 LC-MS method for Protein turnover: mice brain, retina

The resuspended peptides in sample loading buffer (5% acetonitrile and 0.1% formic acid) were fractionated and analysed by an online UltiMate 3000 RSLCnano HPLC system (Thermo Fisher Scientific) coupled online to the Q Exactive HF. Firstly, the peptides were desalted on a reverse phase C18 pre-column (3 cm long, 100µm inner diameter 360 µm outer diameter) for 3 minutes. After 3 minutes the pre-column was switched online with the analytical column (30 cm long, 75 µm inner diameter) prepared in-house using ReproSil-Pur C18 AQ 1.9 µm reversed phase resin (Dr. Maisch GmbH). The peptides separated with a linear gradient of 5–30% buffer B (80% acetonitrile (Lichrosolv) and 0.1% formic acid) at flow rate of 10 nL/min over 88 min and 58 min gradient time. The pre-column and the column temperature was set to 50°C during the chromatorgraphy. The MS data was acquired by scanning the precursors in mass range from 350 to 1600 Da at a resolution of 60,000 at m/z 200. Top 30 precursor ion were chosen for MS1 by using data-dependent acquisition (DDA) mode at a resolution of 15,000 at m/z 200 with maximum IT of 50 ms. For MS2, HCD fragmentation was performed with the AGC target fill value of 1e5 ions. The precursors were isolated with a window of 1.4 Da.

2.2.4.9 LC-MS method for iBAQ quantification: bovine brain, retina SV proteome

Each biological replicate was analyzed in three replicate (technical) on the mass spectrometer. For LC-MS analysis, the samples were reconstituted in sample-running buffer (5% acetonitrile containing 0.1% formic acid in water) and corresponding digested peptides were injected. LC separation was carried on ThermoFisher nano-flow LC system (Agilent Technologies). Buffer A was 0.1% formic acid in water buffer B was 95% acetonitrile, 0.1% formic acid in water. Injected peptides were loaded on an in-house packed C18 trap column (1.5 cm, 360 µm outer diameter, 150 µm inner diameter, Reprosil-Pur 120 Å, 5 µm, C18-AQ, Dr. Maisch) at flow rate 10 µl/min and washed for 5 min with Buffer A. Peptide separation was done on an analytical C18 capillary column (15 cm, 360 µm outer diameter, 75 µm inner diameter, Reprosil-Pur 120 Å, 5 µm, C18-AQ, Dr. Maisch) at a flow rate of 300 nl/min with a gradient from 5-38% of Buffer B for 120 min. Eluting peptides were analyzed on a LTQ-Orbitrap Velos hybrid mass

spectrometer (Thermo Electron) in positive ion mode. The instrument was operated in a Data Dependent acquisition mode where the 15 most intense ions in the MS scan (*m/z* range from 400 to 1200, resolution set to 30,000 at *m/z* 400) were selected for fragmentation by collision induced dissociation (CID) and analyzed in the ion trap. Automatic gain control target was set at 30,000 and 10^6 for Ion Trap and FTMS respectively. Sequenced precursors were put on an exclusion list for 30 sec. The lock mass option (*m/z* 445.1200 (Olsen et al., 2005)) was used for internal recalibration.

2.2.4.10 LC-MS method for label-free absolute protein quantification: rat brains synaptosomes and SVs

Each biological replicate was analyzed in three replicate (technical) on the mass spectrometer. So, for every biological replicate (batch 1, 2, 3 and 4), there were 5 experimental replicates (8, 12, 16, 24 and 48 hours) and each of these experimental replicate had three technical replicates (a, b, and c). For LC-MS analysis, the samples were reconstituted in sample-running buffer (5% acetonitrile containing 0.1% formic acid in water) and peptides corresponding to 1 µg of digested sample were injected. LC separation was carried on an Agilent 1100 nano-flow LC system (Agilent Technologies). Buffer A was 0.1% formic acid in water buffer B was 95% acetonitrile, 0.1% formic acid in water. Injected peptides were loaded on an in-house packed C18 trap column (1.5 cm, 360 µm outer diameter, 150 µm inner diameter, Reprosil-Pur 120 Å, 5 µm, C18-AQ, Dr. Maisch) at flow rate 10 µl/min and washed for 5 min with Buffer A. Peptide separation was done on an analytical C18 capillary column (15 cm, 360 µm outer diameter, 75 µm inner diameter, Reprosil-Pur 120 Å, 5 µm, C18-AQ, Dr. Maisch) at a flow rate of 300 nl/min with a gradient from 5-38% of Buffer B for 90 min. Eluting peptides were analyzed on a LTQ-Orbitrap Velos hybrid mass spectrometer (Thermo Electron) in positive ion mode. The instrument was operated in a Data Dependent acquisition mode where the 15 most intense ions in the MS scan (m/z range from 400 to 1200, resolution set to 30,000 at m/z 400) were selected for fragmentation by collision induced dissociation (CID) and analyzed in the ion trap. Automatic gain control target was set at 30,000 and 10^6 for Ion Trap and FTMS respectively. Sequenced precursors were put on an exclusion list for 30 sec. The lock mass option (m/z 445.1200 (Olsen et al., 2005)) was used for internal recalibration.

2.2.4.11 Data analysis for protein quantification: bovine brain and retina

The acquired RAW data was analysed using MaxQuant software (Cox and Mann, 2008) version 1.0.3.5 based on Andromeda search engine (Cox et al., 2011). Each sample was given unique name. Trypsin was selected as protease and iBAQ option was highlighted. The bovine UniProt database (downloaded on; containing reviewed entries) was used for identifying proteins. Protein quantification was based on unique and razor peptides.

2.2.4.12 Data analysis for protein turnover: mice brain and retina

The acquired RAW data was analysed using MaxQuant software (Cox and Mann, 2008) version 1.0.3.5 based on Andromeda search engine (Cox et al., 2011). Each sample was given unique name. Trypsin was selected for protease category. The mouse UniProt database (downloaded on; containing reviewed entries) was used for identifying proteins. For defining the quantification based on peptides containing $lysine_0$ and $lysine_6$, multiplicity was selected to 2 and label $lysine_6$ was ticked in heavy label. Protein quantification was based on unique and razor peptides.

For protein quantification:

The technical replicates were averaged to minimize the variability due to different runs. The amount of a protein (in moles) is directly proportional to its iBAQ value (Schwanhausser et al., 2011). Therefore, the logarithms of known amounts of UPS2 proteins were plotted against the logarithm of iBAQ values. The slopes and intercepts of UPS2 proteins was calculated in various samples by linear regression. The iBAQ value for every protein was transformed into moles by linear regression of the UPS2 proteins. The proteins were assigned to functional categories manually based on available literature and UniProt.

2.2.4.13 Data analysis for for label-free absolute protein quantification: rat brains synaptosomes and SVs

Proteins were identified using MaxQuant software (Cox and Mann, 2008) version 1.3.0.5 using the Andromeda search engine (Cox et al., 2011) with rat SwissProt (March 2013; containing 7842 entries) and Human Universal Proteome Standard (UPS2, Sigma-Aldrich) protein databases. For the database search, tolerance of 6 ppm (for MS) and 10 ppm (for MS/MS) were set. Oxidation of methionine and carbamidomethylation of cysteines were set as variable and fixed modifications respectively. Tryptic specificity with no proline restriction and up to 2 missed

cleavages was used. False discovery rate (FDR) was set at 1%. Additionally, the iBAQ option was enabled for quantification (using the log10 fit).

For synaptosomal protein quantification:

The technical replicates were averaged to minimize the variability due to different runs. Absolute quantification can be acquired accurately (i) when a protein is fully digested and ii) no post-digestion modification has taken place to the peptides (Shuford et al., 2012). This is the reason why we chose to digest the four biological replicates for 8, 12, 16, 24 and 48 hours. For every protein, the maximum of the averaged experimental replicates from each of the biological replicate was chosen for quantification. This was to make sure that the quantification is carried out when there is maximum iBAQ intensity for every protein.

The slopes and intercepts of UPS2 proteins was calculated in various samples by linear regression. The iBAQ value for every protein was transformed into moles by linear regression of the UPS2 proteins. All the proteins were later converted into weights (μg percentage). The mean percentage for every protein was calculated by taking the average of the biological replicates. The contaminants were removed from the protein list. DAVID Functional Annotation Bioinformatics Microarray Analysis (Huang et al., 2007) was used to assign various categories to identified and quantified proteins. Assigned GO annotations were later confirmed manually.

The amount of a protein (in moles) is directly proportional to its iBAQ value (Schwanhausser et al., 2011). Therefore, the logarithms of known amounts of UPS2 proteins were plotted against the logarithm of iBAQ values.

2.2.4.14 Data Processing and plotting

The acquired output files were analysed and used for plotting data by various scatter-plot and histograms using Excel, Venny, Biovenn, DAVID Bioinformatics Resources and R softwares.

All the western blots given in this study were analysed and quantified by imageJ software.

3 Results

The scope of the study is to answer the most intriguing question: what makes the retina synapses 'special' as compared to brain synapses? It is well known that the presence of cone and rod cells is unique to the retina tissue, but apart from the basic light capturing machinery, one can speculate that the synaptic proteome of retina differ from brain synapses and how are such differences related to communication and transduction of the light-evoked signals to the brain. Moreover, what are the proteins, commonly expressed in retina and brain? Is the majority of the synaptic proteome of retina very similar to that of the brain? Or can we identify, if at all, the "special" proteins unique to the retina synapses that may contribute to their ultimate special function? Can we quantify the absolute copies present per SV?

Thus, here I combined biochemical and biophysical techniques to dissect the proteome and its dynamics occurring at the two differentially located neuronal tissues namely retina and brain, in order to gain an in-depth understanding of subtle but unique differences of the two nervous systems at the molecular level.

3.1 Retina Synapses

As mentioned previously (section 1.1.1.2), ribbon synapses are special synapses present in our sensory system. The ribbon synapses are distinguished by special proteinaceous structure called 'ribbon' surrounded by thousands of synaptic vesicles as has been seen by electron microscopy (fig. 1-1b). The major problem while working with retina samples is the limited availability of the amount of sample. Recently, Uthaiah and Hudspeth (2010) published preparation of various SV-associated complexes from hair cell. They also applied the same protocol to ~2000 chicken retina for isolation of SV-associated protein complexes (Uthaiah and Hudspeth, 2010). For establishing a protocol, the number of used retinas by Uthaiah and Hudspeth seems to be impractical. An alternative to such number was the use of big eyes for dissection of retina, which might represent large synapses proportionally. The bovine retina synaptic complexes were prepared by following their protocol. However, lately we realized major pitfalls in the protocol while applying to the retina tissue (section 4.1.1, appendix A12-14).

The isolation of bovine retina ribbons has been established and its molecular signatures were elucidated by biochemical studies and mass spectrometry

(Kantardzhieva et al., 2012; Schmitz et al., 1996; Schmitz et al., 2000; Von Kriegstein et al., 1999). Despite the large body of literature, the proteome of ribbon synapses has not been elucidated. It is still not clear how and why ribbon synapses manage to perform sustained exocytosis faithfully at such higher rates. Is the ribbon machinery alone responsible for higher rates of exocytosis function? Or do various protein assemblies like SVs also play a crucial role simultaneously in ribbon synapses? If it is so, than what are these protein complex machineries?

In order to shed light on these questions, we aimed to study the synaptic vesicles and associated proteins of retina ribbon synapse to understand the molecular details that distinguish them functionally from conventional synapse.

3.1.1 Characterization and proteomic analysis of bovine retina ribbon

As mentioned previously (section 1.1.1.2), the major component of ribbon is RIBEYE proteins that are made up of two domains; A and B. Unfortunately, the sequence of RIBEYE protein is yet not available in the genomic library. While nothing is known about the A domain and the B domain is homologous to a nuclear co-repressor C-terminal binding protein 2 (CtBP2). It has been predicted that the A domain predominantly has structural role while the B domain faces the cytoplasmic part that binds to NADH. The antibody against CtBP2 was used to show the presence of RIBEYE by immunostaining or immunoblotting (Alpadi et al., 2008; Schmitz et al., 2000).

The ribbons were isolated from bovine retina and the purified ribbon fraction (section 2.2.1.1 and 2.2.1.2) was probed for RIBEYE protein with the commercially available antibody (Abcam) (Von Kriegstein et al., 1999), (fig. 3-1). However, this antibody also yielded many non-specific signals with strong signals for proteins around 75 and 25 kDa, in addition to a strong signal for CtBP2, a nuclear protein (50 kDa) and CtBP2 homologue, RIBEYE (100 kDa) (fig. 3-1a).

The purified ribbon fraction was processed for in-solution digestion (section 2.2.4.1) followed by iBAQ-MS protein quantitation (section 2.2.4.7). The protein quantification data by iBAQ-MS showed approximately 30% of mitochondrial proteins, 30% of structural proteins, 2% of synaptic proteins, 15% cytosolic proteins containing mostly ribosomal and spliceosomal proteins (fig. 3-1b). Almost 20% of the proteins were uncharacterized proteins (fig. 3-1b, appendix A2). A major drawback in this preparation was the fact that CtBP2 protein, which is homologue of RIBEYE protein was quantified equals ~1% of the total protein in abundance as assessed by iBAQ-MS. Thus, it is clear that at least the preparation did not

specifically enrich the RIBEYE proteins, but also co-isolated many unrelated protein complexes. These co-isolated protein complexes include mitochondrial, ribosomal proteins which are the true contaminants. The structural and uncharacterized proteins might be ribbon associated. However, considering that the preparation of ribbons is not highly pure, it is difficult to correlate the identified structural and uncharacterized proteins with ribbon. Alternatively, to obtain pure preparations, immunoprecipitation seems to be a better method. However, since the available antibody is very unspecific, the idea to immunoprecipitate ribbons was not pursued.

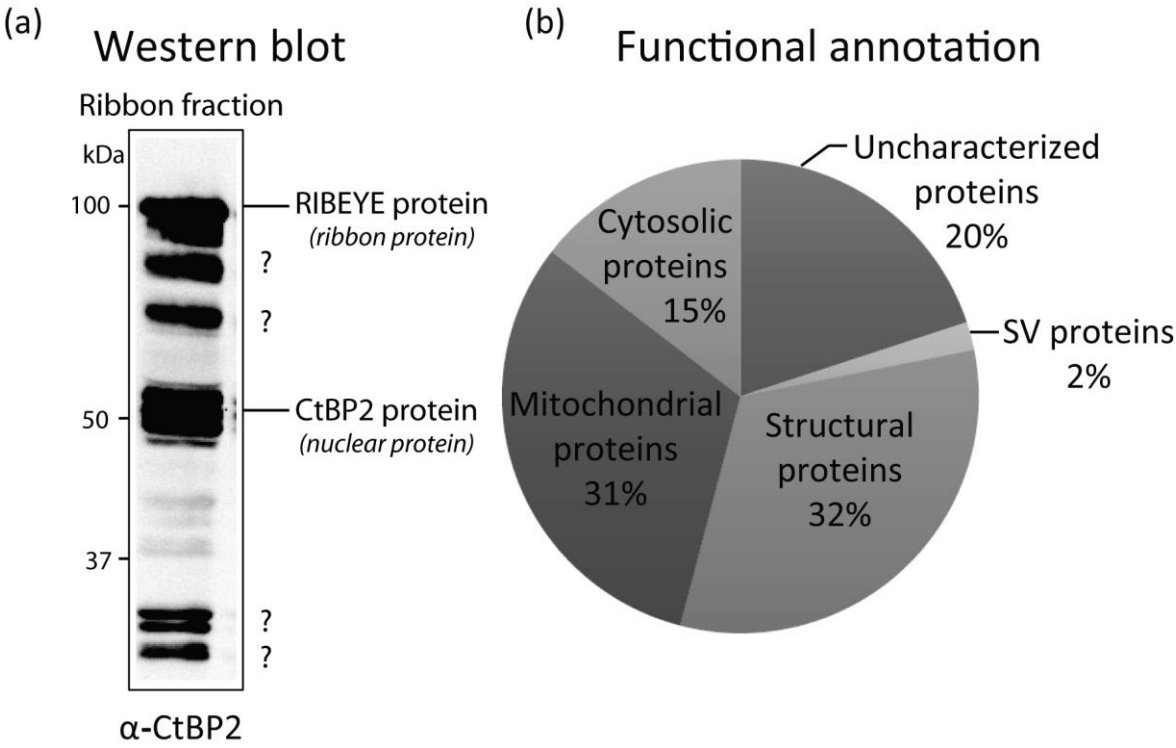

Figure 3-1: ***Characterization and proteomic analysis of purified ribbon.*** (a) Western blot of purified ribbons isolated by following the protocol described by Schmitz F et al., 1996 against commercially available CtBP2 antibody (Abcam). (b) GO Functional annotation of proteins identified and quantified by iBAQ-MS of purified ribbon. Purified ribbons were in-solution digested and run in Velos mass spectrometer. CtBP2 protein, which is homologous to a part of B domain of RIBEYE, was found to be only 0.8% of total protein in abundance.

In parallel, Kanthardhzhieva *et al*., 2012 used their in-house prepared antibody to immunoprecipitate ribbons and processed the data for label-free quantitative mass spectrometry using emPAI technique (Ishihama et al., 2005), a well-known technique to quantify protein abundance by mass spectrometry (Kantardzhieva et al., 2012). Despite the isolation of ribbons by in-house prepared antibody, all the proteins identified and quantified in this study were also found in our study. For

extensive comparison of the data and proteins see discussion (section 4.1.6) (appendix A1 and A2).

3.1.2 Isolation and characterization of SVs from bovine retina

After our attempt to investigate the ribbon proteome, the next aim was to understand the proteome of SVs in retina. There are many available SV isolation protocols for brain tissue (Ahmed et al., 2013; Huttner et al., 1983; Nagy et al., 1976). All these SV isolation protocols are basically divided into categories: one that ensures the purity based on mild homogenization while the other ensures high yield of SVs based on a harsh homogenization approach (Hell et al., 1988).

Apart from brain, sensory systems like retina are the source of large number of SVs. This is because of the presence of ribbon synapses in retina. So far, there has been no attempt to isolate SVs from retina. Since the two tissues are distantly located and perform different functions, the SVs proteome from the brain and retina is very promising to explore the similarities and differences.

Therefore, the next aim was to establish a novel protocol that facilitates isolation of the SVs from a small quantity of starting material. This will provide further detailed insights to understand the retina ribbon synapses at molecular level.

3.1.2.1 Establishment of a novel protocol for isolation of SV from retina

In order to study the proteome of retina SVs, first, a method to isolate SVs from retina was established (fig. 3-2). The advantages of this protocol are that (1) it allows isolation of SVs from as low as eight bovine retinas; (2) it isolates the SVs with high yield and good purity. Additionally, snap-frozen retinae over long time were used for this study.

The brain SV isolation protocols are divided into two types. The classical method of SV isolation protocols are based on the fact that upon homogenization, the nerve terminal reseals back to form synaptosomes. The pure synaptosomal fraction is devoid of nucleus and other cell debris, hence results in SVs of high purity (Nagy 1978). The other type of isolation protocol is based on rupturing the brain tissue by harsh homogenization (like grinding the whole brain in liquid nitrogen using mortar and pestle) to release most of the SVs into the supernatant (Hell et al., 1988). This type of isolation protocol provides high yield of SVs.

Whittaker (Whittaker et al., 1964) for the first time observed the formation of synaptosomes in brain tissue while attempting to purify SVs. Neal (1974) also

applied the same protocol to rabbit retina. It led to a surprise finding that although retina is a neuronal tissue, its nerve terminals do not disrupt efficiently upon mild homogenization. In addition, the ribbon nerve terminals are very large in size, thus do not re-seal back to form synaptosomes. Thus, the concept of formation of synaptosomes to isolate pure SVs cannot be applied to retina tissue (Neal and Atterwil.Ck, 1974).

The protocol started with dissection of retina from bovine eyes. The retina were dissected from bovine eyes and snap-frozen (method section 2.2.1.1). The next step was homogenization of frozen retina to release the SVs from the neuron. Since, the retina is a tougher tissue than brain. Thus, harsh homogenization technique was applied to disrupt the retina tissue. The frozen retina was ground to fine powder in liquid nitrogen using mortar and pestle. This way of lysis has been reported previously for isolation of SVs from brain tissue (Jahn 2006). In addition, the finely powdered retina was re-homogenized using Ultra-turax. Use of Ultra-turax has been reported to efficiently disrupt the retina cells and has been applied for purification of ribbon from bovine retina (Schmitz et al., 1996).

After the disruption of neuronal cell membrane of retina, the next step was isolation of SVs by a combination of various well-known fractionation techniques based on their size, shape and density. Briefly, the homogenate was pelleted at moderate g-force to remove the huge cell debris. The pellet was re-homogenized using Ultra-turax and re-centrifuged to release the maximum amount of SVs from the retina cells. Finally, the supernatants from the two consecutive steps of homogenization and centrifugation were pooled and a short ultracentrifugation was applied to remove huge cell debris. To avoid contaminations from very small and large protein complexes like proteasome complex, mitochondria etc, rate-zonal centrifugation was applied. The supernatant acquired from the previous ultracentrifugation step was overlayed on a 2-step-discontinuous density gradient and subjected to ultracentrifugation. The introduction of 2-step discontinuous density gradient was a combination of 1 M and 0.7 M sucrose. SVs are known to exhibit a density of 1.11ρ, thus they will migrate at the interface of 0.7M and 1M sucrose. The heavier cell debris and protein complexes will pellet at 1 M sucrose while the small proteins will float above the 0.7M sucrose layer. The SV fraction was carefully collected from the interface of 0.7M and 1M sucrose and pelleted (P4).

Following this novel protocol, we observed almost 4-fold enrichment of SVs in the P4 fraction as compared to the homogenate. However, the electron microscopy revealed that although the P4 fraction is enriched with SVs, it also contained several non-SV components. Since, our ultimate aim was to comprehensively

study the SV proteome by mass spectrometry, it was very important to exclude such non-SV components from the preparation. This is due to the fact that mass spectrometry is an unbiased technique for identification of proteins.

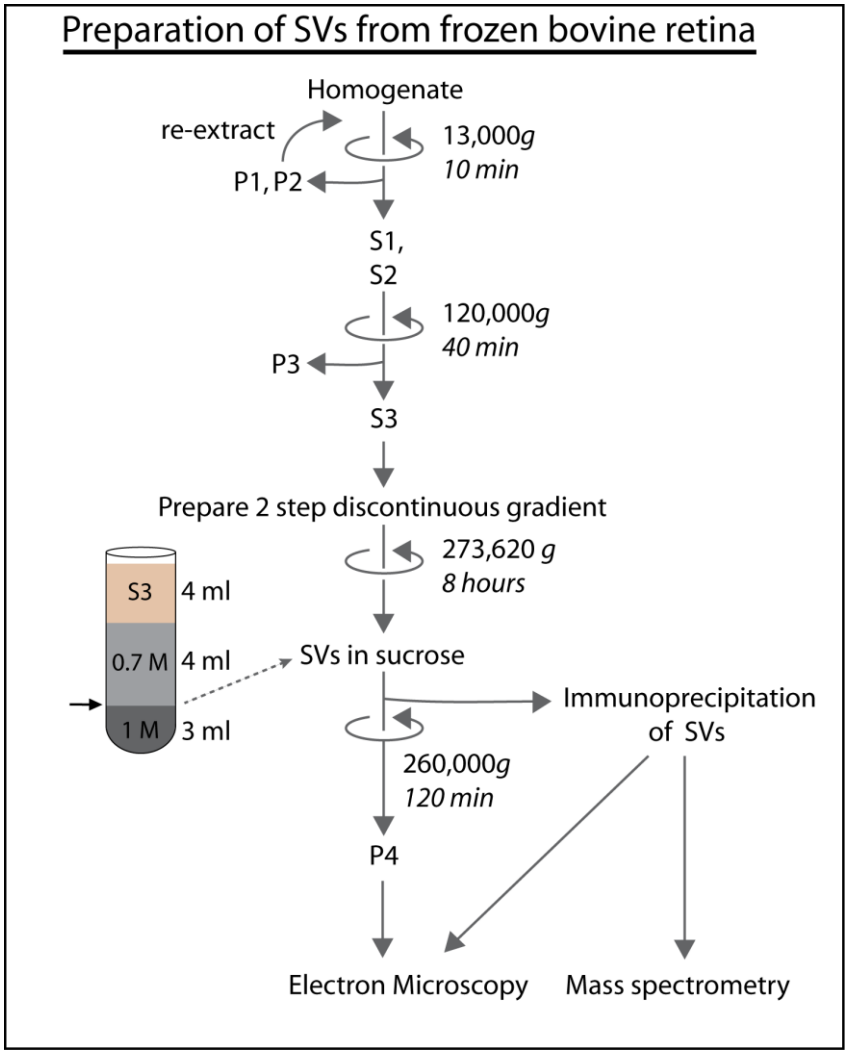

Figure 3-2: ***Schematic representation of our established protocol for isolation of retina SVs.*** (a) Workflow diagram of SV purification after dissection (section 2.2.1.1) and homogenization in liquid nitrogen (section 2.2.1.3). P represents pellet while S represents supernatant at various centrifugation steps. Purified SV should be carefully extracted from the interface of 0.7 M and 1 M sucrose (area marked by arrow sign in Fig 3-2). This fraction was used for immunoprecipitation using Synaptophysin-coupled to Eupergit beads (section 2.2.2.5 and 2.2.2.6) and finally analysed by embedding electron microscopy and mass spectrometry. P4 was used for negative staining electron microscopy.

Recently, Boyken et al., (2013) isolated pure preparations of docked and free SVs of brain synapses by co-immunoprecipitation and studied the proteome differences by quantitative mass spectrometry. Thus, immunoprecipitation technique was introduced as the final step of purification for isolation of pure SVs in our preparation. In the above mentioned study, antibodies against three SV integral proteins: synaptophysin, VGlut1 and VGAT was used to immunoprecipitate the

SVs. For synaptophysin antibody cl. 7.2 was used to immunoprecipitate SVs from rat brain (Boyken et al., 2013). In addition, the same antibody was used for immunostaining of various layers of bovine retina. It was observed that synaptophysin is localized predominantly in OPL (section 1.1.1.2) and a small fraction in IPL (section 1.1.1.2) (Brandstatter et al., 1996a; Von Kriegstein et al., 1999). Synaptophysin protein is known to be integral-SV protein (Jahn et al., 1985), localized in all the synapse forming regions of retina (Von Kriegstein et al., 1999) and its antibody *Cl.* 7.2 has been well known to immunoprecipitate the SVs (Boyken et al., 2013) and importantly has ability to recognize the epitope of bovine synaptophysin protein (section 3.1.2.3). Thus, synaptophysin *Cl.* 7.2 antibody was chosen for immunoprecipitation in our study. Finally, highly pure SVs were isolated by immunoprecipitating integral SV protein- synaptophysin using the antibody *Cl.* 7.2 (see discussion 4.1.1).

3.1.2.2 Optimization of the isolation protocol for retina SVs

While establishing the novel protocol, certain factors were considered. Firstly, the starting material for the established protocol should be easily accomplishable. For our established protocol, a minimum of eight frozen bovine retinae are required as starting material.

Secondly, the material meant for isolation should be minimally lost during various steps of isolation. For efficient rupturing of all the retina cells, certain modifications were introduced in the isolation protocol. The first step added for lysing the retina cells was by powdering the retina tissue in liquid nitrogen using mortar and pestle (section 3.1.2.1). Use of liquid nitrogen to lyse brain neurons was been previously reported (Hell et al., 1988).

In addition, the P1 fraction was re-blended to maximize the SV recovery (Fig 3-2). By re-blending the P1 fraction, almost 40% of the total protein amount was recovered and an increase of 0.8% enrichment in SV yield as compared to the homogenate (fig. 3-3a, b; S2 lane).

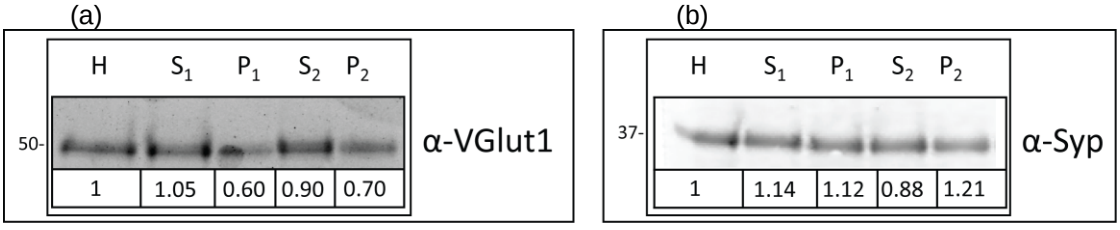

Figure 3-3: ***Improvement in protocol by re-homogenizing the pellet P1.*** Immunoblotting of various fractions H, S1, P1, S2, P2 obtained from SV preparation following protocol (fig 3.3) against (a) VGlut and (b) synaptophysin proteins. The bands were quantified using ImageJ software.

Thirdly, the large membranuous/proteinaceous substances were removed from the preparation by the introduction of a 2-step sucrose gradient. (fig. 3-4).

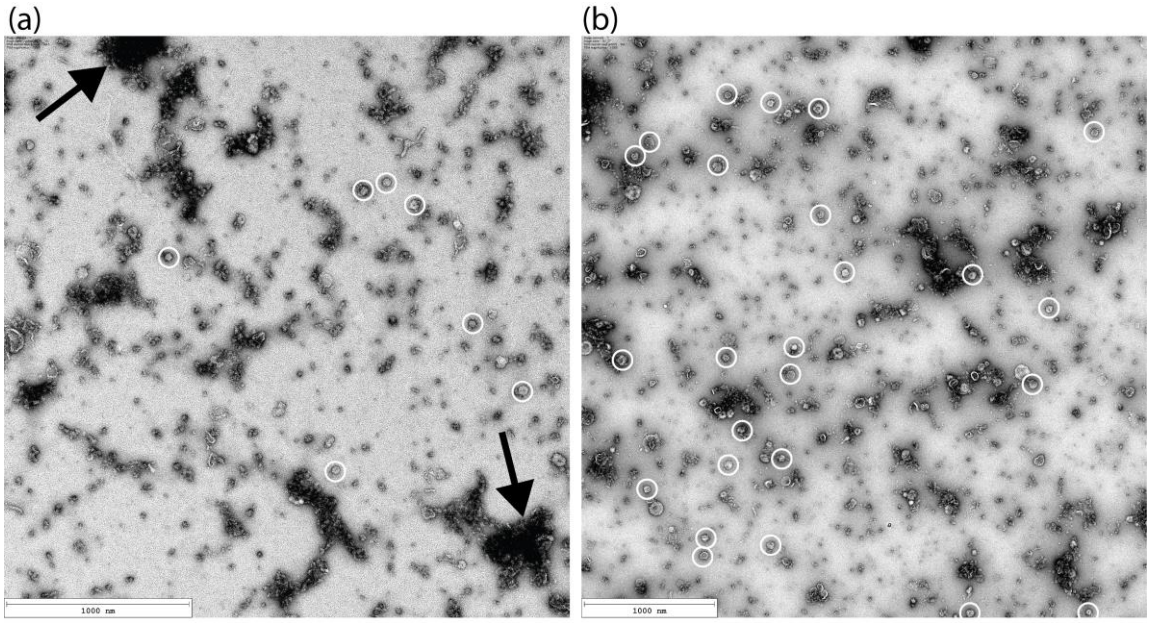

Figure 3-4: ***Improvement in protocol by introducing a 2 step-discontinuous sucrose gradient.*** Negative staining electron microscopy pictures of P4 fraction (a) without and (b) with 1 M sucrose underneath the 0.7 M sucrose cushion. White circles depict the possible SVs from the preparation in the picture. Huge proteinaceous particulates (see a; arrow) are less in number (see b) when 1 M sucrose was laid beneath the 0.7 M sucrose cushion. Note the increase in the number of SVs in (b) as compared to that in (a).

The P4 SV fraction, yet after the introduction of 2-step discontinuous gradient ultracentrifugation showed certain contamination of large proteinaceous complexes (fig. 3-4b). Thus, immunoprecipitation was introduced as the final step for SV isolation. In fact, after inclusion of this immunoprecipitation step, clearly the material was free of any large sized protein complexes, as evidenced by a homogenous size distribution (fig. 3-9).

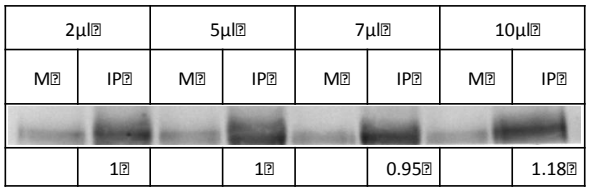

Figure 3-5: ***Titration of beads for optimum amount of beads required for Co-IP.*** Various amounts of Eupergit beads (2µl, 5µl, 7µl, 10µl) were used for immunoprecipitation of SVs of fraction obtained from the interface of 0.7 M and 1 M sucrose gradient from bovine retina. The samples were run for immunoblotting and probed against VGlut1 protein. M and IP represents mock and immunoprecipitated samples respectively.

For this, we coupled the antibody synaptophysin to the Eupergit® beads. Not to waste a lot of coupled antibody, variable amounts of beads were titrated against a

constant amount of input SV fraction (fig. 3-5). It was found that 2 µl of beads was just enough to immunoprecipitate most of the SVs present in 500 µl of SV fraction obtained from 0.7 M - 1 M interface. Thus, by the introduction of above-mentioned optimizations, the novel established protocol contained minimal contamination.

3.1.2.3 Biochemical characterization of retina SVs

Using the novel protocol, approximately 2 mg of P4 fraction was obtained with approximately 90 mg of total protein as starting material (homogenate). We found that our final P4 fraction was approximately three times enriched than the homogenate (table 3-1).

Table 3-1: Quantification of retina SV enrichment during our isolation protocol. Given are the total protein recovery and percentage of protein acquired at every step of the protocol. For relative quantification, equal amount of proteins was loaded on SDS-PAGE and probed against synaptophysin protein using G96 polyclonal primary antibody followed by anti-rabbit coupled to Cy3 secondary antibody. The quantification of signals was done using ImageJ software and enrichment in fractions was calculated against the amount of synatophysin in the homogenate.

Fractions	Protein Concentration	Volume	Total protein	Synaptophysin %	Enrichment %
H	4.39±0.44	20±0.00	87.75±8.84	100±0.00	1
P1	2.23±0.24	21.50±2.2	48.25±9.83	54.70±5.69	1.12
S1	2.08±0.31	16.50±0.7	34.18±3.71	38.94±0.30	1.14
P2	3.51±0.41	6.00±0.00	21.07±2.44	24.00±0.36	1.21
S2	1.02±0.21	18.25±2.4	18.88±6.40	21.25±5.15	0.88
P3	2.29±1.15	5.75±0.35	13.35±7.42	14.86±6.96	1.21
S3	0.71±0.12	50.00±0.0	35.36±6.02	40.15±2.81	2.59
P4	5.03±1.79	0.90±0.14	4.66±2.32	5.20±2.12	3.25
Cyt	0.36±0.33	64.00±19.8	20.04±14.0	22.14±13.82	0.38

There are two pre-requisites for a reliable established SV isolation protocol. First, it should allow enrichment of SV integral and SV associated proteins, and

secondly, it should not enrich the contaminants. Traditionally, the structure and size based features were checked by electron microscopy while the protein based characterizations were tested either by the respective protein activity assays or by western blotting. For the novel protocol of SV isolation, a combination of western blotting, electron microscopy and mass spectrometry was used to measure (or compute) the enrichment of SV integral proteins, SV-associated proteins and SV contaminant proteins.

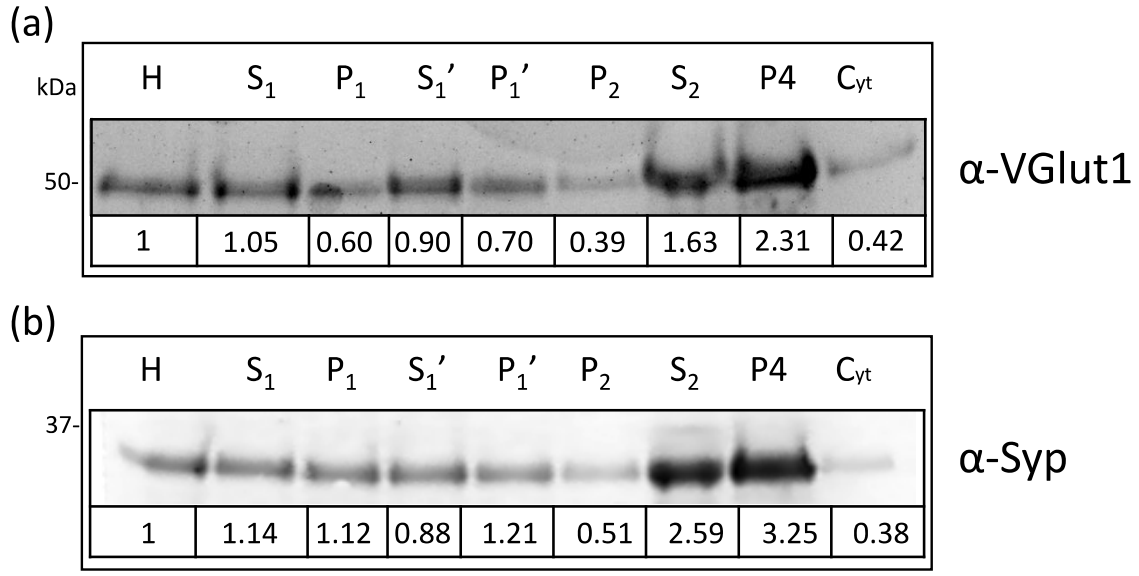

Figure 3-6: Enrichment of SV-integral proteins in bovine retina during the isolation protocol. Immunoblotting of various fractions obtained from SV preparation following protocol (fig 2) against (a) VGlut, (b) synaptophysin protein. The quantification of signals for the corresponding proteins was done using ImageJ software.

SV integral, SV-associated and possible SV contaminant proteins were analyzed by western blots using their respective antibodies. SV-integral proteins like synaptophysin, Glutamate transporters and Synaptotagmin were enriched almost 3 times in fraction P4 as compared to the homogenate by quantitative western blotting (fig. 3-6).

Out of the total population of SVs present in tissue, there is a certain percentage of SVs associated to various active zone proteins for protein-protein interaction. In brain SVs, various SV-associated proteins like unc18 and clathrin do enrich in the preparation (Takamori et al., 2006). Thus, the SV-associated proteins like Rab3a, NSF, clathrin and syntaxin were analyzed by western blot (fig. 3-7). However, many

available antibodies did not bind to the bovine proteins because of lack of interacting epitopes.

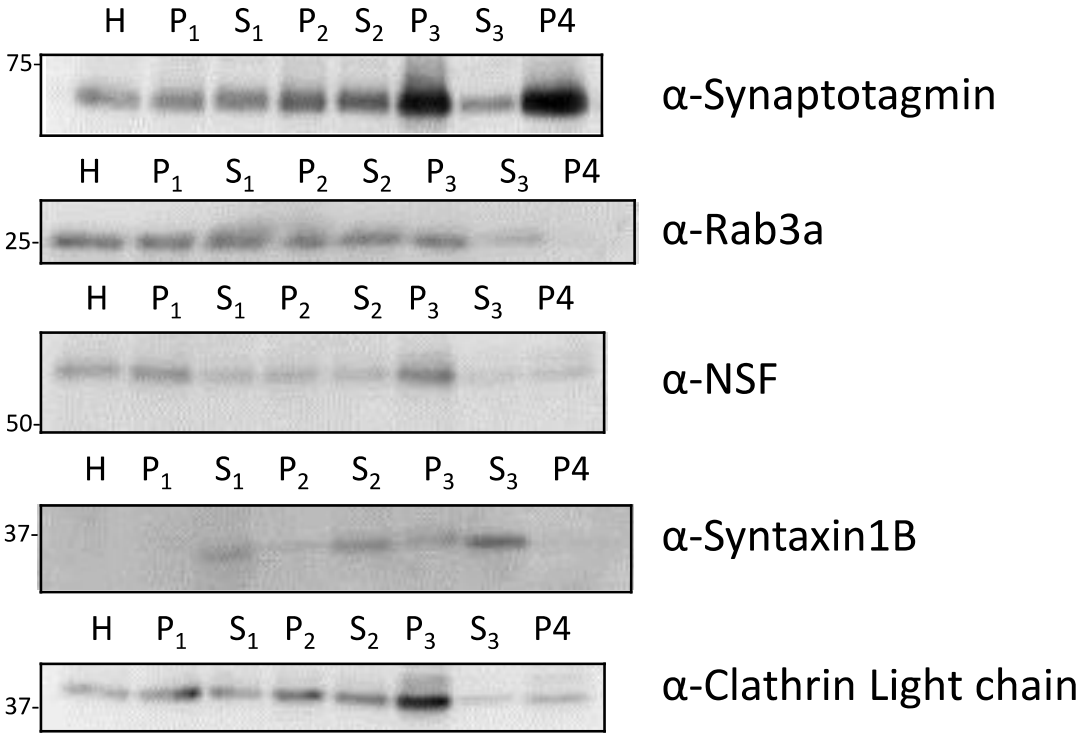

Figure 3-7: Immunoblotting of SV-associated proteins in isolated bovine retina SV. Immunoblotting of various fractions obtained from SV preparation following protocol (fig 2) against (a) synaptotagmin1, (b) Rab3a, (c) NSF, (d) syntaxin1B, (e) Clathrin light chain protein.

Several SV-associated proteins like synapsins, clathrin chains, AP-2 involved in SV recycling are known to enrich in SVs in rat brain (Takamori et al., 2006). This suggests interaction of various SV interacting partners for SV recycling in brain. However, synapsins, Syntaxin1 and Rab3 are known to be totally absent in SVs of retina (Brandstatter et al., 1996b; Grabs et al., 1996; Mandell et al., 1990; Morgans, 2000a, b; Morgans et al., 1996; Von Kriegstein et al., 1999). Strikingly, Syntaxin 1 and Rab3 did not enrich in the purified P4 fraction. It was reported that instead of Syntaxin1, Syntaxin3 is present in ribbon synapses to form SNARE complex with VAMP2 and SNAP25 (Morgans et al., 1996). Except for synaptotagmin, we did not observed any significant enrichment for proteins Rab3a, syntaxin1B in the retina SVs. In addition to this, we also found that NSF protein was almost absent in SV fraction (fig. 3-7).

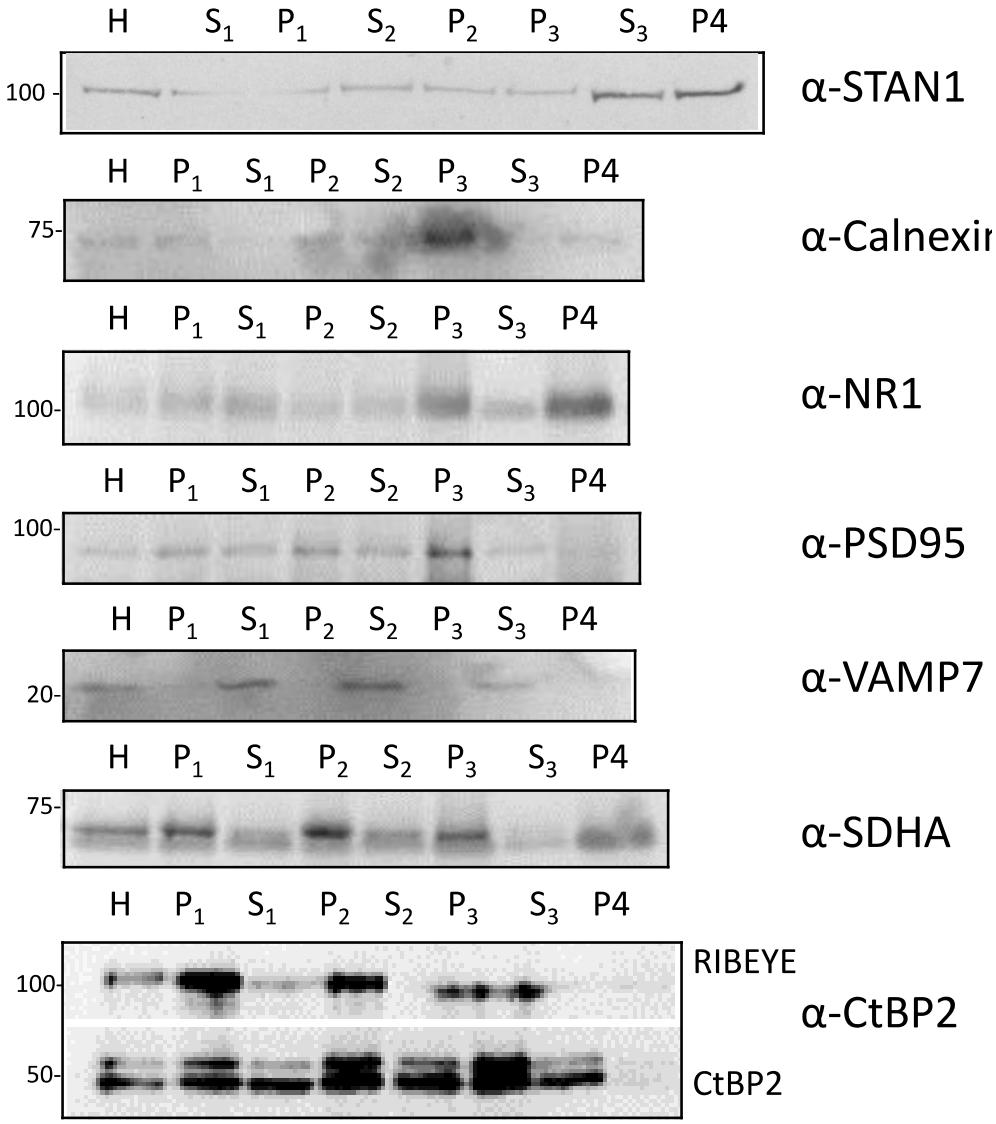

Figure 3-8: ***Enrichment of contaminant proteins in bovine retina with the novel isolation protocol.*** Immunoblot of various fractions obtained from SV preparation following protocol (fig 2) against (a) 150kDa spliceosomal proteins, (b) calnexin, (c) NR1, (d) PSD95, (e) VAMP7, (f) SDHA, (g) CtBP2 proteins.

The SV fraction may contain contamination from any part of cell. There can be contamination from plasma membrane, ER, mitochondria, nucleus, endosomes and cytoplasmic proteins. Thus, western blot analysis was performed for organelle-specific proteins in order to test the contaminations from these organelles. It was observed that some amount of post-synaptic proteins like NR1 and PSD95 were present in the SV fraction P4 (fig. 3-8 c, d). Remarkably, major contamination of proteins such as succinate dehydrogenase (SDHA) from mitochondria and 115 kDa protein from spliceosomes were observed (fig. 3-8 a, f). However, contamination from endosomal proteins like VAMP7 and calnexin were present in negligible amounts (fig. 3-8 b, e).

In addition, no enrichment of nuclear and ribbon protein was observed as shown by CtBP2 specific antibody. Although ribbon interacts with SVs, however, since the protocol separation is based on density, thus, the SVs associated with ribbon not co-isolate in the SV preparation.

There was no contamination from organelle and cell-debris observed after the P4 fraction was immunoprecipitated as depicted by the EM data (fig. 3-9). Thus, above-mentioned non-SV specific protein complexes were excluded from the preparation (section 2.2.2.5, 2.2.2.6).

3.1.2.4 Functional characterization of retina SVs

After the establishment of isolation protocol for SV, the first question was if at all, the isolated SVs are functionally active. Do the biochemical data and mass spectrometric proteome reflect the biologically functional SV?

In order to answer this aspect, Dr. Julia Preobraschenski (Prof. Reinhard Jahn lab, MPIbpc, Germany) performed glutamate uptake assay (section 2.2.3.3) with fraction P4 (fig 3-3) obtained from bovine retina. It was observed that the 14 μg of P4 fraction isolated from bovine retina gave radioactivity counts ~20,000 cpm. Thus, the SVs obtained from aforementioned protocol (section 3.1.2.1) are functional and capable of uptaking freely available glutamate in the surrounding when provided with ATP.

3.1.2.5 Characterization of SVs by Electron Microscopy (EM)

EM is one of the best techniques to visualize organelle-based contamination like plasma membrane, mitochondria, Golgi, and nucleus. It has been used as the sole technique to observe structural details and to purify organelles of cells (Sjostrand, 1953a, b, c, e, f, g, 1958). In late 80's, electron microscopy technique was used to check contamination in the SV preparation from mitochondria (Hell et al., 1988). Since, we were establishing a novel protocol to isolate SVs from retina for the first time, it was very crucial to observe the SV preparations under EM. This ensured the isolation of the component of interest; SVs in this study and indicates the amount of contaminant membranes in the sample.

A wide range of sizes for SVs have been reported (Takamori et al., 2006). Moreover, retina is known to exhibit wide range of SV size based on exposure to light (Derobertis and Franchi, 1956). The P4 fraction was processed for negative

staining under EM (fig. 3-4) and it was observed that retina SVs have an average diameter of 45 nm.

As mentioned previously, introduction of a two-step sucrose gradient strikingly minimized some proteinaceous contamination in the preliminary preparations (fig. 3-4b). Finally, immunoprecipitation was chosen as the final step of purification to isolate SVs from bovine retina as discussed previously. In order to compare the size distribution of SVs from brain and retina, bovine brain and retina were processed, following the aforementioned established protocol (section 3.1.2.1) and observed under embedding-EM (fig. 3-9; (a) brain SVs, (b) retina SVs).

(a) (b)

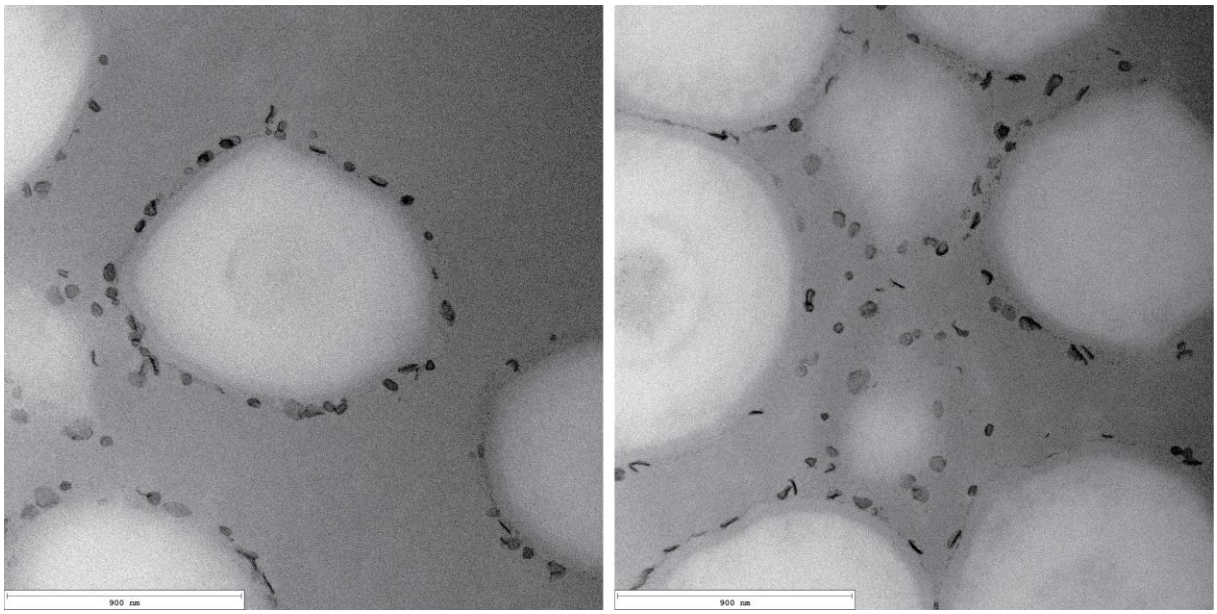

Figure 3-9: Embedding electron microscopy picture of immunoprecipitated SVs of brain and retina. The immunoprecipitated SVs from (a) bovine brain and (b) bovine retina were processed for embedding electron microscopy. Both images show large spherical (approximately 1 μm) Eupergit beads surrounded by numerous SVs. Immunoprecipitated SVs from bovine (a) brain and (b) retina looks clean and free from membranous particulates. (scale bar represents 900 nm)

The EM pictures depict SVs arranged at the periphery of the Eupergit beads used for purification of bovine brain (fig. 3-9a) as well as retina (fig. 3-9b) SVs. There were almost no membranous components observed in the acquired images. Since the final SV fraction seemed convincingly pure, we decided to analyse the proteome of brain and retina SVs by mass spectrometry (section 3.2).

Based on the embedding EM, the diameter of SVs was measured by Dr. Dietmar Riedel (MPIbpc, Germany). For precise diameter measurement, two orthogonal axes were averaged using ITEM Soft image Solution software, version 5.2. This measurement was acquired for more than 200 SVs from brain and retina. Fig. 3.10

shows the size distribution of immunoprecipitated SVs from brain (fig. 3-10a) and retina (fig. 3-10b).

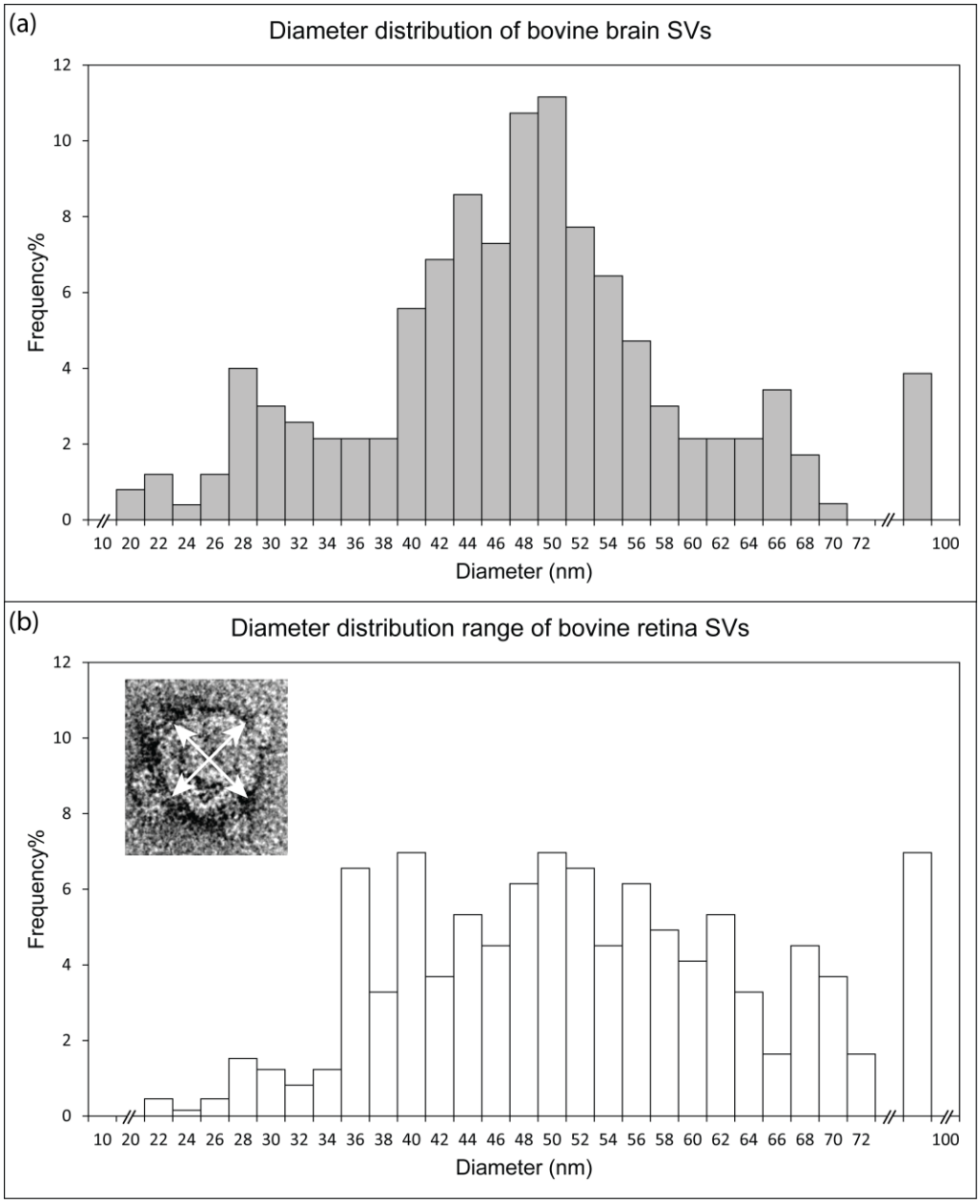

Figure 3-10: ***Size distribution of SVs determined by electron microscopy.*** The outer diameter of SVs immunoprecipitated from bovine (a) brain (n = 235) and (b) retina (n = 247) was measured. For accurate diameter calculation, two orthogonal axis measurements were average using ITEM Soft image Solution, version 5.2.

The size distribution of SVs from brain showed Gaussian distribution with its maxima around 40-50 nm. Interestingly, the retina SVs showed a broad range of size distribution varying between 35-70 nm. This broad range of size distribution may be because of isolation of SVs from various types of neuronal cells like bipolar cells, rod cells, amacrine cells, ganglions etc. present in retina tissue. However, these differences cannot be explained from the present studies.

3.2 Quantitative proteomic analysis of SVs from bovine brain and retina

After establishing the protocol for isolation of retina SVs, the next step was to conduct an in-depth analysis of the retina SV proteome. In addition, the major question was, if the retina SV proteome similar to the brain SV proteome?

In order to answer the above questions, the SVs were isolated from frozen bovine retina as well as brain by following the established protocol (section 3.1.2.1). The isolated SV samples were digested (section 2.2.4.3) and desalted (section 2.2.4.4) followed by mass spectrometric analysis (sections 2.2.4.5, 2.2.4.9, 2.2.4.11 and 2.2.4.14) (fig. 3-11).

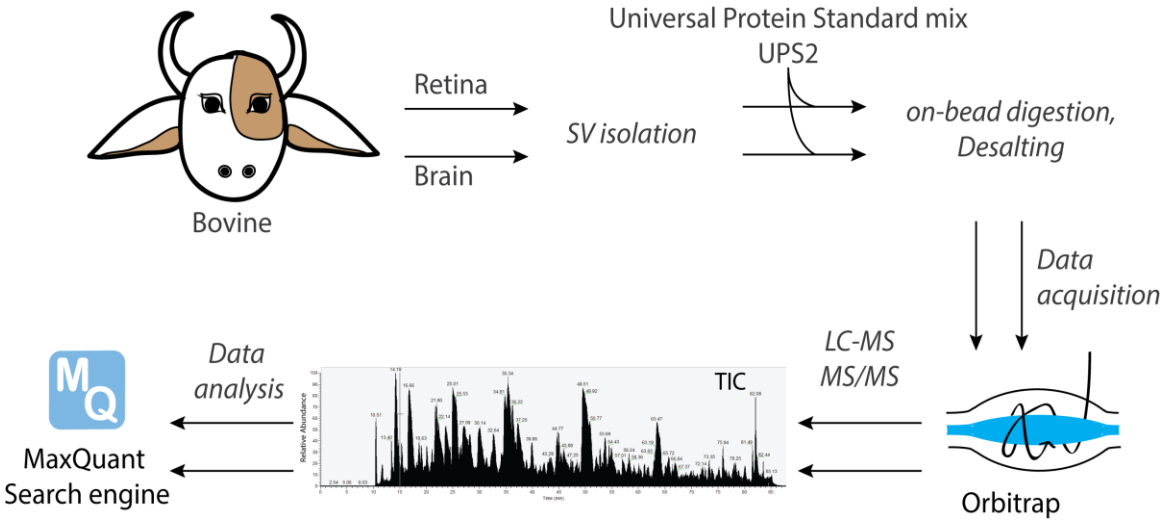

Figure 3-11: ***Schematic representation of workflow for quantitative proteome analysis of SVs from brain and retina*****.** The bovine eyes and brain tissue were collected from slaughterhouse. Isolation of SVs following the established protocol was performed for retina as well as brain separately. The immunoprecipitated SV proteins were spiked-in with standard UPS2 proteins, digested by trypsin using on-bead digestion protocol and the extracted peptides were run on Orbitrap-Velos for 120 min gradient. The RAW files were analysed for identification and quantification by MaxLFQ and iBAQ using MaxQuant software based on Andromeda search engine.

A total of 476 proteins were identified and quantified from immunoprecipitated SVs obtained from bovine retina and brain by mass spectrometric analysis. Out of total of 476, 368 proteins were identified in brain while 214 proteins were identified in retina. All the identified proteins were sub-categorized into various functional categories based on the information provided by UniProt data (available online) as shown in fig. 3-12a, b.

Not surprisingly, 95 proteins which contributed ~53% of protein amounts and 154 protein which contributed ~25% of protein amounts were identified as contaminations originating from mitochondria, ER/Golgi, ribosomes, nucleotide

metabolism pathway and cytosolic enzymes in mass spectrometric analysis of brain and retina respectively (fig. 3-12a, b). Most of the contaminant proteins in this study are due to cytosolic enzymes (~14% protein in brain contributing ~13% protein amounts; 19% proteins in retina contributing 16% protein amounts) and ribosome machinery (~17% in brains and ~2% in retina) (fig. 3-12a, b). In contrast, in another study with similar approach using rat brain, major contamination (~42%) in the immunoprecipitated SVs was by mitochondrial proteins (Boyken J, dissertation 2012). Surprisingly, mitochondrial protein contaminants in our study were found to be 6-8% of the total identified proteins in brain as well as retina; however, they contribute only 1% of the total protein amounts/abundances. The differences in different kinds of contaminant proteins could be due to different approaches of SV preparations.

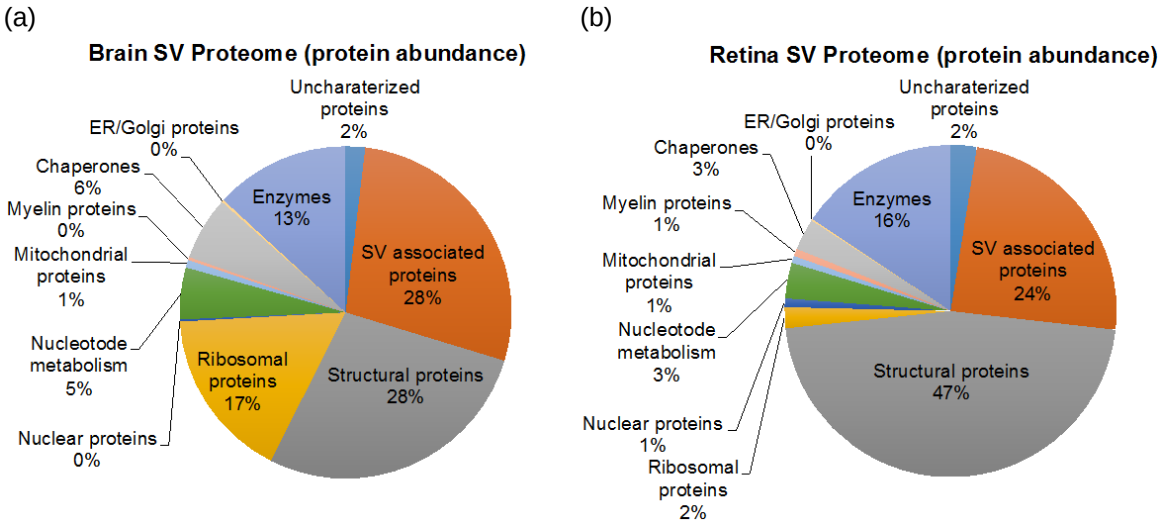

Figure 3-12: ***Pie chart showing the abundance of identified proteins in immunoprecipitated bovine SVs from brain and retina by mass spectrometry.*** The identified proteins from immunoprecipitated SV from brain and retina were manually classified into various functional categories based on the information provided by UniProt. Pie diagram of protein abundances (shown in percentage) identified in (a) brain and (b) retina for various functional categories. Percentage values shown in the pie diagram as 0% have real values less than 1%.

Due to an unknown reason, a striking difference was observed where the ribosomal protein was found to be ~17 % in brain SV while only 2% in retina by abundance (fig. 3-12a and b; dark yellow colour). Protein contaminants from ER/Golgi, myelin and nucleus contributes ≤1% of the total immunoprecipitated protein amount (fig. 3-12a, b). Interestingly, no contamination was observed from post-synaptic proteins.

Apart from the contaminant proteins, structural proteins were also identified in the analysis. Almost 16% and 19% of the total identified proteins were structural contributing to 28% and 47% of protein amounts in brain and retina respectively.

Interestingly, tubulin (20% in brain and 30% in retina) and actin (5% in brain and 11% in retina) contributed mostly to the total abundance of protein identified. Furthermore, some proteins from chaperone machinery and nucleotide metabolism were also identified. Various functional categories of proteins identified along with the SV preparation not necessarily mean contaminations but also represent the existence of several molecular processes occurring in SV cycle. All the proteins in above-mentioned functional categories were not considered for further studies.

In this study, 67 uncharacterized proteins (48 protein in brain (~2% by abundance) and 26 proteins in retina (~2% by abundance)) were identified according to gene prediction (appendix A1 and A2).

3.2.1 Protein copy number per SV

The quantitative model for rat brain SV proteome is already available and a comparison of bovine brain and bovine retina quantitatively with it may help to better understand the retina synapse SV proteome (section 1.1.1.1.1) (Takamori et al., 2006). From the above quantitative mass spectrometric analysis, it is clear that at least the structural proteins co-immunoprecipitated in larger amounts for retina than brain (fig. 3-12a, b grey coloured). Apart from the differences in the number of proteins identified from various functional categories, it is also important to inspect the individual proteins quantitatively. The proteome of retina and brain SV may or may not have similar abundances. From the total identified proteins, it was clear that number of proteins identified in brain were larger than retina. The quantified proteins were also remarkably less in retina than brain.

In order to compare the relative abundances of proteins identified in brain and retina, the well-known mass spectrometric technique “intensity-based-absolute-quantitation” or iBAQ-MS was performed (section 1.2.4.1.1). This technique was first introduced to determine absolute amounts of HeLa lysate proteins (Schwanhausser et al., 2011). In this thesis work, the two sub-types of iBAQ-MS: label-free iBAQ and spiked-in iBAQ were used to quantify absolute amounts of proteins of rat brain synaptosomes and SVs respectively, that are explained in details in a later section (section 3-4). It was observed that absolute amounts calculated using iBAQ-MS technique correlate remarkably well with the amounts derived by quantitative western blotting, thus, iBAQ-MS was also used to quantify absolute amounts of proteins in isolated SVs from bovine retina and brain.

As mentioned previously, synaptophysin was used for immunoprecipitation because it is an integral protein of SVs. The amount of synaptophysin coupled to beads used for all the preparations was kept constant. Thus, the absolute amount of synaptophysin derived by iBAQ-MS in all the preparations was multiplied by a factor to make it equal in all the preparations. This factor was multiplied with every protein present in that preparation to normalize their amounts proportionally. Hence, all the synaptophysin obtained from the immunoprecipitated preparation has equal mass spectrometric iBAQ amount (section 2.2.4.11).

For determination of protein copies per vesicle, the total count of SVs is required. The determination of the exact number of immunoprecipitated SVs present has not yet, been reported and needs optimization. Thus, to determine the copy number per SV, we applied a different approach. We assumed that the copies of synaptophysin per SVs were constant in bovine brain, bovine retina and rat brain. The absolute amount of synaptophysin per rat brain SV (=32 copies) was already determined previously (Takamori et al., 2006). Thus, for determination of copies of proteins per SV, first, the protein-to-synaptophysin ratio was calculated. The number of molecules of every protein was divided by the number of molecules of synaptophysin protein gives the protein-to-synaptophysin ratio. Finally, the copy number of proteins per SV was determined by multiplying the calculated protein-to-synaptophysin ratio by 32 (absolute copy of synaptophysin per rat brain SV) for a given SV preparation (equation 1).

For protein X,

$$Copy\ number\ per\ SV = \frac{normalized\ iBAQ\ amount\ of\ X\ protein}{normalized\ iBAQ\ amount\ of\ synaptophysin} * 32$$

… Equation [1]

The assumption that the copies of synaptophysin per brain SV equals to 32 hold true (Takamori et al., 2006), but since there is no such estimate in the literature available for retina SV, it may not be true in the case of our retina SV preparation. For immunoprecipitated SVs, the exact count of the SVs was not known. Also, it is possible that the copy number of synaptophysin per SVs of retina might not be equal to that of brain. Thus, depending upon the variation of synaptophysin amounts in retina and brain samples, the analysis of results will vary accordingly.

Correlation is a broad class of statistical tool to determine dependence. The coefficient of correlation (R^2) determines the degree of correlation. The closer is the value of coefficient of correlation to 1; the stronger is the correlation between

the two comparing parameters. For comparing the copies/stoichiometry of proteins present in brain and retina SVs, the proteins with missing values for copy numbers either for brain or retina were deleted from the list and a scatter-plot was plotted (fig. 3-13).

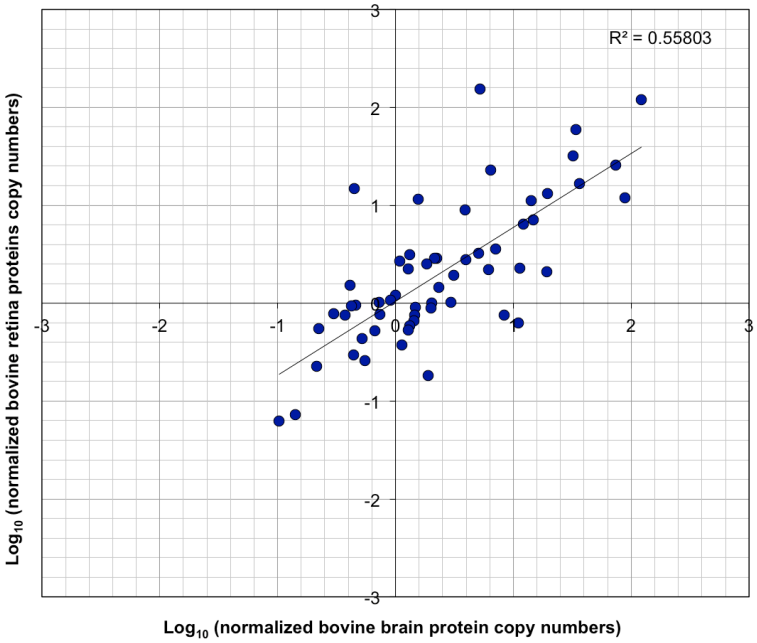

Figure 3-13: Correlation of copy numbers of SV proteins present in bovine brain and retina. Scatter-plots showing correlation of the copy numbers of various proteins identified from immunoprecipitated SVs of bovine brain (x-axis) and retina (y-axis). The coefficient of correlation, R^2 improved from 0.32 (data not shown) to 0.55 (fig. 3-14), when the retina proteins with missing values were deleted.

It is interesting to note that there is a poor correlation in the copy numbers of proteins present in retina and brain. Although, some proteins show similar copies per retina and brain SV, however, the majority of the proteins vary in their copy number in the two tissues; retina and brain. Apparently, these deviations might be because of differences in the two kinds of synapses.

The comparison of synaptic proteins has been discussed in detail in later section (section 3.2.2). The list of copy numbers of rest of the proteins from this study are listed in table (table 3-2 to 3-5; appendix A3 and A4)

3.2.2 Synaptic protein copy numbers per SV

SV is the best-studied organelle in terms of protein composition. Almost a decade ago, in-depth proteome analysis of rat brain SV was accomplished. In addition, 14 SV proteins were quantified using quantitative western blotting (Takamori et al.,

2006). In our study, we identified a total of 86 SV proteins out of which 77 and 33 were identified in brain and retina respectively. These proteins contributed around 28% and 24% of the total protein amount immunoprecipitated from bovine brain and retina respectively (fig. 3-12a, b, c, d; orange colour).

Finally, we compared the ratios to correlate the corresponding copy numbers. By this analysis, we determined the copy numbers of those proteins whose copy numbers were previously determined (Takamori et al., 2006).

We used the protein copy number from Takamori et al., as a reference for our study. The SVs from rat brain were purified following the classical isolation protocol (Takamori et al., 2006) and were analysed using FCS for counting the SVs followed by iBAQ mass spectrometric analysis (section 3.4.1). The protein copy numbers of rat brain (Takamori et al., 2006) and bovine brain may or may not correlate because of differences in species (rat versus bovine) and/or use of different techniques (quantitative western blot versus iBAQ mass spectrometry) for protein quantitation. It was observed that the estimation of abundances by iBAQ-MS and quantitative western blotting correlates remarkably well (fig. 3-31, 3-32). This observation was also reported previously (Schwanhausser et al., 2011). Thus, the protein copy number correlation between bovine brain and bovine retina will truly reflect the proteome differences in the two differentially located neuronal cells.

A scatter-plot that compares the copy numbers of known SV proteins in rat brain and bovine brain (fig. 3-14a) suggested that the protein copy number of rat brain and bovine brain SV strongly correlate. Similarly, a scatter-plot for bovine brain and retina SV proteins was drawn to compare the SV proteome of bovine brain and retina (fig. 3-14b). The correlation suggests that the quantitative proteome of bovine retina SV is similar to brain SV.

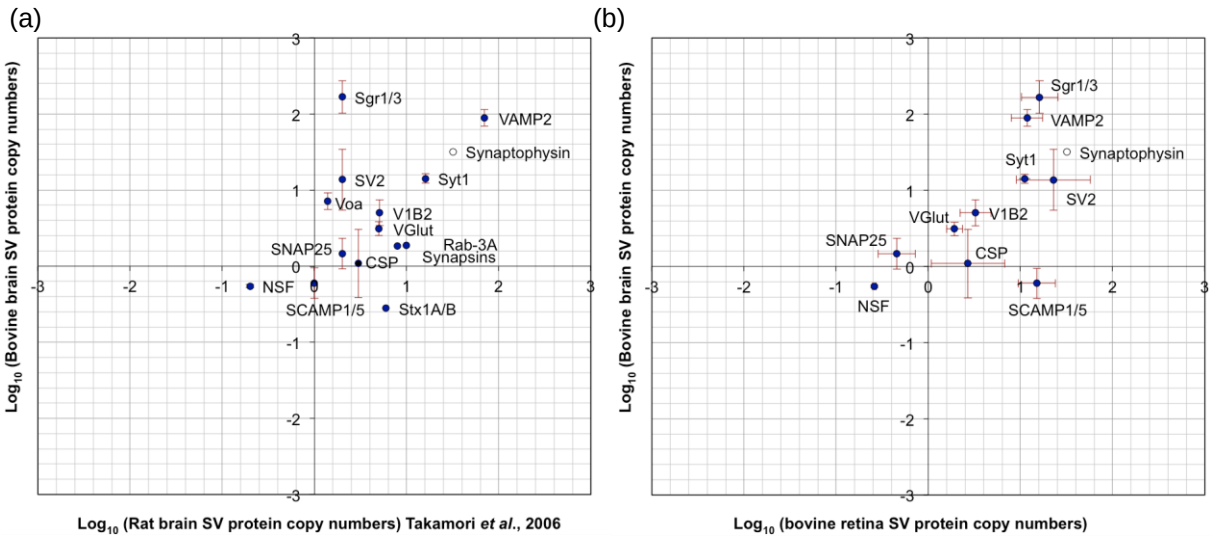

***Figure 3-14: Comparison of protein copy number per SV*.** Scatter plot depicting the correlation of SV proteins from (a) rat brain from Takamori *et al*., 2006 study versus bovine brain from our data with $R^2 = 0.79$, and (b) bovine brain versus bovine retina with $R^2 = 0.43$. Each protein is represented as a *dot*. All the deep blue coloured dots are synaptic proteins, while the white dot represents synaptophysin. The amount of synaptophysin was kept constant for brain and retina SVs.

The copy number of proteins obtained from this study for bovine retina and bovine brain SV and previously published protein copy numbers for rat brain SV were inspected individually to compare the differences and similarity in proteome of SV. According to their different classes and functions, the SV proteins have been sub-classified into various categories as mentioned below (see discussion 4.1.2, 4.1.3 and 4.1.4).

3.2.2.1 SV-integral proteins

Fig. 3-15 shows the comparison of protein copy number of integral SV proteins from bovine brain, bovine retina (present study) and previously published rat brain (Takamori et al., 2006).

The exact function of synaptophysin is not yet known, however, it is suggested that it might play a role in maintaining the curvature of the SV (Thiele et al., 2000). In present iBAQ-MS absolute protein amount analysis, it is assumed that the copies of synaptophysin present on bovine brain SV and retina SV is constant (32 copies). Thus, it is difficult to conclude any information about synaptophysin.

VAMP2 is a SNARE forming SV membrane protein. It is the most abundant protein (70 copies) present on rat brain SV. Our iBAQ-MS quantification data shows the presence of approximately 90 copies of VAMP2 present on bovine brain SV. Similar to the rat brain SVs, VAMP2 remains the most abundant proteins in bovine

brain SV. However, the absolute amount of VAMP2 is drastically low in bovine retina SV. Our data suggests around 12 copies of VAMP2 present per retina SV. VAMP2 is an essential protein that forms the synaptic exocytic SNARE complex with syntaxin and SNAP25. It is possible that the 10 copies of VAMP2 present on retina SV may be just enough for forming the exocytic SNARE complex. In addition, it is also possible that there may be existence of other protein that may replace the role of VAMP2 to form ribbon exocytic SNARE complex.

The ratio of synaptophysin-to-synaptobrevin (syp-to-VAMP2) in the previously published rat brain SV is 1:2. Our data from iBAQ quantification shows 1: 2.8 for syp-to-VAMP2 in Bovine brain SVs, which suggests that this ratio is also maintained in bovine brain SVs. Despite well-established functions of these two proteins, the significance of such ratio maintenance is not known. Remarkably, we find that in bovine retina, this ratio is inversed to make it 3:1 (instead of 1:2 as observed in the rat brain) (section 3.4.1). Of note, this is the first report of such a drastic differences in the ratio of these proteins observed, however, our data does not explain the significance of such a reverse ratio on the molecular function.

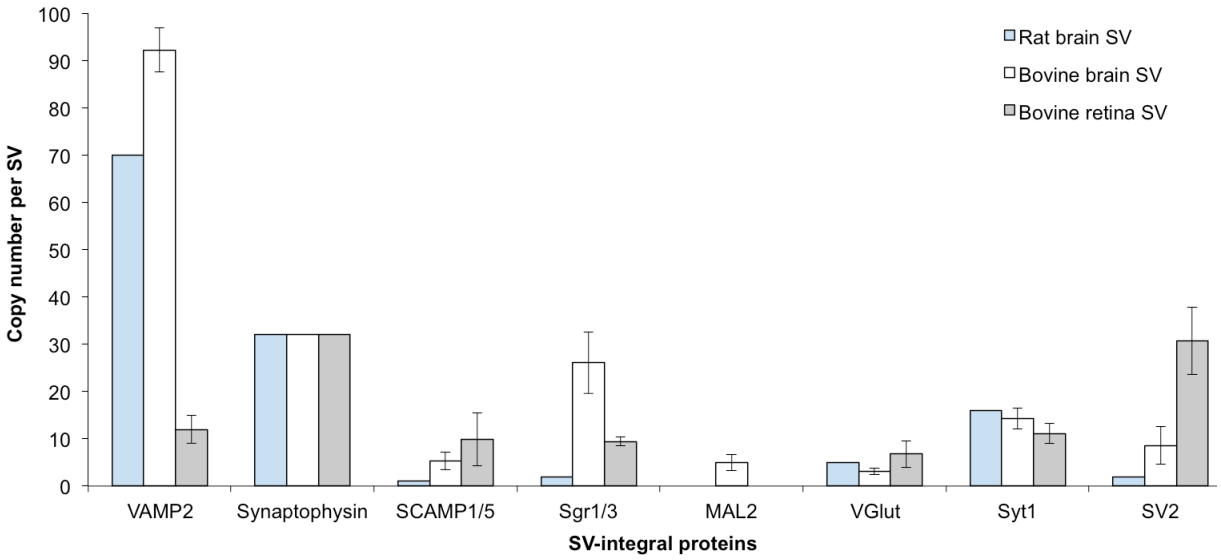

Figure 3-15: ***Comparison of copy numbers of various SV-integral proteins in bovine brain, retina and rat brain per SV.*** Histogram representing the absolute amounts of SV-integral proteins calculated for rat brain SVs (blue columns, Takamori *et al*., 2006) by quantitative western blotting, bovine brain SV (white column) and bovine retina SV (grey columns) by iBAQ-MS.

Tetraspanin family of proteins contain integral membrane proteins with four transmembrane domains including synaptophysin (syp), secretory carrier-associated membrane proteins (SCAMPs), synaptogyrins (sgr) and MAL2. Like synaptophysin, the exact function of synaptogyrin is also not known. There are 2 copies of synaptogyrin protein reported previously for rat brain SV by quantitative

western blot (Takamori et al., 2006). Our data shows presence of ~14 copies and 7 copies in bovine brain and retina SVs for synaptogyrin1. In addition, 11 and 2 copies of synaptogyrin3 were identified in bovine brain and retina SVs respectively. SCAMPs function as carriers for post-golgi recycling pathway and help in endosomal sorting and maintaining the integrity of the SV (Singleton et al., 1997). SCAMPs were found to be present in low (two) copies previously as well as in our data. We quantified approximately similar amounts of SCAMP proteins present on bovine brain (~3 copies for SCAMP5 and ~1 copy for SCAMP1) and retina (~8 copies for SCAMP5 and 1 copy for SCAMP1) SVs.

MAL2, a tetraspanin protein, has been recently identified as integral brain SV protein. It is a component of lipid raft and functions in intracellular transport pathway to deliver membrane bound proteins (Gronborg et al., 2010). It is interesting to note that MAL2 was found only in brain with 5 copies and not in retina SV proteomic analysis (fig. 3-15).

Another class of proteins present on SV are transporters. This includes Vesicular Glutamate transporters (VGlut1/2/3), Synaptic vesicle transporter-2 (SV2A/B/C), vacuolar proton pump (vATPase), SVOP and Zinc transporters Znt3.

VGluts are responsible for uptake of glutamate in excitatory synapses. The retina synapses are mainly excitatory (Pereda, 2014). Brain mainly contains isoforms VGlut1/2 (Herzog et al., 2006; Takamori et al., 2000, 2001), while VGlut3 is known to be predominantly present at auditory systems like hair cell (Ruel et al., 2008; Takamori et al., 2002). The antibody used for quantitative western blotting of rat brain SV was not specific for its isoforms, thus the copy number given for rat brain SV i.e. 10 copies, is the sum of copies of VGlut1/2 isoforms. We quantified 3 copies and 6 copies of VGlut1 present on bovine brain and bovine retina SVs. Unfortunately, we did not quantify the other isoform VGlut2 in bovine brain as well as retina.

SVs contain vacuolar ATPases, integral to its membrane. They are responsible for transport of proton inside the SV lumen. These are called vATPase, consist of many subunits: the V0 subunit is transmembranous while the V1 is cytoplasmic forming a ‘cap like structure’ (fig. 3-16). vATPase pumps proton inside the lumen of the SV to generate the membrane potential. The generated membrane potential drives the influx of various neurotransmitters like glutamate by their respective transporters (VGlut for glutamate) into the SV lumen.

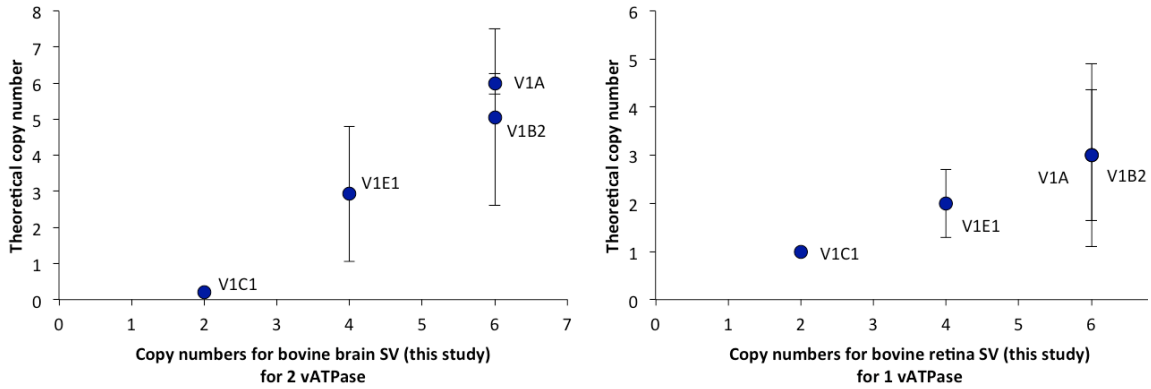

Figure 3-16: Schematic comparison of copy numbers of various subunits of vATPase complex for 1 and 2 copies of bovine brain and retina SV. Scatter-plot comparing the theoretical copies (y-axis) and copies obtained by iBAQ-MS (x-axis) for bovine brain *(left)* and retina *(right)*.

In literature, the stoichiometry of vATPase has always been mentioned to be definite (Harvey et al., 1992) (Finbow and Harrison, 1997; Muench et al., 2011). The VoA subunit of vATPase is a membrane protein present in one copy per protein complex. The hydrophobic peptides obtained from membrane proteins are difficult to solubilize and ionize in the mass spectrometer. The huge standard deviation in VoA proteins might be because of inefficient extraction of peptides in different preparations. The cytosolic or the cap region of vATPase protein contains 3 copies of V1A as well as V1B sunbunit. The amount of vATPase present on rat brain was quantified to be 1-2 copies. In order to compare the theoretical and the absolute amounts of various subunits of vATPase, a scatter-plot was drawn (fig. 3-16). Our data suggests presence of 1 and 2 copies of vATPase present on bovine retina and brain SV respectively. The theoretical and experimental amounts of various subunits of vATPase correlate well.

SV2s are another class of transporters present integral to SVs. They contain 12 transmembrane regions. However, the exact molecule that the protein SV2 transports is not yet clear. We observed ~6 copies for SV2A and ~2 copies for SV2B per bovine brain SV, while it remained 2 copies for SV2B but increased to 27 for SV2A per bovine retina SV. However, SV2C was not at all quantified in our data.

For some proteins, we identified the copy number values in fractional numbers below 1. In principle, the copy number given in fractions is practically possible only when a little population of SVs contains this protein. Zinc transporter- Znt3 was found to be present in 1 copy per bovine brain SV, while we quantified 0.2 copies for retina SV. Similarly, synaptoporin, a tetraspanin, we quantified 0.9 and 0.8 copies on SVs of bovine brain and retina respectively (table 3-2). The inhibitory

synapses, glycine is the major component of SVs, which is transported by Vesicular inhibitory amino acid transporter (VIAAT or VGAT). We quantified 0.4 copies and 0.9 copies of VIAAT per SV derived from bovine brain and retina respectively (table 3-2).

Table 3-2: Copy numbers of SV proteins quantified by iBAQ-MS. List of SV proteins with their quantified copy numbers and standard deviations of three biological replicates in bovine brain and retina.

SV protein					
ID	PROTEIN NAME	COPY NUMBER BRAIN SV	σ	COPY NUMBER RETINA SV	σ
SLC32A1	VIAAT	0.42	0.28	0.93	0.43
SYNPR	Synaptoporin	0.90	0.88	1.48	0.64
ZNT3	Zinc transporter 3	1.30		0.28	

Another class of SV-integral proteins includes synaptotagmins. These are calcium sensors and function in calcium evoked SV fusion. The C2A domain binds to 3 ions calcium of calcium. Studies show that synaptotagmin1 is present in brain as well as retina, although the amount of synaptotagmin1 is relatively low in retina than brain SV (Von Kriegstein et al., 1999). Our data showed similar copies of synaptotagmin1 for rat brain, bovine brain and bovine retina SVs. We quantified ~14 copies and ~11 copies of synaptotagmin1 on SVs of bovine brain and retina respectively. Only a fraction of synaptotagmin2 was identified for bovine brain SV (0.1 copies); however, it was not at all identified in bovine retina SVs.

3.2.2.2 SV-associated proteins

SV-associated proteins are the proteins that interact with SV for various synaptic processes like exocytosis and endocytosis. It was observed that SV-associated proteins also co-purify along with mice and rat brain SV while isolation. The interactions of various proteins are not transient and thus, a population of SVs enriches its associated proteins. The presence of certain number of copies per SVs does not necessarily mean the presence of these associated proteins on SV. However, it means that certain population of isolated SVs have these associated proteins still adhered. The copy numbers for protein calculated by quantification techniques like quantitative western blotting and iBAQ-MS solely represents an average of copies present for SVs. Therefore, it has to be noted that the actual amounts of these associated proteins can be higher than these calculated copies.

SNARE proteins are SNAP (**S**oluble **N**SF **A**ttachment **P**rotein) **R**eceptor, a family of large proteins approximately 60 members in mammals and yeasts. The primary role of SNARE proteins is to mediate exocytosis of SV. SNAP-25, VAMP2 and syntaxin-1A/B form the exocytic SNARE machinery to induce fusion of SV to the plasma membrane in synapses (Jahn 2006). However, in ribbon synapses of retina, syntaxin1A/B is replaced by syntaxin-3 (Morgans 2006). As mentioned in previous section, SV-integral proteins VAMP2 is present relatively in very low amounts in retina (12 copies) than brain (90 copies) SVs. We observed 1.4 and 0.7 copies for SV-associated proteins SNAP-25, in bovine brain and retina respectively (fig. 3-17). It should be noted that SNAP-25 was quantified with high standard deviation. It has been previously reported to be 2 copies per rat brain SV (Takamori et al., 2006).

In addition, 6 copies of syntaxin-1A/B were quantified per SV of rat brain. We observed only 0.3 and 1.1 copies of syntaxin-1A and syntaxin-1B for bovine brain respectively. Interestingly, we quantified 0.3 and 3.6 copies for syntaxin-1B and syntaxin-3 in bovine retina SVs respectively (fig. 3-17). Syntaxin-1A was totally absent in the bovine brain SVs. It may be concluded that the exocytic SNARE machinery is relatively less prominent: rat brain SVs > bovine brain SVs > bovine retina SVs.

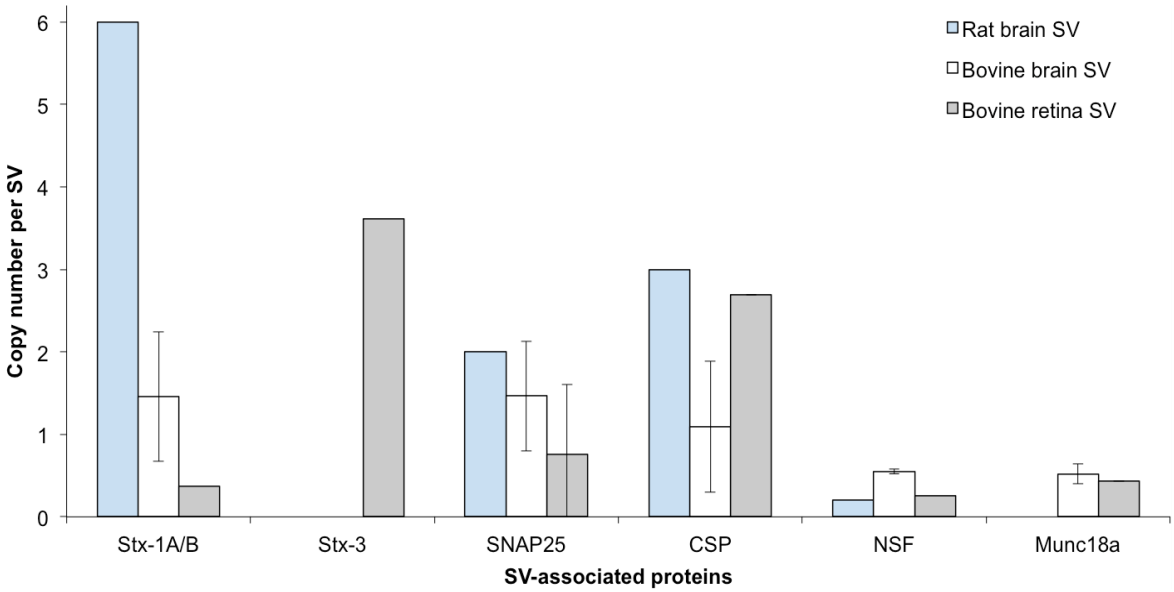

Figure 3-17: ***Comparison of copy numbers of various SV-associated proteins in bovine brain, retina and rat brain per SV.*** Histogram showing copies of SV-associated proteins in rat brain SVs (blue columns, Takamori *et al*., 2006), bovine brain SVs (white columns) and bovine retina SVs (grey columns).

Our data clearly suggests that there are differences in SV proteome of brain with retina. VAMP2 protein, which forms synaptic SNARE complex, is present in very less number on retina SV. The copies of syntaxin and SNAP-25 were very less similar to copies of VAMP2 on retina SV (see discussion 4.1.4).

We quantified priming proteins Munc18a, NSF and co-chaperone proteins cysteine-string protein (CSP); however, these proteins were identified only in one of the replicates of the experiment with retina SV preparation (fig. 3-17). The amount of Munc18a was not determined previously for rat brain. We quantified almost similar amounts of Munc18a 0.5 and 0.4 copies for bovine brain and retina respectively. There are 0.2 copies and 3 copies reported for NSF and CSP proteins in rat brain SV (Takamori et al., 2006). However, we quantified 1 copy and 2.6 copies of CSP protein in bovine brain and retina SV respectively. We quantified almost similar amounts as previously reported for NSF, 0.5 and 0.2 in bovine brain and retina SVs respectively (fig. 3-17).

Presence of SV-associated proteins Rab3 and synapsins is of contradiction in ribbon synapse literature (Mandell et al., 1990; Von Kriegstein et al., 1999). Rab3a was reported to be present in OPL layer of retina by immunolabeling (Ullrich and Sudhof, 1994); however when similar preparation was observed under electron microscopy, it was found that the Rab3a/b/c/d was totally absent in ribbon synapses of retina (Grabs et al., 1996). Similarly, synapsins are reported to be absent in ribbon synapses (Mandell et al., 1990; Von Kriegstein et al., 1999) however, it was reported to be associated to ribbons by western blotting (Schmidt 1999). Presence of synapsin in ribbon synapses was observed to be species-specific. It was concluded that synapsins were absent in OPL layer of murine (rat or mice) while present in bovine retina.

The western blot data shows an absence of enrichment in rab3 during the course of preparation of bovine retina SV (fig. 3-7b). In addition, western blot against synapsin did not show any sign of detection for synapsin specific region. Our western blot data is consistent with the mass spectrometric analysis (fig. 3-18).

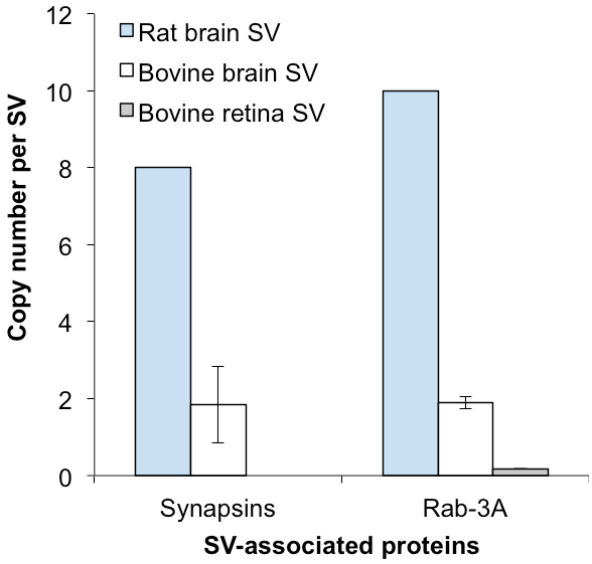

Figure 3-18: ***Copy number of synapsin and rab3a proteins per SV.*** *Histogram representing copies of SV-associated protein: synapsin and rab3a present in rat brain (blue* column, Takamori *et al*., 2006), bovine brain (white column) and bovine retina (grey column) SVs.

We identified rab3a/c and synapsin1/2/3 by mass spectrometric analysis, however; only rab3a and synapsin1/2 were quantified. For rab3a, we quantified only 1.8 copies for bovine brain, while the previously determined copy for rab3 was 8 (Takamori et al., 2006). Interestingly we quantified only 0.1 copies of rab3a in bovine retina. In addition, the rab3a iBAQ amounts quantified in bovine retina SVs for replicates were missing. For synapsins: We quantified 1 copy synapsin1 and 0.6 copy synapsin2 for bovine brain SV. Interestingly, supporting Grabs et al., findings, no synapsin was identified or quantified in bovine retina SVs (fig. 3-18) (see discussion 4.1.5).

Apart from above mentioned SV-associated proteins, we quantified amphiphysin (0.1 copies) and SNAP29 (0.2 copies), only in brain SVs (table 3-3) (see discussion 4.1.5).

Table 3-3: Copy numbers of SV proteins quantified by iBAQ-MS. List of SV proteins with their quantified copy numbers and standard deviations of three biological replicates in bovine brain and retina.

SV protein					
ID	PROTEIN NAME	COPY NUMBER BRAIN SV	σ	COPY NUMBER RETINA SV	σ
AMPH	Amphiphysin	0.11	0.24		
STXBP1	Munc18a	0.52	0.43	0.12	
SNAP29	Synaptosomal-associated protein 29	0.22		0.05151913	

Apart from exocytic SNAREs, docking and priming proteins, various endocytic proteins such clathrin chains, AP-2 complex, dynamin, also interact with the plasma-membrane to form empty SV. Thus, various endocytic proteins also co-purifies with SVs. Table 3-4 shows the copies of various clathrin mediated endocytic pathway proteins for bovine brain and retina per SV (table 3-4). These proteins were although reported to enrich with SVs, however were not quantified (Takamori et al., 2006).

Table 3-4: Copy numbers of SV endocytic proteins quantified by iBAQ-MS. List of SV endocytic proteins with their quantified copy numbers and standard deviations of three biological replicates in bovine brain and retina.

Endocytic proteins					
ID	PROTEIN NAME	COPY NUMBER BRAIN SV	σ	COPY NUMBER RETINA SV	σ
AP2A1	AP-2alpha-2	0.23		0.25	0.036
AP2B1	AP-2beta	1.24	0.097	2.26	0.057
AP2S	AP-2 complex subunit sigma	1.87		0.83	
AP2M1	AP-2mu	1.01	0.040	0.56	0.024
CLHC1	Clathrin heavy chain 1	0.20	0.010	0.15	0.011
SHLB2	Endophilin-B2	0.16		0.07	
SNAP91	synaptosomal-associated protein, 91kD	0.24		0.28	0.019
DNM1	Dynamin-1	1.70	0.587	0.23	

We quantified ~1 copy each for AP-2, clathrin, dynamin1 in bovine brain; however the copies for these proteins were significantly less than one copy in bovine retina.

In addition to synaptic protein, as mentioned earlier, we also quantified certain structural proteins and uncharacterized proteins (table 3-5).

Table 3-5: Copy numbers of bovine SV proteins quantified by iBAQ-MS. List of various proteins with their quantified copy numbers (third column) and standard deviations (fourth column) of three biological replicates.

ID	PROTEIN NAME	COPY NUMBER BRAIN SV	σ	COPY NUMBER RETINA SV	σ
TBB4B	Tubulin beta-4B chain	74.30	53.299	25.54	13.507
TBA4A	Tubulin alpha-4A chain	36.23	20.156	16.61	4.288
	Tubulin alpha-1	19.50	5.237	13.10	6.885
ACTG	Actin, cytoplasmic 2	12.16	4.522	6.41	3.300
	002687307 Tax; Uncharacterized	1.33	0.409	3.12	2.761
MYPR	Myelin proteolipid protein	2.24	30.640	2.86	1.092
TCPZ	T-complex protein 1 subunit zeta	1.29	1.534	2.26	2.248

TUBB2A	Tubulin 2A	19.35	4.076	2.09	2.400
TCPG	T-complex protein 1 subunit gamma	0.41	0.469	1.52	0.984
TCPD	BOVIN T-complex protein 1 subunit delta	1.00	0.578	1.20	1.535
G5E531	T-complex protein 1 subunit alpha	2.03	1.661	1.01	1.672
GNAT1	Guanine nucleotide-binding protein G(t) subunit alpha-1	0.00	0.000	1.00	1.364
TBB5	Tubulin beta-5 chain	2.00	0.590	0.89	1.034
F1MWR8	T-complex protein 1 subunit eta (Fragment)	0.74	0.372	0.77	0.983
GNAO	Guanine nucleotide-binding protein G(o) subunit alpha	8.37	5.489	0.75	2.169
GBB1	Guanine nucleotide-binding protein G(I)/G(S)/G(T) subunit beta-1	2.34	1.22	1.31	0.86
TBB3	Tubulin beta-3 chain	11.10	5.202	0.63	0.781
TBB4A	Tubulin beta-4A chain	1.32	1.034	0.59	0.430
ACTR1A	001180177;XP	0.67	0.442	0.52	0.422
F1MFT4	Uncharacterized protein (Fragment)	0.00	0.000	0.51	0.351
DYNC1H1	001193067;XP	0.14	0.029	0.07	0.182
REFSEQ:XP	opioid-binding protein/cell adhesion molecule-like, partial	0.10	0.073	0.06	0.082

It is interesting that lot of actin and tubulin isoforms are found associated with the brain as well as retina SVs. In addition, we observe myelin proteins in our preparation (table 3-5, appendix A3 and A4). Myelin proteins are well known sticky proteins that tend to contaminate most of the synaptic preparations. The only way to avoid myelin contamination is working with very young animals (2 months mice or rat) for synaptic preparations. Since, our preparations are from bovine brain and retina, which were raised primarily for slaughterhouse purpose, myelin contamination was obvious and cannot be avoided.

Another interesting finding in our study was the identification of T-complex proteins. They are molecular chaperones and play important role in cytoskeletal maintenance and neurotransmitter trafficking. Single nucleotide polymorphism in T-complex has been reported to be associated with Schizophrenia in China Han population (Yang et al., 2004).

The next major question was if there is any difference in the proteome-dynamics in the two neuronal tissues over time. Do the two differentially located synapses have differences in the turnovers of synaptic proteins?

3.3 Protein turnover study

Transcription and translation regulate the rate of synthesis of proteins inside the cells, while degradation machineries take care of disposing the unfunctional cellular proteins. The study of rate of synthesis or degradation of proteins in a cell is referred to as protein turnover.

The classical way to determine protein turnover is by metabolic labelling termed as a pulse- chase experiment. In such experiments, a cellular process can be studied is examined by exposing the cells to a labelled compound *(pulse)*, and later the phenomenon is followed by addition of the unlabelled compound *(chase)*. Traditionally, the radioactive isotope containing amino acids was used for pulsing. Recently, the radioactive amino acids has been replaced with amino acid containing stable isotopes in the media known as the pulse Stable Isotope Labelling with Amino-acids in Cell culture (pSILAC). It has been reported to work as good as traditional method (Schwanhausser et al., 2011).

3.3.1 Establishment of pulsed stable isotope labelling in mice (pSILAM)

In synapses, similar to other subcellular compartments, synthesis and degradation are two essential mechanisms contributing to the homeostasis of the cell. Since neurons virtually do not divide and regenerate, the protein homeostasis is crucial for plastic events that are at the basis of brain functioning. Synaptic plasticity is the ability of synapses to maintain their definite function over time.

In order to understand the differences in temporal protein dynamics of retina and brain tissue, we performed a pulse experiment using stable isotope labelled amino acid diet for feeding mice (mammals) (section 2.2.1.4). This experiment was performed in collaboration with Eugenio F. Fornasiero (Prof. Silvio O. Rizzoli group, Uni-Göttingen, Germany).

C57BL/6 strain mice were pulsed with heavy lysine$_6$ containing food (Silantes, Germany) for 1 week, 2 weeks and 3 weeks (section 2.2.1.4). Each time frame was performed for three cohorts of mice to have three independent results. The three time frames were randomly chosen to quantify a wide range of proteins. The mice were decapitated and the brain and retina tissues were dissected (section 2.2.1.1) (fig. 3-19). The brain and retina homogenate were prepared (section 2.2.1.4) and fractionated on NuPAGE gel followed by in-gel digestion (section 2.2.4.2) separately. For in-gel digestion, the endo-protease trypsin was used. Trypsin cleaves the carboxylic end of lysine and arginine while Lys-C cleaves only at the

carboxylic end of lysine (Manea et al., 2007; Schaller et al., 1987; Vickery and Schmidt, 1931). In recent studies, long peptides (>1000 Da) were observed to be difficult to ionize in mass spectrometer; thus, the endo-protease trypsin was preferred to Lys-C in our study. Finally, the digested proteins were analysed on a Q-Exactive-HF mass spectrometer (section 2.2.4.6 and 2.2.4.8). Each sample was injected for LC-MS thrice for accurate quantification. The RAW files obtained were processed by Andromeda search engine (Cox et al., 2011) using MaxQuant (Cox and Mann, 2008) (section 2.2.4.12 and 2.2.4.14). The software identifies the peptides generated by trypsin, however the quantitation is solely dependent on lysine containing peptides for the respective proteins.

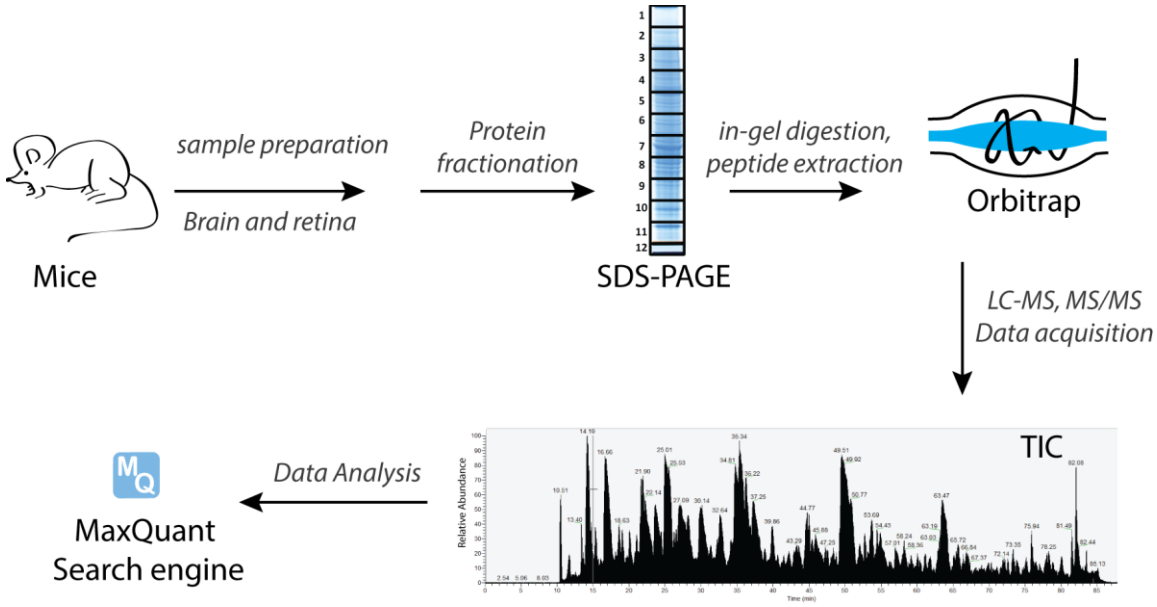

Figure 3-19: ***Schematic representation of workflow for pSILAM*****.** The mice were fed with lysine$_6$ containing food for 5, 14 and 21 days (pulse). At the end of pulse, the mice were decapitated, brain and retina were dissected out and the proteins were fractionated on a Nu-PAGE gel. The gel was cut and digested with trypsin endo-protease. The extracted peptides were run on Q-Exactive-HF on a 88 min gradient. The RAW files were analysed using Andromeda search engine coupled to MaxQuant.

A total of 6489 proteins were identified in the mass spectrometric analysis, out of which only 3843 proteins were quantified by the mass spectrometric analysis. The half-life of all the quantified proteins present in both in retina as well brain was calculated by using following formula:

$$T_{1/2} = \frac{1}{2}\left[\frac{(t * log_2)}{\{log_{10}(1+X)\}}\right] \quad [2]$$

where,

$T_{1/2}$ = half-life of protein in days,

t = time duration of pulse in days,

X = (H/L) or heavy-to-light-ratio.

Out of the 3843 proteins, only 1889 proteins were quantified in retina as well as brain. The average half-life of proteins in brain and retina were measured to be 13 and 11 days respectively. It may be hypothesized that the faster turnover in retina for above-mentioned proteins might be a result of combined peptides obtained from conventional as well as ribbon synapses of retina.

In order to compare the protein turnovers in the two tissues, the difference of protein half-life in retina over brain was calculated (fig. 3-20). fig. 3-20 shows distribution of protein turnover differences in retina over brain for 1889 proteins. It is interesting to note that some proteins have high protein turnover in brain (fig. 3-20; protein id (x-axis) 1 to 200), while the majority of the proteins show higher turnover in retina than brain (fig. 3-20; protein id (x-axis) ~700 to 1889). In addition, some proteins show almost no difference in their half-lives despite of their locations (brain or retina) (fig. 3-20; protein id ~200 to ~700).

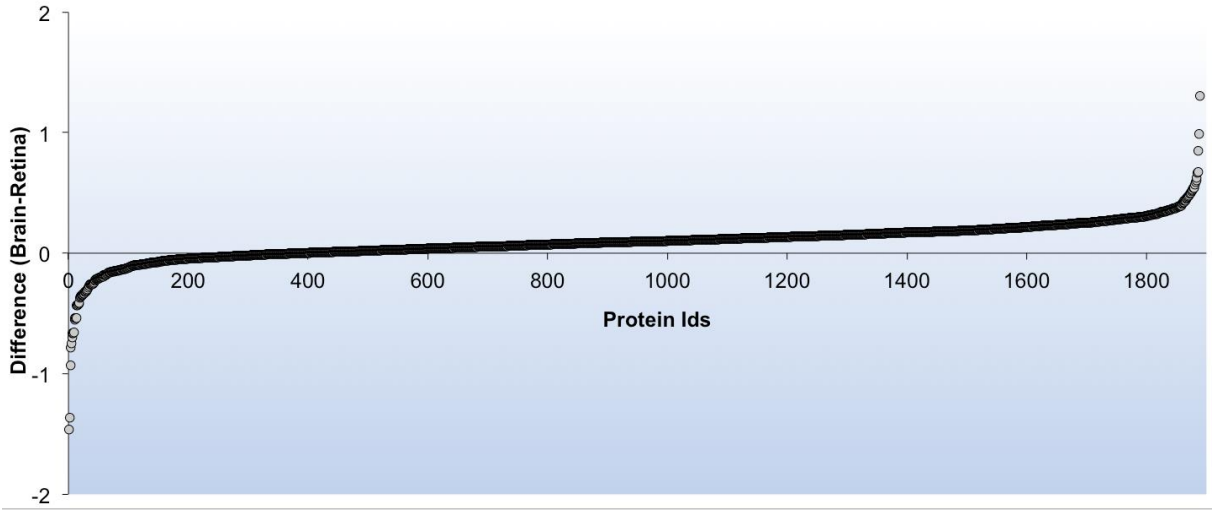

Figure 3-20: ***Distribution of proteins in brain and retina.*** The scatter-plot represents the distribution of number of retina proteins (x-axis) with their difference in turnover (in days) with respect to their turnovers in brain.

In addition, to decipher the differences and similarities between protein turnovers of two distally located nervous tissues; a scatter plot was drawn using the logarithm values of the proteins quantified in retina and brain (fig. 3-21). Each dot in the scatter plot represents a protein, representing its turnover in retina (corresponding x-axis value) and in brain (corresponding y-axis value). This scatter plot was drawn only for 1889 proteins that were quantified in retina as well as in brain. The proteins quantified exclusively in brain or retina were not considered in the scatter plot because of their missing x- or y- axis values.

The coefficient of correlation (R^2) has a value of 0.47. The R^2 value close to 1 is a sign of highly correlating properties. There is a correlation between turnover of proteins present in retina and brain; however, it is does not show a good correlation.

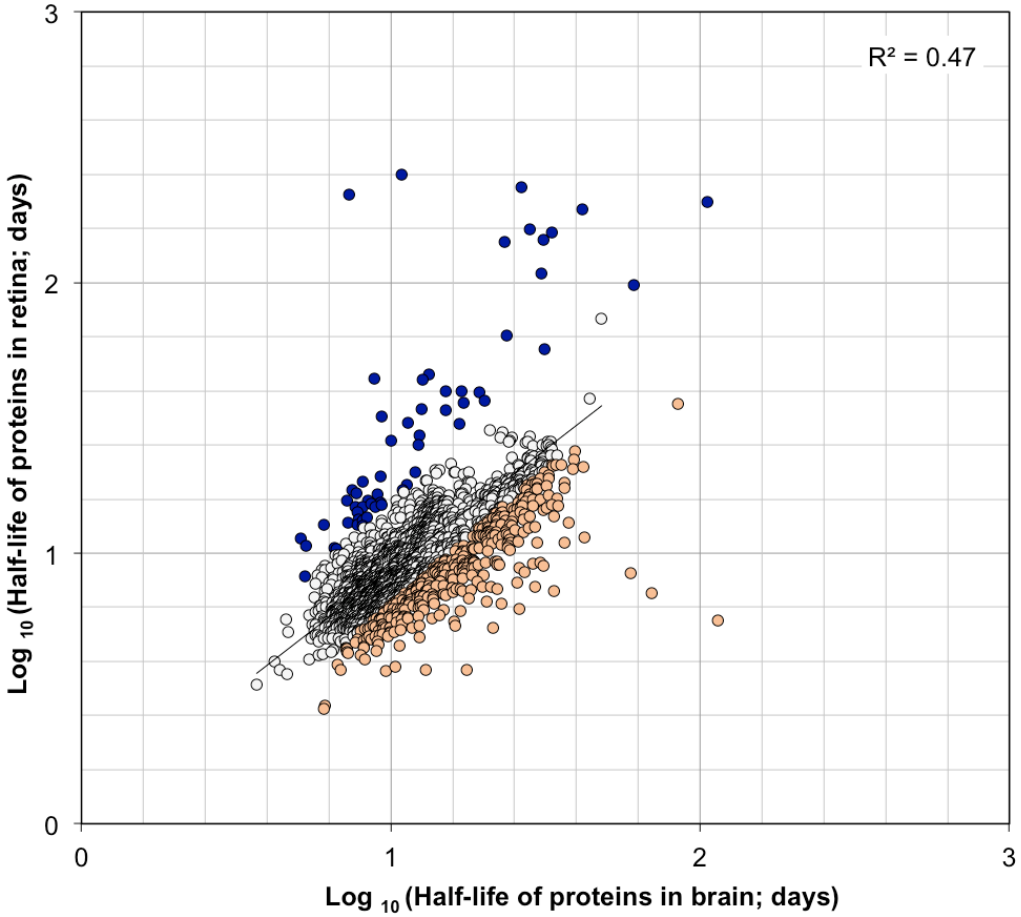

Figure 3-21*: Correlation curve of turnovers of brain and retina proteins from mice*. A scatter-plot representing the half-lives of proteins obtained from mice brain (x-axis; logarithm) and retina (y-axis; logarithm), (R^2 = 0.47). Each dot in the plot represents a protein. For specific proteins, the corresponding x-axis value represents its half-life in brain, while y-axis represents its half-life in retina. The proteins in the scatter plot are coloured differently on the basis of the following criteria: proteins with half-life faster in retina than brain (colour-orange; threshold ≥5 days), similar half-life (colour-white; threshold within 5 days) and half-life faster in brain than retina (coloured-blue; threshold ≥5 days).

Majority of the proteins have almost the same turnover rates in retina and brain (fig. 3-21, white coloured dots). This includes the proteins that will not have any difference in their stability or activity despite being brain neuron or retina neuron in origin. This includes proteins like albumin, haemoglobin (blood), neuroligin, neuronexin (synaptic structural protein but do not play role in synaptic processes) and house-keeping proteins. In addition, it also includes spliceosomal, ribosomal, nuclear and mitochondrial proteins. Interestingly, the vacuolar proton pump of synapse was also observed to have similar half-life (~11 days) in brain and retina.

Apart from the similar half-life proteins in brain and retina, there are some proteins that have higher half-life in retina than brain or vice-versa (fig. 3-21, fast lifetime in brain – blue coloured dots; fast lifetime in retina – orange coloured dots). The majority of proteins with faster turnover in brain mainly include spliceosomal proteins (fig. 3-21 blue coloured dots).

A major population of brain proteins shows an overall slower turnover when compared to the retina (fig. 3-21 orange coloured dots). In other words, the protein turnover is faster in retina than brain.

3.3.2 SV protein turnover

In the proteins list that we considered, we quantified more than hundred synaptic proteins. In order to understand the differences in synaptic protein turnover in the two tissues (retina and brain), the half-lives of synaptic proteins were compared. It should be noted that the major population of synaptic proteins is shifted towards the x-axis (fig. 3-22).

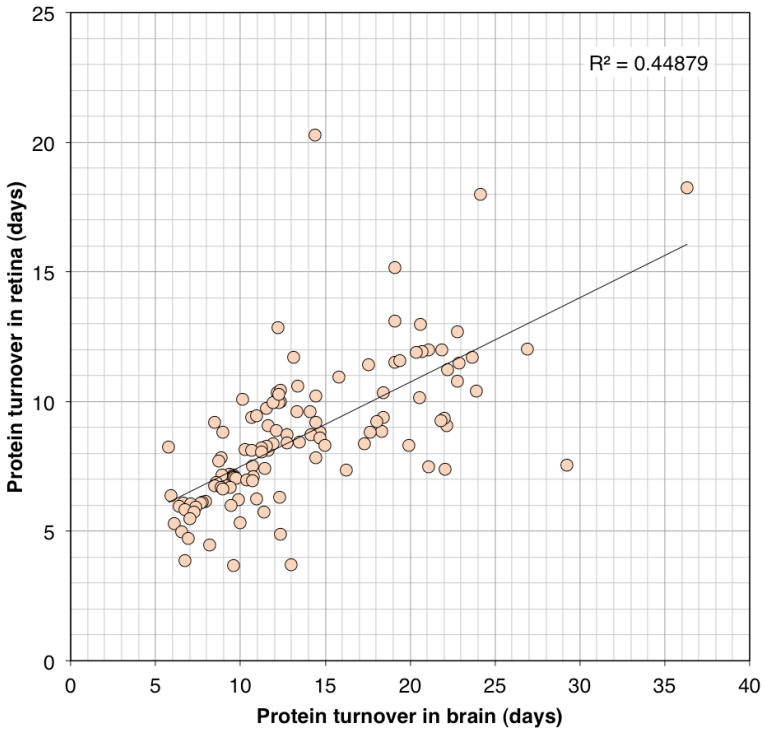

Figure 3-22: ***Correlation curve of turnovers of brain and retina synaptic proteins from mice.*** Here shown is a scatter-plot representing the half-lives of synaptic proteins obtained from mice brain (y-axis; logarithm) and retina (x-axis; logarithm). The half-lives were calculated. Each dot in the plot represents protein. For specific proteins, the corresponding x-axis value represents its half-life in brain while y-axis represents its half-life in retina. The synaptic protein half-lives in brain and retina shows a poorly correlated with the coefficient of correlation (R^2) equals to 0.44. The correlation coefficient suggests that most population of proteins have faster turnover in retina than brain.

In addition, most of the synaptic proteins have their half-lives distributed from 4 to 30 days in brain, while the half-lives of most of the synaptic proteins is restricted to 20 days in retina (fig. 3-23). The average half-life of overall proteins in brain and retina is 13 and 11 days respectively, Interestingly, the average half-life for synaptic proteins in brain remains 13 days while decreases in retina to 9 days.

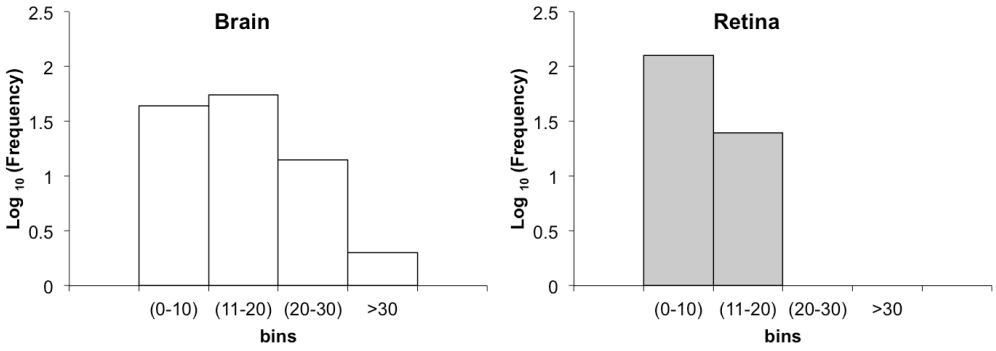

Figure 3-23: ***Half-life distribution of the synaptic proteins*****.** Histogram representing half-life distribution in brain (left; white column) and retina (right; grey column). The x-axis bins represent half-life of proteins in days.

It is very interesting that all the synaptic proteins show higher turnover in retina than brain with few exceptions. The reason why most of the synaptic proteins show faster turnover in retina than brain is not known, however it may be predicted that the fast exo- and endocytic processes occurring at ribbon synapses may result in higher activity of synaptic proteome, resulting in faster turnover of proteins. Retina synapses are known for sustained, rapid exocytosis of SVs. In particular, the ribbon synapses may undergo exocytosis of ~100 SVs per second. However, in brain synapses this number is limited to 8-10 SV per second. This exo- and endocytic activity of retina and brain has never been reported in reference to protein dynamics.

The synaptic proteins were manually categorized into various functional categories and their turnovers were compared in scatter plot (fig. 3-24, 3-25, 3-26, 3-27,3-28, 3-29, 3-30). The proteins shown in blue dots have almost similar turnover in brain and retina.

3.3.2.1 SV integral membrane proteins

As mentioned previously, SV-integral proteins form the core of SVs, which includes proteins of tetraspanin family, transporter proteins, calcium sensors and fusion machinery proteins. fig. 3-24 shows the protein turnover of integral SV proteins in brain and retina.

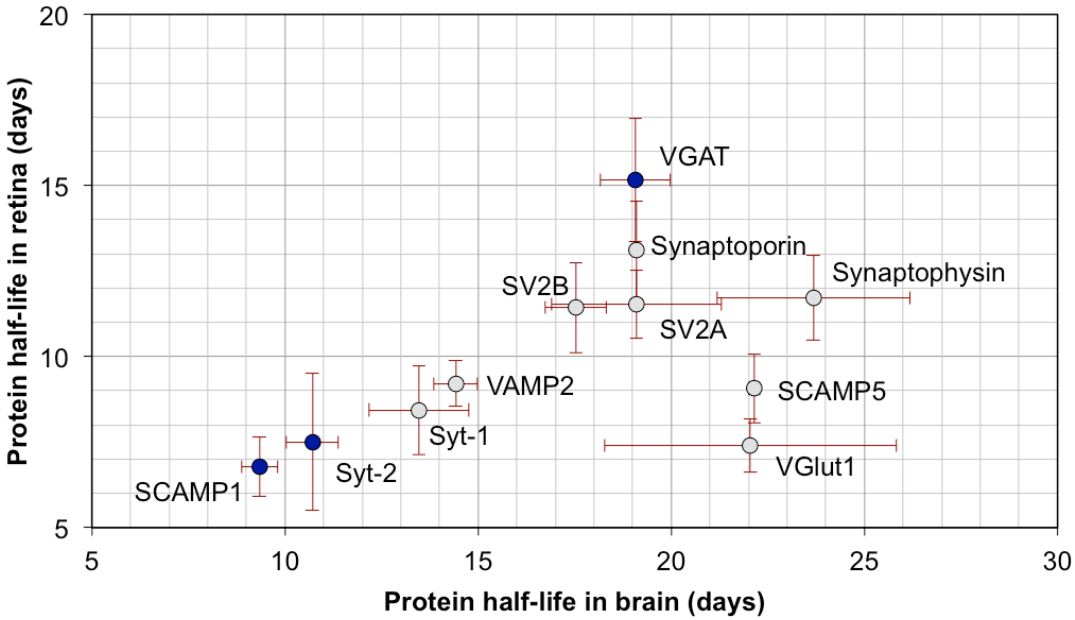

Figure 3-24: ***Scatter-plot depicting protein half-life of integral SV proteins in brain and retina.*** Comparison of turnover of SV-integral proteins present in brain (x-axis) and retina (y-axis). The protein denoted in blue coloured dots do not have significant difference in their turnover in brain and retina.

Our data shows that turnover for tetraspanin proteins like synaptophysin, synaptoporin and SCAMP5 have almost two-fold faster turnover in retina than brain (fig. 3-24).

The retina synapses are majorly glutamergic (Pereda, 2014; Wassle, 2004). The Vesicular glutamate transporters (VGlut) and vesicular inhibitory amino acid transporters (VIAAT/VGAT) are responsible for transporting glutamate and glycine inside the SV lumen respectively. Our data shows almost four-fold faster turnover in retina for VGlut1 than in brain (fig. 3-24). On the other hand, there is no significant difference in the turnover of VIAAT/VGAT in retina and brain (fig. 3-24).

Our data for the membrane glycoprotein SV2 protein turnover of SV2 isoforms is almost 1.5 times faster in retina than brain. It should be noted that the amount of newly synthesized SV2A/B is almost twice in retina than brain over time.

Another class of membrane proteins present on SV are synaptotagmins (Syt1/2), which are calcium sensors. Our data suggests that the synaptotagmin1 has ~1.2 times faster turnover in retina than brain. However, its isoform synaptotagmin2 does not show any significant difference in turnover in brain and retina (fig. 3-24).

As mentioned previously, our data shows that the vATPase complex has similar turnover in retina and brain. Not only the turnovers of the protein complex in two nervous systems (brain and retina) is similar, but its subunits: cytosolic and transmembrane, also show similar turnovers (see discussion 4.2.1).

The reason for similar turnover for some proteins like synaptotagmin2, VGAT and vATPase and faster turnover of other set of SV-integral proteins such as SCAMP5, synaptophysin, VGlut1, SV2; in retina than brain, has not been investigated so far.

3.3.2.2 Active zone proteins

Docking is a key event that allows the interaction of SVs with the release sites at the active zone. The docked SVs interact with various proteins at active zone. This process allows SVs to interact with the plasma membrane. Primed SVs are ready to perform exocytosis. The following plots show the comparison of turnovers of various proteins that aid in docking and priming at retina and brain synapse (fig. 3-25).

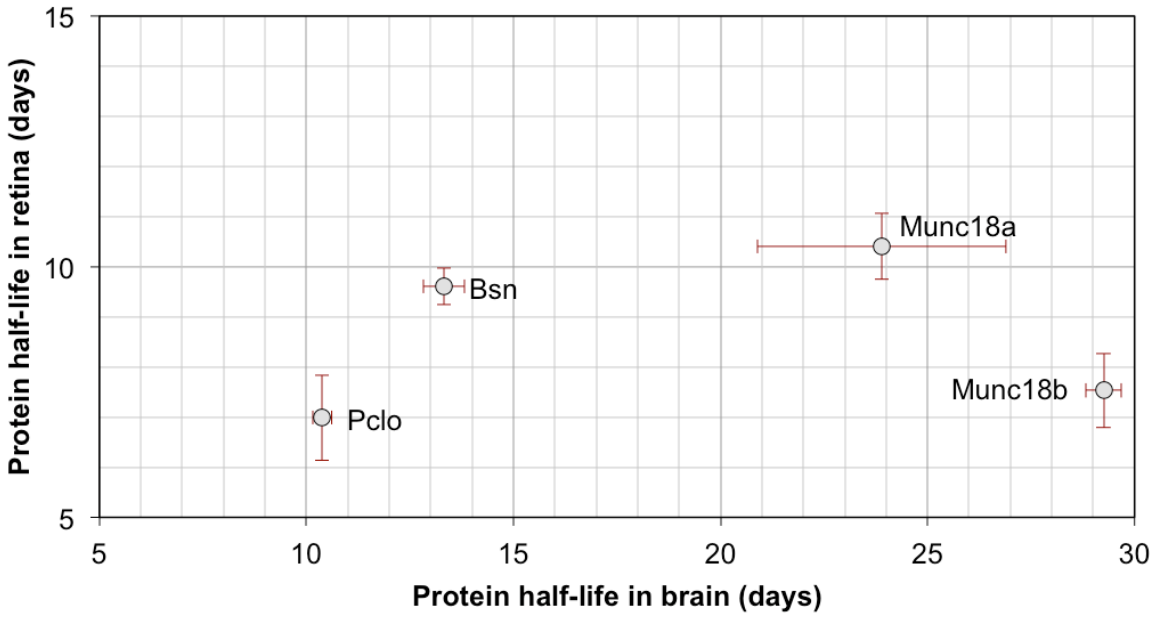

Figure 3-25: ***Scatter-plot of protein turnover of active zone proteins quantified in brain and retina.*** Comparison of turnovers of active zone proteins: Piccolo (Pclo), Bassoon (Bsn) and Munc18a/b in mice brain (x-axis) and retina (y-axis).

Our analysis shows that multi-domain containing large proteins like bassoon (Bsn) and piccolo (Pclo) shows approximately 1.5 times faster turnover in retina than brain. In addition, the priming active zone protein Munc18a/b showed significantly faster turnover in retina than brain. It is approximately two and three times faster for Munc18a and Munc18b respectively. For other active zone proteins like ERC and liprin, there is no significant difference in the turnover in retina and brain.

Proteins like RIM1/2, Munc13a/c are known to be responsible for ATP independent priming. Although we could not quantify most of these proteins, because of absence of one of the SILAC pair (heavy or light labelled peptides) for quantification. For these proteins, with quantification from one of the replicates suggest faster turnover in the retina than in the brain.

3.3.2.3 Synaptic SNARE complex

Synaptic SNARE complex is formed by VAMP2, SNAP-25 and syntaxins. In brain, the SNARE complex utilizes syntaxin-1A/B while in retina it contains syntaxin-3 (Brandstatter et al., 1996b; Morgans, 2000a, b; Morgans et al., 1996).

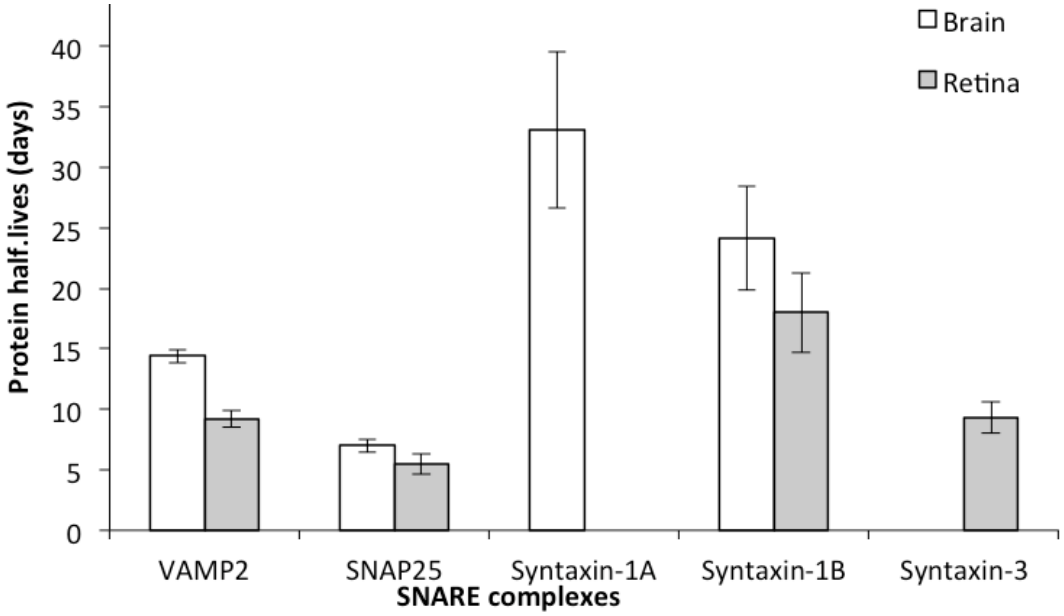

Figure 3-26: ***Comparison of protein turnover of SNARE-complexes of brain and retina*****.** VAMP2, SNAP25 and syntaxin form the synaptic SNARE complex are responsible for exocytosis. In brain, the syntaxin isoforms are syntaxin1A and syntaxin 1B, while in ribbon synapses of retina it is replaced by syntaxin3.

Our data shows that VAMP2 has 1.5 fold faster turnover in retina than brain. There is no significant increase in turnover observed for SNAP-25 (fig. 3-26). Surprisingly, syntaxin-1A was only quantifiable in brain synapses, while syntaxin-1B was observed in brain as well as retina. Interestingly, syntaxin-3 was only quantified in retina. It should be noted that the standard deviations of turnover within the biological replicates for syntaxin1B in brain and retina is not significant (fig. 3-26). This suggests that the syntaxin-1B quantified in retina is due to the presence of conventional synapses (amacrine cells) in retina. As a result of which, its turnover appears to be similar in both the tissues. It may be hypothesized that syntaxin-1B is exclusively present in conventional synapses of retina and thus, its turnover is almost similar in brain and retina (see discussion 4.2.1).

3.3.2.4 Complexins

Another interesting example to dissect the retina and brain proteins is the complexin proteome. Complexin also known as synaphin are a class of proteins, which bind to the SNARE proteins with high affinity. Complexin 1/2 and complexin 3/4 are important in the brain and in the retina respectively (fig. 3-27).

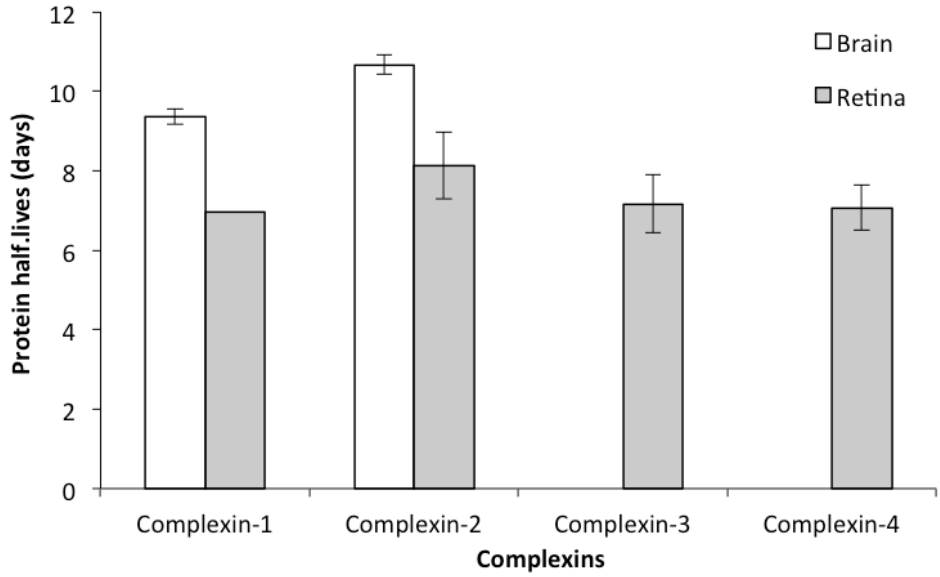

Figure 3-27: Histogram of protein turnover of complexins of brain and retina. Comparison of various isoforms of complexin found in brain (white columns) and retina (grey columns). In ribbon synapses, the complexin 1 and 2 are replaced by complexin 3 and 4.

It is interesting that pSILAM data show presence of complexin 1 and 2 in brain as well as retina while complexin 3 and 4 were quantified exclusively in retina (fig. 3-27). Thus, the complexin 1 and 2 quantified from retina might be as a result of presence of conventional synapses present in retina. Since, it is well known that complexin 3 and 4 are present only in retina, it may be hypothesized that complexin 3 and 4 are present in ribbon synapses of retina (see discussion 4.2.1).

3.3.2.5 Rabs and synapsin family members

Different rab isoforms perform various functions in the cells. For synaptic transduction, rabphilin and rab3 play an important role in triggering exocytosis of SV. Rab3 protein is known to exhibit GTPase activity and aids in priming of SVs. The quantification of rab proteins are represented as a scatter plot (fig. 3-29).

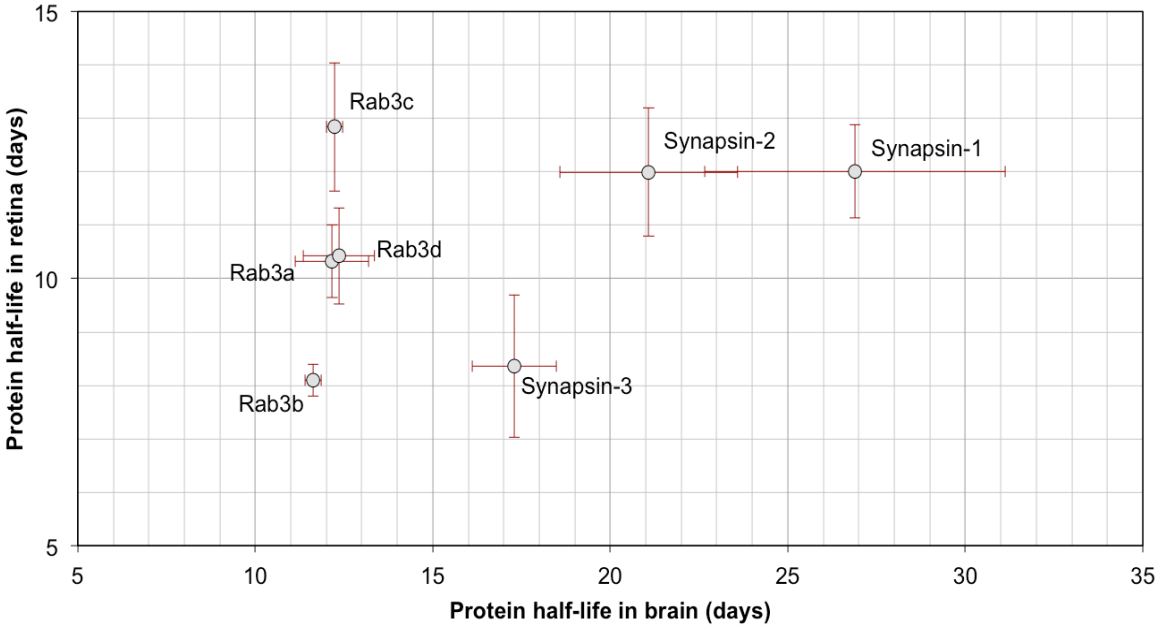

Figure 3-28: ***Scatter-plot of protein turnover of Rab3 and synapsins quantified in brain and retina.*** Scatter-plot showing the protein turnovers of various Rab proteins quantified in brain (x-axis) and retina (y-axis).

From our pSILAM data, it was observed that most of the rabs including rabphilin, rab3a/b/c/d shows almost similar turnover in retina than brain. The existence of Rab3a/b/c/d in ribbon synapses is a debated issue. According to Ulrich and Südhof (1994), rab3a was found to be present in retina while later Grabs and collaborators (1996) concluded its absence in the ribbon synapse (Grabs et al., 1996; Ullrich and Sudhof, 1994). In our isolated SVs from bovine retina, we did not observe enough amounts of Rab3a to quantify i.e. less than one copy per bovine retina SV (section 3.2.2.2, fig 3-18). However, we do identify and quantify rab3a/b/c/d in the homogenate of mice retina. Thus, it could be possible that rab3 is present only in the conventional synapses of mice retina and thus, represent almost similar protein turnover in retina and brain. The pSILAM data suggests that the rab3 isoforms do not have any significant differences in retina and brain (fig. 3-28) (see discussion 4.2.1).

Similar to Rabs, the presence of synapsin family members in ribbon synapses has been debated. It was reported that synapsins are absent in murine (mice or rat) ribbon synapses (Geppert et al., 1994; Mandell et al., 1992; Mandell et al., 1990). Later, it was reported that presence of synapsin in retina is species specific. It was found by immunostaining that synapsins are absent in murine retina OPL (section 1.1.1.2) but present in bovine retina OPL (section 1.1.1.2). However, our pSILAM data shows presence of synapsins in the retina (fig. 3-28). Similar to Rabs, overall

synapsin isoforms do not show differences in their turnovers between retina and brain. A single exception to this is synapsin 3, which showed a faster turnover in the retina than in the brain.

3.3.2.6 Key proteins responsible for endocytosis of SV

As explained in the introduction (section 1.1.1.1.2), there are 4 modes describing endocytosis of SVs. The clathrin-mediated pathway is the most explicitly studied endocytic pathway. Various proteins like clathrin, the AP2 complex, epsin and dynamin aid during the endocytosis of empty SV at the pre-synapse.

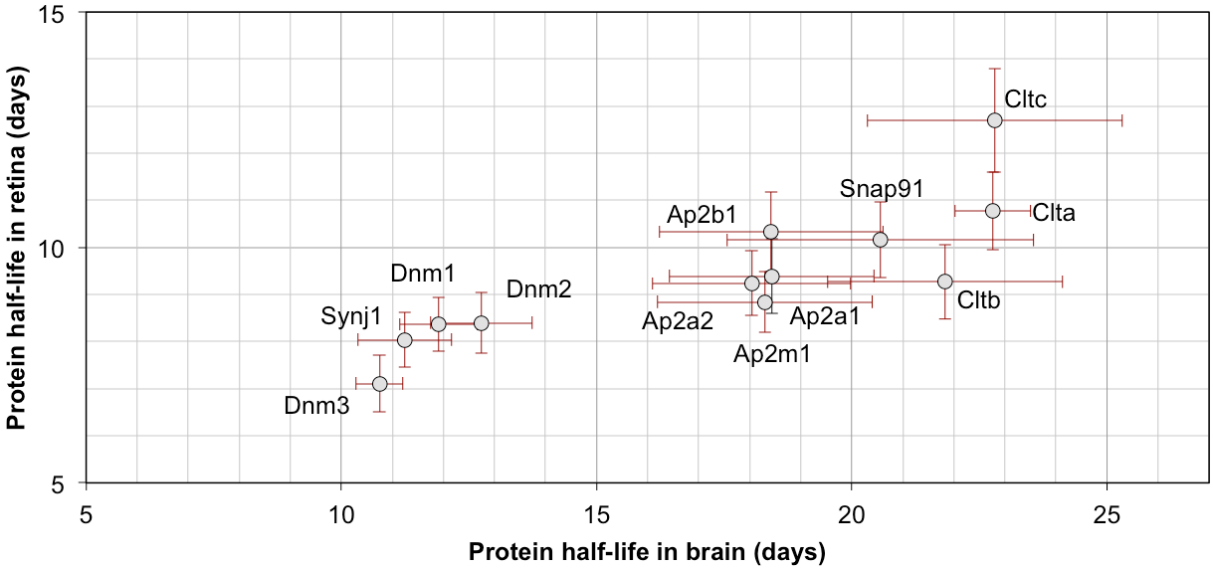

Figure 3-29: ***Scatter-plot of turnovers of clathrin-mediated endocytic proteins quantified in brain and retina.*** Comparison of turnovers of various endocytic proteins: clathrin-complex, AP-2 complex, dynamin isoforms and SNAP91 in brain (x-axis) and retina (y-axis).

Our data suggests that the turnover of AP-2 subunits, clathrin (Clt a/b/c) subunits, dynamin isoforms (Dnm 1/2/3) and SNAP91 are faster in retina than brain (fig. 3-29). Interesting, the subunits of complexes like AP-2 (Ap2a1, Ap2a2, Ap2b1, Ap2m1) have almost similar turnovers in a given tissue (~17 days in brain and ~9 days in retina). In addition, the turnover of AP-2 complex is around 1.5 times faster in retina than brain (fig. 3-29). The similar turnover of AP-2 subunits, clathrin chains in a given tissue supports the hypothesis that the different subunits of a multi subunit protein are synthesized together (Price et al., 2010).

3.3.2.7 Retina specific proteins

Apart from above-mentioned retina specific proteins: syntaxin-3, complexin 3 and 4, RIBEYE is known to be present only in ribbons (section 1.1.1.2.1). RIBEYE is difficult to analyse using our data because its sequence is so far not available in the genomic library for any of the species. RIBEYE protein is known to have two domains: A and B domain. The sequence of A domain of RIBEYE is not sequenced. However, the sequence of B domain is known to be homologous with the sequence of a nuclear co-repressor protein called C-terminal binding proteins or CtBP2 that is also expressed in neurons (fig. 3-30a) (Schmitz, 2009; Schmitz et al., 2000).

(a) FASTA sequence of CtBP2 protein (UniProt; mice)

```
10    MALVDKHKVK RQRLDRICEG IRPQIMNGPL HPRPLVALLD GRDCTVEMPI
51    LKDLATVAFC DAQSTQEIHE KVLNEAVGAM MYHTITLTRE DLEKFKALRV
101   IVRIGSGYDN VDIKAAGELG IAVCNIPSAA VEETADSTVC HILNLYRRNT
151   WLYQALREGT RVQSVEQIRE VASGAARIRG ETLGLIGFGR TGQAVAVRAK
201   AFGFSVIFYD PYLQDGIERS LGVQRVYTLQ DLLYQSDCVS LHCNLNEHNH
251   HLINDFTIKQ MRQGAFLVNA ARGGLVDEKA LAQALKEGRI RGAALDVHES
301   EPFSFAQGPL KDAPNLICTP HTAWYSEQAS LEMREAAATE IRRAITGRIP
351   ESLRNCVNKE FFVTSAPWSV IDQQAIHPEL NGATYRYPPG IVGVAPGGLP
401   PAMEGIIPGG IPVTHNLPTV AHPSQAPSPN QPTKHGDNRE HPNEQ
```

(b)

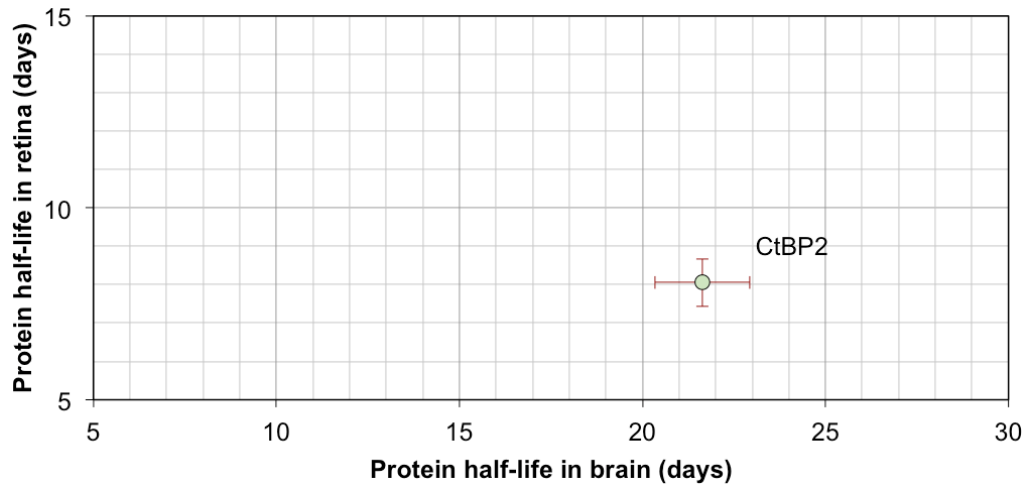

Figure 3-30: Sequence and turnover of CtBP2 protein in brain and retina. (a) Sequence of mouse CtBP2 protein from UniProt showing quantified peptides shown in red colour. (b) Scatter-plot depicting the turnover of RIBEYE B domain homologue protein CtBP2 in brain and retina.

RIBEYE is a ribbon protein; its presence has not been reported in brain synapses. Since, ribbons are absent in brain synapses, the protein turnover given by brain synapses is solely from the nuclear CtBP2. While in retina, the turnover of CtBP2 will be as a result of peptides derived from nuclear as well as synaptic ribbon CtBP2.

We observed an enhanced turnover (~2.7 times) for CtBP2 protein in retina than brain. This may reflect the overall faster rates of synthesis and degradation for CtBP2 protein, and hence RIBEYE protein in retina. In future, if the RIBEYE protein will be sequenced, the determination of its turnover based on its unique peptides will provide accurate turnover values. Moreover, if any of the quantified peptide derived from CtBP2 protein does not shows its origin in RIBEYE protein, the protein turnover provided in fig. 3.30 will change for retina.

3.4 Label-free absolute quantitation of brain synaptic protein components

One of the most common way to quantify absolute amount of protein in a biological sample is quantitative western blotting or immunoblotting. Recently, mass spectrometry has also advanced in the field of protein quantitation. Using mass spectrometry for precise protein quantification, SRM/MRM (selected reaction monitoring/ multiple reaction monitoring) is the most accurate known ways to quantify proteins with the help of isotopically labelled peptides called 'AQUA' peptides (Gerber et al., 2007; Gerber et al., 2003; Kettenbach et al., 2011). However, this technique is not cost-efficient. With improvement in stability of various attributes of mass spectrometry like nano-liquid chromatography, spray, column oven and highly sensitive analyzers and detectors, label-free protein quantitation techniques have competed well and proved to be quite well correlating the absolute amount approximation. Among several known label-free mass spectrometric techniques for absolute quantification of proteins, iBAQ is known to be best working label-free quantitation technique. In addition, it has also been shown in correlation with the western blot data performed for HeLa cell proteins (Schwanhausser et al., 2011).

In this thesis, iBAQ based quantitation method was established in our lab and applied on rat brain synaptosomes to validate the technique (section 2.2.1.5) in collaboration with Benjamin Wilhlem (Prof. Silvio O Rizzoli, Uni-Göttingen, Germany) and rat brain synaptic vesicles (section 2.2.1.6) in collaboration with Zohreh Farsi (Prof. Reinhard Jahn, MPI-bpc, Göttingen, Germany). The samples were digested in-solution (section 2.2.4.1, 2.2.4.4) and mass spectrometric analyses were carried on Orbitrap-Velos mass spectrometer (section 2.2.4.7, 2.2.4.10, 2.2.4.13 and 2.2.4.14).

3.4.1 Protein quantification of Synaptic Vesicle by iBAQ-MS

As mentioned previously, the in-depth proteomic analysis of rat brain SVs was first established by two independent studies. In these studies, 185 and 419 proteins were reported (Morciano et al., 2005; Takamori et al., 2006). In order to quantitate the proteins of SVs, rat brain SVs were isolated (section 2.2.1.6). The purified SVs were counted and processed for iBAQ-MS (sections: 2.2.4.1, 2.2.4.7, 2.2.4.9, 2.2.4.10, 2.2.4.13, 2.2.4.14). Proteomic analysis from this study of purified SV resulted in identification of 639 proteins excluding the spiked-in Universal Human standard (UPS2) proteins. Almost all the proteins (~99%) reported previously were also identified in our study. The additional proteins identified in our study were

cytosolic, mitochondrial and ribosomal proteins. An interesting observation was the identification of chloride channels Clc3 and Clc6. These channels are highly structured integral proteins of SV that mediate transport of chloride ions (Takamori et al., 2001). These proteins were not identified by mass spectrometry in the previous studies (Morciano et al., 2005; Takamori et al., 2006). The additional proteins identified in our SV analysis are due to the improvement in the detectors and analyzers of mass spectrometer instruments and improvement in the computational algorithm for identification and quantitation of proteins.

Apart from the whole proteome, absolute amounts of 14 integral and associated SV proteins were quantified previously by quantitative western blot (Takamori et al., 2006). In the present study, for quantitation of SV proteins by iBAQ-MS, the amounts of SV proteins were calculated using the slopes of UPS2 proteins by linear regression (appendix A10). Finally, the absolute amounts of proteins per SV were calculated by dividing the absolute amounts obtained by iBAQ-MS with the number of counted SVs as shown in equation 3.

$$Copy\ number\ per\ SV = \frac{iBAQ\ amounts\ of\ X\ protein}{number\ of\ SVs\ in\ the\ preparation} \quad [3]$$

In order to compare the absolute amounts of proteins per SV, the amounts obtained by iBAQ-MS from this study and previously published data were plotted (fig. 3-31).

(a)

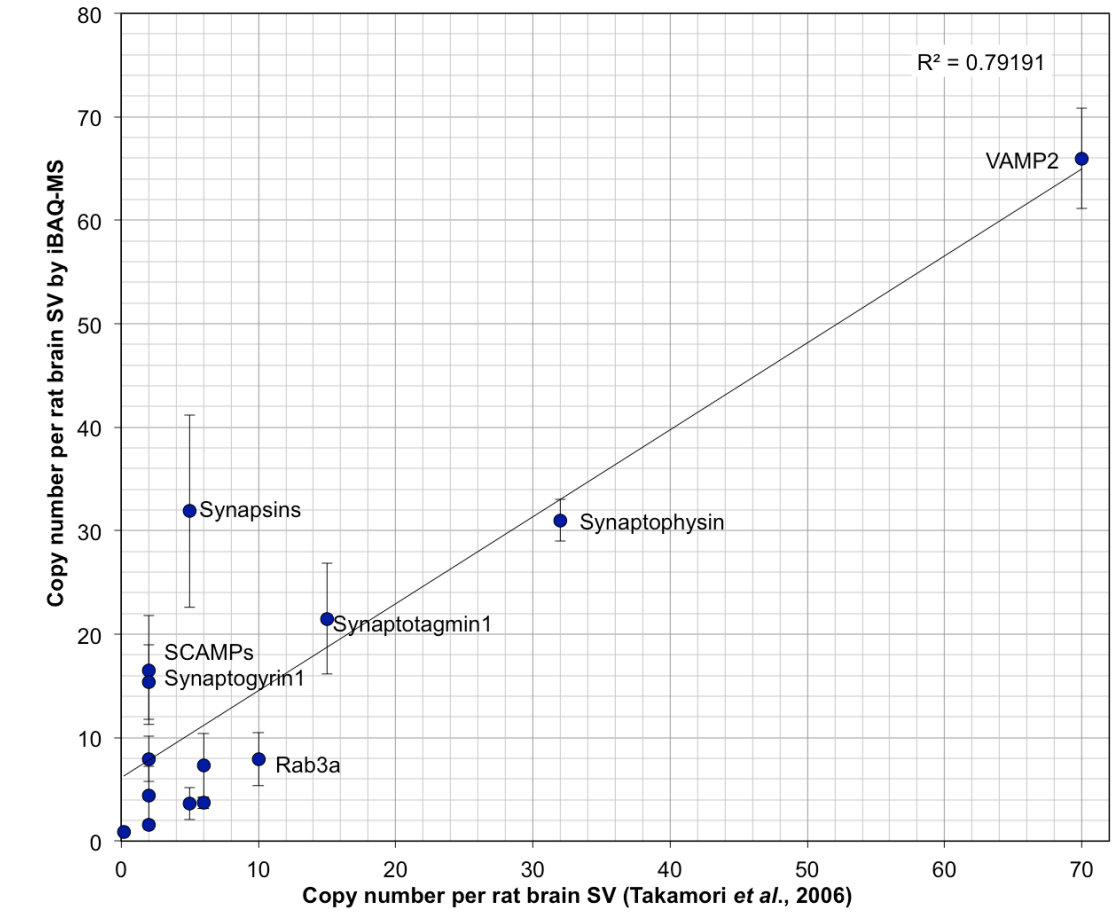

(b)

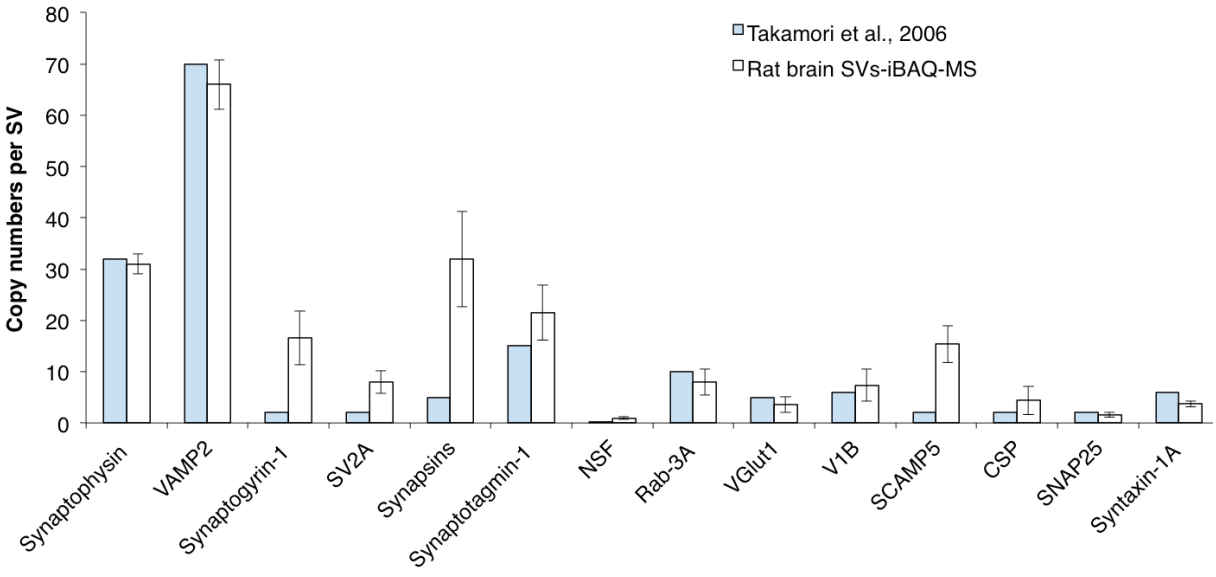

Figure 3-31: ***Comparison of SV protein copy numbers derived from iBAQ-MS and previously published study*** **(Takamori *et al*., 2006).** (a) Scatter-plot comparing the absolute amounts of SV proteins quantified by iBAQ-MS (x-axis) and quantitative western blot (y-axis). R^2 = 0.79. (b) Histogram depicting the copy numbers of SV proteins quantified by western blot (Takamori et al., 2006, blue columns) and iBAQ MS (white columns).

The iBAQ-MS quantitation of SV proteins correlated well with the western blot data from previous studies (fig. 3-31). As expected, VAMP2 is the most abundant protein (~68 copies), followed by synaptophysin (~31 copies). As mentioned previously (section 3.2.2.1), indeed, synaptophysin and VAMP2 also maintain a similar ratio of 1:2 in this study. Synaptotagmin1 (~21 copies) was quantified a little more than previously (15 copies) reported. In addition, we quantified little low copies for VGluts (4 copies for VGlut1, 0.8 copies for VGlut2), rab3a (8 copies) as reported previously (10 copies each). Vacuolar proton pump is an SV-integral protein that transports protons inside the lumen of SV. We observed huge variation in the copy numbers of Voa subunit. This huge variation is possibly due to inability of long, hydrophobic peptides to ionize in mass spectrometer. A similar trend was also observed in amounts for Voa subunit while quantifying copy numbers of vATPase per SV of bovine brain and retina (section 3.2.2.1, fig 3-16). Thus, the copies of vATPase was quantified based on its cytosolic cap region. Previously, it was reported that the SVs might have either 1 or 2 copies of vATPase (Takamori et al., 2006). In this study, 7 copies (± 2 copies) of V1B subunit were quantified suggesting presence of 2-3 copies of vATPase per SV. In addition, 8 copies for SV2 (SV2A ~6 copies, SV2B ~2 copies, SV2C ~0.07 copies) and ~14 copies for synaptogyrin1 were observed from our data, which is more than the previously reported study (2 copies). As mentioned in the previous section (section 3.2.2.1), this could be due to the inefficiency of SV2 antibody to react with the heavily glycosylated SV2 proteins. We quantified ~16 copies for SCAMPs, which are higher than the reported (2 copies each) due to unknown reasons. Although, this discrepancies may be attributed to the two different techniques and can be resolved with the use of another absolute quantification method like AQUA.

Various SV-associated proteins from this study did not correlate well with previously reported copies per SV. The exocytic SNARE machinery was also quantified in the brain SVs by iBAQ-MS. Syntaxin1, was reported 6 copies per SV in previous studies, while the iBAQ-MS based quantitation showed only half of the previously reported copies (syntaxin-1A ~0.8 copies and syntaxin-1B ~2.8 copies). However, SNAP25 was observed similar to the (~2 copies per SV) previous study. Synapsin is also reported to be present on purified SVs (Takamori et al., 2006). They were reported to be 5 copies per SV, however, we quantified almost five-fold excess of synapsins (synapsin1 ~29 copies, synapsin2 ~ 2 copies and synapsin 3 ~0.3 copies) by iBAQ-MS. Since, these are all associated proteins to SVs, their average copy numbers may vary from preparation to preparation and thus could have discrepancies in copy numbers than reported.

Certain other SV-associated proteins like NSF (~0.9 copies) and co-chaperone-CSP (~4.4 copies) proteins were almost the same as reported (0.2 and 2 copies respectively) previously.

Due to the absence of a good antibody, the copy number of several other SV proteins were not reported by quantitative western blot. Since mass spectrometry is an unbiased technique for identification of proteins and so is the iBAQ-MS approach (Schwanhausser et al., 2011), thus, the iBAQ-MS provided a large dataset of list of proteins with their copy numbers. However, it should be noted that not every protein was quantified. Table 3-2 shows list of quantified proteins classified into various categories.

Table 3-6: Copy numbers of rat SV proteins quantified by iBAQ-MS. List of proteins classified into various categories based on their functions along with their quantified copy numbers (third column) and standard deviations (fourth column) of three biological replicates.

Various SV proteins			
ID	Protein	Copy number	σ
SYNPR	Synaptoporin	4.63	2.29
TPRGL	Tumor protein p63-regulated gene 1-like protein	1.02	0.29
VAMP1	VAMP1	3.61	0.91
VIAAT	VGAT	2.90	0.72
SYT2	Synaptotagmin-2	1.80	0.42
SYT5	Synaptotagmin-5	0.03	0.01
SYT12	Synaptotagmin-12	0.55	0.27
VAMP7	VAMP 7	0.16	0.07
VGLU2	VGlut 2	0.83	0.23
VAPA	Vesicle-associated membrane protein-associated protein A	0.08	0.03
SNP29	Synaptomal-associated protein 29	0.09	0.03
VAT1	Synaptic vesicle membrane protein VAT-1 homolog	0.82	0.25
Endocytic proteins			
ID	Protein	Copy number	σ
AP2B1	AP-2 complex subunit beta	4.773	1.410
AP2M1	AP-2 complex subunit mu	5.928	1.562
AP2A2	AP-2 complex subunit alpha-2	2.949	1.015
AP2S1	AP-2 complex subunit sigma	6.121	2.086
CLH1	Clathrin heavy chain 1	0.000	0.000
DYN1	Dynamin-1	0.239	0.127
SHLB2	Endophilin-B2	0.006	0.014
SHLB1	Endophilin-B1	0.005	0.011
Active Zone proteins			
ID	Protein	Copy number	σ
BSN	Protein bassoon	0.001	0.001
CPLX2	Complexin-2	0.059	0.002

Interestingly, the copy number of various SV-integral proteins: synaptoporin (4 copies), VAMP1 (3 copies) were quantified for the first time (table 3-6). The inhibitory synapses contain VIAAT or VGAT transporter proteins to transport glycine into the lumen of SV. Interestingly, we quantified an average of ~3 copies of VIAAT protein per SV of brain (table 3-6). Recently, the protein mover or 'tumor protein p63-regulated gene 1-like' was reported to be associated with SVs. Our data suggests that there is 1 copy of mover associated with rat brain SV (Kremer et al., 2007).

In addition, endocytic proteins especially proteins involved in clathrin-mediated pathway were also quantified by iBAQ-MS (table 3-6). Based on the data, we conclude that ~5 copies of AP-2 complex are associated on an average rat brain SVs.

In addition, we quantified several active zone proteins: bassoon, Munc18a, complexin2 and piccolo, however, their copies quantified were in very small fractions (table 3-6). From this data, it can be concluded that these proteins are not present on each SVs but on a fractional population of SVs.

Table 3-7: Copy numbers of rab machinery quantified by iBAQ-MS. List of rab proteins with their quantified copy numbers (third column) and standard deviations (fourth column) of three biological replicates.

Rab machinery			
ID	Protein	Copy number	σ
RAB1A	Ras-related protein Rab-1A	2.575	0.405
RAB1B	Ras-related protein Rab-1B	0.120	0.038
RAB2A	Ras-related protein Rab-2A	2.733	1.086
RAB3B	Ras-related protein Rab-3B	0.175	0.044
RAB3C	Ras-related protein Rab-3C	1.453	1.245
RAB3D	GTP-binding protein Rab-3D	4.776	0.566
RAB4A	Ras-related protein Rab-4A	0.065	0.031
RAB4B	Ras-related protein Rab-4B	0.214	0.083
RAB6A	Ras-related protein Rab-6A	4.232	0.630
RAB7A	Ras-related protein Rab-7a	1.308	0.416
RAB8A	Ras-related protein Rab-8A	0.025	0.012
RAB10	Ras-related protein Rab-10	0.255	0.297
RB11B	Ras-related protein Rab-11B	1.122	0.251
RAB12	Ras-related protein Rab-12	0.070	0.020
RAB15	Ras-related protein Rab-15	0.056	0.018
RAB18	Ras-related protein Rab-18	0.099	0.035
RAB21	Ras-related protein Rab-21	0.003	0.020
RB27B	Ras-related protein Rab-27B	0.066	0.046
RAB34	Ras-related protein Rab-34	0.726	0.351
RAB35	Ras-related protein Rab-35	0.140	0.139

Apart from endocytic machinery, we also quantified several rab proteins (table 3-7). Rabs are mostly involved in membrane trafficking and regulating the SV-recycling. Besides above mentioned proteins, there were many more proteins quantified by iBAQ-MS. Most of these proteins were found to be cytosolic, mitochondrial and ribosomal proteins that tend to stick to every preparation and have been reported regularly in every other mass spectrometric analysis (appendix A5).

Furthermore, we applied the iBAQ-MS quantitation technique to quantify a much more complex synaptic sample i.e. synaptosomes of rat brain.

3.4.2 Protein quantification of Synaptosome by iBAQ-MS

The synaptosomes were prepared according to standard protocol with slight modifications (section 2.2.1.5) (Nagy et al., 1976; Takamori et al., 2006; Wilhelm et al., 2014a). The measurement of physical properties like average number, size, shape of synaptosome and other organellar structures of synaptosomes such as SVs and mitochondria were accomplished using electron microscopy. The localization of 76 proteins and their abundance distribution in the (a) synaptosomes, (b) primary neuronal cultured cells and (c) neuro-muscular junctions was performed by super-resolution microscopy called Stimulated emission depletion (STED) microscopy. The absolute amount of proteins were calculated by the classical quantitative western blotting as well as the label-free mass spectrometric iBAQ-MS approach. The physical characterization, STED microscopy data and the western blot protein quantification were performed by Dr. Benjamin Wilhelm, Sven Truckenbrodt and coworkers (Prof. Dr. Silvio O Rizzoli, Uni-Göttingen, Germany). The methods and results have been extensively explained in doctoral thesis work (Benjamin, W.B.,2013) and corresponding publication (Wilhelm., 2014). Thus, the methods and results are not explicitly explained in this thesis.

Spike-in iBAQ was used to quantify proteins of SVs from rat brain (section 3.4.1), bovine retina and brain (section 3.2). Apparently, spike-in iBAQ was not used for quantifying proteins of synaptosome due to the presence of the Universal Standards (UPS2) Proteins in the synaptosomes. Although, the UPS2 proteins were majorly derived from human, but there were many identical peptides between rat and human UPS2. Thus, spike-in of the UPS2 proteins into synaptosomes will results in higher iBAQ amount than the actual amount.

In order to avoid mixing the UPS2 and the synaptosomes, label-free iBAQ quantification was performed. In such an approach, the standards and experimental samples were analysed by mass spectrometer as separate samples. This has been possible because of the improvement in the spray, chromatography and MS stability. In addition, there were almost 66 recombinant synaptic proteins available. These recombinant proteins were also used as a standard for quantitative western blotting. These 66 recombinant proteins were also used as standards to calculate the absolute amounts of synaptosomal proeteins by label-free-iBAQ-MS (section 2.2.4.1, 2.2.4.4, 2.2.4.7, 2.2.4.10). Similarly, the absolute amounts of the rest of the synaptosomal proteins were calculated using the slope of UPS2 protein standard using linear regression (section 2.2.4.13 and 2.2.4.14).

iBAQ based quantitation approach provide the information of isoforms of protein present in the database. Since there are various isoforms for synaptic vesicle proteins, for accurate comparison with the quantitative western blot data, the protein amounts obtained from iBAQ-MS were summed for those isoforms. Thus, the fig. 3-32 contains comparison of only 43 instead of 66 proteins. The estimates of absolute protein amounts obtained from iBAQ-MS correlated well with the amounts obtained by quantitative western blot for these 43 proteins (fig. 3-32)

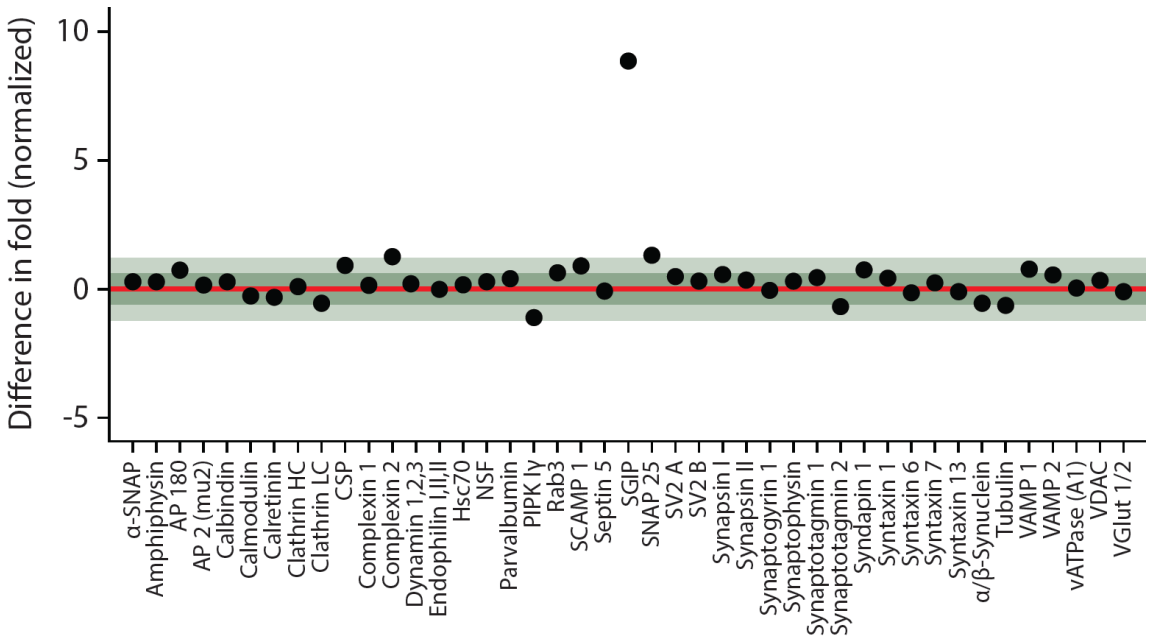

Figure 3-32: ***Comparison of protein quantification by iBAQ-MS and quantitative western blot.*** X-axis represents various synaptic proteins while the Y-axis represents the difference in fold obtained by iBAQ-MS as compared to quantitative western blotting. Proteins touching the red line have almost the same copy numbers calculated by the two techniques of protein quantification. The proteins with values above zero have a higher quantification amount given by iBAQ-MS. Similarly, protein with low amounts by iBAQ-MS have negative values in this plot. Figure adapted from Wilhelm *et al*., (2014) with permission.

Except for SGIP proteins, the absolute amounts obtained by quantitative western blot and iBAQ-MS were almost equal. The slight variation in the amounts may be due to differences in the techniques. The reasons of the differences in the two techniques have not been yet studied.

In addition, the amounts observed from this study were also compared with previously published results. It was observed that the average number of SVs per synapse are 380, thus the copy numbers of proteins per SVs obtained from previously published and our study were compared (fig. 3-33).

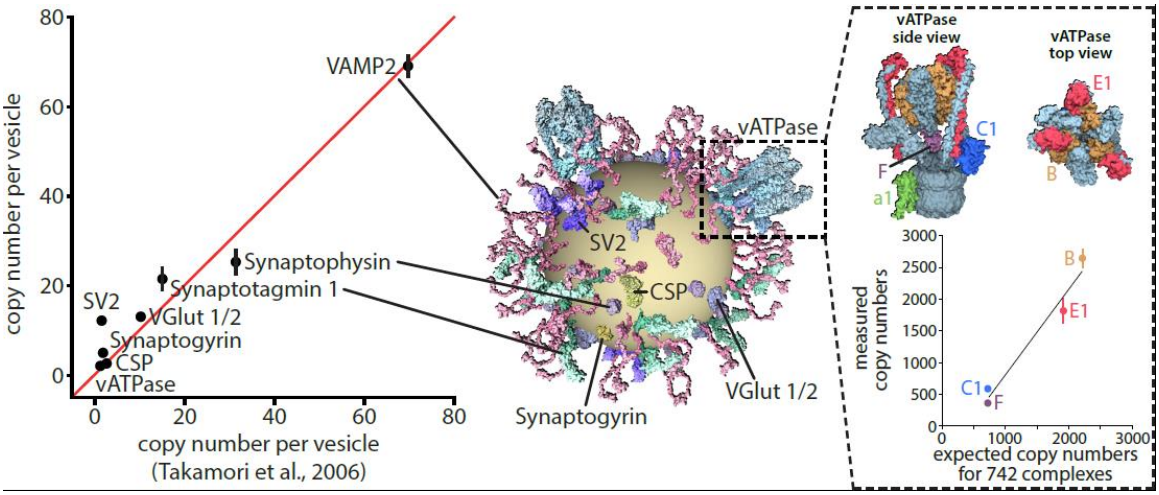

Figure 3-33: Comparison of copy numbers of SV proteins of previously published and our study. The comparison of protein copy number per SV obtained from previously published data (x-axis) with our data (y-axis) *(left)*. The comparison of expected copy number of vATPase subunits (x-axis) versus observed copy numbers (y-axis) for a total of 742 Voa subunits *(right)*. Figure adapted from Wilhelm *et al*., (2014) with permission.

As expected, the copy number of proteins correlated very well (fig. 3-33, left) although there were slight variations between the data from these two studies. The copies of SV-integral proteins VAMP2, synaptophysin, synaptotagmin1, VGlut1/2 correlated well (Takamori et al., 2006). As opposed to the previous published data, very high copies of SV2 were observed in synaptosomes. As mentioned previously (section 3.3.2.1 and 3.4.1), this may be due to the heavy glycosylation of SV2, which hinders the detection by quantitative western blot.

As a proof of principle, the experimental and theoretical amounts of subunits of vATPase were also compared (fig. 3-33, right). A total of 380 SVs should have 742 V0a subunits. The comparison of copies of various subunits of vATPase with its transmembrane subunits V0a also gave a good correlation.

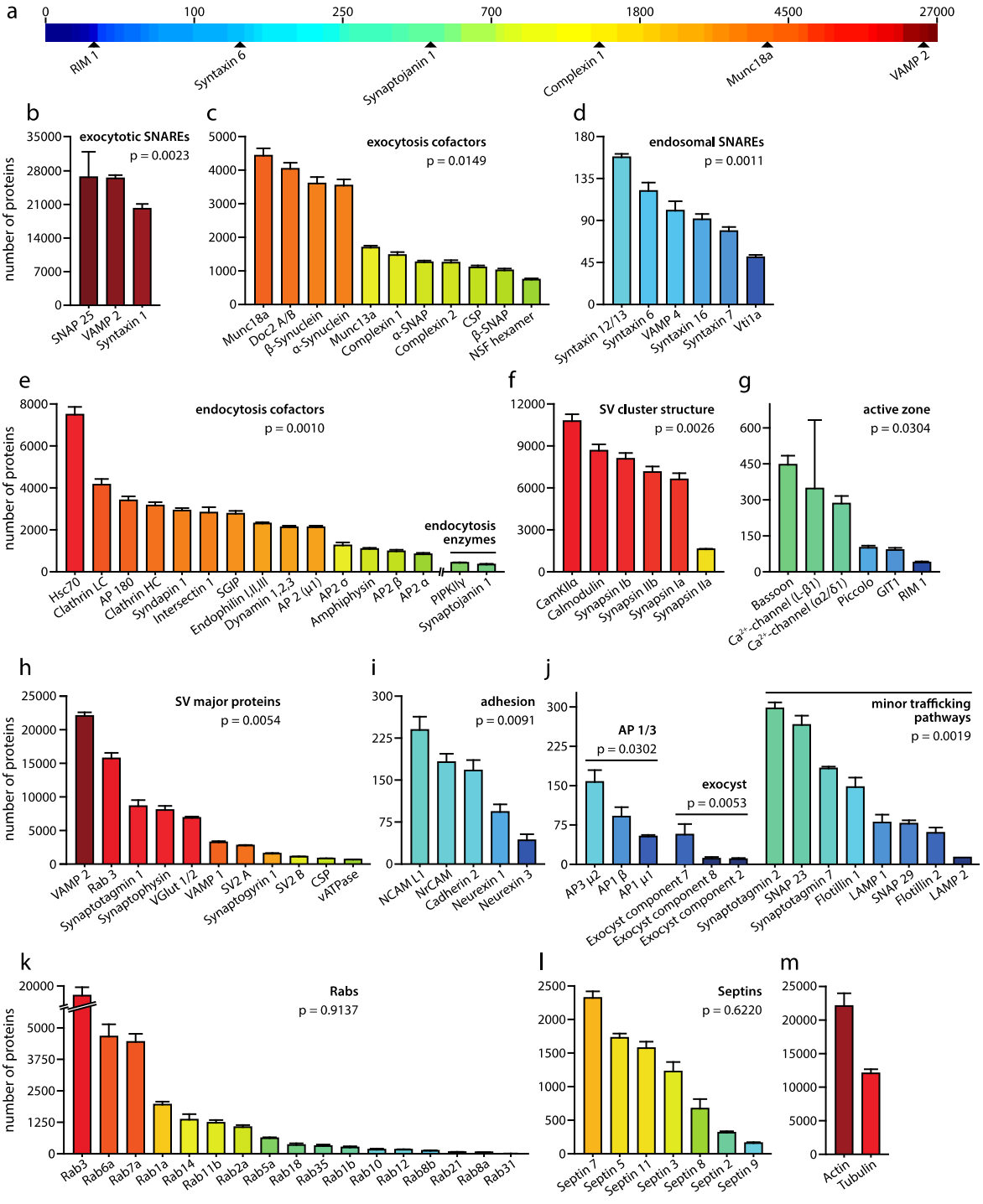

Figure 3-34: Distribution of absolute amounts of synaptic proteins. (a) Absolute amount distribution of synaptic proteins. (b) Distribution of amounts of synaptic proteins. The colour of the columns represents the absolute copies of proteins per synaptosome (decreasing: red to blue). All the synaptic proteins were classified manually into various functional categories; (b) exocytic SNAREs, (c) exocytic cofactors, (d) endosomal SNARES, (e) endocytic cofactors, (f) SV cluster structure, (g) active zone, (h) SV major proteins, (i) adhesion proteins, (j) AP1/3 complex *(left)* and minor trafficking pathway proteins *(right)*, (k) rab machinery and structural proteins (l) septins, (m) actin and tubulin. The color of the columns denotes the abundances of the proteins depicted in (a). Figure adapted from Wilhelm *et al*., (2014) with permission.

In addition to the 66 proteins, iBAQ-MS also provided quantification for approximately 1100 proteins. Out of these 1100, 124 proteins were synaptic. The synaptic proteins vary from as low as 2 to 27,000 copies per synaptosome (fig. 3-34a). The proteins were classified manually into various functional categories and their abundances were compared (fig. 3-34 b to m).

Interestingly, the copy numbers of protein involved in the same functional pathways were almost similar. In other words, the proteins resulting in a particular function correlated well in their copies.

For example, VAMP2 protein is the most abundant protein of SVs and apparently, the exocytic SNAREs: VAMP2, SNAP25 and syntaxin1 were observed as the most abundant synaptic proteins after synapsins in the synaptosome. Similarly, the absolute amounts of proteins involved in various exo- and endocytic functions of the synapse were similar (fig. 3-34 b to m).

It should be noted that the endosomal proteins were the least abundant proteins and their amounts may not be sufficient to carry out endosomal-mediated endocytosis in the synapse. The reason for their low abundance is not known, however, this suggests that endosomal pathway is the least used pathway for generation of SV.

Clathrin-mediated pathway is the most studied pathway of endocytosis in the synapse for regeneration of empty SV. It was observed that the absolute amounts of proteins involved in this pathway were fairly abundant (fig. 3-35e). However, it should be noted that defined number of clathrin-mediated proteins act together to result in the endocytosis of single empty SV. For example, there were approximately 1000 AP-2 complexes present per synaptosomes. However, each vesicle requires approximately 110 AP-2 complexes to aid in endocytosis of empty vesicles. Thus, on an average synaptosome, only 10 empty vesicle may be endocytosed at a given time. Similarly, we obtained just enough amount of dynamins to help in cleavage of ~11 empty vesicles.

In general, the endocytic pathway proteins were less abundant than the exocytic proteins (fig 3-34 d, e). This suggests that the endocytic pathway is the regulating step for SV-recycling.

The data obtained by various techniques used in characterization of synaptic bouton was combined together to generate a 3-D architecture of the synaptic nerve terminal (fig. 3-35). The model was generated by Dr. Burckhard Rammner. (Prof. Dr. Silvio O Rizzoli, Uni-Göttingen, Germany).

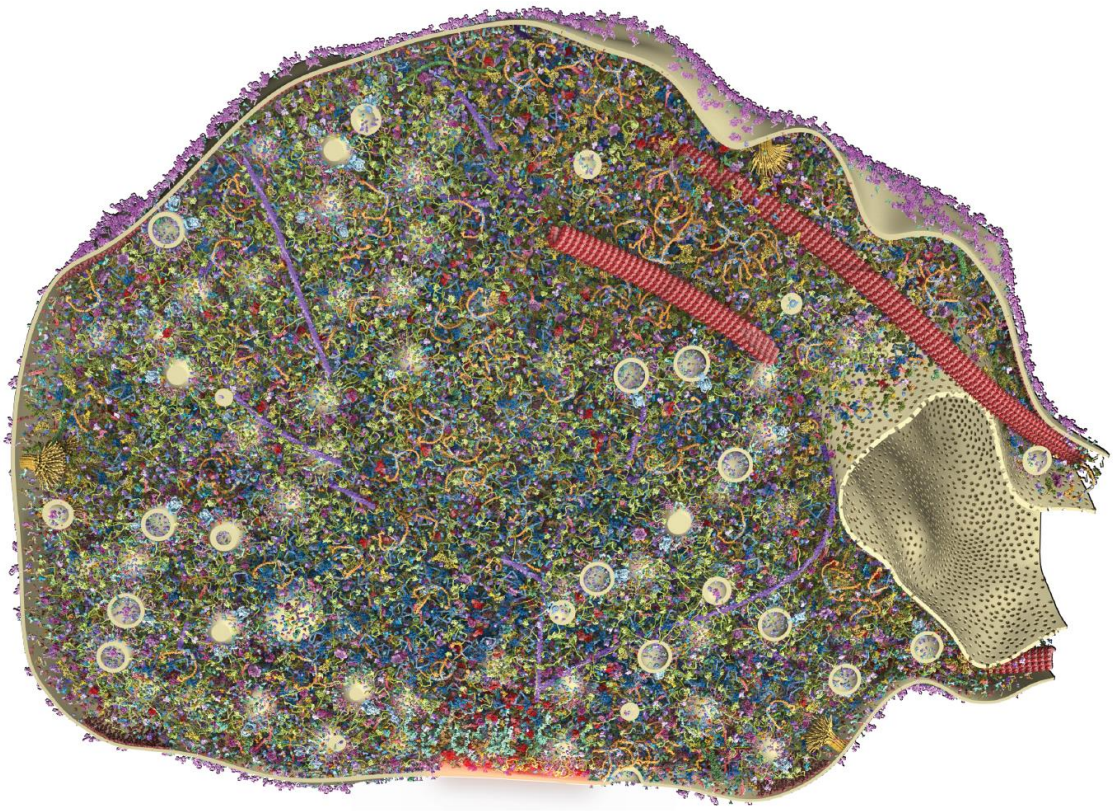

Figure 3-35: 3-Dimensional model for synaptic nerve terminal. The data from electron microscopy, super-resolution STED microscopy, quantitative western blotting and quantitative mass spectrometry was combined to generate the 3-dimensional graphical model of nerve terminal. The 3-dimensional structure of all the proteins was adapted from various model and PDB database available online. Figure adapted from Wilhelm *et al*., (2014) with permission.

4 Discussion

Synaptic vesicles (SVs) play a crucial role in the transfer of information in brain and retina synapses. The fidelity and efficiency of SV function is orchestrated by a variety of proteins that are either integrated or associated to a SV. Elucidation of the proteome of a SV would thus provide insights into the molecular mechanism of SV function and regulation. In this study, by establishing a novel protocol for isolation of SVs from bovine brain and retina, a comprehensive analysis of the brain and retina SV proteome was performed. The data presented in this study show that retina SV proteome significantly differs from that of brain, thus providing insights into the specialized functionality of retina synapses. In addition, a new dimension of proteomics called the temporal proteome dynamics was also performed to understand the synaptic proteome turnover in mice retina and brain.

4.1 Elucidation of the molecular anatomy of ribbon SV from bovine retina

4.1.1 A novel isolation protocol for isolation of SVs

One of the major impediments common to all high-throughput analyses is the availability of starting material in sufficient quantities. This is particularly true for analysis of sensory synaptic structures, for example from retina, where only limited quantities of neuronal tissue can be obtained. This is exemplified by just a single study reported so far (Uthaiah and Hudspeth, 2010). Although this study provides a comprehensive dataset for proteome similarities and differences in brain, cochlea and retina, the authors used ~2000 chicken brains, retinas and cochlea to isolate their synaptic complexes. In addition to requiring a large quantity of starting material, the published report suffered from two other drawbacks; the yield was not high and the synaptic preparation was not pure enough. The protocol established in the present study overcomes the above-said shortcomings, thus requiring less starting material but resulting in high yield and purity.

The SV isolation method established in this study required just eight frozen bovine retinas (section 3.1.2.1). The classical isolation protocol for SVs is based on requirement of 20 rat brains (Jahn et al., 1985; Nagy et al., 1976; Takamori et al., 2006). As low as one rat brain has also been reported using harsh homogenization protocol but resulting in an impure fraction of SV (Hell et al., 1988). Recently, a small-scale SV isolation protocol was established on single mouse brain resulting

in highly pure SVs (Ahmed et al., 2013). Our protocol is comparable to the later two studies (Ahmed et al., 2013; Hell et al., 1988). The starting material in terms of protein amounts (~90 mg) used in our study is almost similar to that of previously published studies (Ahmed et al., 2013; Hell et al., 1988). Although, scaling up similar amounts for mice or rat retina is not feasible. An average mice or rat retina yields approximately 200 μg of protein, thus for 90 mg, at least 200 rat or mice needs to be sacrificed. Thus, bovine retinas were the best choice of starting material to establish the protocol.

The introduction of a combination of two harsh homogenization steps viz., powdering of tissue in liquid nitrogen using mortar and pestle (Jahn and Hell, 2006) and subsequent homogenization using Ultra-turrax (Schmitz et al., 1996) proved to increase the yield as compared to the previously published study (Uthaiah and Hudspeth, 2010). This is in line to the observations made by Neal et al., which led to the finding of two important features to be taken care while aiming for isolation of ribbon SVs: (1) the retina tissue requires a harsh homogenization and (2) the classical method cannot be applied for isolation of SVs from retina (Neal and Atterwil.Ck, 1974; Schmitz et al., 1996). In deed, the retina which were processed using mild homogenization procedures, led to a loss of a major population of ribbon proteome in waste fraction P1, as shown by EM. Thus, the preparation reported by Hudspeth and Uthaiah allowed enrichment of non-ribbon synaptic complexes thus undermining the purity of the whole preparation (Neal and Atterwil.Ck, 1974).

Although the combined harsh homogenization technique improved the yield, it compromised the purity of the preparation. Even after the regular differential centrifugations, large membranous and proteinaceous substances were observed in fraction P4; however, these contaminants were depleted by a two-step density gradient centrifugation (fig. 3-5). The data from immune-blot analysis (fig. 3-6 and 3-7), electron microscopy (fig. 3-4 and 3-9) and mass spectrometric analysis (fig. 3-12) show that the preparation is of high purity. Further, spliceosomal and mitochondrial protein contaminants were significantly lowered by introduction of immunoprecipitation of SVs (fig. 3-13). Most of the contamination (2% of total protein) was observed due to ribosomal proteins; the common contaminations in every other mass spectrometric analysis and have been reported to be present in similar studies (Boyken et al., 2013; Pavlos et al., 2010).

The classical protocol for high purity SV isolation has been reported with 1-3% of enrichment at LP2 fraction (Jahn et al., 1985; Nagy et al., 1976; Takamori et al., 2006). Recently reported SV isolation protocol from single mice brain was reported with 4% enrichment for SV-P fraction (Ahmed et al., 2013). The P4 fraction (fig. 3-

2) in our protocol corresponds to the above-mentioned LP2 and SV-P fractions. Indeed, the enrichment value of P4 is ~ 3% (fig. 3-6) and quite comparable to the corresponding fractions of published methods (Ahmed et al., 2013; Jahn et al., 1985; Nagy et al., 1976; Takamori et al., 2006). Our established protocol is even comparable to the high yield SV isolation protocols, which was reported with 3% enrichment (Hell et al., 1988). Thus, this is the first report of an established isolation protocol that allows preparation of retina SVs with purity and yield.

Moreover, our established protocol follows harsh homogenization steps, yet keeps the proteins like vacuolar ATPases and glutamate transporters in their functionally active form (section 3.1.2.4). Thus, our established protocol isolates functional SVs from retina.

In conclusion, our SV isolation method outperforms previously published protocols. A future direction of this work is to apply the protocol to ~200 retinas of murine i.e. mice or rat. Since the genome of rat and mice is well sequenced, the proteome analysis of murine retina SVs will provide better proteome coverage than the present (reported in this thesis). Also, this will provide appropriate comparison with previously published rat brain and retina SV proteome quantitatively.

4.1.2 iBAQ-MS quantification as a reliable method for estimation of abundances of proteins in synaptic preparations

Label-free quantitation using mass spectrometry is a method to quantitate most of the proteins present in biological sample in single experiment. Till date, iBAQ is the most accurate label-free quantitation technique (Schwanhausser et al., 2011). However, this technique has never been used for quantitation of synaptic proteome. In this thesis, iBAQ was used to determine the differences in the proteome of bovine brain SV and bovine retina SV (fig. 3-14). In addition, iBAQ was also applied to determine the estimates of proteins present in rat brain SV (section 3.4.1) and rat brain synaptosome (section 3.4.2).

Remarkably, the protein quantification of synaptic samples: bovine brain SVs, rat brain SVs and rat brain synaptosomes, correlated well with the quantitative western blot data (fig. 3-14, 3-31a, 3-32 and 3-33). We also observe a fairly good correlation with the theoretical and iBAQ experimental number of subunits of complexes such as vATPase, AP-2, Clathrin chains (fig. 3-16; 3-33 and 3-34). In addition, for complex biological sample like rat brain synaptosome, the copy numbers of proteins involved in the similar pathways correlated well (fig. 3-34). The copy

numbers per SV for various SV-integral proteins quantified from bovine brain (section 3.3.2) and rat brain (section 3.4.1) correlates remarkably well (fig. 4-1).

For few proteins, the iBAQ data did not show a good correlation with the quantification data obtained by quantitative western blot. Some proteins for example SV2 and synaptogyrin-1 were quantified with similar copies by iBAQ for bovine brain and rat brain SV, however they did not correlate with previously published copies. For these proteins, the low copy numbers given by quantitative western blot could be due to masking of their antibody specific region with heavy post-translational modification like glycosylation (Buckley and Kelly, 1985; Chang and Sudhof, 2009; Stenius et al., 1995). Some proteins were quantified with similar amounts of proteins in brain SVs of either bovine or rat with the previously published study. However, their copies differed with species. This includes VAMP2, SCAMP5 and transmembrane subunit of vacuolar ATPase protein. For these proteins, the probable reason could be the differences in the species or it is also possible that these proteins were not accurately quantified by iBAQ. It should be noted that iBAQ is an approximation of the estimates of protein (Schwanhausser et al., 2011). The deviation from expected amounts may be re-examined by other well-known absolute protein quantification techniques like quantitative western blotting or SRM/MRM by AQUA peptides using mass spectrometry (Bantscheff et al., 2007; Gerber et al., 2007; Gerber et al., 2003).

In addition, the SV proteome of retina and brain showed subtle differences. It is important to note that the difference in the copies of individual proteins in brain SV (rat and bovine) with that of retina SV reflects the biological differences in the SVs of distally located tissues; brain and retina (see discussion 4.1.4).

Finally, the advantage of using iBAQ is that it can quantify proteins in wide dynamic range in a single run/experiment. The iBAQ quantitation allowed quantitation of ~50, ~30, ~150 and ~1100 proteins from bovine brain SVs, bovine retina SVs, rat brain SVs and rat brain synaptosomes respectively. In addition, iBAQ enables the quantitation of proteins for which the quantitative western blot is not possible. This includes synaptic proteins VAMP1, synaptotagmin 2, VIAAT, synaptoporin, protein Mover (Table 3-6). Moreover, iBAQ can also be applied for quantification of proteins in complex sample preparations like synaptosomes (Wilhelm et al., 2014a). An iBAQ-based quantification performed in this thesis work allowed for confirmation of biochemical quantitation of synaptosomal proteome, based on which a three-dimensional model representing real abundance of proteins was generated (fig. 3-35).

The method or the workflow, established in this thesis work, for isolation (section 3.2.2) and quantification (section 3.3) of retina SVs represents the state of the art in SV proteomics, which may be applied directly to isolate and quantify proteins of SVs from sensory systems like cochlea.

4.1.3 Our novel protocol enriches mostly free ribbon SVs

It is known that there are many types of neuronal cells present in retina (section 1.1.1.2). In fact, in retina, the conventional and ribbon synapses lie in close proximity (Dowling and Boycott, 1966; Dowling and Werblin, 1969) (fig. 1-4). This explains why we observed non-ribbon proteins like complexin 1 and 2, syntaxin 1B in our retina homogenate as well (Reim et al., 2009) (section 3.4). Surprisingly, it was observed that 88% of retina cells form ribbon synapses, while the remaining 12% forms the conventional synapses (Jeon et al., 1998). Since, an average number of SVs present in ribbon synapse and conventional synapse is 10^6 and 200 respectively (table 1-1), combining the data of total number of cells in retina (Jeon et al., 1998) and SVs per cell in retina (table 1-1), would give the estimate of ribbon SVs and non-ribbon SVs in retina. Interestingly, the calculated estimate shows that ~99% of the total SVs are derived from ribbon synapses especially rod and bipolar cells. In other words, out of every 100 SVs obtained by homogenizing retina; there will be 99 SVs from ribbon synapses.

In addition, the estimate of the total free SVs in ribbon synapses is 99% (table 1-1). Thus, out of the total SVs of retina (90% ribbon SVs and 10% conventional SVs), almost 99% of the SVs (calculated from table 1-1) obtained from lysates of retina will be free SVs from ribbon synapses. Thus, our SV preparation contains 99% free ribbon SVs. This is supported by the fact that most of the proteins that interact with free SV for assisting in docking and priming are missing in our preparation as judged by western blot (fig. 3-7 and 3.8) and mass spectrometric analysis (section 3.2.2.2). However, it can also be argued that since in the present study, the isolation protocol is based on the density of SV, it might enrich mostly the free or undocked SVs.

In our study, the isolated SVs proteome is the average proteome of retina SV reflecting majorly SV proteins of rod and bipolar cells. Thus, it can be concluded that the obtained results mostly correlate to the SVs of rod photoreceptors and bipolar cells. Arguably, the rab3, synapsins and syntaxin 1 proteins are absent in ribbon synapses (Brandstatter et al., 1996b; Grabs et al., 1996; Mandell et al., 1990; Morgans, 2000a, b; Morgans et al., 1996; Von Kriegstein et al., 1999). Complete absence of synapsins (Mandell et al., 1990; Von Kriegstein et al., 1999)

(fig. 3-18) and presence of very low amount of rab3 (Grabs et al., 1996) (fig. 3-7; 3-18) and syntaxin 1B (Brandstatter et al., 1996b; Morgans, 2000a, b; Morgans et al., 1996) (fig. 3-7; 3-17) in our isolated SVs from bovine retina support our hypothesis that the isolated SVs are enriched in ribbon SVs. It should be noted that the absence of these non-ribbon proteins was not only supported by our western blot analysis (section 3.1.2.3) but also the mass spectrometric analysis (section 3.2).

4.1.4 Molecular anatomy of brain and retina SV

In a landmark study by Takamori et al., the molecular anatomy of rat brain SV with exact copy number of each protein obtained by biochemical analysis was reported. Based on a good correlation between the reported copy number of all proteins (except SCAMP5) and the iBAQ-MS based quantification of copy numbers in rat brain SV performed in the present study (fig. 3-31), one can assume that the data obtained from frozen bovine brain SV is therefore reliable. Although, there is possibility of mistake in proteome quantitation because of the fact that the starting material (frozen retina and brain from bovine source) were not freshly processed. The bovine retina and brain were dissected and snap frozen for long time, further thawed and used for this study. Accordingly, we propose a quantitative proteome model for bovine brain SV (fig. 4-1; top left). By combining the copy numbers of bovine brain SV and rat brain SV (fig. 4-1; top right), one can arrive at an average copy number of proteins for brain SV in general viz., 32 copies of synaptophysin, 3-4 copies of VGlut1, ~70 copies of VAMP2, 14-20 copies of synaptotagmin1, 2 copies of vATPase, 14 copies of synaptogyrin1 and 8 copies of SV2. SCAMP5 may have wide range of copies (3-16 copies) (for more details see section 3.4.1, 4.1.2).

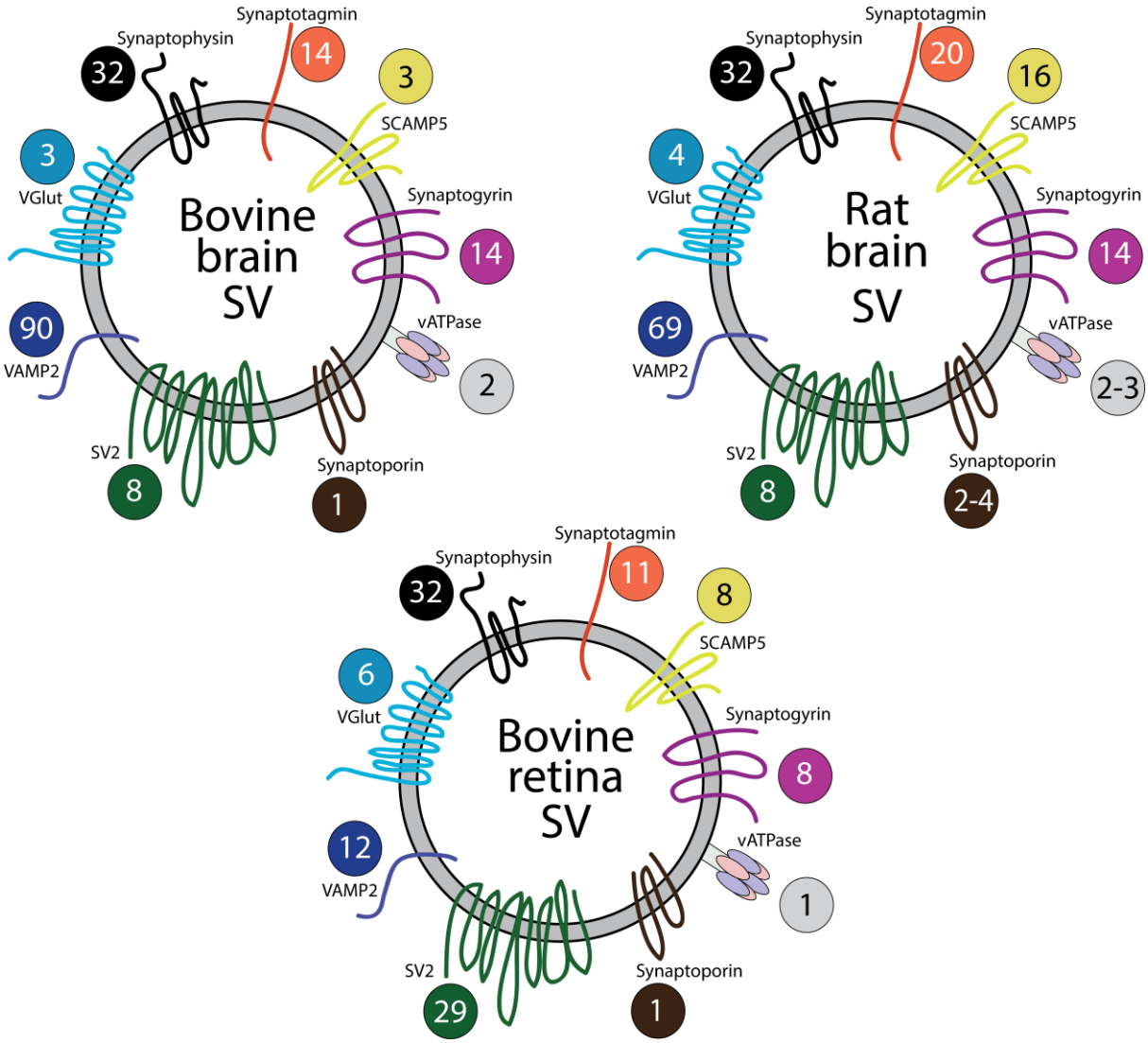

Figure 4-1: ***Schematic model representing various SV-integral proteins with their copy numbers per vesicle.*** Putative model representing SV-integral proteins: synaptophysin (black), synaptotagmin 1 (orange), SCAMP5 (yellow), synaptogyrin (purple), vATPase (multi-subunits in different colours), SV2 (green), VAMP2 (blue) and VGlut1 (cyan). The numbers represent their absolute copy numbers as quantified by iBAQ-MS.

Based on the obtained iBAQ quantification data, we also propose a model for retina SV (fig. 4-1 *bottom*). It is obvious that the copies of synaptotagmin1 and SCAMP5 of retina SV is almost similar to that of brain SV. However, the other SV-integral proteins are not similar in copy number to that of brain SV. These proteins include SV2 (29 copies) and VAMP2 (12 copies) or synaptogyrin-1 (8 copies) which are staggeringly high and low in number, respectively, compared to that brain SV. Since, the function of SV2 and synaptogyrin is not known, thus the biological relevance of the difference in copies of these proteins could not be assessed. Interestingly, the vesicular transporter VGlut1 is another notable protein with a two-fold increase in retina SV as compared to that in brain. Considering that VGlut1 is

responsible for transportation of glutamate inside the lumen of SV and since the retina synapses are majorly glutamergic, thus it is possible that more copies of VGlut1 are required to carry out its function efficiently in ribbon synapses (Johnson et al., 2003; Sherry et al., 2003). However, it has to be noted that the number of VGlut copies per SV corresponding to the effect on rate of transport of glutamate has never been reported.

The copy number of exocytic SNARE forming protein VAMP2 in retina is ~6 times less than brain SV. Exocytic SNARE machinery is very crucial for exocytosis of SV and VAMP2 forms a SNARE complex with syntaxin, SNAP25 and complexin. Although a drastic decrease in the copies of VAMP2 in retina (~12 copies) than brain (~70 copies) has been observed, a biochemical evidence to explain this observation is lacking. The low copy number of such a functionally important protein raises the question on how fusion of ribbon SVs could occur.

However, one cannot exclude the possibility of the presence of other ribbon-specific uncharacterized proteins that complement VAMP2 function in ribbon synapses. Ribbon synapses are well known to have special proteins replacing the conventional synaptic proteins to perform their functions efficiently. For example, the conventional synaptic protein- synaptotagmin is replaced by a totally new class of protein known as Otoferlin in cochlea (Helfmann et al., 2011; Pangrsic et al., 2012; Reisinger et al., 2011; Roux et al., 2006). Interestingly, a previously published report that SNAP25, an interacting partner for VAMP2, is absent in ribbon synapses also supports this view. Thus, it is possible that the alternative of VAMP2 might form the SNARE zippers without SNAP25 but alternatively with SNAP25-like-protein of ribbon synapses.

On the other hand, it is also possible that the quantified 12 copies of VAMP2 are just enough to carry out the ribbon synapse function efficiently. Studies show that syntaxin 3 has almost 10 times higher affinity to form SNARE complex with VAMP2 and SNAP25 than syntaxin-1 (Brandstatter et al., 1996b; Morgans, 2000a, b; Morgans et al., 1996). It is possible that this increased affinity has been developed in the ribbon synapses to compensate the probability of SNARE forming activity with low abundant VAMP2 present on SV. In addition, it is not known what causes a free SV to undergo docking in ribbon synapses. Docking in ribbon synapses means tethering of SVs to the ribbon. It is not known what protein leads to the adhering of SV to the ribbon. It is possible that ribbon SVs have a specialized ribbon-tethering protein present in ribbon synapses for docking the free SV to ribbon. The low copies of VAMP2 are compromised with the above-said ribbon-

tethering protein for docking. Subsequently, the docked SV is placed in right position protruding its low copies of VAMP2 to form exocytic SNARE machinery.

4.1.5 SV-associated proteins in bovine brain and retina

In addition to the difference in the integral protein copy number in SV between brain and retina, our data also identified differences in SV associated proteins.

SNAP25 was arguably reported to be absent in ribbon synapses (Grabs et al., 1996; Von Kriegstein et al., 1999). Our data does not show the presence of SNAP 25 (0-1 copies) significantly in immunoprecipitated bovine retina SVs (fig. 3-17). Although, since SNAP25 is an SV-associated protein, it is possible that it may not adhere to the SV in same number in every SV preparation resulting in large deviation in the quantification analysis (fig. 3-17). However, the turnover of SNAP25 does not significantly differ in brain and retina (fig. 3-26), suggesting similar or constant rate of synthesis and degradation in the two tissues: retina and brain. Thus, based on our data, SNAP25 is not a ribbon protein.

Syntaxin 1A/B is present in brain synapses while syntaxin 3 is specific for ribbon synapses. Syntaxin 1A (1-6 copies) was identified only in brain synaptic preparations. Interestingly, we observed syntaxin1B and syntaxin 3 (~3 copies) in isolated bovine retina SVs as well as mice retina homogenates (fig. 3-17), while the amount of syntaxin1B quantified in isolated bovine retina SVs was far less than with very high p value. In addition the turnover of syntaxin1B had similar rates of turnover in retina and brain. Syntaxin1 was reported to be present in the amacrine cell bodies of mice retina (Sherry et al., 2006). Hence, it could be suggested that identification of syntaxin1B could be as a result of the presence of 1% conventional SVs (fig. 3-26).

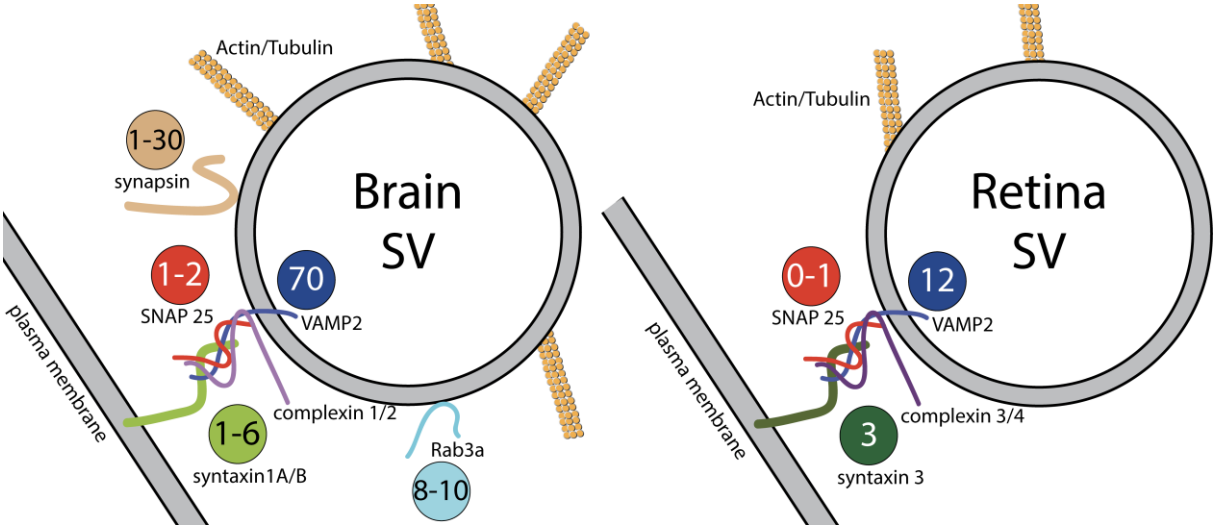

Figure 4-2: ***Comparison of SV associated proteins of brain and retina*****.** Pictorial representation of various proteins or isoforms present in brain and retina along with their copy numbers (written in circle; the colour of the circle represents the colour of proteins in the picture) per SV.

In brain synapses, the synapsin tethers the SVs, upon arrival of action potential; the synapsin phosphorylates and releases the free SV. Further, the released SVs undergo docking, priming and exocytosis to release the neurotransmitters into the synaptic cleft. Unlike brain synapses, the synapsin does not forms a matrix for tethering the retina free SVs. Our data supports the absence of synapsin SV in ribbon synapses (fig. 3-18). In 1999, Von Kriegstein et al., referred the presence or absence of synapsin in ribbon synapses to be species-specific. They observed no synapsin in the OPL region of mice retina by immunostaining. While for bovine retina, synapsin was detected in the homogenate but not in crude ribbons by western blotting. In addition, since synapsin is SV-associated protein, thus does not co-purifies with ribbon. Based on this result, it was hypothesized that synapsin is present in ribbon synapses of bovine retina while absent in murine retina. In contrast to their finding, we observed presence of synapsin in mice retina homogenate, while total absence of synapsin in isolated bovine retina SVs. By combining the previously observed results for synapsin and our results, it can be speculated that the identification of synapsin in retina homogenate is based on the presence of synapsin in the conventional synapses of retina. The identification of synapsin in mice retina in our study is due to the improvement in the sensitivity and detection limits of the mass spectrometers to detect as low as picomol amounts of protein. It should be noted that in the previous studies, the absence of synapsin was not based on mass spectrometric identification. Although, we do not provide any experimental proof of presence of synapsin in conventional synapses of retina. However, presence of faint signals for various synaptic layers of retina: OPL and

IPL by immunostaining clearly support our concept of presence of synapsin in conventional synapses of retina (Geppert et al., 1994; Mandell et al., 1990). Since, synapsin is not a ribbon synapse protein, it has not been observed even with isolated ribbons and isolated SVs obtained in our study (fig. 3-18).

As mentioned previously (section 1.1.1.2.2), till now, there is no evidence of how a free SVs is held in the cytoplasm, and interestingly what signals the retina free SV to migrate to the ribbon for docking. It is well known that apart from synapsin, the tubulin and actin also holds the conventional synapse SVs. While the ribbon SVs exists in a more mobile state than the brain SVs. This high mobility of ribbon SVs was studied by fluorescent labelling of SVs using internal fluorescence microscopy (Usukura and Yamada, 1987). It was found that the ribbon SVs do not show microtubule or actin filament directed movement. In fact, our isolated bovine retina SVs have ~2 folds less actin and tubulin than the bovine brain SVs. Hence, our data indicates that the isolated retina SVs are potentially from ribbon synapses (table 3-5).

Rab3a was reported to be abundantly present in the OPL fraction of retina (Sudhof 1995). Soon, it was found that Rab3a, including its isoforms is absent in the ribbon synapses using immunogold labeling EM (Grabs 1999). In support, our data suggest absence of Rab3a/b/c/d in immunoprecipitated bovine retina SVs. In addition, the rab3 isoforms quantified in mice retina show insignificant difference in their turnovers in brain and retina (fig. 3-28) As suspected, these rab3 isoforms in retina may be derived from conventional synapses of retina. Also, we suspect that there could be alternative proteins in ribbon synapses serving the role of GTPase activity, which is very crucial for exocytosis.

4.1.6 Synaptic ribbon proteome

Ribbon is a special structure present only in ribbon synapses as has been first observed by EM (Sjostrand, 1953g, 1958). The exact function and composition of ribbon is not yet known (Schmitz, 2009; Schmitz et al., 1996; Schmitz et al., 2000; Von Kriegstein et al., 1999).

An uncharacterized and not yet sequenced protein RIBEYE is proposed to form the skeleton of ribbon (Schmitz, 2009; Schmitz et al., 1996; Schmitz et al., 2000; Von Kriegstein et al., 1999). The bovine synaptic ribbon isolated and purified following the standard protocol (Schmitz et al., 1996), is not very pure as judged by the western blot (fig. 3.1 *left*) and iBAQ analysis (fig. 3-1 *right*). Although RIBEYE is known to form the skeleton of ribbon (Schmitz et al., 1996), the

percentage amount of RIBEYE in ribbon is never reported. Thus, it is hard to judge the purity of our preparation. Of note, the amount of CtBP2 proteins- homologue for B domain of RIBEYE protein, quantified in our study was 10 times less than amount obtained by the published study. This difference in the final yield could be explained by the use of an extra step of purification by immunoprecipitation, which was not performed in the present study. However, most of the proteins quantified in previously published dataset of immunoprecipitated synaptic ribbons i.e. 42 out of 53 proteins, were also quantified in our synaptic ribbon preparation (Kantardzhieva et al., 2012). These quantified proteins include structural, nuclear, cytosolic, chaperones and few active zone proteins (Kantardzhieva et al., 2012). Assessing the functional relevance of the quantified proteins in ribbon is out of the focus of the present study.

To summarize, true insights into the ribbon proteome can be obtained only by studying the ribbon-specific RIBEYE protein. Immunoprecipitation with RIBEYE specific antibody would enable isolation of ribbon proteome. In addition, protein-protein crosslinking of isolated ribbons may allow better understanding of ribbon-associated proteins.

4.2 Understanding the temporal synaptic proteome dynamics

4.2.1 Synaptic proteins have faster turnover in retina than brain

It is reported that the blood and liver tissue are the fastest known regenerating tissue of body. In addition, after blood, liver has the fastest ability to incorporate stable-isotope in mice (Kruger et al., 2008). Thus, one can derive that the rate of turnover of a protein in a given tissue may reflect its function. Our data clearly shows that proteins specifically, the synaptic proteins show faster turnover in retina than brain. Interestingly, all the retina specific proteins identified and quantified from isolated bovine retina (section 3.2) show faster turnover in mice retina than brain (section 3.3). Considering that the retina ribbon synapses are highly active than the conventional synapses, this supports our proposed hypothesis of relation of protein turnover with function. As mentioned previously (section 4.1.3), 90% of the isolated SVs are of ribbon synapse origin. It is quite possible that the ribbon synapse proteins thus show faster turnover. Specifically, SV-integral proteins: synaptophysin, VAMP2, synaptotagmin1, SV2, synaptoporin and SCAMP5 showed almost 1.5 times faster turnover in retina than brain (fig. 3-24). Interestingly, VGlut1 showed extremely faster (4 times) turnover in retina than brain supported by the fact that retina synapses are glutamergic (Pereda, 2014; Takamori et al., 2000, 2001). It is rarely related for GABAergic, which are restricted

only to the supporting glial cells (Pereda, 2014). As expected, the turnover rate of the GABA transporter VIAAT is similar in retina and brain (fig. 3-24).

Similarly, the SV-associated ribbon synaptic proteins as well show faster turnover in retina than brain. Most of the endocytic proteins especially the proteins involved in clathrin-mediated endocytic pathway show faster turnover in retina than brain. Similarly, the exocytic and active zone proteins also showed faster turnover in retina than brain. This is very prominent for ribbon specific isoforms. The exocytic SNARE protein- syntaxin-3 for retina has almost 2.5 and 3.5 times faster for brain specific isoforms syntaxin 1A and syntaxin 1B respectively (Brandstatter et al., 1996b; Gray and Pease, 1971; Heidelberger et al., 2005; Matthews and Fuchs, 2010; Morgans, 2000a, b; Morgans et al., 1996) (fig. 3-26). In addition, studies show that syntaxin 3 has higher affinity to bind with VAMP2 and SNAP25 *in-vitro* (Morgans et al., 1996*).* Similarly, brain specific- complexin 1 and 2 and retina specific- complexin 3 and 4 in retina ribbon synapses also show similar trend (Reim et al., 2009) (fig. 3-27).

Nevertheless, not all SV-associated proteins show faster turnover in retina than brain. Synapsin and rab3 show similar turnovers in retina and brain. Arguably, synapsin and rab3 are absent in ribbon synapses (Grabs et al., 1996; Ullrich and Sudhof, 1994; Von Kriegstein et al., 1999). Our isolated bovine retina SVs suggests absence of synapsin and rab3, and hence supports our proposed hypothesis that the property of faster turnover is ribbon-specific (fig. 3-18).

Our hypothesis can also be extended from SV to ribbon proteome, since our data for RIBEYE homologue protein CtBP2 showed almost twice as fast turnover rates in retina than brain (fig. 3-30). Although, one can speculate that the turnover of CtBP2 does not truly reflect the turnover of RIBEYE, by EM, it is clear that brain lacks ribbon (Derobertis and Franchi, 1956; Derobertis and Bennett, 1955; Dowling and Boycott, 1966; Dowling and Werblin, 1969; Sjostrand, 1953b, e, g, 1958). Thus, the protein turnover for CtBP2 in brain is truly the turnover for nuclear proteins. There is no reported study suggesting special function of CtBP2 in retina. In general, the turnover data for retina and brain shows that most of the nuclear proteins have almost similar turnovers in the two tissues. Thus, the turnover for CtBP2 in retina represents the additive turnover of nuclear protein CtBP2 and B-domain of RIBEYE. Another issue for considering CtBP2 a ribbon homologue is that there is no evidence for the percentage similarity of CtBP2 and B domain of RIBEYE. In near future, if the RIBEYE is sequenced, then only its unique/specific peptides should be considered to quantitate its turnover.

Thus, there is a relation between the ribbon synaptic proteome and their turnovers. It is possible that the ribbon synaptic proteins tend to degrade at a much faster rate and thus is the rate of synthesis in retina than brain. This may be or may not be related to the activity of ribbon synapses present in retina. It may be speculated that in order to maintain the very high rates of exocytosis for long periods of time, the ribbon synapses need to revive their synaptic proteome at a slightly faster rate than brain. This may result for maintaining the plasticity of faithful ribbon synapses.

4.2.2 Synaptic proteins have faster turnover *ex vivo* than *in vivo*

The turnover of brain proteins measured in this study is overall slower when compared to the turnover of proteins measured in primary neurons grown in culture (Cohen et al., 2013). Nevertheless, the turnover of synaptic proteins *in vivo* correlates well with the *ex vivo* situation (fig. 4-3).

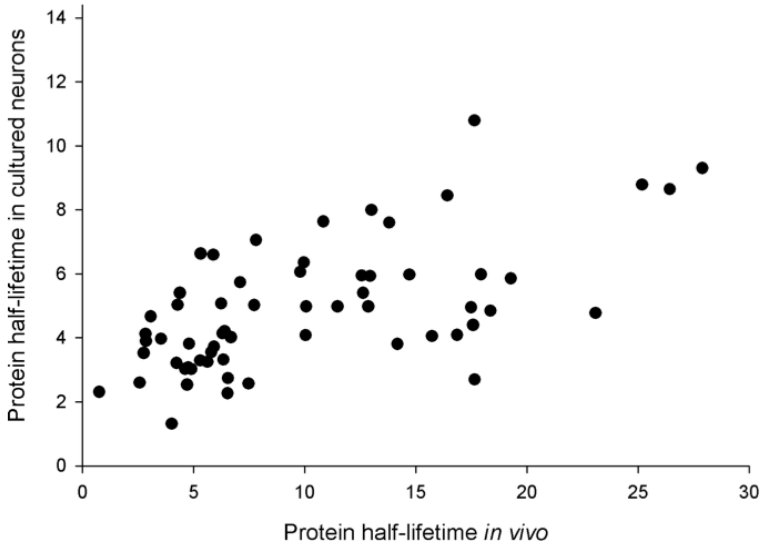

Figure 4-3: *Comparison of protein turnovers in vivo and ex vivo*. Scatter-plot representing turnovers of 56 synaptic proteins in vivo i.e. mice brain (x-axis) and in vitro i.e. cultured neurons (y-axis).

The shorter half-life of synaptic proteins observed in culture is mainly due to the fact that the neurons in this preparation are young cells growing exponentially, while the mice utilized in this study were adult. During development cells that are growing fast will need to synthesize proteins at a high rate, thus the observed half-life will be shorter. Moreover, the continuous flow of nutrients may influence the rate of protein synthesis. The availability of food influences the metabolism and thus the protein turnover (McNurlan and Garlick, 1989). The brain receives nutrients from the blood circulation, which is optimized to supply the physiological

demands of the brain. At variance, in cell culture neurons are submerged in the medium, which may promote to increase the rate of protein synthesis and thus increased rate of turnover (Purves, D. et al., 2001).

4.2.3 Turnover rates of synaptic proteins correlate with their absolute copy numbers

While comparing the copy numbers of synaptic proteins in rat boutons (section 3.4.2) and the turnover in mice (section 3.3), it was interesting to note that there is a correlation between the number and the longevity of proteins at the nerve terminals (fig. 4-4).

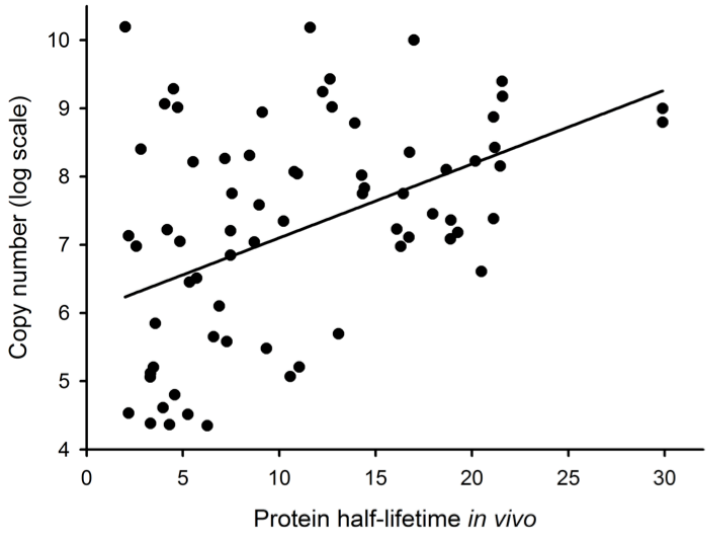

Figure 4-4: Scatter-plot of copy numbers of synaptic proteins per nerve-terminal versus their turnover. Comparison of half-life of 69 brain synaptic proteins of mice brain (section 3.3) and their copy numbers per synaptosome in rat brain (section 3.4.2).

The reason for this intriguing correlation is not known to date. It may be hypothesized that neurons (as well as other cells) are organized in an efficient way, and that the efforts spent in making very abundant proteins are counter-balanced by the reduction of their degradation. In other words, the proteins that are required in large amounts are more stable while proteins that are required in low copy numbers are a less important burden for the translational synthesis machinery and thus, their turnover is fast. However, this is for the moment only a speculation and new experiments will be necessary to test this hypothesis.

An additional observation is that the proteins participating in the same step of synaptic transmissions have similar half-lives (fig. 4-5).

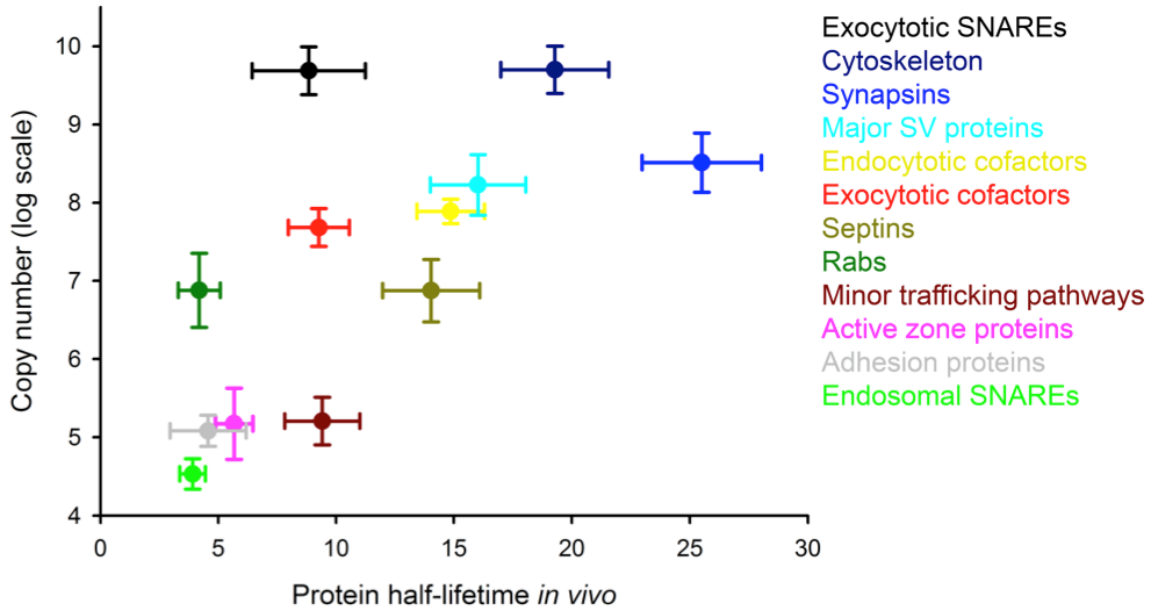

Figure 4-5: ***Scatter-plot of copy numbers of synaptic proteins involved in SV-recycling process per nerve-terminal versus their turnover.*** Comparison of half-life of mice brain synaptic proteins (section 3.3) involved in various SV-recycling pathways with their copy numbers per synaptosomes rat brain (section 3.4.2). Each colour represents unique SV-recycling pathway.

Many of these protein groups are strikingly different, such as the short-lived endosomal SNAREs, or the remarkably long-lived synapsins. The mechanisms behind this type of regulation remain to be investigated. In addition, one caveat of this preliminary work is that the protein lifetimes were obtained in mice, while the protein copy numbers were derived from rat preparations. An approach quantifying both elements in the same animal model will be necessary to strengthen these results.

4.2.4 Absolute protein turnover calculation: some critical insights

Temporal proteome dynamics is one of the missing dimensions in the field of cell biology. The investigation of absolute turnover of proteins in various synaptic structures will extend our knowledge for a deeper understanding of the neuronal processes. As mentioned previously (section 3.3), it is well known that in the central nervous system of adult animals neurons divide and regenerate just in very limited cases, virtually negligible for the purpose of this study. Thus, following developmental neurons can be considered at a protein synthesis “steady state”. The continuous flow of nutrients is used regularly for the synthesis of new proteins.

In order to calculate the absolute value of protein turnover, one should investigate the real amount of newly synthesized proteins and degraded protein over time.

However, there is always re-use of amino acids derived from degraded proteins (Doherty and Beynon, 2006). Thus, while performing a pSILAM experiment, a certain amount of lysine0 amino acid also contribute to the peptide derived from newly synthesized protein. In addition, the mice were fed with ~99% pure lysine6 food. Although this is negligible amount, yet, there is 1% amount of $lysine_0$ being regularly consumed by the mice.

Thus in practice, the calculated protein turnover derived from the SILAC pairs is derived from homogeneous population of lysine pair (heavy and light) containing peptides i.e. all $lysine_0$ for light and all $lysine_6$ for heavy peptides. In this way, the peptides containing heterogeneous tags i.e. $lysine_0$ and $lysine_6$ together in same peptide/protein will not be considered for quantification. Thus, the calculated heavy-to-light ratio derived from SILAC pairs will always be slightly less than the actual turnover. From the experiments performed in this thesis work, this difference cannot be calculated. However, apart from the mentioned experiments, the experiments in progress will solve this issue (discussed below).

For calculations of rates of complex criteria like protein turnover, there are many models described in literature (Guan et al., 2012; Price et al., 2010). The three-compartment model seems to be the best working model for protein turnover calculation and has been suggested previously for liver protein turnover calculations (Guan et al., 2012). Briefly, the first compartment contains the influx of SILAC pair ($lysine_6$-to-$lysine_0$) ratio into the mice body. The first compartment is the lysine pool available for mice as food, which is 99% $lysine_6$. The second compartment is blood stream, which contains the absorbed form of SILAC pair ratio for proteins. The second compartment is the blood stream of mouse that is a direct source of lysine for various organs. The relative amount of lysine present in the blood needs to be determined in order to know the actual availability of heavy lysine to brain. However, this has been reported that within 3 days, the blood stream becomes nearly 100% SILAC. Thus, this value will not be majorly influencing the turnover rates in our experiments because we have chosen longer experimental times for feeding mice. Finally, the third compartment is the freely available pool of $lysine_6$-to-$lysine_0$ ratio present in organ/tissue, which is brain and retina for our study, although, the re-usable amount of $lysine_6$ and $lysine_0$ acquired from degraded proteins will also be present in this pool. This is the most crucial parameter that needs to be defined to calculate the real turnover of a protein. The experiments in this regard are still in progress. We are trying to calculate this ratio using different approaches:

- by quantifying the ratio of extracted free lysine$_6$-to-lysine$_0$ ratio by mass spectrometry.
- by quantitating the SILAC pairs present in signal-induced over-expressed organ specific protein in cortex over time

References

Ahmed, S., Holt, M., Riedel, D., and Jahn, R. (2013). Small-scale isolation of synaptic vesicles from mammalian brain. Nature protocols *8*, 998-1009.

Ahrne, E., Molzahn, L., Glatter, T., and Schmidt, A. (2013). Critical assessment of proteome-wide label-free absolute abundance estimation strategies. Proteomics *13*, 2567-2578.

Alpadi, K., Magupalli, V.G., Kappel, S., Koblitz, L., Schwarz, K., Seigel, G.M., Sung, C.H., and Schmitz, F. (2008). RIBEYE recruits munc119, a mammalian ortholog of the Caenorhabditis elegans protein unc119, to synaptic ribbons of photoreceptor Synapses. Journal of Biological Chemistry *283*, 26461-26467.

Arike, L., Valgepea, K., Peil, L., Nahku, R., Adamberg, K., and Vilu, R. (2012). Comparison and applications of label-free absolute proteome quantification methods on Escherichia coli. Journal of proteomics *75*, 5437-5448.

Bai, F., Witzmann, F.A. (2007) Synaptosome proteomics. Subcell Biochem. *43*, 77-98.

Bantscheff, M., Schirle, M., Sweetman, G., Rick, J., and Kuster, B. (2007). Quantitative mass spectrometry in proteomics: a critical review. Analytical and bioanalytical chemistry *389*, 1017-1031.

Bargmann, C.I. (2012). Beyond the connectome: how neuromodulators shape neural circuits. BioEssays : news and reviews in molecular, cellular and developmental biology *34*, 458-465.

Barnhill, A.E., Hecker, L.A., Kohutyuk, O., Buss, J.E., Honavar, V.G., and Greenlee, H.W. (2010). Characterization of the retinal proteome during rod photoreceptor genesis. BMC research notes *3*, 25.

Bech-Hansen, N.T., Naylor, M.J., Maybaum, T.A., Pearce, W.G., Koop, B., Fishman, G.A., Mets, M., Musarella, M.A., and Boycott, K.M. (1998). Loss-of-function mutations in a calcium-channel alpha(1)-subunit gene in Xp11.23 cause incomplete X-linked congenital stationary night blindness. Nature genetics *19*, 264-267.

Bellhorn, M.B., and Lewis, R.K. (1976). Localization of Ions in Retina by Secondary Ion Mass-Spectrometry. Experimental eye research *22*, 505-518.

Benfenati, F., Greengard, P., Brunner, J., and Bahler, M. (1989). Electrostatic and hydrophobic interactions of synapsin I and synapsin I fragments with phospholipid bilayers. The Journal of cell biology *108*, 1851-1862.

Bennett, M.V., and Zukin, R.S. (2004). Electrical coupling and neuronal synchronization in the Mammalian brain. Neuron *41*, 495-511.

Berntson, A.K., and Morgans, C.W. (2003). Distribution of the presynaptic calcium sensors, synaptotagmin I/II and synaptotagmin III, in the goldfish and rodent retinas. Journal of vision *3*, 274-280.

Booth, F.J., Connell, G.J., Docherty, J.R., and Mcgrath, J.C. (1978). Isolation of Non-Adrenergic Motor-Nerve Response in Rat Vas-Deferens by Elimination of Adrenergic Motor Component. J Physiol-London *280*, P19-P20.

Borst, J.G.G., and van Hoeve, J.S. (2012). The Calyx of Held Synapse: From Model Synapse to Auditory Relay. Annual Review of Physiology, Vol 74 *74*, 199-224.

Boyken, J (2012) Molecular profiling of presynaptic docking sites, Doctoral thesis, Uni-Goettingen.

Boyken, J., Gronborg, M., Riedel, D., Urlaub, H., Jahn, R., and Chua, J.J. (2013). Molecular profiling of synaptic vesicle docking sites reveals novel proteins but few differences between glutamatergic and GABAergic synapses. Neuron *78*, 285-297.

Brandstatter, J.H., Lohrke, S., Morgans, C.W., and Wassle, H. (1996a). Distributions of two homologous synaptic vesicle proteins, synaptoporin and synaptophysin, in the mammalian retina. The Journal of comparative neurology *370*, 1-10.

Brandstatter, J.H., Wassle, H., Betz, H., and Morgans, C.W. (1996b). The plasma membrane protein SNAP-25, but not syntaxin, is present at photoreceptor and bipolar cell synapses in the rat retina. The European journal of neuroscience *8*, 823-828.

Buckley, K., and Kelly, R.B. (1985). Identification of a transmembrane glycoprotein specific for secretory vesicles of neural and endocrine cells. The Journal of cell biology *100*, 1284-1294.

Cajal, S.R. (2006). The impossible interview with the man of the neuron doctrine. Interview by Edward G Jones. Journal of the history of the neurosciences *15*, 326-340.

Catsicas, S., Catsicas, M., Keyser, K.T., Karten, H.J., Wilson, M.C., and Milner, R.J. (1992). Differential expression of the presynaptic protein SNAP-25 in mammalian retina. Journal of neuroscience research *33*, 1-9.

Chang, W.P., and Sudhof, T.C. (2009). SV2 renders primed synaptic vesicles competent for Ca2+ -induced exocytosis. The Journal of neuroscience : the official journal of the Society for Neuroscience *29*, 883-897.

Chua, J.J., Kindler, S., Boyken, J., and Jahn, R. (2010). The architecture of an excitatory synapse. Journal of cell science *123*, 819-823.

Cohen, L.D., Zuchman, R., Sorokina, O., Muller, A., Dieterich, D.C., Armstrong, J.D., Ziv, T., and Ziv, N.E. (2013). Metabolic turnover of synaptic proteins: kinetics, interdependencies and implications for synaptic maintenance. PloS one *8*, e63191.

Connors, B.W., and Long, M.A. (2004). Electrical synapses in the mammalian brain. Annual review of neuroscience *27*, 393-418.

Cox, J., and Mann, M. (2008). MaxQuant enables high peptide identification rates, individualized p.p.b.-range mass accuracies and proteome-wide protein quantification. Nature biotechnology *26*, 1367-1372.

Cox, J., Neuhauser, N., Michalski, A., Scheltema, R.A., Olsen, J.V., and Mann, M. (2011). Andromeda: a peptide search engine integrated into the MaxQuant environment. Journal of proteome research *10*, 1794-1805.

Cueva, J.G., Haverkamp, S., Reimer, R.J., Edwards, R., Wassle, H., and Brecha, N.C. (2002). Vesicular gamma-aminobutyric acid transporter expression in amacrine and horizontal cells. The Journal of comparative neurology *445*, 227-237.

Deremer, M.F., Saeli, R.J., Brautigan, D.L., and Edelman, A.M. (1992a). Ca2+-Calmodulin-Dependent Protein Kinase-Ia and Kinase-Ib from Rat-Brain .2. Enzymatic Characteristics and Regulation of Activities by Phosphorylation and Dephosphorylation. Journal of Biological Chemistry *267*, 13466-13471.

Deremer, M.F., Saeli, R.J., and Edelman, A.M. (1992b). Ca2+-Calmodulin-Dependent Protein Kinase-Ia and Kinase-Ib from Rat-Brain .1. Identification, Purification, and Structural Comparisons. Journal of Biological Chemistry *267*, 13460-13465.

Derobertis, E., and Franchi, C.M. (1956). Electron Microscope Observations on Synaptic Vesicles in Synapses of the Retinal Rods and Cones. J Biophys Biochem Cy *2*, 307-&.

Derobertis, E.D.P., and Bennett, H.S. (1955). Some Features of the Submicroscopic Morphology of Synapses in Frog and Earthworm. J Biophys Biochem Cy *1*, 47-&.

Dieck, S.T., Altrock, W.D., Kessels, M.M., Qualmann, B., Regus, H., Brauner, D., Fejtova, A., Bracko, O., Gundelfinger, E.D., and Brandstatter, J.H. (2005). Molecular dissection of the photoreceptor ribbon synapse: physical interaction of Bassoon and RIBEYE is essential for the assembly of the ribbon complex. Journal of Cell Biology *168*, 825-836.

Doherty, M.K., and Beynon, R.J. (2006). Protein turnover on the scale of the proteome. Expert review of proteomics *3*, 97-110.

Dole, M., Mack, L.L., and Hines, R.L. (1968). Molecular Beams of Macroions. J Chem Phys *49*, 2240-&.

Dowling, J.E., and Boycott, B.B. (1966). Organization of the primate retina: electron microscopy. Proceedings of the Royal Society of London Series B, Biological sciences *166*, 80-111.

Dowling, J.E., and Werblin, F.S. (1969). Organization of retina of the mudpuppy, Necturus maculosus. I. Synaptic structure. Journal of neurophysiology *32*, 315-338.

Edman, P. (1949). A method for the determination of amino acid sequence in peptides. Archives of biochemistry *22*, 475.

Elliott, T. R. (1905) The action of adrenalin. J. Physiol. 32, 401–467

Elliot, T.R. (1905). The action of adrenalin. British medical journal *1905*, 127-130.

Fabre, B., Lambour, T., Garrigues, L., Ducoux-Petit, M., Amalric, F., Monsarrat, B., Burlet-Schiltz, O., and Bousquet-Dubouch, M.P. (2014). Label-free quantitative proteomics reveals the dynamics of proteasome complexes composition and stoichiometry in a wide range of human cell lines. Journal of proteome research *13*, 3027-3037.

Fenn, J.B. (2002). Electrospray ionization mass spectrometry: How it all began. Journal of biomolecular techniques : JBT *13*, 101-118.

Fenn, J.B., Mann, M., Meng, C.K., Wong, S.F., and Whitehouse, C.M. (1989). Electrospray ionization for mass spectrometry of large biomolecules. Science *246*, 64-71.

Ferguson, S.M., Brasnjo, G., Hayashi, M., Wolfel, M., Collesi, C., Giovedi, S., Raimondi, A., Gong, L.W., Ariel, P., Paradise, S.*, et al.* (2007). A selective activity-dependent requirement for dynamin 1 in synaptic vesicle endocytosis. Science *316*, 570-574.

Finbow, M.E., and Harrison, M.A. (1997). The vacuolar H+-ATPase: A universal proton pump of eukaryotes. Biochemical Journal *324*, 697-712.

Firth, S.I., Morgan, I.G., Boelen, M.K., and Morgans, C.W. (2001). Localization of voltage-sensitive L-type calcium channels in the chicken retina. Clin Exp Ophthalmol *29*, 183-187.

Ford, M.G., Mills, I.G., Peter, B.J., Vallis, Y., Praefcke, G.J., Evans, P.R., and McMahon, H.T. (2002). Curvature of clathrin-coated pits driven by epsin. Nature *419*, 361-366.

Furshpan, E.J., and Potter, D.D. (1959). Transmission at the giant motor synapses of the crayfish. The Journal of physiology *145*, 289-325.

Geiger, T., Wehner, A., Schaab, C., Cox, J., and Mann, M. (2012). Comparative Proteomic Analysis of Eleven Common Cell Lines Reveals Ubiquitous but Varying Expression of Most Proteins. Molecular & Cellular Proteomics *11*.

Geppert, M., Ullrich, B., Green, D.G., Takei, K., Daniels, L., De Camilli, P., Sudhof, T.C., and Hammer, R.E. (1994). Synaptic targeting domains of synapsin I revealed by transgenic expression in photoreceptor cells. The EMBO journal *13*, 3720-3727.

Gerber, S.A., Kettenbach, A.N., Rush, J., and Gygi, S.P. (2007). The absolute quantification strategy: application to phosphorylation profiling of human separase serine 1126. Methods in molecular biology *359*, 71-86.

Gerber, S.A., Rush, J., Stemman, O., Kirschner, M.W., and Gygi, S.P. (2003). Absolute quantification of proteins and phosphoproteins from cell lysates by tandem MS. Proceedings of the National Academy of Sciences of the United States of America *100*, 6940-6945.

Gomis, A., Burrone, J., and Lagnado, L. (1999). Two actions of calcium regulate the supply of releasable vesicles at the ribbon synapse of retinal bipolar cells. Journal of Neuroscience *19*, 6309-6317.

Goodenough, D.A., and Paul, D.L. (2009). Gap junctions. Cold Spring Harbor perspectives in biology *1*, a002576.

Grabs, D., Bergmann, M., Urban, M., Post, A., and Gratzl, M. (1996). Rab3 proteins and SNAP-25, essential components of the exocytosis machinery in conventional synapses, are absent from ribbon synapses of the mouse retina. European Journal of Neuroscience *8*, 162-168.

Gratzl, M., Dahl, G., Russell, J.T., and Thorn, N.A. (1977). Fusion of neurohypophyseal membranes in vitro. Biochimica et biophysica acta *470*, 45-57.

Gray, E.G., and Pease, H.L. (1971). Understanding Organisation of Retinal Receptor Synapses. Brain research *35*, 1-&.

Gray, E.G., and Whittaker, V.P. (1962). The isolation of nerve endings from brain: an electron-microscopic study of cell fragments derived by homogenization and centrifugation. Journal of anatomy *96*, 79-88.

Greenlee, M.H., Roosevelt, C.B., and Sakaguchi, D.S. (2001). Differential localization of SNARE complex proteins SNAP-25, syntaxin, and VAMP during development of the mammalian retina. The Journal of comparative neurology *430*, 306-320.

Griffiths, J (2008) A Brief History of Mass Spectrometry. Analytical Chemistry *80*, 5678-5683.

Gronborg, M., Pavlos, N.J., Brunk, I., Chua, J.J.E., Munster-Wandowski, A., Riedel, D., Ahnert-Hilger, G., Urlaub, H., and Jahn, R. (2010). Quantitative Comparison of Glutamatergic and GABAergic Synaptic Vesicles Unveils Selectivity for Few Proteins Including MAL2, a Novel Synaptic Vesicle Protein. Journal of Neuroscience *30*, 2-12.

Guan, S.H., Price, J.C., Ghaemmaghami, S., Prusiner, S.B., and Burlingame, A.L. (2012). Compartment Modeling for Mammalian Protein Turnover Studies by Stable Isotope Metabolic Labeling. Analytical chemistry *84*, 4014-4021.

Heidelberger, R. (2001). ATP is required at an early step in compensatory endocytosis in synaptic terminals. Journal of Neuroscience *21*, 6467-6474.

Heidelberger, R., Sterling, P., and Matthews, G. (2002). Roles of ATP in depletion and replenishment of the releasable pool of synaptic vesicles. Journal of neurophysiology *88*, 98-106.

Heidelberger, R., Thoreson, W.B., and Witkovsky, P. (2005). Synaptic transmission at retinal ribbon synapses. Progress in retinal and eye research *24*, 682-720.

Heidelberger, R., Wang, M.M., and Sherry, D.M. (2003). Differential distribution of synaptotagmin immunoreactivity among synapses in the goldfish, salamander, and mouse retina. Visual neuroscience *20*, 37-49.

Helfmann, S., Neumann, P., Tittmann, K., Moser, T., Ficner, R., and Reisinger, E. (2011). The crystal structure of the C(2)A domain of otoferlin reveals an unconventional top loop region. Journal of molecular biology *406*, 479-490.

Hell, J.W., Maycox, P.R., Stadler, H., and Jahn, R. (1988). Uptake of GABA by rat brain synaptic vesicles isolated by a new procedure. The EMBO journal *7*, 3023-3029.

Henne, W.M., Boucrot, E., Meinecke, M., Evergren, E., Vallis, Y., Mittal, R., and McMahon, H.T. (2010). FCHo proteins are nucleators of clathrin-mediated endocytosis. Science *328*, 1281-1284.

Herzog, E., Takamori, S., Jahn, R., Brose, N., and Wojcik, S.M. (2006). Synaptic and vesicular co-localization of the glutamate transporters VGLUT1 and VGLUT2 in the mouse hippocampus. Journal of neurochemistry *99*, 1011-1018.

Heuser, J.E., Reese, T.S., Dennis, M.J., Jan, Y., Jan, L., and Evans, L. (1979). Synaptic vesicle exocytosis captured by quick freezing and correlated with quantal transmitter release. The Journal of cell biology *81*, 275-300.

Higashide, T., McLaren, M.J., and Inana, G. (1998). Localization of HRG4, a photoreceptor protein homologous to Unc-119, in ribbon synapse. Investigative ophthalmology & visual science *39*, 690-698.

Hildebrand, J.D., and Soriano, P. (2002). Overlapping and unique roles for C-terminal binding protein 1 (CtBP1) and CtBP2 during mouse development. Molecular and cellular biology *22*, 5296-5307.

Hirano, A.A., Brandstatter, J.H., and Brecha, N.C. (2005). Cellular distribution and subcellular localization of molecular components of vesicular transmitter release in horizontal cells of rabbit retina. The Journal of comparative neurology *488*, 70-81.

Honing, S., Ricotta, D., Krauss, M., Spate, K., Spolaore, B., Motley, A., Robinson, M., Robinson, C., Haucke, V., and Owen, D.J. (2005). Phosphatidylinositol-(4,5)-bisphosphate regulates sorting signal recognition by the clathrin-associated adaptor complex AP2. Molecular cell *18*, 519-531.

Hsueh, Y.P. (2006). The role of the MAGUK protein CASK in neural development and synaptic function. Current medicinal chemistry *13*, 1915-1927.

Huang, D.W., Sherman, B.T., Tan, Q., Kir, J., Liu, D., Bryant, D., Guo, Y., Stephens, R., Baseler, M.W., Lane, H.C*., et al.* (2007). DAVID Bioinformatics Resources: expanded annotation database and novel algorithms to better extract biology from large gene lists. Nucleic acids research *35*, W169-175.

Hurlbut, W.P., and Ceccarelli, B. (1974). Transmitter release and recycling of synaptic vesicle membrane at the neuromuscular junction. Advances in cytopharmacology *2*, 141-154.

Husi, H., Ward, M.A., Choudhary, J.S., Blackstock, W.P., and Grant, S.G. (2000). Proteomic analysis of NMDA receptor-adhesion protein signaling complexes. Nature neuroscience *3*, 661-669.

Huttner, W.B., Schiebler, W., Greengard, P., and De Camilli, P. (1983). Synapsin I (protein I), a nerve terminal-specific phosphoprotein. III. Its association with synaptic vesicles studied in a highly purified synaptic vesicle preparation. The Journal of cell biology *96*, 1374-1388.

Ishihama, Y., Oda, Y., Tabata, T., Sato, T., Nagasu, T., Rappsilber, J., and Mann, M. (2005). Exponentially modified protein abundance index (emPAI) for estimation of absolute protein amount in proteomics by the number of sequenced peptides per protein. Molecular & cellular proteomics : MCP *4*, 1265-1272.

Jackman, S.L., Choi, S.Y., Thoreson, W.B., Rabl, K., Bartoletti, T.M., and Kramer, R.H. (2009). Role of the synaptic ribbon in transmitting the cone light response. Nature neuroscience *12*, 303-310.

Jahn, R. (2006). Exocytosis - spotlight on the trafficking organelle. European journal of cell biology *85*, 15-15.

Jahn, R., and Scheller, R.H. (2006). SNAREs--engines for membrane fusion. Nature reviews Molecular cell biology *7*, 631-643.

Jahn, R., Schiebler, W., Ouimet, C., and Greengard, P. (1985). A 38,000-dalton membrane protein (p38) present in synaptic vesicles. Proceedings of the National Academy of Sciences of the United States of America *82*, 4137-4141.

Jahn, R., and Sudhof, T.C. (1994). Synaptic vesicles and exocytosis. Annual review of neuroscience *17*, 219-246.

Jellali, A., Stussi-Garaud, C., Gasnier, B., Rendon, A., Sahel, J.A., Dreyfus, H., and Picaud, S. (2002). Cellular localization of the vesicular inhibitory amino acid transporter in the mouse and human retina. The Journal of comparative neurology *449*, 76-87.

Jeon, C.J., Strettoi, E., and Masland, R.H. (1998). The major cell populations of the mouse retina. The Journal of neuroscience : the official journal of the Society for Neuroscience *18*, 8936-8946.

Jia, W.G., Beaulieu, C., Liu, Y.L., and Cynader, M. (1992). Calcium Calmodulin Dependent Kinase-Ii in Cat Visual-Cortex and Its Development. Dev Neurosci-Basel *14*, 238-246.

Johnson, J., Tian, N., Caywood, M.S., Reimer, R.J., Edwards, R.H., and Copenhagen, D.R. (2003). Vesicular neurotransmitter transporter expression in developing postnatal rodent retina: GABA and glycine precede glutamate. The Journal of neuroscience : the official journal of the Society for Neuroscience *23*, 518-529.

Jordan, B.A., Fernholz, B.D., Boussac, M., Xu, C., Grigorean, G., Ziff, E.B., and Neubert, T.A. (2004). Identification and verification of novel rodent postsynaptic density proteins. Molecular & cellular proteomics : MCP *3*, 857-871.

Jordan, B.A., Fernholz, B.D., Neubert, T.A., and Ziff, E.B. (2006). New Tricks for an Old Dog: Proteomics of the PSD. In The Dynamic Synapse: Molecular Methods in Ionotropic Receptor Biology, J.T. Kittler, and S.J. Moss, eds. (Boca Raton (FL)).

Kantardzhieva, A., Peppi, M., Lane, W.S., and Sewell, W.F. (2012). Protein Composition of Immunoprecipitated Synaptic Ribbons. Journal of proteome research *11*, 1163-1174.

Katz, B. (Liverpool Univ. Press, 1969)The Release of Neural Transmitter Substances (Sherrington Lecture)

Karas, M., Bachmann, D., and Hillenkamp, F. (1985). Influence of the Wavelength in High-Irradiance Ultraviolet-Laser Desorption Mass-Spectrometry of Organic-Molecules. Analytical chemistry *57*, 2935-2939.

Karas, M., and Hillenkamp, F. (1988). Laser Desorption Ionization of Proteins with Molecular Masses Exceeding 10000 Daltons. Analytical chemistry *60*, 2299-2301.

Katz, B., and Miledi, R. (1969). Spontaneous and evoked activity of motor nerve endings in calcium Ringer. The Journal of physiology *203*, 689-706.

Kessels, M.M., and Qualmann, B. (2004). The syndapin protein family: linking membrane trafficking with the cytoskeleton. Journal of cell science *117*, 3077-3086.

Kettenbach, A.N., Rush, J., and Gerber, S.A. (2011). Absolute quantification of protein and post-translational modification abundance with stable isotope-labeled synthetic peptides. Nature protocols *6*, 175-186.

Kremer, T., Kempf, C., Wittenmayer, N., Nawrotzki, R., Kuner, T., Kirsch, J., and Dresbach, T. (2007). Mover is a novel vertebrate-specific presynaptic protein with differential distribution at subsets of CNS synapses. FEBS letters *581*, 4727-4733.

Kruger, M., Moser, M., Ussar, S., Thievessen, I., Luber, C.A., Forner, F., Schmidt, S., Zanivan, S., Fassler, R., and Mann, M. (2008). SILAC mouse for quantitative proteomics uncovers kindlin-3 as an essential factor for red blood cell function. Cell *134*, 353-364.

Kummel, D., Krishnakumar, S.S., Radoff, D.T., Li, F., Giraudo, C.G., Pincet, F., Rothman, J.E., and Reinisch, K.M. (2011). Complexin cross-links prefusion SNAREs into a zigzag array. Nature structural & molecular biology *18*, 927-U1603.

Kuster, B. (2014). Mass Spectrometry Based Draft of the Human Proteome. Molecular & Cellular Proteomics *13*, S15-S15.

Lasansky, A. (1973). Organization of Outer Synaptic Layer in Retina of Larval Tiger Salamander. Philos T Roy Soc B *265*, 471-&.

Lenzi, D., and von Gersdorff, H. (2001). Structure suggests function: the case for synaptic ribbons as exocytotic nanomachines. BioEssays : news and reviews in molecular, cellular and developmental biology *23*, 831-840.

Li, F., Pincet, F., Perez, E., Giraudo, C.G., Tareste, D., and Rothman, J.E. (2011). Complexin activates and clamps SNAREpins by a common mechanism involving an intermediate energetic state. Nature structural & molecular biology *18*, 941-U105.

Loewi, O. (1924) Über humorale Übertragbarkeit der Herznervenwirkung. Pflugers Arch. Gesamte Physiol. Menschen Tiere 204, 629–640 (in German)

LoGiudice, L., Sterling, P., and Matthews, G. (2009). Vesicle Recycling at Ribbon Synapses in the Finely Branched Axon Terminals of Mouse Retinal Bipolar Neurons. Neuroscience *164*, 1546-1556.

Lu, P., Vogel, C., Wang, R., Yao, X., and Marcotte, E.M. (2007). Absolute protein expression profiling estimates the relative contributions of transcriptional and translational regulation. Nature biotechnology *25*, 117-124.

Luby-Phelps, K. (2000). Cytoarchitecture and physical properties of cytoplasm: Volume, viscosity. diffusion, intracellular surface area. Int Rev Cytol *192*, 189-221.

Ma, C., Li, W., Xu, Y., and Rizo, J. (2011). Munc13 mediates the transition from the closed syntaxin-Munc18 complex to the SNARE complex. Nature structural & molecular biology *18*, 542-549.

Makarov, A. (2000). Electrostatic axially harmonic orbital trapping: A high-performance technique of mass analysis. Analytical chemistry *72*, 1156-1162.

Mallick, P., Schirle, M., Chen, S.S., Flory, M.R., Lee, H., Martin, D., Ranish, J., Raught, B., Schmitt, R., Werner, T.*, et al.* (2007). Computational prediction of proteotypic peptides for quantitative proteomics. Nature biotechnology *25*, 125-131.

Malsam, J., Parisotto, D., Bharat, T.A.M., Scheutzow, A., Krause, J.M., Briggs, J.A.G., and Sollner, T.H. (2012). Complexin arrests a pool of docked vesicles for fast Ca2+-dependent release. Embo Journal *31*, 3270-3281.

Mandell, J.W., Czernik, A.J., De Camilli, P., Greengard, P., and Townes-Anderson, E. (1992). Differential expression of synapsins I and II among rat retinal synapses. The Journal of neuroscience : the official journal of the Society for Neuroscience *12*, 1736-1749.

Mandell, J.W., MacLeish, P.R., and Townes-Anderson, E. (1993). Process outgrowth and synaptic varicosity formation by adult photoreceptors in vitro. The Journal of neuroscience : the official journal of the Society for Neuroscience *13*, 3533-3548.

Mandell, J.W., Townes-Anderson, E., Czernik, A.J., Cameron, R., Greengard, P., and De Camilli, P. (1990). Synapsins in the vertebrate retina: absence from ribbon synapses and heterogeneous distribution among conventional synapses. Neuron *5*, 19-33.

Manea, M., Mezo, G., Hudecz, F., and Przybylski, M. (2007). Mass spectrometric identification of the trypsin cleavage pathway in lysyl-proline containing oligotuftsin peptides. Journal of peptide science : an official publication of the European Peptide Society *13*, 227-236.

Mann, K., and Edsinger, E. (2014). The Lottia gigantea shell matrix proteome: re-analysis including MaxQuant iBAQ quantitation and phosphoproteome analysis. Proteome science *12*, 28.

Mann, K., and Mann, M. (2013). The proteome of the calcified layer organic matrix of turkey (Meleagris gallopavo) eggshell. Proteome science *11*, 40.

Martin, J.A., Hu, Z.T., Fenz, K.M., Fernandez, J., and Dittman, J.S. (2011). Complexin Has Opposite Effects on Two Modes of Synaptic Vesicle Fusion. Current Biology *21*, 97-105.

Matthews, G., and Fuchs, P. (2010). The diverse roles of ribbon synapses in sensory neurotransmission. Nature reviews Neuroscience *11*, 812-822.

Maycox, P.R., Deckwerth, T., Hell, J.W., and Jahn, R. (1988). Glutamate uptake by brain synaptic vesicles. Energy dependence of transport and functional reconstitution in proteoliposomes. The Journal of biological chemistry *263*, 15423-15428.

McClatchy, D.B., and Yates, J.R., 3rd (2008). Stable Isotope Labeling of Mammals (SILAM). CSH protocols *2008*, pdb prot4940.

McClatchy, D.B., and Yates, J.R., 3rd (2014). Stable isotope labeling in mammals (SILAM). Methods in molecular biology *1156*, 133-146.

McMahon, H.T., and Boucrot, E. (2011). Molecular mechanism and physiological functions of clathrin-mediated endocytosis. Nat Rev Mol Cell Bio *12*, 517-533.

McNurlan, M.A., and Garlick, P.J. (1989). Influence of nutrient intake on protein turnover. Diabetes/metabolism reviews *5*, 165-189.

Michalski, A., Damoc, E., Hauschild, J.P., Lange, O., Wieghaus, A., Makarov, A., Nagaraj, N., Cox, J., Mann, M., and Horning, S. (2011). Mass spectrometry-based proteomics using Q Exactive, a high-performance benchtop quadrupole Orbitrap mass spectrometer. Molecular & cellular proteomics : MCP *10*, M111 011015.

Michalski, A., Damoc, E., Lange, O., Denisov, E., Nolting, D., Muller, M., Viner, R., Schwartz, J., Remes, P., Belford, M.*, et al.* (2012). Ultra high resolution linear ion trap Orbitrap mass spectrometer (Orbitrap Elite) facilitates top down LC MS/MS and versatile peptide fragmentation modes. Molecular & cellular proteomics : MCP *11*, O111 013698.

Morciano, M., Burre, J., Corvey, C., Karas, M., Zimmermann, H., and Volknandt, W. (2005). Immunoisolation of two synaptic vesicle pools from synaptosomes: a proteomics analysis. Journal of neurochemistry *95*, 1732-1745.

Morgans, C.W. (2000a). Neurotransmitter release at ribbon synapses in the retina. Immunology and cell biology *78*, 442-446.

Morgans, C.W. (2000b). Presynaptic proteins of ribbon synapses in the retina. Microscopy research and technique *50*, 141-150.

Morgans, C.W. (2001). Localization of the alpha(1F) Calcium channel subunit in the rat retina. Investigative ophthalmology & visual science *42*, 2414-2418.

Morgans, C.W., Brandstatter, J.H., Kellerman, J., Betz, H., and Wassle, H. (1996). A SNARE complex containing syntaxin 3 is present in ribbon synapses of the retina. The Journal of neuroscience : the official journal of the Society for Neuroscience *16*, 6713-6721.

Morgans, C.W., Gaughwin, P., and Maleszka, R. (2001). Expression of the alpha(1F) calcium channel subunit by photoreceptors in the rat retina. Molecular vision *7*, 202-209.

Muench, S.P., Trinick, J., and Harrison, M.A. (2011). Structural divergence of the rotary ATPases. Q Rev Biophys *44*, 311-356.

Muresan, V., Lyass, A., and Schnapp, B.J. (1999). The kinesin motor KIF3A is a component of the presynaptic ribbon in vertebrate photoreceptors. Journal of Neuroscience *19*, 1027-1037.

Nagaraj, N., Wisniewski, J.R., Geiger, T., Cox, J., Kircher, M., Kelso, J., Paabo, S., and Mann, M. (2011). Deep proteome and transcriptome mapping of a human cancer cell line. Molecular systems biology *7*, 548.

Nagy, A., Baker, R.R., Morris, S.J., and Whittaker, V.P. (1976). The preparation and characterization of synaptic vesicles of high purity. Brain research *109*, 285-309.

Neal, M.J., and Atterwil.Ck (1974). Isolation of Photoreceptor and Conventional Nerve-Terminals by Subcellular Fractionation of Rabbit Retina. Nature *251*, 331-333.

Obled, C., Barre, F., Millward, D.J., and Arnal, M. (1989). Whole body protein synthesis: studies with different amino acids in the rat. The American journal of physiology *257*, E639-646.

Ohya, T., Miaczynska, M., Coskun, U., Lommer, B., Runge, A., Drechsel, D., Kalaidzidis, Y., and Zerial, M. (2009). Reconstitution of Rab- and SNARE-dependent membrane fusion by synthetic endosomes. Nature *459*, 1091-1097.

Olsen, J.V., de Godoy, L.M., Li, G., Macek, B., Mortensen, P., Pesch, R., Makarov, A., Lange, O., Horning, S., and Mann, M. (2005). Parts per million mass accuracy on an Orbitrap mass spectrometer via lock mass injection into a C-trap. Molecular & cellular proteomics : MCP *4*, 2010-2021.

Olsen, O., Moore, K.A., Nicoll, R.A., and Bredt, D.S. (2006). Synaptic transmission regulated by a presynaptic MALS/Liprin-alpha protein complex. Current opinion in cell biology *18*, 223-227.

Ong, S.E., Blagoev, B., Kratchmarova, I., Kristensen, D.B., Steen, H., Pandey, A., and Mann, M. (2002). Stable isotope labeling by amino acids in cell culture, SILAC, as a simple and accurate approach to expression proteomics. Molecular & cellular proteomics : MCP *1*, 376-386.

Paillart, C., Li, J., Matthews, G., and Sterling, P. (2003). Endocytosis and vesicle recycling at a ribbon synapse. The Journal of neuroscience : the official journal of the Society for Neuroscience *23*, 4092-4099.

Palade, G.E. (1954). Electron Microscope Observations of Interneuronal and Neuromuscular Synapses. Anatomical Record *118*, 335-336.

Pangrsic, T., Reisinger, E., and Moser, T. (2012). Otoferlin: a multi-C2 domain protein essential for hearing. Trends in neurosciences *35*, 671-680.

Parsons, T.D., and Sterling, P. (2003). Synaptic ribbon: Conveyor belt or safety belt? Neuron *37*, 379-382.

Pavlos, N.J., Gronborg, M., Riedel, D., Chua, J.J., Boyken, J., Kloepper, T.H., Urlaub, H., Rizzoli, S.O., and Jahn, R. (2010). Quantitative analysis of synaptic vesicle Rabs uncovers distinct yet overlapping roles for Rab3a and Rab27b in Ca2+-triggered exocytosis. The Journal of neuroscience : the official journal of the Society for Neuroscience *30*, 13441-13453.

Peng, J., Kim, M.J., Cheng, D., Duong, D.M., Gygi, S.P., and Sheng, M. (2004). Semiquantitative proteomic analysis of rat forebrain postsynaptic density fractions by mass spectrometry. The Journal of biological chemistry *279*, 21003-21011.

Peng, J., Schwartz, D., Elias, J.E., Thoreen, C.C., Cheng, D., Marsischky, G., Roelofs, J., Finley, D., and Gygi, S.P. (2003). A proteomics approach to understanding protein ubiquitination. Nature biotechnology *21*, 921-926.

Pereda, A.E. (2014). Electrical synapses and their functional interactions with chemical synapses. Nature reviews Neuroscience *15*, 250-263.

Pocklington, A.J., Armstrong, J.D., and Grant, S.G. (2006). Organization of brain complexity--synapse proteome form and function. Briefings in functional genomics & proteomics *5*, 66-73.

Pratt, J.M., Petty, J., Riba-Garcia, I., Robertson, D.H., Gaskell, S.J., Oliver, S.G., and Beynon, R.J. (2002). Dynamics of protein turnover, a missing dimension in proteomics. Molecular & cellular proteomics : MCP *1*, 579-591.

Price, J.C., Guan, S., Burlingame, A., Prusiner, S.B., and Ghaemmaghami, S. (2010). Analysis of proteome dynamics in the mouse brain. Proceedings of the National Academy of Sciences of the United States of America *107*, 14508-14513.

Prokai-Tatrai, K., Teixido, M., Nguyen, V., Zharikova, A.D., and Prokai, L. (2005). A pyridinium-substituted analog of the TRH-like tripeptide pGlu-Glu-Pro-NH2 and its prodrugs as central nervous system agents. Medicinal chemistry *1*, 141-152.

Purves D, Augustine GJ, Fitzpatrick D, et al., editors. (2001) Sunderland (MA): Sinauer Associates; Neuroscience, 2nd edition.

Rappsilber, J., Ryder, U., Lamond, A.I., and Mann, M. (2002). Large-scale proteomic analysis of the human spliceosome. Genome research *12*, 1231-1245.

Rauniyar, N., McClatchy, D.B., and Yates, J.R., 3rd (2013). Stable isotope labeling of mammals (SILAM) for in vivo quantitative proteomic analysis. Methods *61*, 260-268.

Raviola, E., and Gilula, N.B. (1975). Intramembrane organization of specialized contacts in the outer plexiform layer of the retina. A freeze-fracture study in monkeys and rabbits. The Journal of cell biology *65*, 192-222.

Read, D.S., Ball, S.L., Pardue, M.T., Morgans, C.W., Peachey, N.S., McCall, M.A., and Gregg, R.G. (2001). Photoreceptor L-type voltage-dependent Ca2+ channels are required for formation and/or maintenance of ribbon synapses in the OPL. Investigative ophthalmology & visual science *42*, S365-S365.

Reckow, S., and Webhofer, C. (2014). Analysis of individual protein turnover in live animals on a proteome-wide scale. Methods in molecular biology *1156*, 147-154.

Reidel, B., Thompson, J.W., Farsiu, S., Moseley, M.A., Skiba, N.P., and Arshavsky, V.Y. (2011). Proteomic Profiling of a Layered Tissue Reveals Unique Glycolytic Specializations of Photoreceptor Cells. Molecular & Cellular Proteomics *10*.

Reim, K., Regus-Leidig, H., Ammermuller, J., El-Kordi, A., Radyushkin, K., Ehrenreich, H., Brandstatter, J.H., and Brose, N. (2009). Aberrant function and structure of retinal ribbon synapses in the absence of complexin 3 and complexin 4. Journal of cell science *122*, 1352-1361.

Reisinger, E., Bresee, C., Neef, J., Nair, R., Reuter, K., Bulankina, A., Nouvian, R., Koch, M., Buckers, J., Kastrup, L.*, et al.* (2011). Probing the functional equivalence of otoferlin and synaptotagmin 1 in exocytosis. The Journal of neuroscience : the official journal of the Society for Neuroscience *31*, 4886-4895.

Rizo, J., and Rosenmund, C. (2008). Synaptic vesicle fusion. Nature structural & molecular biology *15*, 665-674.

Rizzoli, S.O., and Betz, W.J. (2005). Synaptic vesicle pools. Nature reviews Neuroscience *6*, 57-69.

Rizzoli, S.O., and Jahn, R. (2007). Kiss-and-run, collapse and 'readily retrievable' vesicles. Traffic *8*, 1137-1144.

Rodnight, R., and Wofchuk, S.T. (1992). Roles for protein phosphorylation in synaptic transmission. Essays in Biochemistry, Vol 27 *27*, 91-102.

Rogelj, B., Mitchell, J.C., Miller, C.C.J., and McLoughlin, D.M. (2006). The X11/Mint family of adaptor proteins. Brain Res Rev *52*, 305-315.

Roux, I., Safieddine, S., Nouvian, R., Grati, M., Simmler, M.C., Bahloul, A., Perfettini, I., Le Gall, M., Rostaing, P., Hamard, G.*, et al.* (2006). Otoferlin, defective in a human deafness form, is essential for exocytosis at the auditory ribbon synapse. Cell *127*, 277-289.

Ruel, J., Emery, S., Nouvian, R., Bersot, T., Amilhon, B., Van Rybroek, J.M., Rebillard, G., Lenoir, M., Eybalin, M., Delprat, B.*, et al.* (2008). Impairment of SLC17A8 encoding vesicular glutamate transporter-3, VGLUT3, underlies nonsyndromic deafness DFNA25 and inner hair cell dysfunction in null mice. American journal of human genetics *83*, 278-292.

Saheki, Y., and De Camilli, P. (2012). Synaptic vesicle endocytosis. Cold Spring Harbor perspectives in biology *4*, a005645.

Schagger, H. (2006). Tricine-SDS-PAGE. Nature protocols *1*, 16-22.

Schagger, H., and von Jagow, G. (1987). Tricine-sodium dodecyl sulfate-polyacrylamide gel electrophoresis for the separation of proteins in the range from 1 to 100 kDa. Analytical biochemistry *166*, 368-379.

Schaller, J., Akiyama, K., Tsuda, R., Hara, M., Marti, T., and Rickli, E.E. (1987). Isolation, characterization and amino-acid sequence of gamma-seminoprotein, a glycoprotein from human seminal plasma. European journal of biochemistry / FEBS *170*, 111-120.

Schlossman, D.M., Schmid, S.L., Braell, W.A., and Rothman, J.E. (1984). An Enzyme That Removes Clathrin Coats - Purification of an Uncoating Atpase. Journal of Cell Biology *99*, 723-733.

Schmid, S.L., Braell, W.A., Schlossman, D.M., and Rothman, J.E. (1984). A Role for Clathrin Light-Chains in the Recognition of Clathrin Cages by Uncoating Atpase. Nature *311*, 228-231.

Schmied, R., and Holtzman, E. (1987). A phosphatase activity and a synaptic vesicle antigen in multivesicular bodies of frog retinal photoreceptor terminals. J Neurocytol *16*, 627-637.

Schmitz, F. (2009). The Making of Synaptic Ribbons: How They Are Built and What They Do. Neuroscientist *15*, 611-624.

Schmitz, F., Augustin, I., and Brose, N. (2001). The synaptic vesicle priming protein Munc13-1 is absent from tonically active ribbon synapses of the rat retina. Brain research *895*, 258-263.

Schmitz, F., Bechmann, M., and Drenckhahn, D. (1996). Purification of synaptic ribbons, structural components of the photoreceptor active zone complex. The Journal of neuroscience : the official journal of the Society for Neuroscience *16*, 7109-7116.

Schmitz, F., Konigstorfer, A., and Sudhof, T.C. (2000). RIBEYE, a component of synaptic ribbons: a protein's journey through evolution provides insight into synaptic ribbon function. Neuron *28*, 857-872.

Schmitz, F., Tabares, L., Khimich, D., Strenzke, N., de la Villa-Polo, P., Castellano-Munoz, M., Bulankina, A., Moser, T., Fernandez-Chacon, R., and Sudhof, T.C. (2006). CSPalpha-deficiency causes massive and rapid photoreceptor degeneration. Proceedings of the National Academy of Sciences of the United States of America *103*, 2926-2931.

Schoenheimer, R., and Rittenberg, D. (1938). The Application of Isotopes to the Study of Intermediary Metabolism. Science *87*, 221-226.

Schoenheimer, R., Rittenberg, D., Foster, G.L., Keston, A.S., and Ratner, S. (1938). The Application of the Nitrogen Isotope N15 for the Study of Protein Metabolism. Science *88*, 599-600.

Schrimpf, S.P., Meskenaite, V., Brunner, E., Rutishauser, D., Walther, P., Eng, J., Aebersold, R., and Sonderegger, P. (2005). Proteomic analysis of synaptosomes using isotope-coded affinity tags and mass spectrometry. Proteomics *5*, 2531-2541.

Schwanhausser, B., Busse, D., Li, N., Dittmar, G., Schuchhardt, J., Wolf, J., Chen, W., and Selbach, M. (2011). Global quantification of mammalian gene expression control. Nature *473*, 337-342.

Shalit, T., Elinger, D., Savidor, A., Gabashvili, A., and Levin, Y. (2015). MS1-Based Label-Free Proteomics Using a Quadrupole Orbitrap Mass Spectrometer. Journal of proteome research *14*, 1979-1986.

Sherry, D.M., and Heidelberger, R. (2005). Distribution of proteins associated with synaptic vesicle endocytosis in the mouse and goldfish retina. The Journal of comparative neurology *484*, 440-457.

Sherry, D.M., Mitchell, R., Standifer, K.M., and du Plessis, B. (2006). Distribution of plasma membrane-associated syntaxins 1 through 4 indicates distinct trafficking functions in the synaptic layers of the mouse retina. BMC neuroscience *7*, 54.

Sherry, D.M., Wang, M.M., and Frishman, L.J. (2003). Differential distribution of vesicle associated membrane protein isoforms in the mouse retina. Molecular vision *9*, 673-688.

Sherry, D.M., Yang, H.D., and Standifer, K.M. (2001). Vesicle-associated membrane protein isoforms in the tiger salamander retina. Journal of Comparative Neurology *431*, 424-436.

Shevchenko, A., Tomas, H., Havlis, J., Olsen, J.V., and Mann, M. (2006). In-gel digestion for mass spectrometric characterization of proteins and proteomes. Nature protocols *1*, 2856-2860.

Shin, O.H., Rizo, J., and Sudhof, T.C. (2002). Synaptotagmin function in dense core vesicle exocytosis studied in cracked PC12 cells. Nature neuroscience *5*, 649-656.

Shuford, C.M., Sederoff, R.R., Chiang, V.L., and Muddiman, D.C. (2012). Peptide production and decay rates affect the quantitative accuracy of protein cleavage isotope dilution mass spectrometry (PC-IDMS). Molecular & cellular proteomics : MCP *11*, 814-823.

Sihra, T.S., Bogonez, E., and Nicholls, D.G. (1992). Localized Ca2+ Entry Preferentially Effects Protein Dephosphorylation, Phosphorylation, and Glutamate Release. Journal of Biological Chemistry *267*, 1983-1989.

Singleton, D.R., Wu, T.T., and Castle, J.D. (1997). Three mammalian SCAMPs (secretory carrier membrane proteins) are highly related products of distinct genes having similar subcellular distributions. Journal of cell science *110 (Pt 17)*, 2099-2107.

Sjostrand, F.S. (1953a). The Lamellated Structure of the Nerve Myelin Sheath as Revealed by High Resolution Electron Microscopy. Experientia *9*, 68-69.

Sjostrand, F.S. (1953b). The Ultrastructural Organization of Retinal Rods and Cones. J Appl Phys *24*, 117-117.

Sjostrand, F.S. (1953c). The Ultrastructure of the Inner Segments of the Retinal Rods of the Guinea Pig Eye as Revealed by Electron Microscopy. J Cell Compar Physl *42*, 45-70.

Sjostrand, F.S. (1953d). The ultrastructure of the innersegments of the retinal rods of the guinea pig eye as revealed by electron microscopy. Journal of cellular physiology *42*, 45-70.

Sjostrand, F.S. (1953e). The Ultrastructure of the Nerve Myelin Sheaths. J Appl Phys *24*, 117-118.

Sjostrand, F.S. (1953f). The Ultrastructure of the Outer Segments of Rods and Cones of the Eye as Revealed by the Electron Microscope. J Cell Compar Physl *42*, 15-44.

Sjostrand, F.S. (1953g). The Ultrastructure of the Retinal Rod Synapses of the Guinea Pig Eye. J Appl Phys *24*, 1422-1422.

Sjostrand, F.S. (1958). Ultrastructure of retinal rod synapses of the guinea pig eye as revealed by three-dimensional reconstructions from serial sections. J Ultrastruct Res *2*, 122-170.

Smith, P.K., Krohn, R.I., Hermanson, G.T., Mallia, A.K., Gartner, F.H., Provenzano, M.D., Fujimoto, E.K., Goeke, N.M., Olson, B.J., and Klenk, D.C. (1985). Measurement of protein using bicinchoninic acid. Analytical biochemistry *150*, 76-85.

Smith, S.M., Renden, R., and von Gersdorff, H. (2008). Synaptic vesicle endocytosis: fast and slow modes of membrane retrieval. Trends in neurosciences *31*, 559-568.

Soufi, B., Krug, K., Harst, A., and Macek, B. (2015). Characterization of the E. coli proteome and its modifications during growth and ethanol stress. Frontiers in microbiology *6*, 103.

Spellman, D.S., Deinhardt, K., Darie, C.C., Chao, M.V., and Neubert, T.A. (2008). Stable isotopic labeling by amino acids in cultured primary neurons. Molecular & Cellular Proteomics *7*, 1067-1076.

Stenius, K., Janz, R., Sudhof, T.C., and Jahn, R. (1995). Structure of synaptogyrin (p29) defines novel synaptic vesicle protein. The Journal of cell biology *131*, 1801-1809.

Sterling, P., and Matthews, G. (2005). Structure and function of ribbon synapses. Trends in neurosciences *28*, 20-29.

Strom, T.M., Nyakatura, G., Apfelstedt-Sylla, E., Hellebrand, H., Lorenz, B., Weber, B.H., Wutz, K., Gutwillinger, N., Ruther, K., Drescher, B.*, et al.* (1998). An L-type calcium-channel gene mutated in incomplete X-linked congenital stationary night blindness. Nature genetics *19*, 260-263.

Sudhof, T.C. (2002). Synaptotagmins: Why so many? Journal of Biological Chemistry *277*, 7629-7632.

Sudhof, T.C. (2004). The synaptic vesicle cycle. Annual review of neuroscience *27*, 509-547.

Sudhof, T.C., and Rizo, J. (2011). Synaptic vesicle exocytosis. Cold Spring Harbor perspectives in biology *3*.

Sugita, S., Shin, O.H., Han, W., Lao, Y., and Sudhof, T.C. (2002). Synaptotagmins form a hierarchy of exocytotic Ca(2+) sensors with distinct Ca(2+) affinities. The EMBO journal *21*, 270-280.

Syka, J.E., Coon, J.J., Schroeder, M.J., Shabanowitz, J., and Hunt, D.F. (2004). Peptide and protein sequence analysis by electron transfer dissociation mass spectrometry. Proceedings of the National Academy of Sciences of the United States of America *101*, 9528-9533.

Takamori, S., Holt, M., Stenius, K., Lemke, E.A., Gronborg, M., Riedel, D., Urlaub, H., Schenck, S., Brugger, B., Ringler, P.*, et al.* (2006). Molecular anatomy of a trafficking organelle. Cell *127*, 831-846.

Takamori, S., Malherbe, P., Broger, C., and Jahn, R. (2002). Molecular cloning and functional characterization of human vesicular glutamate transporter 3. Embo Rep *3*, 798-803.

Takamori, S., Rhee, J.S., Rosenmund, C., and Jahn, R. (2000). Identification of a vesicular glutamate transporter that defines a glutamatergic phenotype in neurons. Nature *407*, 189-194.

Takamori, S., Rhee, J.S., Rosenmund, C., and Jahn, R. (2001). Identification of differentiation-associated brain-specific phosphate transporter as a second vesicular glutamate transporter (VGLUT2). Journal of Neuroscience *21*.

Taylor, M.J., Lampe, M., and Merrifield, C.J. (2012). A Feedback Loop between Dynamin and Actin Recruitment during Clathrin-Mediated Endocytosis. PLoS biology *10*

Z Taoufiq (2013) A high magnification image of synapse obtained by electron microscopy, OIST

Thiele, C., Hannah, M.J., Fahrenholz, F., and Huttner, W.B. (2000). Cholesterol binds to synaptophysin and is required for biogenesis of synaptic vesicles. Nature cell biology *2*, 42-49.

Thoreson, W.B. (2007). Kinetics of synaptic transmission at ribbon synapses of rods and cones. Molecular neurobiology *36*, 205-223.

Thoreson, W.B., Rabl, K., Townes-Anderson, E., and Heidelberger, R. (2004). A highly Ca2+-sensitive pool of vesicles contributes to linearity at the rod photoreceptor ribbon synapse. Neuron *42*, 595-605.

tom Dieck, S., Altrock, W.D., Kessels, M.M., Qualmann, B., Regus, H., Brauner, D., Fejtova, A., Bracko, O., Gundelfinger, E.D., and Brandstatter, J.H. (2005). Molecular dissection of the photoreceptor ribbon synapse: physical interaction of Bassoon and RIBEYE is essential for the assembly of the ribbon complex. The Journal of cell biology *168*, 825-836.

Towbin, H., Staehelin, T., and Gordon, J. (1989). Immunoblotting in the clinical laboratory. Journal of clinical chemistry and clinical biochemistry Zeitschrift fur klinische Chemie und klinische Biochemie *27*, 495-501.

Toyama, B.H., Savas, J.N., Park, S.K., Harris, M.S., Ingolia, N.T., Yates, J.R., 3rd, and Hetzer, M.W. (2013). Identification of long-lived proteins reveals exceptional stability of essential cellular structures. Cell *154*, 971-982.

Ullrich, B., and Sudhof, T.C. (1994). Distribution of synaptic markers in the retina: implications for synaptic vesicle traffic in ribbon synapses. Journal of physiology, Paris *88*, 249-257.

Ungewickell, E., Ungewickell, H., Holstein, S.E.H., Lindner, R., Prasad, K., Barouch, W., Martin, B., Greene, L.E., and Eisenberg, E. (1995). Role of Auxilin in Uncoating Clathrin-Coated Vesicles. Nature *378*, 632-635.

Usukura, J., and Yamada, E. (1987). Ultrastructure of the synaptic ribbons in photoreceptor cells of Rana catesbeiana revealed by freeze-etching and freeze-substitution. Cell and tissue research *247*, 483-488.

Uthaiah, R.C., and Hudspeth, A.J. (2010). Molecular anatomy of the hair cell's ribbon synapse. The Journal of neuroscience : the official journal of the Society for Neuroscience *30*, 12387-12399.

Valenstein, E. S. (Columbia Univ. Press, 2006) The War of the Soups and the Sparks: The Discovery of Neurotransmitters and the Dispute Over How Nerves Communicate

Verhage, M., and Sorensen, J.B. (2008). Vesicle docking in regulated exocytosis. Traffic *9*, 1414-1424.

Vickery, H.B., and Schmidt, C.L.A. (1931). The history of the discovery of the amino acids. Chemical reviews *9*, 169-318.

Von Kriegstein, K., Schmitz, F., Link, E., and Sudhof, T.C. (1999). Distribution of synaptic vesicle proteins in the mammalian retina identifies obligatory and facultative components of ribbon synapses. The European journal of neuroscience *11*, 1335-1348.

Vongersdorff, H., and Matthews, G. (1994). Dynamics of Synaptic Vesicle Fusion and Membrane Retrieval in Synaptic Terminals. Nature *367*, 735-739.

vonGersdorff, H., Vardi, E., Matthews, G., and Sterling, P. (1996). Evidence that vesicles on the synaptic ribbon of retinal bipolar neurons can be rapidly released. Neuron *16*, 1221-1227.

Wahl, S., Katiyar, R., and Schmitz, F. (2013). A local, periactive zone endocytic machinery at photoreceptor synapses in close vicinity to synaptic ribbons. The Journal of neuroscience : the official journal of the Society for Neuroscience *33*, 10278-10300.

Walikonis, R.S., Jensen, O.N., Mann, M., Provance, D.W., Jr., Mercer, J.A., and Kennedy, M.B. (2000). Identification of proteins in the postsynaptic density fraction by mass spectrometry. The Journal of neuroscience : the official journal of the Society for Neuroscience *20*, 4069-4080.

Wan, L., Almers, W., and Chen, W.B. (2005). Two ribeye genes in teleosts: The role of ribeye in ribbon formation and bipolar cell development. Journal of Neuroscience *25*, 941-949.

Wan, Q.F., Vila, A., Zhou, Z.Y., and Heidelberger, R. (2008). Synaptic vesicle dynamics in mouse rod bipolar cells. Visual neuroscience *25*, 523-533.

Wang, M.M., Janz, R., Belizaire, R., Frishman, L.J., and Sherry, D.M. (2003). Differential distribution and developmental expression of synaptic vesicle protein 2 isoforms in the mouse retina. Journal of Comparative Neurology *460*, 106-122.

Washburn, M.P., Wolters, D., and Yates, J.R., 3rd (2001). Large-scale analysis of the yeast proteome by multidimensional protein identification technology. Nature biotechnology *19*, 242-247.

Wassle, H. (2004). Parallel processing in the mammalian retina. Nature reviews Neuroscience *5*, 747-757.

Wells, J.M., and McLuckey, S.A. (2005). Collision-induced dissociation (CID) of peptides and proteins. Methods in enzymology *402*, 148-185.

Wenk, M.R., and De Camilli, P. (2004). Protein-lipid interactions and phosphoinositide metabolism in membrane traffic: insights from vesicle recycling in nerve terminals. Proceedings of the National Academy of Sciences of the United States of America *101*, 8262-8269.

Whitehouse, C.M., Dreyer, R.N., Yamashita, M., and Fenn, J.B. (1985). Electrospray interface for liquid chromatographs and mass spectrometers. Analytical chemistry *57*, 675-679.

Whittaker, V.P., Michaelson, I.A., and Kirkland, R.J. (1964). The separation of synaptic vesicles from nerve-ending particles ('synaptosomes'). The Biochemical journal *90*, 293-303.

Wilhelm, B.G. (2013) Stoichiometric biology of synapses Doctoral thesis, Uni-Goettingen.

Wilhelm, B.G., Mandad, S., Truckenbrodt, S., Krohnert, K., Schafer, C., Rammner, B., Koo, S.J., Classen, G.A., Krauss, M., Haucke, V.*, et al.* (2014a). Composition of isolated synaptic boutons reveals the amounts of vesicle trafficking proteins. Science *344*, 1023-1028.

Wilhelm, M., Schlegl, J., Hahne, H., Gholami, A.M., Lieberenz, M., Savitski, M.M., Ziegler, E., Butzmann, L., Gessulat, S., Marx, H.*, et al.* (2014b). Mass-spectrometry-based draft of the human proteome. Nature *509*, 582-+.

Xing, Y., Bocking, T., Wolf, M., Grigorieff, N., Kirchhausen, T., and Harrison, S.C. (2010). Structure of clathrin coat with bound Hsc70 and auxilin: mechanism of Hsc70-facilitated disassembly. Embo Journal *29*, 655-665.

Yang, H., Standifer, K.M., and Sherry, D.M. (2002). Synaptic protein expression by regenerating adult photoreceptors. The Journal of comparative neurology *443*, 275-288.

Yang, M.S., Yu, L., Guo, T.W., Zhu, S.M., Liu, H.J., Shi, Y.Y., Gu, N.F., Feng, G.Y., and He, L. (2004). Evidence for association between single nucleotide polymorphisms in T complex protein 1 gene and schizophrenia in the Chinese Han population. J Med Genet *41*, e63.

Yao, P.J., Coleman, P.D., and Calkins, D.J. (2002). High-resolution localization of clathrin assembly protein AP180 in the presynaptic terminals of mammalian neurons. The Journal of comparative neurology *447*, 152-162.

Yoshimura, Y., Yamauchi, Y., Shinkawa, T., Taoka, M., Donai, H., Takahashi, N., Isobe, T., and Yamauchi, T. (2004). Molecular constituents of the postsynaptic density fraction revealed by proteomic analysis using multidimensional liquid chromatography-tandem mass spectrometry. Journal of neurochemistry *88*, 759-768.

Zanazzi, G., and Matthews, G. (2009). The Molecular Architecture of Ribbon Presynaptic Terminals. Molecular neurobiology *39*, 130-148.

Zubarev, R.A. (2004). Electron-capture dissociation tandem mass spectrometry. Current opinion in biotechnology *15*, 12-16.

Zubarev, R.A. (2009). Electron capture dissociation LC/MS/MS for bottom-up proteomics. Methods in molecular biology *492*, 413-416.

Zubarev, R.A., Kelleher, N.L., and McLafferty, F.W. (1998). Electron capture dissociation of multiply charged protein cations. A nonergodic process. Journal of the American Chemical Society *120*, 3265-3266.

CURRICULUM VITAE

PERSONAL DATA

Name	Sunit Mandad
Place, Date of Birth	Pilani, 19/08/1984
Nationality	Indian

EDUCATIONAL QUALIFICATION

2006 – 2008	Master of Science in Marine Biotechnology, Department of Biotechnology, Goa University, India. Grade A+.
2003 – 2006	Bachelors of Science in Botany, Zoology and Chemistry from University of Rajasthan, India. First class with Distinction. Fifth rank in the University merit list.
2000 – 2002	Intermediate of Science (10+2) from Central Board of Secondary Education, India. First Class with Distinction.

RESEARCH EXPERIENCE

2011 – 2015	**Doctoral Thesis** Max Planck Institute for, Germany under the supervision of Prof. Dr. Henning Urlaub. TITLE: **''***A comprehensive characterization of brain and retina synaptic vesicle proteome by quantitative mass spectrometry''*
2008 – 2010	**Junior Research Fellow** Indian Institute of Science, India, under the supervision of Prof P. Balaram. TITLE : *''Isolation and characterization of novel peptides from animal venom and secretions''*
2007 – 2008	**MS Thesis** Department of Biotechnology, Goa University, Goa, India under the supervision of Dr. Urmilla Barros. TITLE : *''Study of Algal-bacterial Association: as a source of Lectins''*
2007	**Summer Training (Masters)** Centre for Cellular and Molecular Biology (CCMB), Hyderabad, India under supervision of Dr. Prabir K. De. TITLE : "*Anomalous late-elution of a hamster urinary 60 kDa protein in a sephadex gel-filtration and its reason: identity and tissue origin of the protein.*"

AWARDS

2014	Selected for *student talk* at 11th Horizons in Molecular Biology at *Max Planck Institute for Biophysical Chemistry*, Germany.
2008	Qualified *Junior Research Fellowship* from the Council of Scientific and Industrial Research (CSIR), Ministry of Human Resource Development, Government of India.
2008	Qualified *Junior Research Fellowship* from the Indian Council of Medical Research (ICMR), Ministry of Human Resource Development, Government of India.
2007	Qualified *Graduate Aptitude Test* (GATE), with 96.4 percentile, a prerequisite for the admission in M.Tech/Ph. D in 'IITs' (Indian Institute of Technology), IISc (Indian Institute of Science), India and many foreign universities and institutes.
2007	Selected through All India Competition for *Summer Training* at *Centre for Cellular and Molecular Biology* (CCMB), Hyderabad, India
2006	Selected for admission to *Master of Science* in *Marine Biotechnology* at Goa University and *National fellowship* from Department of Biotechnology (DBT), Government of India through All India Combined Entrance examination conducted by Jawaharlal Nehru University, New Delhi (2006).
2006	*Fifth* rank at the *University of Rajasthan* in B.Sc (Zoology, Botany and Chemsitry), India.
2005 & 2006	Certificate of Merit for *First* Rank in BSc-II & III year, IMGVS College, University of Rajasthan.
1999	*Qualified* seventh All India General Knowledge test held by *Indian Public school's Conference.*
1999	*Qualified* Science Talent search Examination.

CONFERENCES

2014	Presented *student talk* at 11th Horizons in Molecular Biology, Göttingen Germany. TITLE: *"A Glimpse at the molecular architecture of Brain pre-synaptic nerve terminal"*
2012	*Poster* presentation at 4th MaxQuant summer school, Max Planck Institute of Biochemistry, Germany. TITLE: *"Understanding the molecular mechanism of synaptic vesicles docking in Ribbon synapses"*

2011	*Poster* presentation at 5th European Summer school in Proteomics Basics, Brixen, Italy. TITLE: *''Solubilization of synaptosomal N-methyl-D-aspartate receptor from rat brain for mass spectrometric studies''*
2010	*Poster* Presentation at 7th Horizons in Molecular Biology, *Max Planck Institute for Biophysical Chemistry*, Germany. TITLE: *''De novo sequencing of natural peptides by mass spectrometry''*

Publications

Parts of this thesis have been published previously:

Wilhelm BG, **Mandad S**, Truckenbrodt S, Kröhnert K, Schäfer C, Rammner B, Koo SJ, Claßen GA, Krauss M, Haucke V, Urlaub H, Rizzoli SO (2014). Composition of isolated synaptic boutons reveals the amounts of vesicle trafficking proteins. ***Science*** 344, 6187, 1023-1028.

Acknowledgements

First, I would like to thank my supervisor, **Prof. Henning Urlaub** for giving an opportunity to work in his group. I feel lucky that he chose me for such a challenging and exciting piece of work. I enjoyed working in his friendly, cool laboratory. I am glad that he advised me for various kinds of retreats and the conferences to improve my scientific skills. I am personally thankful that he taught me skiing in few days.

I am deeply grateful to **Prof. Reinhard Jahn**, without whom, major part of my project would not have been possible at all. I am indebted for all his expert advice and discussions from time to time.

I am also thankful to **Prof Tobias Moser** and **Dr. Ellen Reisinger** for helping me throughout my project. I gained great experience, knowledge during my thesis committee, SFB and time-to-time general meetings. Ellen, thank you so much for teaching me the retina dissection.

I am also obliged to **Prof. Silvio O Rizzoli**, for giving me an opportunity to be a part of one of his great publications. It is always a wonderful feeling while discussing with Silvio. He is like an ever-ready person for encouragement, exciting ideas and help. It was a great experience to work with him!

I would like to thank to **Dr. Janina Boyken** with whom I learnt impactful experiments that has helped me to carry on my project successful. I would like to also thank all my collaborators, **Benni**, **Eugenio**, **Iliana**, **Sandra**, **Zohreh** and many more for always being so nice to talk to (apart from the project!).

Thanks **Uwe**, **Moni**, **Annika**… for doing a great job of maintaining the machines is right condition. Uwe and **Steffi**, a warm hug for our Monday long drives (bringing the eyes and brain from the slaughter house)!

A special thank to **Karthik**, **Sarfaraz**, **Gajendar**, **Uzma**, **Eugenio**, **Saskia**, **Christof**, **Momo**, **Ilian**, **Julia** for being my real friend of writing thesis. You all know… how I managed! Dear Karthik, you have always been a great source of inspiration for me. Thank you so much for helping with my thesis writing and (personal as well as professional) time-to-time discussions! Sarfaraz, Uzma and Gajju…Thank you so much for always be with me. Life in Germany without you friends… is not good!

My labmates! Of course! You were the best people to bear me for such a long time. **Miro**, **Ilian**, **Uzma**, **Romi**, **Alex-slothy**, **Samir**, **Saadia**, **Kundan**, **Domi**, **Mahi**…I appreciate your help and discussions from time-to-time. Thank you all for having non-stop fun! I am also thankful to **Reinhard lab** for always being friendly and adjusted me as member of their lab.

I am thankful especially to **Prof. P. Balaram** (Director, IISc, India), late Prof. K S Krishnan (NCBS, India) and **Dr. V. Sabareesh** (IGIB, India) for developing my interest in the mass spectrometry! My teachers who encouraged and taught me to the right way!

My IISc friends **Suhana**, **Deepali**, **Vidhi**, **Dinz**, **Mukky**, **Mou**, **Sunanada, Sunitha, Rangs**….oh now! I missed you so much! My school friends… **Madhu**, **Pooja**, **Anjali**, **Swapna**, **Suman**, **Prerna**, **Dhanusha**, **Charu**, **Vineeta**, **Papiya**, **Kanchan**,…I am so lucky to have you all as my best friends.

My brothers **Manish** and **Pulkit**! …although I never said this… 'you are the best buddies of my life!!!' My **parents**, especially my **mom-** who has always been my best friend of life… Thank you so much for everything!!! Lastly, I would like to extend my thanks to my lovely husband **Ashwani**- for believing, encouraging me and making my life very beautiful!!!

Appendix

A1: Table showing the list of structural proteins identified and quantified in purified bovine retina synaptic ribbons by iBAQ-MS.

FASTA Header	Protein name	Abundance %	stdev
F2Z4C1	TUBA1A	11.600	3.293
A4IFM8	Actin, alpha 1, skeletal muscle	0.241	0.159
A1XEA5	Keratin 18 (Fragment	0.197	0.052
F1MAZ3	Microtubule-associated protein	0.078	0.018
F1MEW3	Microtubule-associated protein	0.060	0.027
G3N2J1	Microtubule-associated protein	0.011	0.002
F1N1H2	Microtubule-associated protein	0.001	
F1N034	Kinesin-like protein	0.001	
E1BJB1	Tubulin beta-2B chain	11.524	2.839
Q862F9	Similar to vimentin (Fragment)	4.623	1.886
F1MRD0	Actin, cytoplasmic 1	3.110	0.363
G3X7R8	Tubulin beta-6 chain (Fragment)	1.244	0.825
B0LJD2	Actin variant 2	1.178	0.457
B0LJ60	Beta-tubulin	0.562	0.127
Q148E2	Tubulin beta-2B	0.563	0.312

A2: Table showing the list of uncharacterized proteins identified and quantified in purified bovine retina synaptic ribbons by iBAQ-MS.

Uniprot ID	*Fasta headers*	*Mol. weight [kDa]*	*Abundance %*	σ
G3MXE1	>tr|G3MXE1|G3MXE1_BOVIN Uncharacterized protein OS=Bos taurus PE=4 SV=1	8.3506	1.539182831	0.097348338
F1MSQ6	>tr|F1MSQ6|F1MSQ6_BOVIN Uncharacterized protein (Fragment) OS=Bos taurus GN=NEFH PE=3 SV=2	118.29	0.935595366	0.149984966
E1B953	>tr|E1B953|E1B953_BOVIN Uncharacterized protein OS=Bos taurus GN=TUBB PE=4 SV=2	49.558	0.624379743	0.184085449
F1MPS1	>tr|F1MPS1|F1MPS1_BOVIN Uncharacterized protein (Fragment) OS=Bos taurus GN=RS1 PE=4 SV=2	25.756	0.312507296	0.271057707
E1BFB0	>tr|E1BFB0|E1BFB0_BOVIN Uncharacterized protein OS=Bos taurus GN=SPTAN1 PE=4 SV=2	284.57	0.208925588	0.166965611
F1MR06	>tr|F1MR06|F1MR06_BOVIN Uncharacterized protein (Fragment) OS=Bos taurus GN=ATP1A3 PE=3 SV=2	113.08	0.190822555	0.069338666

F1MYC9	>tr|F1MYC9|F1MYC9_BOVIN Uncharacterized protein OS=Bos taurus GN=SPTBN1 PE=4 SV=1	274.39	0.15820024	0.159829418
E1BJA2	>tr|E1BJA2|E1BJA2_BOVIN Uncharacterized protein OS=Bos taurus GN=AIFM1 PE=4 SV=1	66.871	0.143940532	0.0626037
G3MY15	>tr|G3MY15|G3MY15_BOVIN Uncharacterized protein (Fragment) OS=Bos taurus GN=LOC782835 PE=3 SV=1	14.007	0.127020492	
E1BMW9	>tr|E1BMW9|E1BMW9_BOVIN Uncharacterized protein OS=Bos taurus GN=PURA PE=4 SV=2	34.88	0.111002149	0.139829621
F1N301	>tr|F1N301|F1N301_BOVIN Uncharacterized protein OS=Bos taurus GN=RPL22 PE=4 SV=2	14.759	0.109412273	
G3MZG7	>tr|G3MZG7|G3MZG7_BOVIN Uncharacterized protein OS=Bos taurus PE=3 SV=1	17.85	0.104767724	0.058240234
E1BDS9	>tr|E1BDS9|E1BDS9_BOVIN Uncharacterized protein (Fragment) OS=Bos taurus PE=4 SV=2	13.592	0.100964886	0.090014933
E1BHK2	>tr|E1BHK2|E1BHK2_BOVIN Uncharacterized protein OS=Bos taurus GN=ADD1 PE=4 SV=1	80.672	0.086308253	0.033323374
F1N1S2	>tr|F1N1S2|F1N1S2_BOVIN Uncharacterized protein OS=Bos taurus GN=MAP1B PE=4 SV=2	270.27	0.077264322	0.070847088

A3: Table showing the copies of synaptic proteins quantified in bovine brains and retina SV by iBAQ-MS. List of proteins with their absolute copies quantified from immunoprecipitated bovine brain and retina SVs by iBAQ-MS. Note that the synaptic proteins (given in the results) are excluded from this list.

ID	PROTEIN NAME	COPY NUMBER BRAIN SV	σ	COPY NUMBER RETINA SV	σ
G3P	Glyceraldehyde-3-phosphate dehydrogenase	121.85	19.787	119.79	22.852
APOC3	Apolipoprotein C-III	33.72	32.814	58.99	26.568
TBB4B	Tubulin beta-4B chain	74.30	53.299	25.54	13.507
TBA4A	Tubulin alpha-4A chain	36.23	20.156	16.61	4.288
LDHA	L-lactate dehydrogenase A chain	0.45	0.489	14.90	12.200
	BOVIN Tubulin alpha-1	19.50	5.237	13.10	6.885
TTHY	Transthyretin	1.55	98.661	11.62	7.104
H11	Histone H1.1 (Fragment)	0.00	0.000	9.56	7.570
ACTG	Actin, cytoplasmic 2	12.16	4.522	6.41	3.300
	002687307 Tax	1.33	0.409	3.12	2.761
MYPR	Myelin proteolipid protein	2.24	30.640	2.86	1.092
RS16	40S ribosomal protein S16	1.83	1.136	2.54	1.580

	LOC618147 histone cluster 1, H2ae-like	0.00	0.740	2.29	2.248
TCPZ	T-complex protein 1 subunit zeta	1.29	1.534	2.26	2.248
TUBB2A	Tubulin 2A	19.35	4.076	2.09	2.400
TCPG	T-complex protein 1 subunit gamma	0.41	0.469	1.52	0.984
TCPD	BOVIN T-complex protein 1 subunit delta	1.00	0.578	1.20	1.535
VATH	Isoform Beta of V-type proton ATPase subunit H	0.72	0.307	1.03	0.599
G5E531	T-complex protein 1 subunit alpha	2.03	1.661	1.01	1.672
GNAT1	Guanine nucleotide-binding protein G(t) subunit alpha-1	0.00	0.000	1.00	1.364
ATP1A3	ATPase, Na+/K+ transporting, alpha 3 polypeptid	0.46	3.476	0.96	0.381
AP2A2	AP-2 complex subunit alpha-2	0.00	0.000	0.95	0.562
PFKL	6-phosphofructokinase, liver type	0.00	0.010	0.91	0.784
TBB5	Tubulin beta-5 chain	2.00	0.590	0.89	1.034
PKM2	Pyruvate kinase	0.30	0.228	0.79	1.221
F1MWR8	T-complex protein 1 subunit eta (Fragment)	0.74	0.372	0.77	0.983
HSPB1	Heat shock protein beta-1	0.37	0.140	0.75	2.191
GNAO	Guanine nucleotide-binding protein G(o) subunit alpha	8.37	5.489	0.75	2.169
EF1A1	Elongation factor 1-alpha 1	1.42	0.218	0.66	0.393
TBB3	Tubulin beta-3 chain	11.10	5.202	0.63	0.781
TBB4A	Tubulin beta-4A chain	1.32	1.034	0.59	0.430
VIME	Vimentin	0.22	0.212	0.55	0.585
ACTR1A	001180177;XP	0.67	0.442	0.52	0.422
F1MFT4	Uncharacterized protein (Fragment)	0.00	0.000	0.51	0.351
GLNA	Glutamine synthetase	0.00	0.289	0.35	0.409
PCBP1	Poly(rC)-binding protein 1	0.44	0.111	0.30	0.199
DYNC1H1	001193067;XP	0.14	0.029	0.07	0.182
REFSEQ:XP	opioid-binding protein/cell adhesion molecule-like, partial	0.10	0.073	0.06	0.082

A4: Table showing the copies of synaptic proteins quantified only in in bovine brains SV by iBAQ-MS. List of proteins with their absolute copies quantified only in immunoprecipitated bovine brain SVs by iBAQ-MS.

Myelin basic protein	123.05	20.91
Uncharacterized protein	7.85	14.44
orphan sodium- and chloride-dependent neurotransmitter transporter NTT4	5.13	2.19
ATPase, H+ transporting, lysosomal 13kDa, V1 subunit G2	4.55	8.32
vacuolar protein sorting 13 homolog C	1.81	1.26
Ras-related C3 botulinum toxin substrate 1	1.79	0.35
Dynamin-1	1.70	0.23
Ribosomal protein S4, Y-linked 1	1.69	0.21
001180044;XP	1.59	0.60

Probable phospholipid-transporting ATPase IA	1.59	0.68
001249299;XP	1.58	1.19
Immunoglobulin J chain	1.52	0.76
Glial fibrillary acidic protein	1.41	0.19
6-phosphofructokinase, muscle type	1.27	0.52
Contactin-1	1.05	1.26
AP-2 complex subunit sigma	1.03	0.34
adaptor-related protein complex 2, alpha 1 subunit	0.99	1.54
40S ribosomal protein S26	0.97	0.79
Uncharacterized protein (Fragment)	0.82	0.87
Neurofilament light polypeptide	0.80	0.35
Actin, alpha cardiac muscle 1	0.78	0.45
ADP-ribosylation factor 4	0.74	0.59
001179819;XP	0.74	0.28
Myelin basic protein	0.68	0.36
Apolipoprotein D	0.66	0.18
Calcium/calmodulin-dependent protein kinase II alpha	0.66	1.21
FARSA protein	0.64	0.37
KIAA0541 protein-like	0.61	1.95
Id	0.61	0.25
40S ribosomal protein S18	0.50	0.31
Dynamin-1-like protein	0.49	0.17
Elongation factor 1-alpha 2	0.49	0.21
001178304;XP	0.49	0.17
Id	0.48	0.33
T-complex protein 1 subunit beta	0.44	0.05
60 kDa heat shock protein, mitochondrial	0.43	0.45
Sodium/potassium-transporting ATPase subunit alpha-1	0.43	0.30
Serum amyloid A protein	0.43	0.26
Guanine nucleotide-binding protein G(I)/G(S)/G(O) subunit gamma-2	0.42	0.16
40S ribosomal protein S5	0.42	0.80
Clathrin heavy chain 1	0.42	0.30
Alpha-crystallin B chain	0.41	0.38
AP2-associated protein kinase 1	0.41	0.17
40S ribosomal protein S6	0.41	0.50
Uncharacterized protein (Fragment)	0.40	0.09
Heat shock cognate 71 kDa protein	0.40	0.54
Uncharacterized protein	0.40	0.63
Rho-related GTP-binding protein RhoB	0.36	0.33
Alpha-internexin	0.35	0.56
D-3-phosphoglycerate dehydrogenase	0.35	0.12
ADP-ribosylation factor-like protein 8B	0.34	0.23
Thy-1 cell surface antigen	0.34	0.14
Id	0.32	0.17
Ras-related protein Rab-13	0.31	0.18
Glutamate dehydrogenase 1, mitochondrial	0.30	0.19
Cell cycle exit and neuronal differentiation 1	0.30	0.29
40S ribosomal protein S13	0.28	0.09

MAP2K1 protein	0.26	0.11
Neurofilament medium polypeptide	0.26	0.24
Uncharacterized protein	0.26	0.26
RAB2A, member RAS oncogene family	0.25	0.13
Cyclin G associated kinase	0.24	0.31
RTN1	0.23	0.06
Ras-related protein Rab-11A	0.23	0.15
Uncharacterized protein (Fragment)	0.23	0.23
26S protease regulatory subunit 10B	0.22	1.42
Visinin-like protein 1	0.21	0.13
SEC22 vesicle trafficking protein homolog B	0.21	0.25
Proteolipid protein 2	0.20	0.15

A5: Table showing the copies of synaptic proteins quantified insignificantly from purified rat brain SV by iBAQ-MS. List of proteins with their absolute copies quantified by iBAQ-MS. Note that the synaptic and rab proteins (given in the results) are excluded from this list.

Syntaxins			
ID	Protein	Copy number	σ
STX6	Syntaxin-6	0.08	0.04
STX7	Syntaxin-7	0.24	0.10
STX12	Syntaxin-12	0.19	0.19
Endocytotic proteins			
ID	Protein	Copy number	σ
DYN1	Dynamin-1	0.239	0.127
SHLB2	Endophilin-B2	0.006	0.014
SHLB1	Endophilin-B1	0.005	0.011
Active Zone proteins			
ID	Protein	Copy number	σ
BSN	Protein bassoon	0.001	0.001
CPLX2	Complexin-2	0.059	0.002
Rab machinery			
ID	Protein	Copy number	σ
RAB1A	Ras-related protein Rab-1A	2.575	0.405
RAB1B	Ras-related protein Rab-1B	0.120	0.038
RAB2A	Ras-related protein Rab-2A	2.733	1.086
RAB3B	Ras-related protein Rab-3B	0.175	0.044
RAB3C	Ras-related protein Rab-3C	1.453	1.245
RAB3D	GTP-binding protein Rab-3D	4.776	0.566
RAB4A	Ras-related protein Rab-4A	0.065	0.031
RAB4B	Ras-related protein Rab-4B	0.214	0.083

RAB6A	Ras-related protein Rab-6A	4.232	0.630
RAB7A	Ras-related protein Rab-7a	1.308	0.416
RAB8A	Ras-related protein Rab-8A	0.025	0.012
RAB8B	Ras-related protein Rab-8B	0.015	0.012
RAB10	Ras-related protein Rab-10	0.255	0.297
RB11B	Ras-related protein Rab-11B	1.122	0.251
RAB12	Ras-related protein Rab-12	0.070	0.020
RAB15	Ras-related protein Rab-15	0.056	0.018
RAB18	Ras-related protein Rab-18	0.099	0.035
RAB21	Ras-related protein Rab-21	0.003	0.020
RB27B	Ras-related protein Rab-27B	0.066	0.046
RAB34	Ras-related protein Rab-34	0.726	0.351
RAB35	Ras-related protein Rab-35	0.140	0.139

A6: Table showing the copies of cytosolic proteins quantified from purified rat brain SV by iBAQ-MS. List of proteins with their absolute copies quantified by iBAQ-MS. Note that the synaptic and rab proteins (given in the results) are excluded from this list.

ID	Protein	Copy #	σ
GLNA	Glutamine synthetase	10.26	3.21
G3P	Glyceraldehyde-3-phphate dehydrogenase	9.27	2.39
ALDOA	Fructe-bisphphate aldolase A	4.50	1.78
THY1	Thy-1 membrane glycoprotein	4.34	2.03
MYPR	Myelin proteolipid protein	2.91	0.60
KCC2A	Calcium/calmodulin-dependent protein kinase type II subunit alpha	2.52	0.64
AT1A3	Sodium/potassium-transporting ATPase subunit alpha-3	2.18	0.68
AAK1	AP2-associated protein kinase 1	2.05	0.54
EF1A1	Elongation factor 1-alpha 1	2.03	0.67
AT1B1	Sodium/potassium-transporting ATPase subunit beta-1	1.83	0.56
MBP	Myelin basic protein S	1.29	0.56
GNAO	Isoform Alpha-2 of Guanine nucleotide-binding protein G(o) subunit alpha	1.28	0.44
GBB1	Guanine nucleotide-binding protein G(I)/G(S)/G(T) subunit beta-1	1.19	0.44
S6A17	Sodium-dependent neutral amino acid transporter SLC6A17	0.98	0.39
BASP1	Brain acid soluble protein 1	0.85	0.22
CN37		0.84	0.37
LDHA	L-lactate dehydrogenase A chain	0.75	0.28
TBA1B	Tubulin alpha-1B chain	0.75	0.23
KCRU	Creatine kinase U-type	0.67	0.26
OPCM	Opioid-binding protein/cell adhesion molecule	0.48	0.15
K6PF	6-phphofructokinase	0.47	0.20
ALDOC	Fructe-bisphphate aldolase C	0.45	0.15
CADM3	Cell adhesion molecule 3	0.42	0.15

CALM	Calmodulin	0.37	0.11
NCAM1	Neural cell adhesion molecule 1	0.37	0.12
AT1A1	Sodium/potassium-transporting ATPase subunit alpha-1	0.31	0.08
TM163	Transmembrane protein 163	0.29	0.07
RHOB	Rho-related GTP-binding protein RhoB	0.28	0.06
RALA	Ras-related protein Ral-A	0.26	0.12
K6PP	6-phphofructokinase type C	0.25	0.09
CALX	Calnexin	0.25	0.10
CD81	CD81 antigen	0.25	0.07
ACTB	Actin	0.24	0.12
1433Z	14-3-3 protein zeta/delta	0.23	0.06
EF1A2	Elongation factor 1-alpha 2	0.22	0.12
TCPD	T-complex protein 1 subunit delta	0.21	0.09
NTRI	Neurotrimin	0.19	0.11
AT2A2	Sarcoplasmic/endoplasmic reticulum calcium ATPase 2	0.19	0.05
LAMP5	Lysome-associated membrane glycoprotein 5	0.18	0.05
ARF3	ADP-ribylation factor 3	0.18	0.06
NUMBL	Numb-like protein	0.17	0.09
GTR3	Solute carrier family 2	0.17	0.10
SHPS1	Tyrine-protein phphatase non-receptor type subste 1	0.15	0.10
HSP7C	Heat shock cognate 71 kDa protein	0.15	0.07
TCPR1	Tectonin beta-propeller repeat-containing protein 1	0.15	0.05
KPCB	Isoform Beta-II of Protein kinase C beta type	0.15	0.06
CD9	CD9 antigen	0.14	0.10
CNTN1	Contactin-1	0.14	0.06
KCC2B	Calcium/calmodulin-dependent protein kinase type II subunit beta	0.13	0.05
K6PL	6-phphofructokinase	0.13	0.06
CD47	Isoform 2 of Leukocyte surface antigen CD47	0.13	0.05
TBB2A	Tubulin beta-2A chain	0.13	0.05
CDIP1	Cell death-inducing p53-target protein 1	0.13	0.06
PUR6	Multifunctional protein ADE2	0.13	0.03
PGRC1	Membrane-associated progesterone receptor component 1	0.12	0.03
KPCG	Protein kinase C gamma type	0.12	0.03
NPTXR	Neuronal pentraxin receptor	0.12	0.05
TBB5	Tubulin beta-5 chain	0.11	0.02
CADM2	Cell adhesion molecule 2	0.11	0.04
RAP2B	Ras-related protein Rap-2b	0.11	0.07
LSAMP	Isoform 2 of Limbic system-associated membrane protein	0.11	0.03
RAP1A	Ras-related protein Rap-1A	0.10	0.02
GPX42	Phpholipid hydroperoxide glutathione peroxidase	0.10	0.04
PDIA3	Protein disulfide-isomerase A3	0.10	0.05
NPTN	Neuroplastin	0.09	0.03
PTPR2	Receptor-type tyrine-protein phphatase N2	0.09	0.05
DPP6	Dipeptidyl aminopeptidase-like protein 6	0.09	0.04
SIR2	NAD-dependent protein deacetylase sirtuin-2	0.08	0.05
TBA1A	Tubulin alpha-1A chain	0.08	0.03
FIS1	Isoform 2 of Mitochondrial fission 1 protein	0.08	0.03
APOE	Apolipoprotein E	0.08	0.02

VISL1	Visinin-like protein 1	0.08	0.08
RHOA	Transforming protein RhoA	0.08	0.03
TPIS	Triephphate isomerase	0.08	0.03
REEP5	Receptor expression-enhancing protein 5	0.07	0.03
FKB1A	Peptidyl-prolyl cis-trans isomerase FKBP1A	0.07	0.05
CAZA2	F-actin-capping protein subunit alpha-2	0.07	0.01
MDHC	Malate dehydrogenase	0.07	0.02
CALR	Calreticulin	0.07	0.03
ARF6	ADP-ribylation factor 6	0.07	0.04
ROGDI	Protein rogdi homolog	0.07	0.03
VMAT2	Synaptic vesicular amine transporter	0.07	0.04
KCRB	Creatine kinase B-type	0.06	0.03
SC6A1	Sodium- and chloride-dependent GABA transporter 1	0.06	0.04
AT2B2	Isoform WB of Plasma membrane calcium-transporting ATPase 2	0.06	0.02
CD59	CD59 glycoprotein	0.06	0.10
ACLY	ATP-cite synthase	0.06	0.04
TPPC3	Trafficking protein particle complex subunit 3	0.06	0.11
LDHB	L-lactate dehydrogenase B chain	0.05	0.03
KPYM	Pyruvate kinase isozymes M1/M2	0.05	0.05
CPNE9	Copine-9	0.05	0.02
NEUM	Neuromodulin	0.05	0.03
MARCS	Myristoylated alanine-rich C-kinase subste	0.05	0.01
PRIO	Major prion protein	0.04	0.03
MAP6	Microtubule-associated protein 6	0.04	0.01
TBA4A	Tubulin alpha-4A chain	0.04	0.03
PPIB	Peptidyl-prolyl cis-trans isomerase B	0.04	0.02
GRP78	78 kDa gluce-regulated protein	0.04	0.03
LAMP1	Lysome-associated membrane glycoprotein 1	0.04	0.02
ATG9A	Autophagy-related protein 9A	0.04	0.01
AT1B3	Sodium/potassium-transporting ATPase subunit beta-3	0.03	0.02
EAA2	Excitatory amino acid transporter 2	0.03	0.02
ERP29	Endoplasmic reticulum resident protein 29	0.03	0.02
ENOG	Gamma-enolase	0.03	0.02
VPS45	Vacuolar protein sorting-associated protein 45	0.03	0.02
OX2G	OX-2 membrane glycoprotein	0.03	0.02
MAP4	Microtubule-associated protein 4	0.03	0.02
GBB2	Guanine nucleotide-binding protein G(I)/G(S)/G(T) subunit beta-2	0.03	0.08
PICA	Phphatidylinitol-binding clathrin assembly protein	0.03	0.02
GNAQ	Guanine nucleotide-binding protein G(q) subunit alpha	0.03	0.02
KCC2G	Calcium/calmodulin-dependent protein kinase type II subunit gamma	0.03	0.02
DYN2	Isoform 2 of Dynamin-2	0.03	0.01
UCHL1	Ubiquitin carboxyl-terminal hydrolase isozyme L1	0.03	1.37
NAC2	Sodium/calcium exchanger 2	0.03	0.01
VDAC2	Voltage-dependent anion-selective channel protein 2	0.03	0.02
SYUA	Isoform Syn2 of Alpha-synuclein	0.03	0.01
RASK	Isoform 2B of GTPase KRas	0.03	0.01
1433E	14-3-3 protein epsilon	0.02	0.02

HPCA	Neuron-specific calcium-binding protein hippocalcin	0.02	0.01
TBB2B	Tubulin beta-2B chain	0.02	0.00
BASI	Basigin	0.02	0.01
TPPC1	Trafficking protein particle complex subunit 1	0.02	0.05
GNAI1	Guanine nucleotide-binding protein G(i) subunit alpha-1	0.02	0.02
TTYH1	Protein tweety homolog 1	0.02	0.01
DYN3	Isoform 5 of Dynamin-3	0.02	0.02
CAPZB	F-actin-capping protein subunit beta	0.02	0.01
PRRT2	Proline-rich transmembrane protein 2	0.02	0.03
NCKX2	Sodium/potassium/calcium exchanger 2	0.02	0.01
L1CAM	Neural cell adhesion molecule L1	0.02	0.01
ODO2	Dihydrolipoyllysine-residue succinyltransferase component of 2-oxoglutae dehydrogenase complex	0.02	0.01
NCEH1	Neutral cholesterol ester hydrolase 1	0.02	0.01
NPTX1	Neuronal pentraxin-1	0.02	0.02
CLC2L	C-type lectin domain family 2 member L	0.02	0.01
MARK2	Serine/threonine-protein kinase MARK2	0.02	0.01
VACHT	Vesicular acetylcholine transporter	0.02	0.01
ITPR1	Initol 1	0.02	0.01
RASM	Ras-related protein M-Ras	0.02	0.01
NCPR	NADPH--cytochrome P450 reductase	0.02	0.01
DPYL2	Dihydropyrimidinase-related protein 2	0.02	0.04
RS4X	40S ribomal protein S4	0.02	0.01
DPYL1	Dihydropyrimidinase-related protein 1	0.02	0.01
CLUS	Clusterin	0.02	0.01
VP33B	Vacuolar protein sorting-associated protein 33B	0.01	0.01
CD166	CD166 antigen	0.01	0.92
NFASC	Neurofascin	0.01	0.01
AT2B1	Plasma membrane calcium-transporting ATPase 1	0.01	0.01
BCAS1	Isoform 5 of Breast carcinoma-amplified sequence 1 homolog	0.01	0.01
	Ras-related protein Rab-31	0.01	
RL8	60S ribomal protein L8	0.01	0.01
ALBU	Serum albumin	0.01	0.01
PSMD2	26S proteasome non-ATPase regulatory subunit 2	0.01	0.01
DHE3	Glutamate dehydrogenase 1	0.01	0.01
CLCN3	H(+)/Cl(-) exchange transporter 3	0.01	0.03
ICA69	Islet cell autoantigen 1	0.01	0.01
KCC2D	Calcium/calmodulin-dependent protein kinase type II subunit delta	0.01	0.01
DCLK1	Serine/threonine-protein kinase DCLK1	0.01	0.00
CEND	Cell cycle exit and neuronal differentiation protein 1	0.01	0.00
AT1A2	Sodium/potassium-transporting ATPase subunit alpha-2	0.01	0.01
MARK1	Serine/threonine-protein kinase MARK1	0.01	0.01
PGK1	Phphoglycee kinase 1	0.01	0.01
MAG	Myelin-associated glycoprotein	0.01	0.00
RL31	60S ribomal protein L31	0.01	0.01
ANXA3	Annexin A3	0.01	0.01
GRM2	Metabotropic glutamate receptor 2	0.01	0.00
PI3R4	Phphoinitide 3-kinase regulatory subunit 4	0.01	0.01

RS16	40S ribomal protein S16	0.01	0.01
KPCD	Protein kinase C delta type	0.01	0.01
GNAZ	Guanine nucleotide-binding protein G(z) subunit alpha	0.01	0.01
PRS6B	26S protease regulatory subunit 6B	0.01	0.01
MAP2	Microtubule-associated protein 2	0.01	0.01
PDIA1	Protein disulfide-isomerase	0.01	0.00
S12A5	Solute carrier family 12 member 5	0.01	0.00
DYHC1	Cytoplasmic dynein 1 heavy chain 1	0.01	0.00
VGF	Neurecretory protein VGF	0.01	0.01
CNTP1	Contactin-associated protein 1	0.01	0.00
KAP3	cAMP-dependent protein kinase type II-beta regulatory subunit	0.01	0.01
NAC1	Isoform 2 of Sodium/calcium exchanger 1	0.01	0.00
SPRY7	SPRY domain-containing protein 7	0.01	0.00

A7: Size-exclusion chromatogram: The elution profile of highly pure rat brain SVs

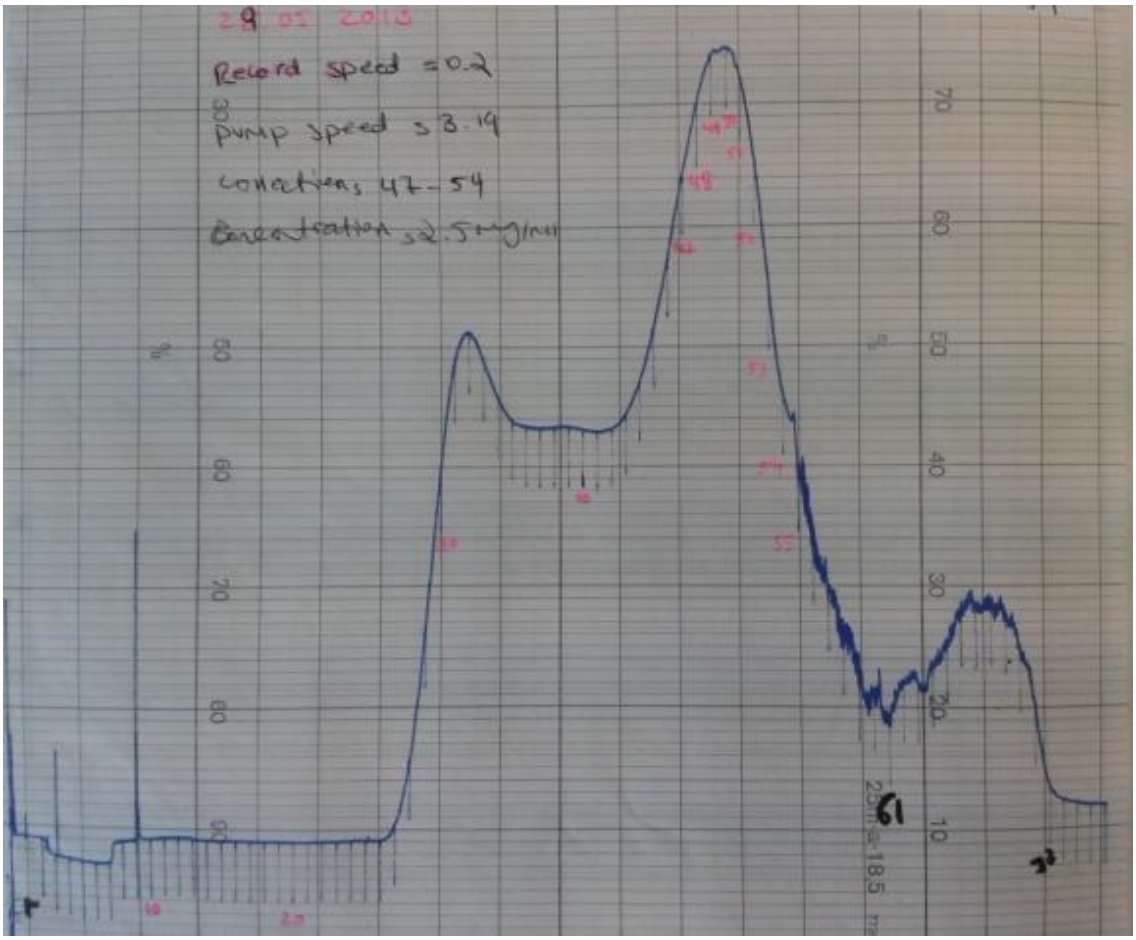

A8: Venn diagram: Comparison of retina proteome and brain proteome

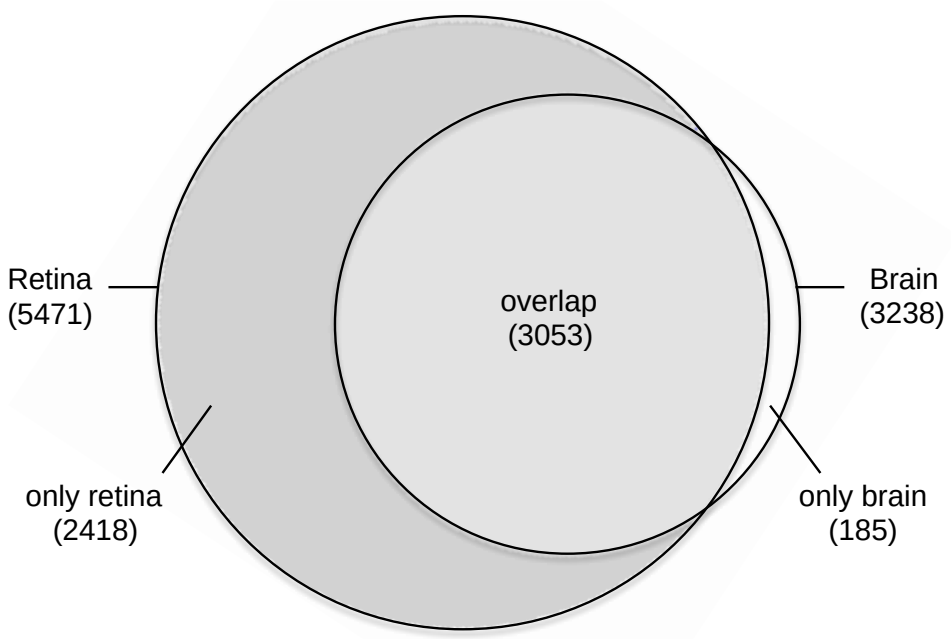

A8: Functional annotation of retina proteins

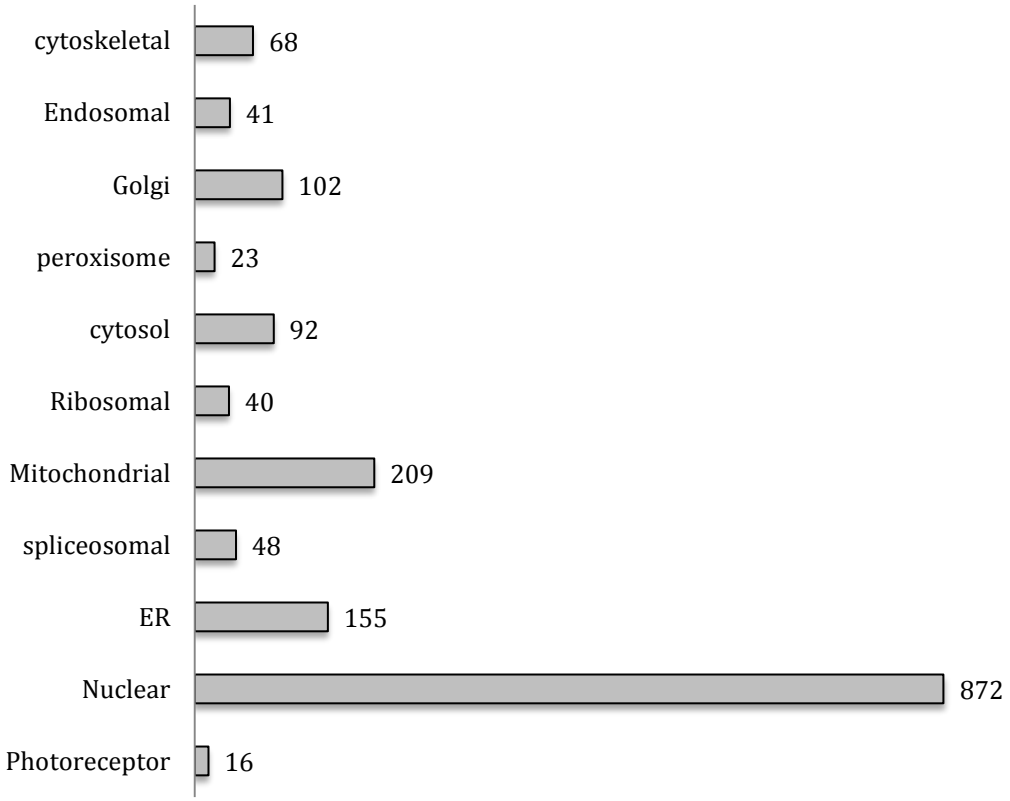

A9: Proteome comparison: Bovine brain SVs and Bovine retina SVs

(a)

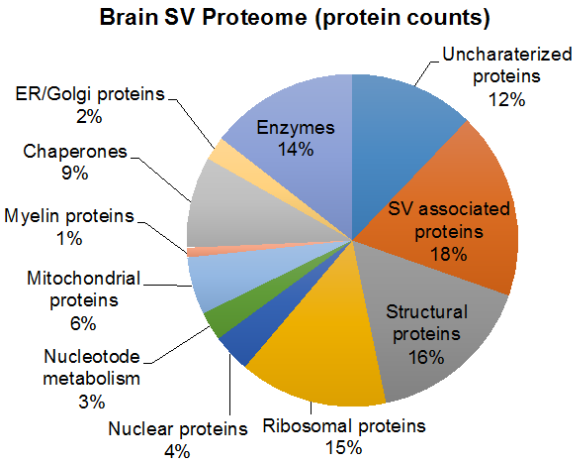

(b)

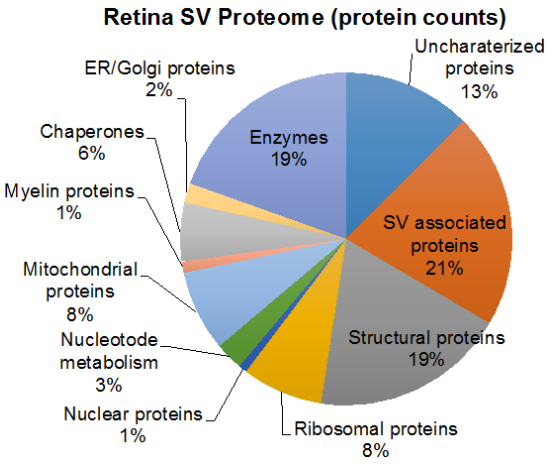

A10: Log (amount) v/s Log (iBAQ) plots of various marker protein of rat brain SVs

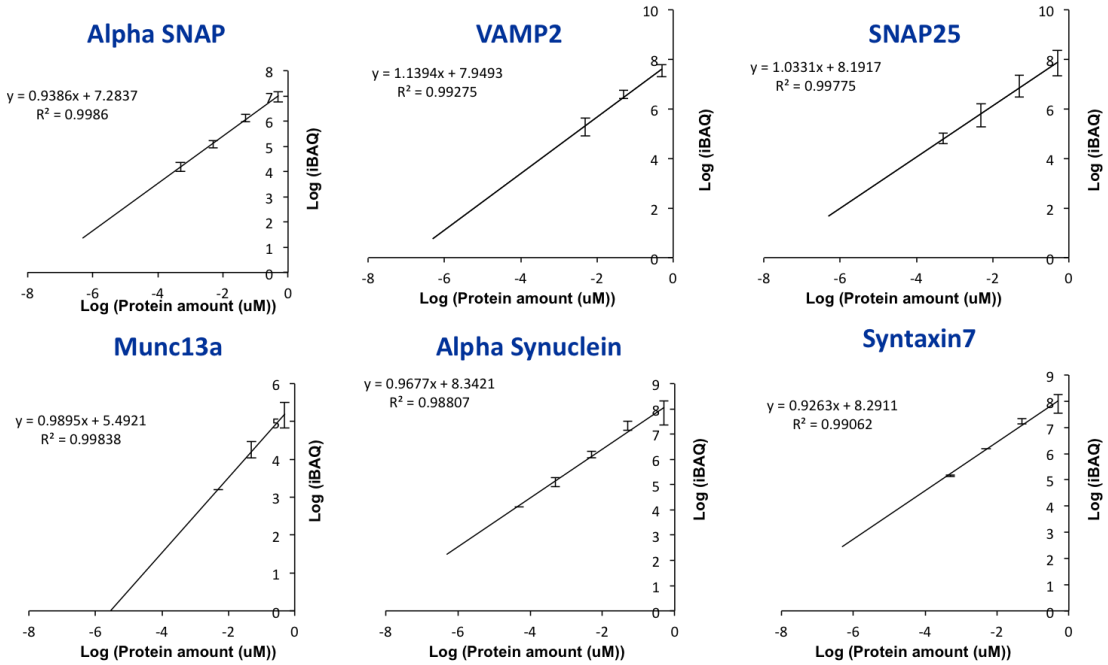

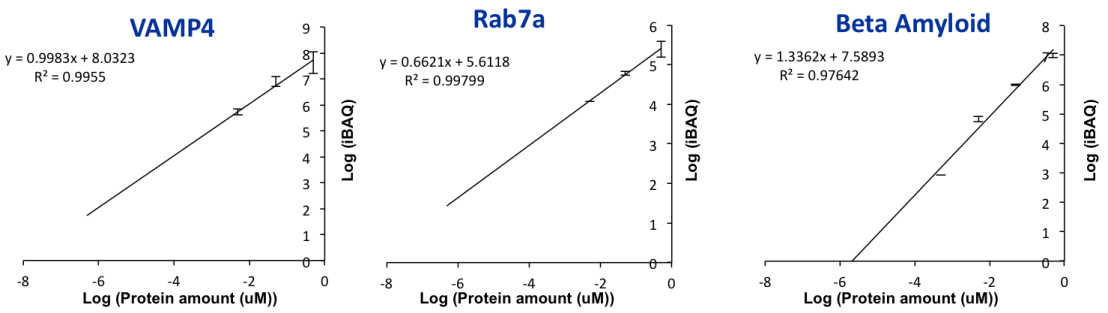
VAMP4
y = 0.9983x + 8.0323
R² = 0.9955
Log (iBAQ)
Log (Protein amount (uM))
Rab7a
y = 0.6621x + 5.6118
R² = 0.99799
Log (iBAQ)
Log (Protein amount (uM))
Beta Amyloid
y = 1.3362x + 7.5893
R² = 0.97642
Log (iBAQ)
Log (Protein amount (uM))

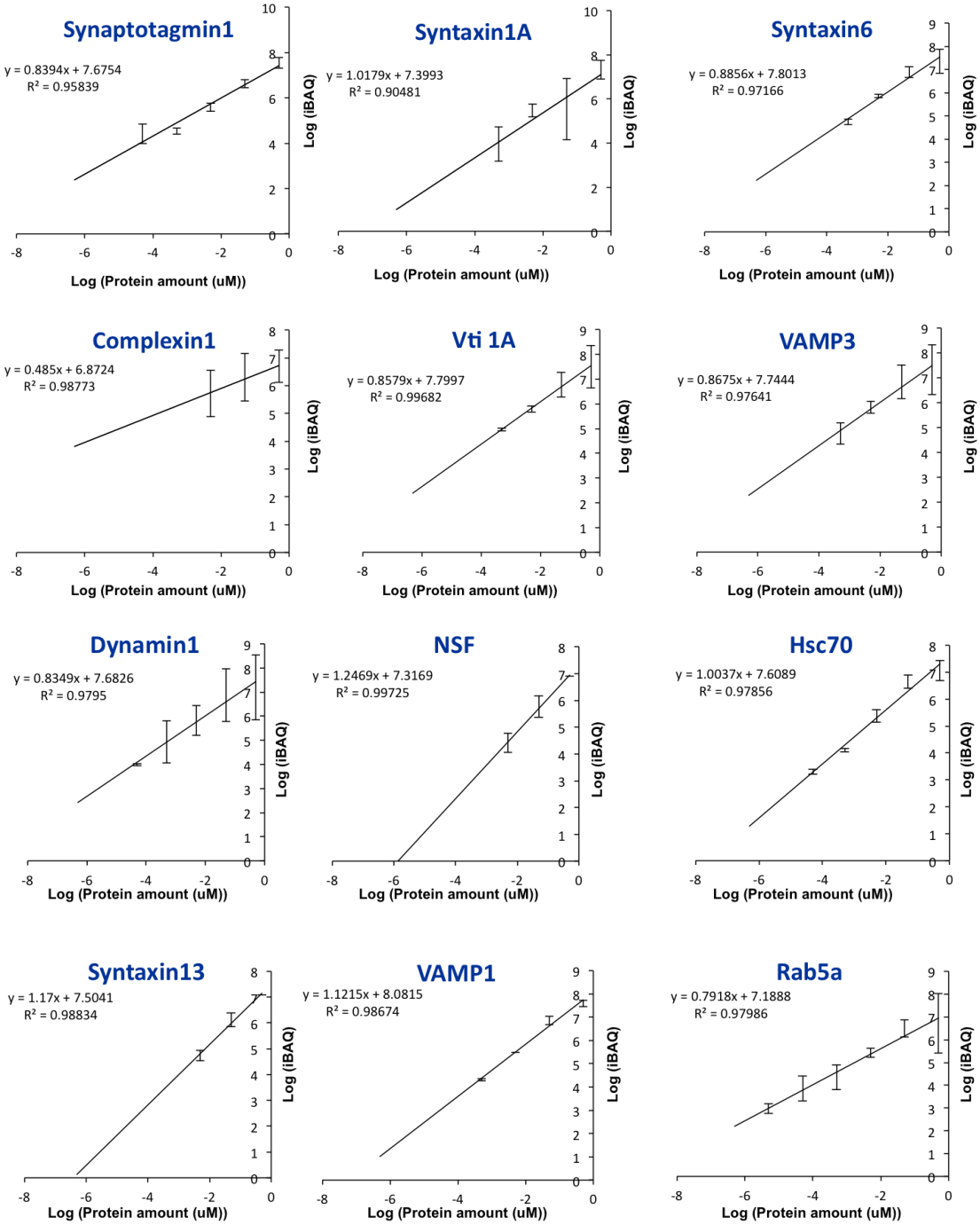
Synaptotagmin1
y = 0.8394x + 7.6754
R² = 0.95839
Syntaxin1A
y = 1.0179x + 7.3993
R² = 0.90481
Syntaxin6
y = 0.8856x + 7.8013
R² = 0.97166
Complexin1
y = 0.485x + 6.8724
R² = 0.98773
Vti 1A
y = 0.8579x + 7.7997
R² = 0.99682
VAMP3
y = 0.8675x + 7.7444
R² = 0.97641
Dynamin1
y = 0.8349x + 7.6826
R² = 0.9795
NSF
y = 1.2469x + 7.3169
R² = 0.99725
Hsc70
y = 1.0037x + 7.6089
R² = 0.97856
Syntaxin13
y = 1.17x + 7.5041
R² = 0.98834
VAMP1
y = 1.1215x + 8.0815
R² = 0.98674
Rab5a
y = 0.7918x + 7.1888
R² = 0.97986
Log (iBAQ)
Log (Protein amount (uM))

A11: Incorporation of Heavy lysine$_6$ –to-lysine$_0$ in brain (white column) and retina (grey column) synaptic proteins overtime

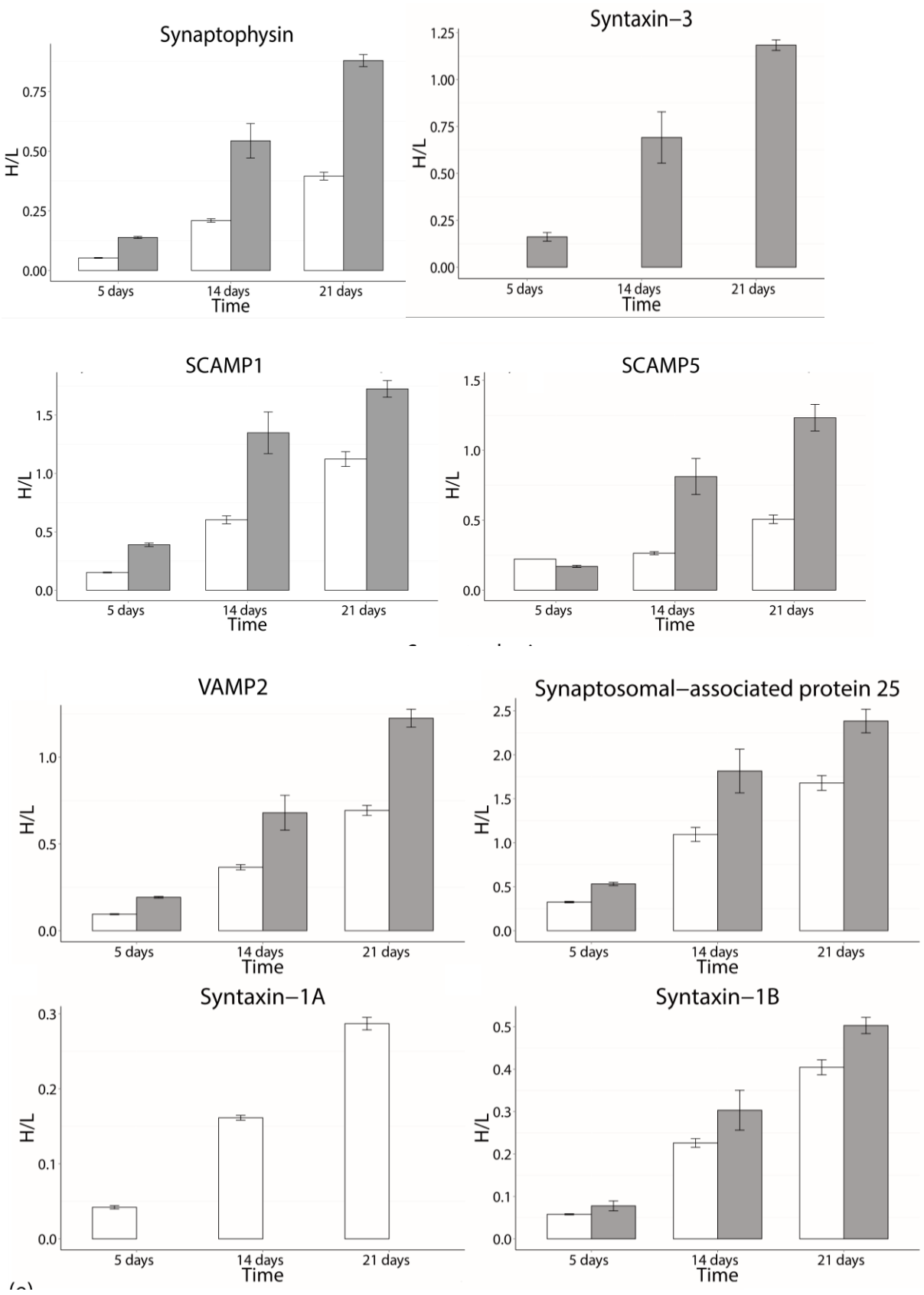

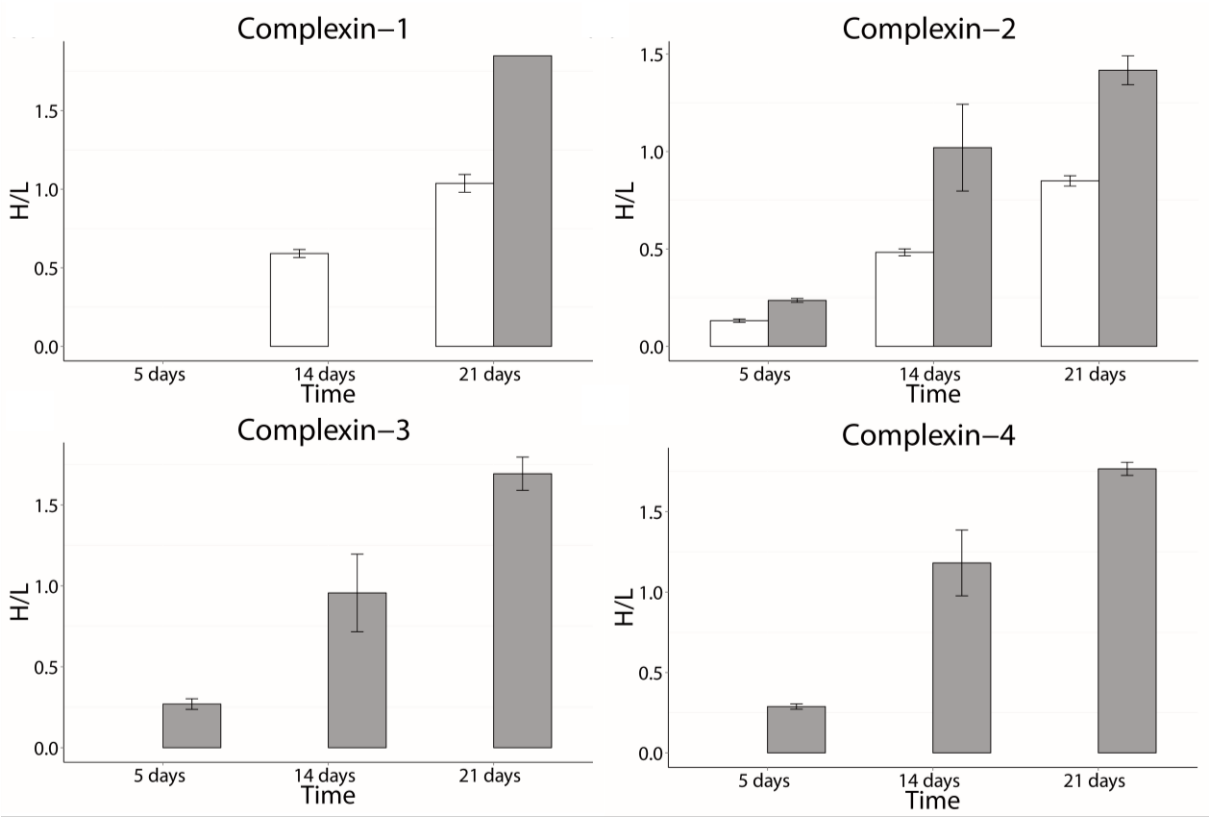
Complexin−1
Complexin−2
Complexin−3
Complexin−4
H/L
Time
5 days
14 days
21 days

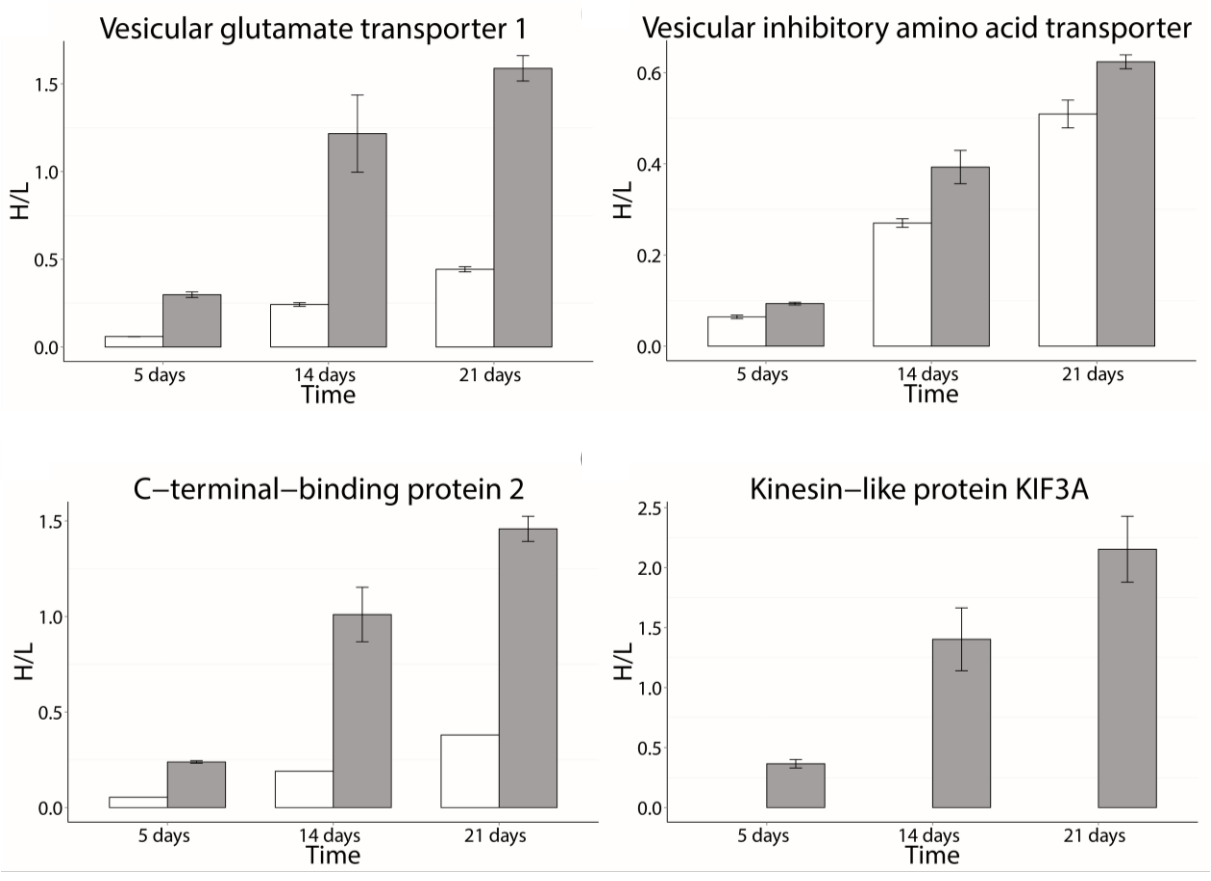
Vesicular glutamate transporter 1
Vesicular inhibitory amino acid transporter
C−terminal−binding protein 2
Kinesin−like protein KIF3A
H/L
Time
5 days
14 days
21 days

A12: Separation of docked and free SVs using hybrid protocol of Uthaiah and Hudspeth, 2010 and Boyken et al., 2013

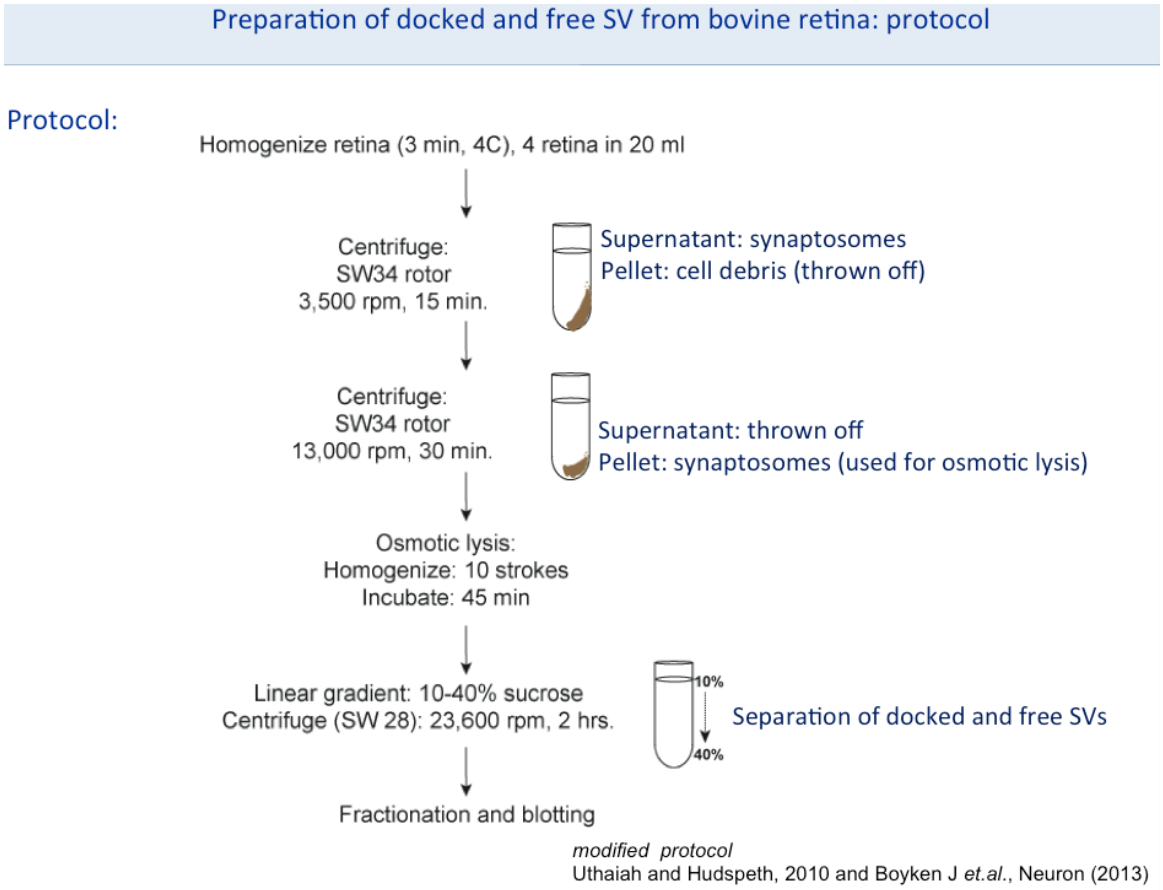

A13: Separation of bovine retinal Docked and free synaptic vesicles on a sucrose gradient

- **Docking marker**: Ribeye (homologue of CtBP2) is known docking protein for ribbon synapses
- **Synaptic vesicle markers**: VGlut, Synaptophysin, Synaptobrevin 2 (VAMP2)

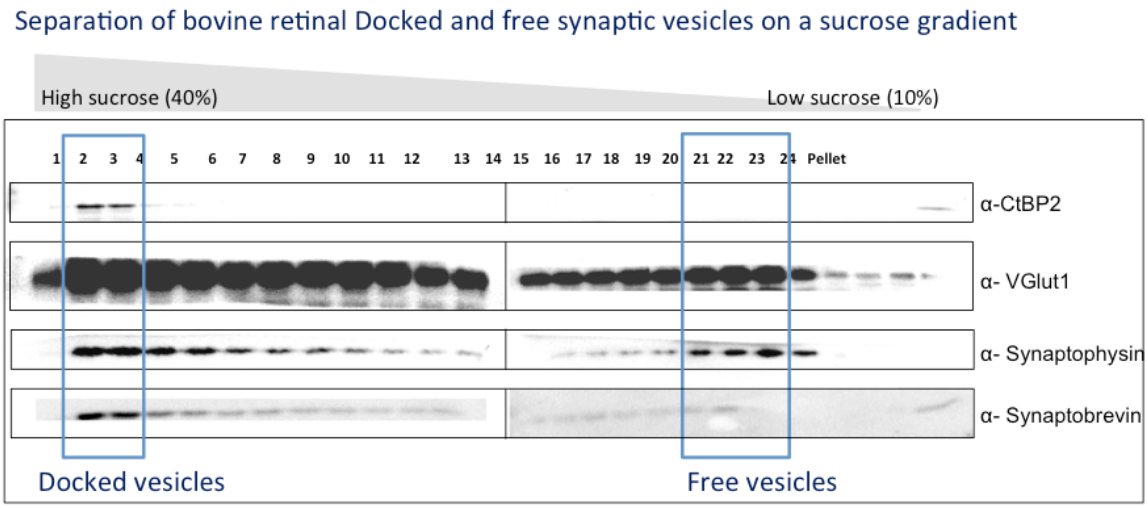

A14: Western blot of immunoprecipitation of docked and free vesicles

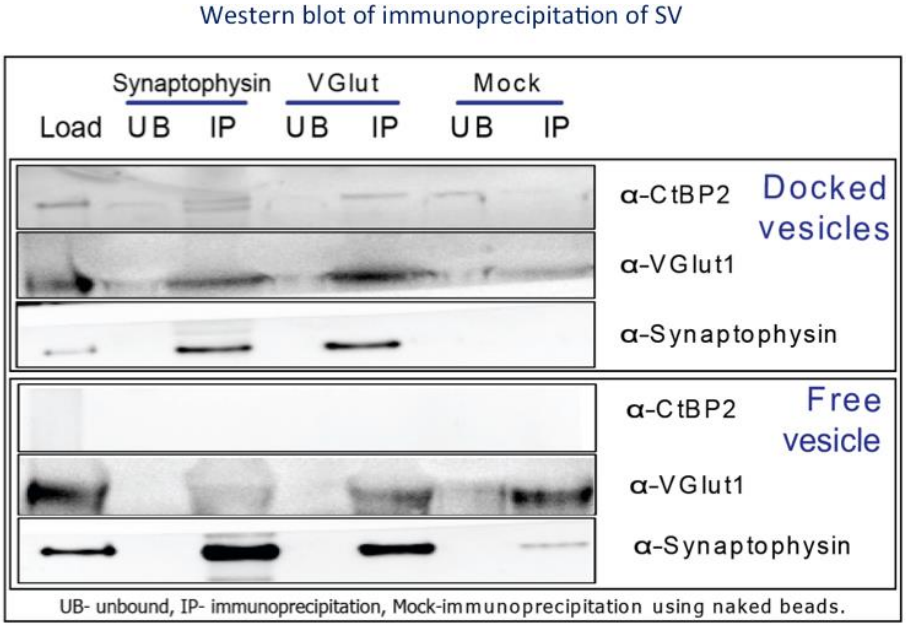

Immunoprecipitation of SVs is possible using Synaptophysin and VGlut (SV marker proteins) coupled to eupergit beads.